Molecular mechanisms of monoaminergic neurons development in *Caenorhabditis elegans*

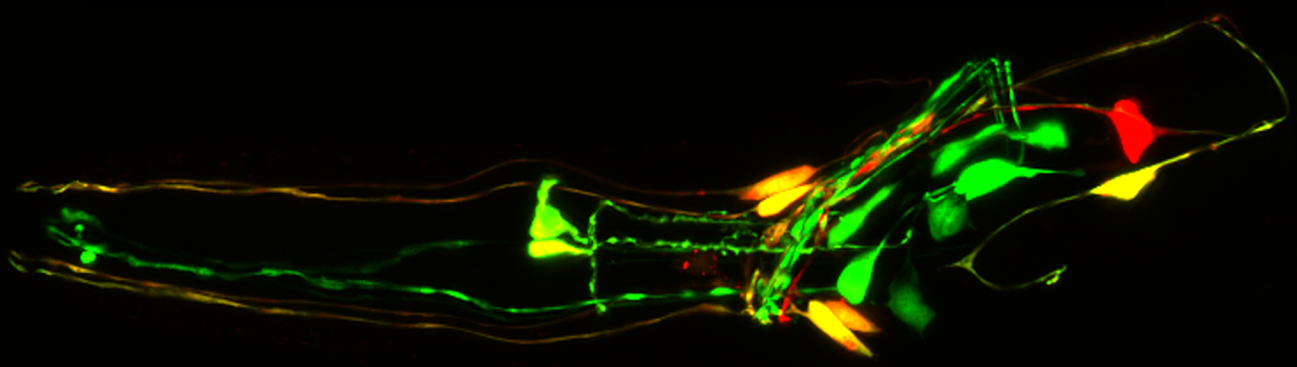

Doctoral Thesis by Ángela Jimeno Martín
Thesis Supervisor: Dr. Nuria Flames Bonilla
University Advisor: Dr. Isabel Fariñas Gómez

Doctoral Programme in Neuroscience, Universitat de València Estudi General
Instituto de Biomedicina de Valencia (IBV) -
Consejo Superior de Investigaciones Científicas (CSIC)

Valencia, June 2018

INSTITUTO DE BIOMEDICINA DE VALENCIA CSIC

CSIC
CONSEJO SUPERIOR DE INVESTIGACIONES CIENTÍFICAS

INSTITUTO DE BIOMEDICINA DE VALENCIA CSIC

Nuria Flames, PhD.
Developmental Neurobiology Unit
Instituto de Biomedicina de Valencia
e-mail: nflames@ibv.csic.es

Nuria Flames Bonilla, Doctora en Ciencias Biológicas, Científico Titular y Directora de la Unidad de Neurobiología del Desarrollo del Instituto de Biomedicina de Valencia del CSIC,

CERTIFICA:

Que Ángela Jimeno Martín, licenciada en Biotecnología por la Universidad de Salamanca, ha realizado bajo mi supervisión, la Tesis Doctoral titulada "Molecular mechanisms involved in monoaminergic neurons development in *Caenorhabditis elegans*".

En Valencia, 12 de Junio de 2018

MARIA ISABEL FARIÑA GOMEZ

Firmado digitalmente por MARIA ISABEL FARIÑA GOMEZ
Fecha: 2018.06.11 10:49:03 +02'00'

Directora de tesis
Dra. Nuria Flames Bonilla

Tutora académica
Dra. Isabel Fariñas

IBV. C/Jaime Roig, 11, 46010-Valencia, Spain Tel. 34-96-3391776

La Naturaleza nos es hostil porque no la conocemos: sus crueldades representan la venganza contra nuestra indiferencia

Ramón y Cajal

Biblioteca del IBV, Valencia, Junio 2018

Después de tantas palabras como he utilizado en la redacción de esta Tesis, ahora me faltan para dar a las gracias a todos aquellos que han hecho posible que llegue hasta aquí.

Mis andanzas en este mundo científico comenzaron muy lejos, en el INCyL, en el laboratorio de la Dra. Conchi Lillo, con mis primeros maestros Jedi, Saúl y Antonio. Siempre les estaré sumamente agradecida por sus enseñanzas y su apoyo y recordaré con mucho cariño los tres años que pasé con ellos en mi adorada Salamanca.

Y es que sin aquella primera etapa no hubiera conseguido que la Dra. Nuria Flames, mi Directora de Tesis, me diera la oportunidad de unirme a su laboratorio. No solo conseguí con ella mi primer contrato para formarme como investigadora, en tiempos económicamente muy complicados, sino que además me llevó a mi segunda familia, las Flames, por lo que nunca podré darle suficientemente las gracias.

Porque las Flames (sí Carlos, ya sabes eres una Nina más), querido lector, son la mejor familia EVER, son TOP, son las más inteligentes, locas, divertidas, guapas, cariñosas, adorables, trabajadoras e infinidad de adjetivos más que uno pueda aplicar para describir al mejor equipo de personas donde integrarse para hacer la tesis. Porque después de tantas horas en el laboratorio, lugar que empieza a ser como tu casa y por el que no te importaría caminar en calcetines o practicar el limbo, primero tus compañeras pasan a ser tus amigas y después, simplemente, te das cuenta de que son tu familia.

Como sabéis, soy una tía (porque tengo 5 sobrinos) muy dura y nada emocional, pero quiero dejar constancia de lo mucho que agradezco a todas todo lo que me habéis dado estos años. Quiero agradecer a Miren, mi maestra Jedi, todo lo que me ha enseñado, no solo de la ciencia sino también de la vida, y toda la paciencia y cariño que ha tenido conmigo, porque es muy responsable de que esta tesis haya salido adelante. A Carla, mi otra maestra Jedi, con la que he aprendido las maravillas de *C. elegans*, a ser una buena compañera de laboratorio y a pelear sin descanso por lo que uno quiere. Os recomiendo que leáis su tesis ¡¡está tan bien escrita!! A Rebeca, por cuidar de mí y hacerme sentir como en casa, por compartir desde enseñanzas a fotos y risas. A Carlos, que es nuestro genio loco, por las teorías estrambóticas, las discusiones y por compartir el éxito de nuestro Awesome Contamination Instagram. A Isa, que es fuerte como una montaña y me ha ayudado tantas veces con la serenidad y la alegría con la que mira la vida. A mi querida Ricitos, a la que voy a echar muchos de menos porque entiende muy bien mis legen-esperaunmomento-darias idas de olla. A la Reme, que con su desenvoltura y cariño sembró de buen rollo el laboratorio. A Laura, que siempre sabe escucharte y darte ánimo cuando lo necesitas. A Mireia, de la que puedes aprender miles de cosas y que es para mí

un ideal de mujer a seguir. Y por último, pero no menos importante, a nuestra Junior, que tiene una energía y alegría arrolladoras.

Y para continuar, de una familia a otra, porque desde luego que no hubiera llegado hasta aquí sin mis padres, Eusebio y Conchi. La pareja más luchadora, valiente y amorosa que conoceré jamás, que llenos de esfuerzo y cariño sacaron adelante, entre gallinas y tuppers, a esta pequeña científica. Porque lo que yo soy hoy, se asienta en lo que vosotros habéis construido. No hay palabra suficientemente grande para expresaros mi agradecimiento por todo lo que me habéis dado.

Por supuesto no me olvido de vosotras, Eva y Celeste, que también habéis estado apoyándome estos años, desde largas charlas telefónicas a nuestras quedadas en familia. ¡¡Tenemos pendientes muchas aventuras!!

Aunque si alguien ha vivido de cerca todo el trabajo de estos años, es mi Fran. Quizá parezca exagerado si digo que no lo habría conseguido sin él, pero es que Fran es mi mejor amigo y mi maestro. Porque somos compañeros en el duro proceso de sacar la tesis adelante y formamos el mejor equipo para sobrevivir y disfrutar de la vida. Porque da igual que estemos estudiando o que crucemos el mundo en tren, siempre lo mejor es estar en tu compañía. Sin duda esta tesis no habría sido posible sin ti, sin tu paciencia, cariño y tus chistes malos. Te mereces un Gracias tan grande que resuene en todos los universos.

Finalmente, quiero dar las gracias a todos los que han participado en mi formación estos años, a las profesoras Hortensia Rico y María Iranzo de la Universidad de Valencia por permitirme colaborar en tareas docentes. Un gracias especial al Dr. Mark Alkema, por acogerme en su laboratorio durante mi estancia en la Universidad de Massachusetts. Allí no solo aprendí técnicas nuevas, sino una nueva perspectiva de hacer ciencia, donde conté con la ayuda y apoyo de Jeremy, Jeff, Wookyo, Amit, Yung-Chi; también de mi compañera de cumpleaños, Laura, y del resto de integrantes de la familia hispanohablante de Worcester que me acogió y quienes con su cariño hicieron que los tres meses pasaran volando. Así mismo, a la Generalitat Valenciana por su apoyo económico a través del programa VALi+D.

En definitiva, a todos aquellos que habéis participado, aunque no os haya nombrado aquí, en el largo proceso que me ha llevado hasta el título de Doctora.

¡GRACIAS!

INDEX

INDEX OF FIGURES AND TABLES

- **INTRODUCTION**

- **METHODS**

- **RESULTS**

Figures

Tables

ABBREVIATIONS AND ACHRONYMS

5-HT serotonin
5-HTP 5 hydroxytryptophan
A Adrenaline
AADC amino acid decarboxylase
ADE Anterior dirid, sensory neuron
ADF Amphid neuron Dual F
BAS-1 biogenic amine synthesis related 1
bHLH basic Helix-Loop-Helix
bp base pair
BS binding site
C. elegans *Caenorhabditis elegans*
CGC Caenorhabditis Genetic Center
CEPD Cephalic neuron dorsal
CEPV Cephalic neuron ventral
CRISPR Clustered Regularly Interspaced Short Palindromic Repeats
CRM *cis*-regulatory module
DA Dopamine
DNA Deoxyribonucleic acid
E. coli *Escherichia coli*
ESR enhanced slowing response
Fwd forward
GCH1 GTP cyclohydrolase 1
GFP Green Fluorescent Protein
HD Homeodomain
HSN Hermaphrodite specific neuron
IPTG Isopropyl β-D-1-thiogalactopyranoside
kb kilo base
NA Noradrenaline
NSM Neurosecretory motorneuron
nt nucleotide
OA Octopamine
PCR Polymerase Chain Reaction
PDE Postdeirid sensillum neuron
PWM position weight matrix
p p value
Rev reverse
RIC Ring interneuron
RIM Ring motorneuron
RNA Ribonucleic acid
RNAi RNA interference
SEM standard error of the mean
SEP standard error of the proportion
SERT serotonin transporter
SLC18A1/2 Solute Carrier Family 18 Member A1/A2
SLC6A4 Solute Carrier Family 6 Member A4.
SNP Single Nucleotide Polymorphism
TA Tyramine
TF transcription factor
TFBS transcription factor binding site
TPH-1 tryptophan hydroxylase
Trp tryptophan
TSS transcription starting site
UTR untranslated region
VC ventral cord motorneuron
VMAT vesicular monoamine transporter
wt wild type

INTRODUCTION

INTRODUCTION

Specific cell identities are defined by the expression of selected transcriptomes that allow the cell to fulfill its specific functions (Spitz and Duboule 2008). Activation of gene expression is regulated by *trans*-acting elements, known as transcription factors (TF), that bind to *cis*-regulatory elements to recruit and promote the activity of RNA polymerase II and the rest of the transcription machinery. To gain further insights into the molecular mechanisms of transcriptional regulation it is essential to understand the link between transcription factors and their target genes. Furthermore, to better understand the establishment of specific cell identities we need to study how TFs act in a coordinated manner to select cell type specific transcriptomes.

The establishment of cell type diversity is particularly important in the nervous system which is composed by hundreds of different neuronal types each one defined by specific transcriptomes. Large efforts have been made to deeply characterize cell fate specific programs that trigger neuron subtype gene expression profiles (Hobert 2016a).

In this Thesis we aim to increase our knowledge on the transcriptional programs that control neuron subtype specification of monoaminergic (MA) neurons. This group of neurons synthesizes their neurotransmitters from aromatic amino acids, such us tyrosine and tryptophan that metabolize into dopamine, serotonin, adrenaline or noradrenaline among others. MA neurons are very ancient in evolution, being present in all animal groups (Turlejski 1996). Functionally, they are very diverse, and, in humans, MA dysfunction is linked to several pathological conditions such as Parkinson disease, depression, schizophrenia or bipolar disorder (Wang and Pereira 2016; Otte et al. 2016; Willis 1987). Thus, understanding the transcriptional regulatory programs controlling MA subtype specification is important not only for fundamental biology but also because it can help us understand the genetic component of some of these disorders.

In this work we take advantage of the phylogenetic conservation of MA systems and use the model organism *Caenorhabditis elegans* to identify new TFs required for MA subtype specification. Our strategy consisted in the performance of an RNAi screen against all TFs in the *C. elegans* genome to identify new candidates involved in MA specification. To provide the required background for this project, the Introduction is divided in three chapters: in Part I offers a general overview of the regulation of gene expression and neuronal specification; Part II describes *C. elegans* as a model organism, with a brief description of reverse genetic screen in the worm, and the organization of the nervous system of *C. elegans* and Part III is focused on monoaminergic systems across phylogeny and we review the TFs known to be required for MA specification in different model organisms with special attention to *C. elegans*.

Part I. Regulation of gene expression and neural cell fate specification

1. *trans*-acting elements: Transcription factors

Transcription of coding genes is carried out by RNAi polymerase II (Pol II) and all the accessory machinery able to stabilize the polymerase, unwind the DNA and separate their strands. However, the binding of the polymerase to the core promoter is prompt by the timely binding of regulatory transcription factors.

Typically, TF scan long DNA sequences until they find motif matches where they bind (Spitz and Furlong 2012). This specific genomic sequences, about 6-12 nucleotides in length are called TF binding sites (TFBS) (Shlyueva, Stampfel, and Stark 2014). Each TF binds a range of TFBS, meaning that specific nucleotide positions can vary in each TFBS. The set of TFBS of a TF determine a consensus sequence named transcription factor binding motif. This motif is a degenerate sequence that can be represented through position weight matrices (PWM) that provide the frequencies at which individual nucleotides are found at each position of the motif. This PWM are graphically represented as logos, which illustrate by letters the nucleotides of each position and the probability of each one keeps direct relation to the letter size (Gao, Liu, and Ruan 2017) (Figure I.1).

PWMs are a reflection of the interaction established between the DNA and the TF. Logically, the motif the TF binds is the result of aminoacid interactions and three-dimensional conformation of the protein domain that conforms its DNA-binding domain (DBD)(Yang and Ramsey 2015). The characteristics of this DBD provide the specificity of the TF to the DNA sequence it binds. Accordingly, TFs can be classified into different groups according to their DBDs (Wingender, Schoeps, and Dönitz 2013).

In humans, the classification of TFs according to their DBD follows a hierarchical structure that groups them in 10 superfamilies and 40 classes (Wingender, Schoeps, and Dönitz 2013). Superfamilies are based on the structural properties of the DBD, like helix-turn-helix, immunoglobulin fold, zinc-coordinated DNA-binding domains or basic domains and the classes are defined upon sequence similarities regarding DNA-binding motifs. Additionally, classes are integrated by different families which contain members with particular related sequence and function similarities. In humans there are 111 TF families. In *C. elegans*, TFs are grouped in 48 families and subfamilies, again according to their DBD characteristics (Table I.1) (Weirauch et al. 2014; Narasimhan et al. 2015).

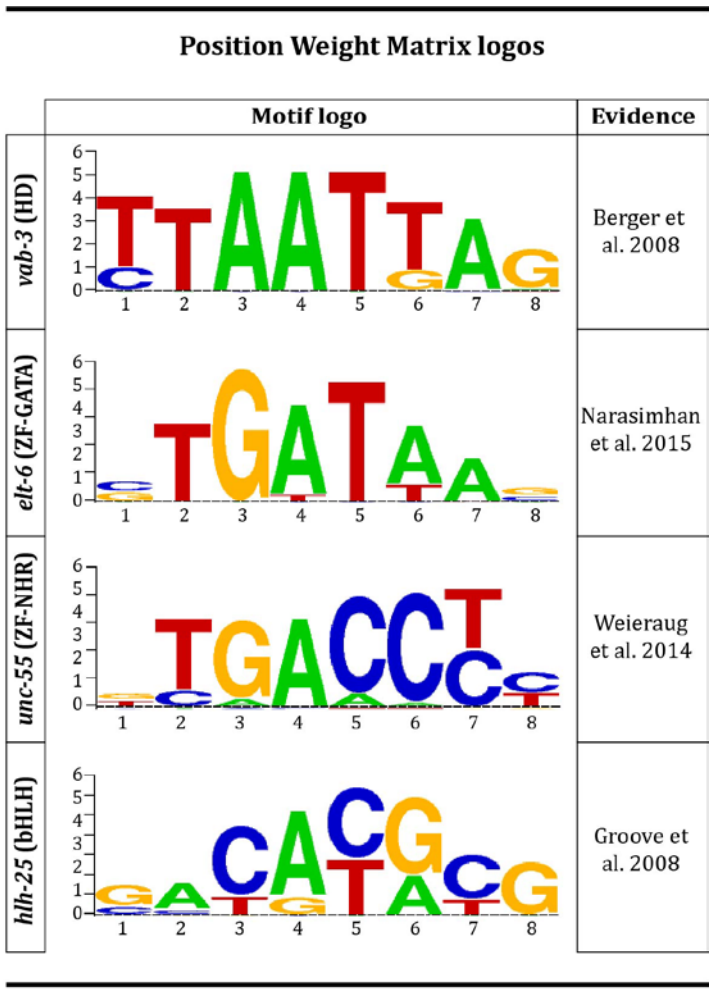

Figure I.1 Position weight matrixes logos. This image shows some examples of PWM of distinct TFs from different families represented as logos.

Table I.1. *C. elegans* TF families		
DNA-binding Domain	**Family description**	**Total members**
β-catenin/armadillo		3
AP-2	Activator protein-2	5
ARID/BRIGHT	AT-rich interaction domain	5
AT Hook		16

bHLH		Basic region helix loop helix	42
Brinker			2
bZIP		Basic region leucine zipper	36
CBF		CCAAT-binding factor	9
CENPB		Centromer protein B	1
CSD		Cold-shock domain	5
CP2			1
CSL		CBF1, Supressor of Hairless, LAG-1	1
CxC		GC-rich DNA-binding domain	2
HD	-	Homeodomain	19
	CUT		7
	HNF		1
	HOX	Homeobox	18
	LIM	Lin11, Isl-1 and Mec-3	7
	NK		18
	POU	Pit-1, Oct-1, Unc-86	3
	PRD	Paired domain	17
	PROX	Homeo Prospero domain	1
	SIX		4
	TALE	Three aminoacids loop extension	6
HMG box		High mobility group	16
HTH		Helix turn helix	3
IPT/TIG		Ig-like, plexins, TFs	2
MADF		Mothers against Dpp factor	12
MADS box		MCM1/AG/DEF/SRF	2
MDB		Methyl-CpG binding domain	1
MH1		MAD homology 1	7
MTERF		mitochondrial transcription termination factors	2
MYB		Myb (myeloblastosis)-like TFs	13
p53			3
PRD-FULL		Paired domain	3
PRD-NPAX		Paired domain	4
RNT			1
SAND		Sp100, AIRE-1, NucP41/75, DEAF-1	2
SART-1			1

STAT		Signal transducers and activators of transcription	1
T-box			22
TBP		TATA-binding protein	3
TEA/ATTS		Transcriptional enhancer activator	1
TSC-22/DIB/BUN			3
WH	-	Winged helix	2
	DAC	Dachshund	1
	HSF	Heat shock factor	11
	RFX	X-box binding regulatory factor	15
	ETS	Erythroblast transformation specific	1
	FKH	Fork head	1
	TDP	TF E2F dimerisation partner	4
WT1		Wilms tumor1	1
YEATS		YNK7, ENL, AF-9 and TFIIF small subunit	1
ZF - BED		BEAF/DREF-like ZF	4
ZF - C2H2		Zinc finger Cys(2)His(2)	192
ZF - C2CH		Zinc finger Cys(2)His	1
ZF - CCCH		Zinc finger	1
ZF - DM		Dsx and Mab-3-like ZF	11
ZF - FLYWCH			4
ZF - GATA		Zinc finger GATA binding motif	14
ZF - MIZ		Msx interacting ZF	1
ZF - NF-X1 - 10 domains		Nuclear factor	1
ZF - NHR		Nuclear hormone receptor	272
ZF - THAP		Zinc finger Thanatos associated proteins	5
Unknown			2
TOTAL TFs			876

Several computational and experimental approaches have been developed to determine TF binding across the genome and to determine specific TF DNA binding motifs. Some of the most commonly employed techniques are chromatin immunoprecipitation followed by deep sequencing (ChIP-seq), protein binding microarrays (PBMs), systematic evolution of ligands by exponential enrichment (SELEX) or yeast-one-hybrid (Y1H), among many more (Levo and Segal 2014). However, the high

number of TFs across species hampers *in* vivo motif determination and there, bioinformatic models, using K-mers or hidden Markov models predict in a confident manner TFBS (Yang and Ramsey 2015). Experimental data about determination of TFBS are systematically collected in motif databases such us JASPR or TRANSFAC.

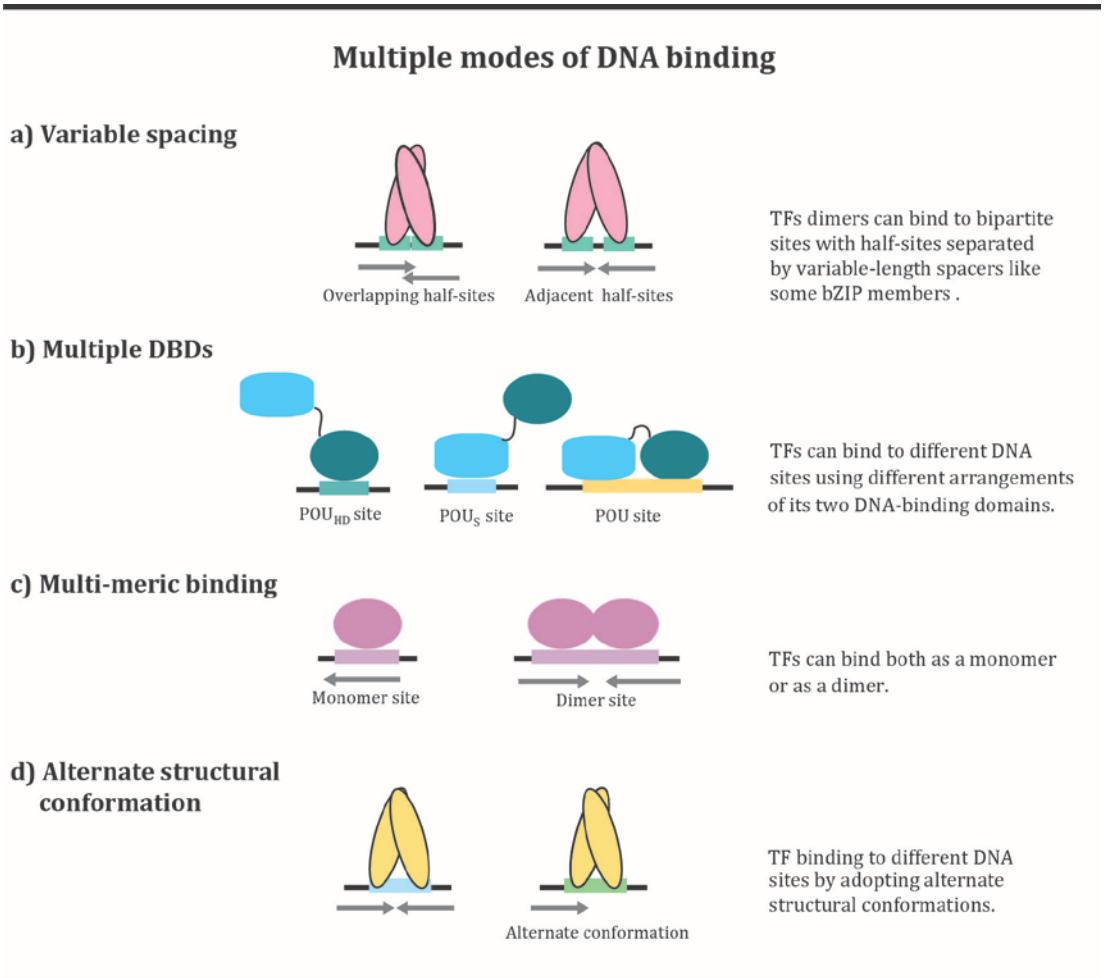

Figure I.2. Multiple modes of DNA binding. The possibilities of TF binding to DNA motifs are exemplified. These models show how the recognition of binding sites can change because of protein structure. Adapted from *Siggers and Gordân 2014*.

Normally, there is high accuracy between *in vitro* predicted binding sequences and the *in vivo* reported binding site for a given TF. Nevertheless, there are still some cases where the *in vitro* affinities do not reflect *in vivo* binding specificities and this is mainly provoked, on the one hand, by cofactors that are only present *in vivo* and that can alter the TF sequence preferences (Siggers and Gordân 2014) and on the other hand, by the

flanking base pairs to the core TFBS that can also contribute to the binding specificity. One example of this are two members of bHLH in yeast, *Cbf1* and *Tye7*, which were shown to have highly similar DNA-binding motifs *in vitro* (E-box) but seem to bind to different sets of genomic targets *in vivo*. (Gordân et al. 2013). This study used genomic context protein binding microarrays (gcPBMs) to show the binding differences of *Cbf1* and *Tye7* to the E-box motif when it was embedded into 30 bp flanking sequences that shape and deform the DNA surrounding the binding site.

The interaction between TFs and the DNA has been described as a rather simple interaction, based on establishment of hydrogen bonds or hydrophobic contacts. However, proteins can use two or more modes of binding, which can be classified into four categories. The first of them alludes to proteins that bind to bipartite DNA motifs (compose of two half-sites) working as homodimers or heterodimers. In such cases, the TF can recognize distinct classes of motifs in which the half-sites are separated by different numbers of bases depending on the conformation of the dimer (Figure I.2a), this was observed, for example, in basic leucine zipper (bZIP) AP-1 (Kim and Struhl 1995).

Secondly, proteins can present more than one DNA-binding domains (DBD) that allow the protein to alternatively recognize different DNA elements (Figure I.2b). One example is the mouse TF *Oct1*, this POU TF has a homeodomain DBD ($POU_{HD)}$ and POU-specific domain (POU_S). This protein can recognize three different binding sites using both domains alone or in combination (Klemm et al. 1994).

On the other hand, proteins form multimers that can expand the diversity in DNA-binding specificity of the TF (Figure I.2c), as is the case of *Elk1* that binds as monomer and as homodimer (Jolma et al. 2015). Moreover, the recognition of distinct binding sites can be altered by external residues to the DBD, as is the case of human sterol regulatory element (FigureI.2d) (Parraga et al. 1998).

Although DNA binding specificity of a TF is essential to determine where it will bind along the genome, the transcriptional regulation often involves the assembly of DNA multi protein complexes (Lelli, Slattery, and Mann 2012). These complexes can exhibit not only different affinities for distinct DNA sequences, but also yield different types of output of gene expression depending on TF interactions. Usually, these interactions lead to cooperative binding when protein-protein interactions occur between TF that are adjacently bound and achieve an increased stability on DNA and enhance their individual contributions for a gene transcription (Wolberger 1999). The interaction can enhance the affinity for weak motifs (Figure I.3a1), but also the proximity between TFs can modify the inherent binding specificity through more stable or alternate conformations of the protein structure (Figure I.3a2), as is the case of *Ets1* and *Pax5* (Garvie, Hagman, and

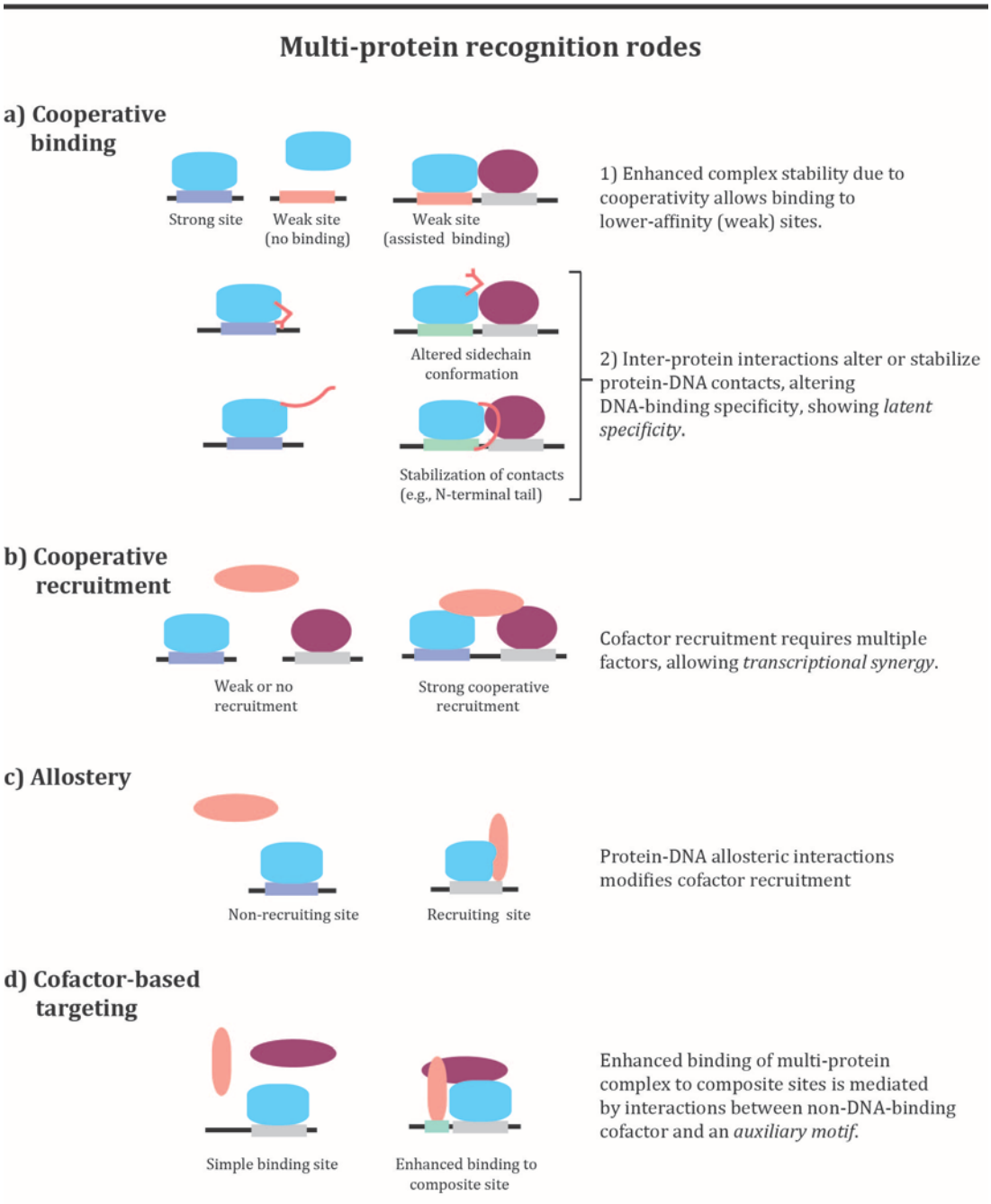

Figure I.3. Multi-protein recognition codes. Here we represent four distinct mechanism by which proteins can interact to regulate binding to DNA in multi protein complexes. Adapted from *Siggers and Gordân 2014*.

Wolberger 2001). Moreover, this highlights how intrinsic specificity of a monomeric

protein can be altered or redefined through interactions with a cofactor showing a *latent specificity*, well exemplified in *Drosophila* Hox proteins (Joshi et al. 2007).

Other possible scenario involves cofactors, these proteins do not bind to DNA directly but through their interaction with TFs they can repress or enhance transcription (Levine and Tjian 2003). Currently, multiple TFs contribute to recruit a common cofactor to make simultaneous contact with it and, as a result, the overall protein interaction integrates the contributions of the TFs to achieve maximum gene expression, what is called *synergistic enhancement* (Figure I.3b). The binding specificity of the cofactor is determined by the coincident presence of multiple TFs (Carey 1998), as observed in the recruitment of p300-CREB binding protein to the regulation of INFβ promoter (Merika et al. 1998). Nevertheless, DNA architecture can also function as sequence-specific allosteric ligand for a TF to promote structural rearrangements in protein structure (rotations or translations) and thus, alters the cofactor recruitment (Figure I.3c). This situation has been described for glucocorticoid receptor (GR) (Meijsing et al. 2009; Leung, Hoffmann, and Baltimore 2004). Traditionally, cofactors interact with already DNA bound TFs, however there are some cases where cofactors interact directly with DNA when they are part of a larger multiprotein complex through their recognition of an auxiliary motif named *recruitment motif*. One example is found in sulfur metabolism TFs in yeast, composed of the bHLH TF *Cbf1* and two non-DNA binding proteins *Met28* and *Met4* (Figure I.3c) (Blaiseau and Thomas 1998).

All these mechanisms of TF binding and multiprotein complexes targeting DNA sequences provide a flavor of the complexity of the regulation of gene expression, however, they only comprise a small part of the elements involved in transcriptional regulation. Gene expression is also integrated by many *cis*-regulatory elements from core promoters to enhancers, silencers, insulators and tethering elements. In the following section we will summarize the role of DNA regulatory elements in gene expression.

2. *cis*-regulatory elements: promoters and enhancers

As previously mentioned, to carry out gene transcription, RNA-pol II and the transcriptional machinery binds to DNA, more exactly, in the promoter of the target gene that is going to be transcribed. Promoters are the loci overlapping the transcription start site (TSS), where the regulatory input of a gene is integrated in order to initiate transcription, thus, promoters are crucial for gene regulation. However, this rather simplistic definition is actually more complex *in vivo*. In Metazoans, for instance, the regulatory elements that control promoter activity can be spread over a large genomic space. This has led to the definition of a *core promoter*, which would be the immediate adjacent region of the TSS and that is assumed to dock the RNA-pol II and the rest of

elements belonging to the pre-initiation transcriptional complex (Figure I.4) (Lenhard, Sandelin, and Carninci 2012).

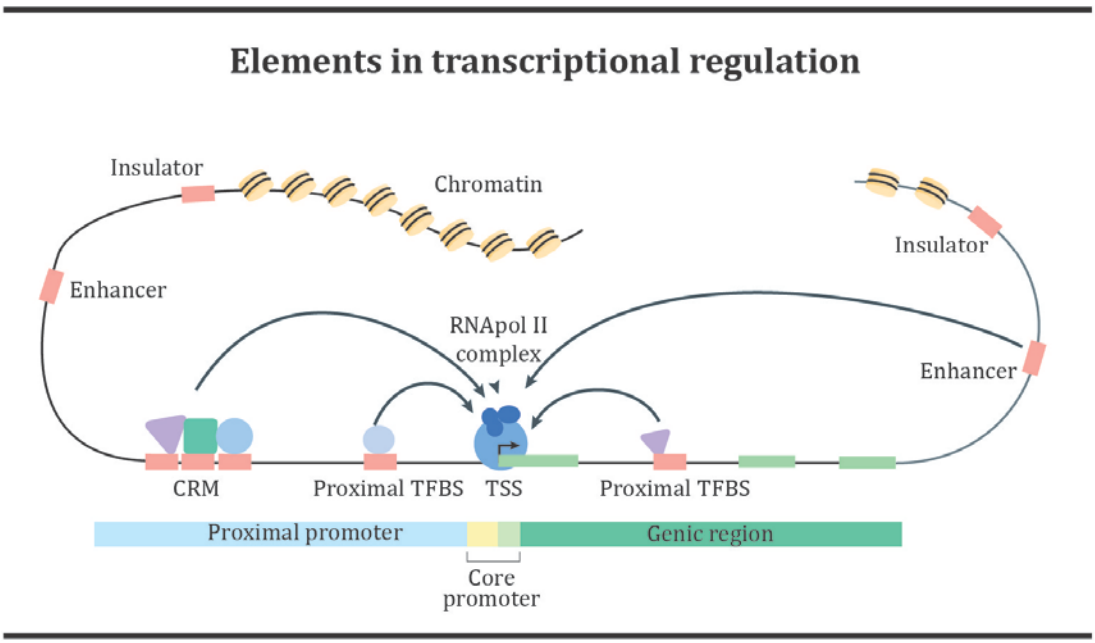

Figure I.4. Elements in transcriptional regulation. Summary of the elements involved in gene expression. The structure of chromatin is formed by DNA wrapped around histone octamers. This tight association can impede the access of positive transcriptional signals from enhancers and negative signals from silencers. In this regard, insulators are considered the chromatin barriers delimiting boundaries between heterochromatin and accessible sequences. The region upstream transcription start site (TSS) is commonly divided into core and proximal promoter elements. TFBS are usually clustered into *cis*-regulatory modules (CRM) but it is possible to find them also inside introns. Adapated from *Lenhard, Sandelin and Carninci 2012.*

Nevertheless, transcription is often weak in the absence of regulatory regions that are more distal from TSS. This regions are called enhancers or *cis*-regulatory modules (CRMs) (Shlyueva, Stampfel, and Stark 2014). Some authors distinguish between these two terms, arguing that CRM are located in proximities of core promoters whereas enhancers are found hundreds of kilobases further to TSS (Lenhard, Sandelin, and Carninci 2012), however as they share the same architecture features, most authors consider the terms enhancer and CRM synonyms. Both are small segments of DNA, around a few hundred base pairs in length, whose main function is to recruit TFs through clusters of TF binding motifs (Long, Prescott, and Wysocka 2016). These *cis*-elements seem to act independently of the distance and orientation to their target genes, by forming DNA loops, and they function as modules, contributing additively and even

redundantly to convert relaxed individual activities into more specific genetic programs (Spitz and Furlong 2012).

The link between enhancer architecture and its functional output is determined by the combinatorial and spatiotemporal occupancy. This means that is not simply the window of expression of TFs, but the timing of enhancer occupancy what defines the temporal control of gene expression. The regulation of this feature is extremely important in gene regulatory networks that control developmental progress or organ formation (Wilczyński and Furlong 2010). Accordingly, it has been shown that the combinatorial interplay between different TFs, each with its own expression interval, is key in the regulation of context-specific binding: enhancers contain distinct TF motifs, that lead to time-dependent occupancy which, in turn can cooperatively recruit additional TFs for occupancy later on development (Yáñez-Cuna, Kvon, and Stark 2013).

Nevertheless, not only motif composition is relevant in enhancers to drive expression, but also motif disposition has been seen to play a role in some contexts. Disposition means that the relative order, orientation and spacing between TF motifs within an enhancer is important for gene regulation (Evans, Swanson, and Barolo 2012; Levine 2010). This is intrinsically related with the mechanisms by which multiprotein complexes recognize DNA, as we previously described (Figure I.2). For instance, the cooperative binding or cofactor recruitment is conditioned by correct motif positioning that allows TFs interactions. One of the best studied examples is the interferon-β enhancer that contains a 55bp sequence and it is occupied by eight TFs, any variation in the relative order, distance or orientation of TFBS abolish enhancer function (Kim and Maniatis 1997). This highly ordered model of enhancer occupancy led to the *enhanceosome* model of activity, which requires a strict and specific disposition of TF binding motifs in a relative order between them and thus, this triggers a sharp, switch-like activation (Figure I.5a).

Although the rapid response achieved through the enhanceosome model can be essential in sudden events like virus infection, most of the enhancers, especially those related to development, seem to be occupied by cooperativity and also in additive or independent manner. This observation lead to the proposal of the of the *billboard* model of enhancer activity (Figure I.5b), which suggests that enhancers serve as information display elements where TFs can cooperate but with few constraints between the position of their binding sites (Kulkarni and Arnosti 2003). Supporting evidence about this model is based on sequence analysis of enhancers with similar activities and diversity in motif positioning that points towards no generalize motif positioning rules (Liberman and Stathopoulos 2009).

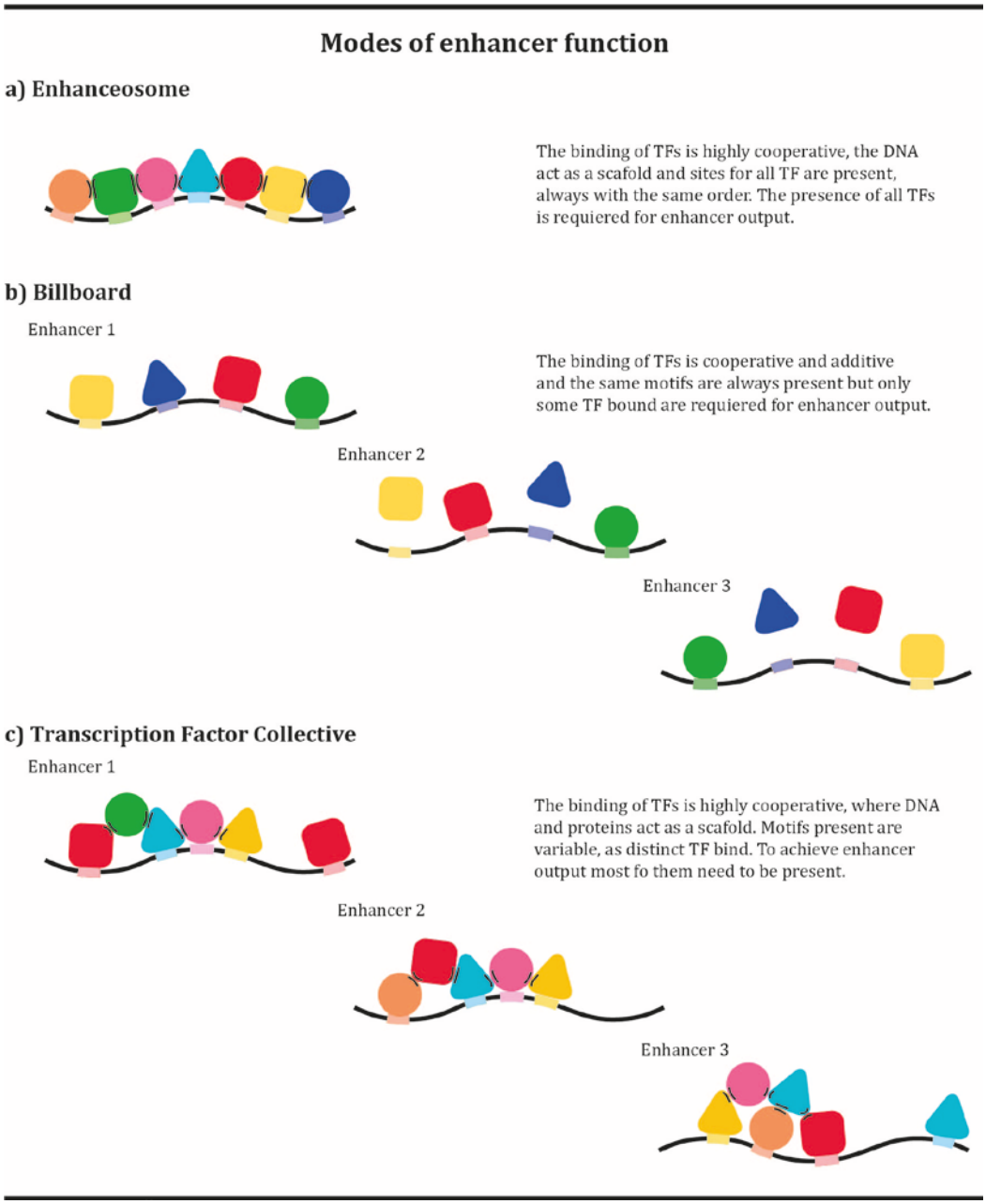

Figure I.5. Modes of enhancer function. a) In the enhanceosome model enhancer activity requires cooperative occupancy of all the TFs in strict order. b) On the other side of the spectrum, the billboard model requires less rigorous TF binding that can be additive or cooperative, and only some TFBS are occupied in a given moment. c) In the TF collective model, the whole group of TFs that integrate the collective is required in order to activate expression of the many enhancers they control, but the interactions among them can vary depending on the motif composition and disposition. Adapted from *Spitz and Furlong 2012*.

Finally, a third model, termed the *TF collective*, proposes a balance between the rigidity of the enhanceosome model and the lack of TF interactions of the billboard model. This model was proposed based on the regulatory logic of cardiac development in Drosophila. A group of TFs co-bind and regulate a large set of enhancers with no apparent motif grammar, however, when one TF of that group is removed, the rest fail to activate enhancers, suggesting cooperative binding through protein-protein interactions (Figure I.5c) (Junion et al. 2012). The *TF collective* model would be able to withstand some motif divergence while having little effect over TFs bound. This feature could buffer changes in sequences or in TF levels of expression, as long as they reach minimum threshold, which could alter complex genetic developmental programs, making them more robust (Masel and Siegal 2009).

3. Regulatory landscapes: interplay between regulatory elements and epigenetics

Both *trans* and *cis* elements are immersed in a three-dimensional environment where DNA is wrapped by nucleosomes, highly condensed through chromatin and as a result, the final conformation inside the nucleus of the cell is hinder to access. Thus, the expression of a gene demands the interplay between TFs, enhancers and promoters to achieve a genomic architecture that allows the activation of genetic programs.

As stated above, TFs bind and activate enhancer functions. However, the accessibility to those enhancer sequences can be hampered by DNA packaging around nucleosomes adding a new layer of complexity to regulate gene expression. Nevertheless, some TFs have the ability to bind to DNA that is inaccessible for other TFs, they open chromatin and recruit cooperatively other *trans*-acting elements that occupy the enhancer (Figure I.6a). This type of TF is termed *pioneer TF* and they have been described to act on top of gene regulatory networks (Mercer et al. 2011). Its ability is related mainly with recruitment of chromatin remodeling complexes that lead to nucleosome repositioning (Zaret and Carroll 2011).

This modification of chromatin structure, that affects gene expression but do not involve changes in DNA sequence is called epigenetics. Epigenetic changes can be located at DNA level, such cytosine methylation, or as a posttranslational modification over histones that integrate the nucleosomes (Dupont, Armant, and Brenner 2009). This includes a great variety of protein modifications but the ones studied in more detail are lysine methylation and acetylation. Usually, methylation either in DNA or histones leads to transcriptional repression although depending on the lysine position and the number of methyl groups added, the result can be transcription activation.

Interplay between TFs and chromatine structure

a) Chromatine remodeling (pioneer TF)

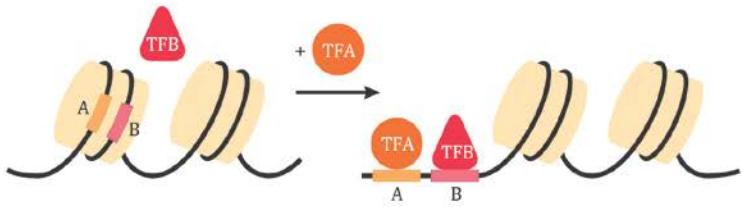

b) Nucleosome repositioning

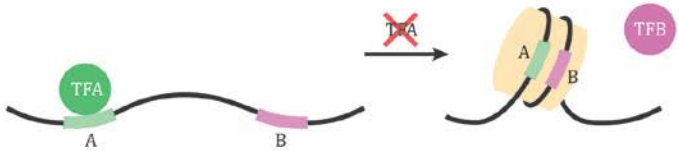

c) DNA architecture

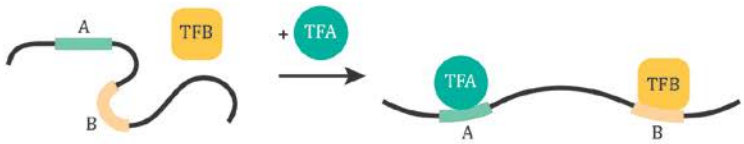

d) DNA loops

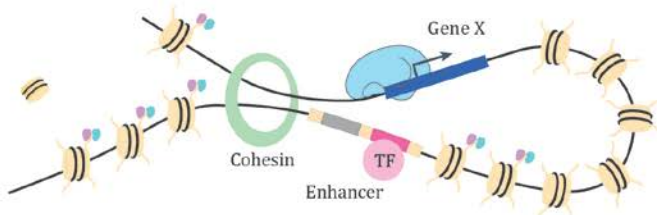

e) Transcription factories

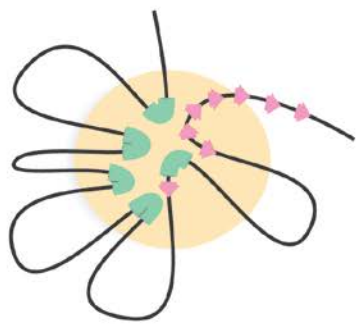

Figure I.6. Interplay between TFs and chromatin structure. a) One of the first interactions between transcriptional complexes and chromatin is currently through pioneer TFs that have the intrinsic ability to bind DNA regions wrapped in nucleosomes and expose other binding motifs for other TFs. b) By remaining bound to the DNA, some TFs (as pioneers) avoid nucleosome repositioning keeping an active loading state. c) Protein-DNA interactions can induce conformational changes and bends that exhibit motifs otherwise inaccessible. All these mechanisms, although indirectly, enable the establishment of transcriptional complexes. d) When enhancers become active, DNA loops bring them together with promoters. This action is thought to be mediated through cohesins and other multiprotein complexes. e) The formation of a three-dimensional environment where distal regions interact originates spaces where transcription is enhanced and involves the genes located there, these regions are called TADs. Thus, transcription cannot be dissociated from a three-dimensional space. Adapted from *Spitz and Furlong 2012* and *Shlyueva et al. 2014.*

Conversely, histone acetylation is commonly associated to gene expression (Wenzel, Palladino, and Jedrusik-Bode 2011). *C. elegans* does not methylate its DNA, and therefore, promoter silencing triggered by this mechanism is substituted for other regulatory mechanisms in the worm. Finally, TFs recognize and interact with epigenetic marks through recruiting histone modification machinery or can bind an provoke architectural modifications over DNA through shape bends (Figure I.6c), to make motifs for other TFs more accessible (Andreeva et al. 2017).

DNA topology goes further than protein-DNA interactions. One of the features of enhancers is that they can be located hundreds of kilobases away of the regions they regulate. Thus, interaction of enhancers with their target promoters requires large chromatin loops to bring these two elements together (Figure I.6d). These structures facilitate that previously unrelated regions of the genome become closer in three-dimensional space, what is named topologically associated domains (TADs) (Hansen et al. 2018). Recent techniques of chromosome conformation capture, such as Hi-C (Belton et al. 2012) and others have revealed that this structures are conserved among different organisms and cell types and seem to be the way for enhancer-promoter interactions (Gibcus and Dekker 2013). The boundaries of these TADs, are enriched in CCCTC-binding motifs that recruit the CTCF transcription factor (Bell, West, and Felsenfeld 1999). CTCF interacts through cohesins with DNA to settle the interaction areas of distal regions. Interestingly, the vicinity of these areas where chromatin is open, by action of pioneer TFs or recruitment of TF collectives, leads to active transcriptional environment termed transcription factories (Figure I.6e) (Papantonis and Cook 2010; Razin et al. 2011; Rieder, Trajanoski, and McNally 2012).

Consequently, the crosstalk of all the regulatory elements, transcriptions factors, enhancers, insulators, chromatin modifications and chromosomal architecture, is key in

the regulation of gene expression. The overall architecture of all these elements in a given cell at a specific time in development configures its regulatory landscape (Spitz, Gonzalez, and Duboule 2003). Accordingly, regulatory landscapes ensure precise spatio-temporal and robust gene expression (Spitz and Duboule 2008).

4. Terminal selector codes activate neuron type specific transcriptional profiles

Regulation of gene expression needs to be tightly coordinated in specific genetic programs that result in cell-type specific transcriptomes. Currently, many efforts are aimed to understand how this cell-type specific regulatory programs are implemented in a cell.

The study of nervous system specification has traditionally followed a *top-down* approach to define the events and signaling patterns that progressively give rise to differentiated neuronal fate. In this approach, selected signaling molecules or TFs are studied through loss of function and gain of function experiments to see if specific cell fates are affected (Sengupta and Bargmann Cornelia 1998). The advantage of using a simple model organisms such as *C. elegans*, with a much compact regulatory genome is that it allows to combine the *top-down* approach with *bottom-up* approaches where, the regulatory regions of sets of genes expressed in mature neurons, such as the synaptic machinery, can be directly studied through *in vivo* reporter analysis to identify the regulatory logic directing its activation (Hobert 2016a).

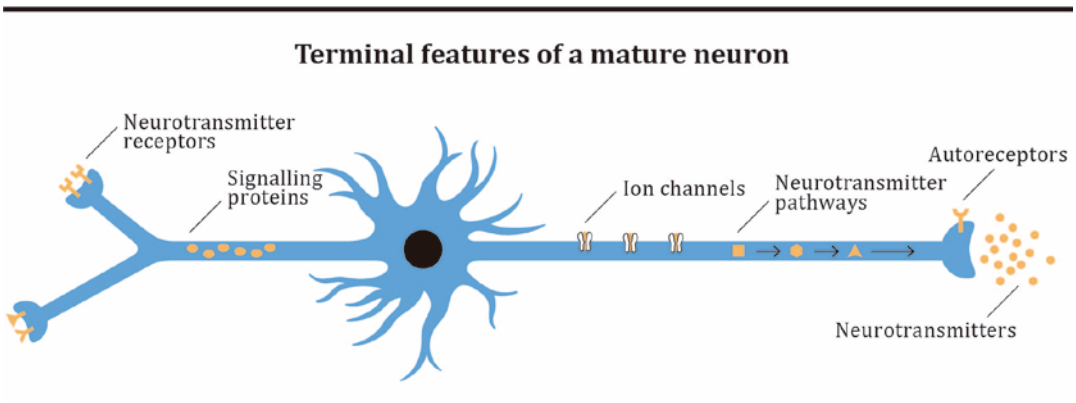

Figure I.7. Terminal features of a mature neuron. A neuron is characterized by the expression of effector genes (also known as terminal features) that encode for neurotransmitter synthesis machinery, receptors, ion channels, etc that allow to fulfill its specific functions. Adapted from *PhD manuscript of Carla Lloret.*

One successful strategy to identify genetic programs controlling differentiation of specific neuron types was to select and study the regulatory regions of a group of effector genes (genes coding for proteins required for cell type specific functions such as neurotransmitter biosynthesis enzymes, ion channels, receptors, etc.) that need to be co-regulated in a given neuronal type (Figure I.7). The expression of these genes characterizes the terminal features of a mature neuron. The regulatory regions controlling the expression of the effector genes contain the molecular signature that uniquely characterizes the core identity of a neuron type (Hobert 2011). By means of this methodology, it was revealed that, within a neuron type, each gene battery of effector genes is co-regulated by specific combinations of TFs. Thus, given the role of these TFs, they receive the name of *terminal selectors* (Hobert 2008).

The term terminal selector is the extension of the selector gene concept originally proposed by García-Bellido in 1975 (García-Bellido 1975) to designate genes that affect the identity of organs. Terminal selectors involve TFs that act directly on effector genes to initiate and maintain the terminally differentiated state of a neuron (Deneris and Hobert 2014; Doitsidou et al. 2013; Flames and Hobert 2009) (Fig. I.8a). It is important to highlight that terminal selectors, act in the last steps of differentiation, to directly activate effector genes, other TFs are required earlier in development to commit progenitors towards specific neuronal fates, but, as these TFs do not act directly on effector genes they are not considered terminal selectors.

TFs are broadly expressed in a wide variety of cells and have pleiotropic functions. To achieve their context-specific functions TFs act in a combinatorial manner. The same TF can be part of two different terminal selector combinations to select completely different neuronal types. For example, in dopaminergic neurons, *ast-1* TF acts in a collective together with *ceh*-20, and *ceh-43* (Doitsidou et al. 2013; Flames and Hobert 2009) while in AVG neuron works with *lin-11* to select a different set of genes (Pereira et al. 2015). Combinations of TFs explain how an individual TF can be required for control specific features but are not sufficient to induce genetic a program (summarized in Figure I.5). Moreover, it is also in agreement with the multiplicity and modularity of enhancers controlling expression of a single gene: different combinations of terminal selectors recognize distinct enhancers to drive cell type specific expression (Figure I.8b).

Interestingly, terminal selector codes seem to regulate cell type specific effector genes but not ubiquitous or panneuronal genes. For example, the removal of terminal selectors of some neurons does not affect pan-neuronal genes (Stefanakis, Carrera, and Hobert 2015). This argues that terminal selectors act in a parallel routine together with other regulatory programs that control other neuronal features, like pan-neuronal function or structure formation, such as cilia (Figure I.8a).

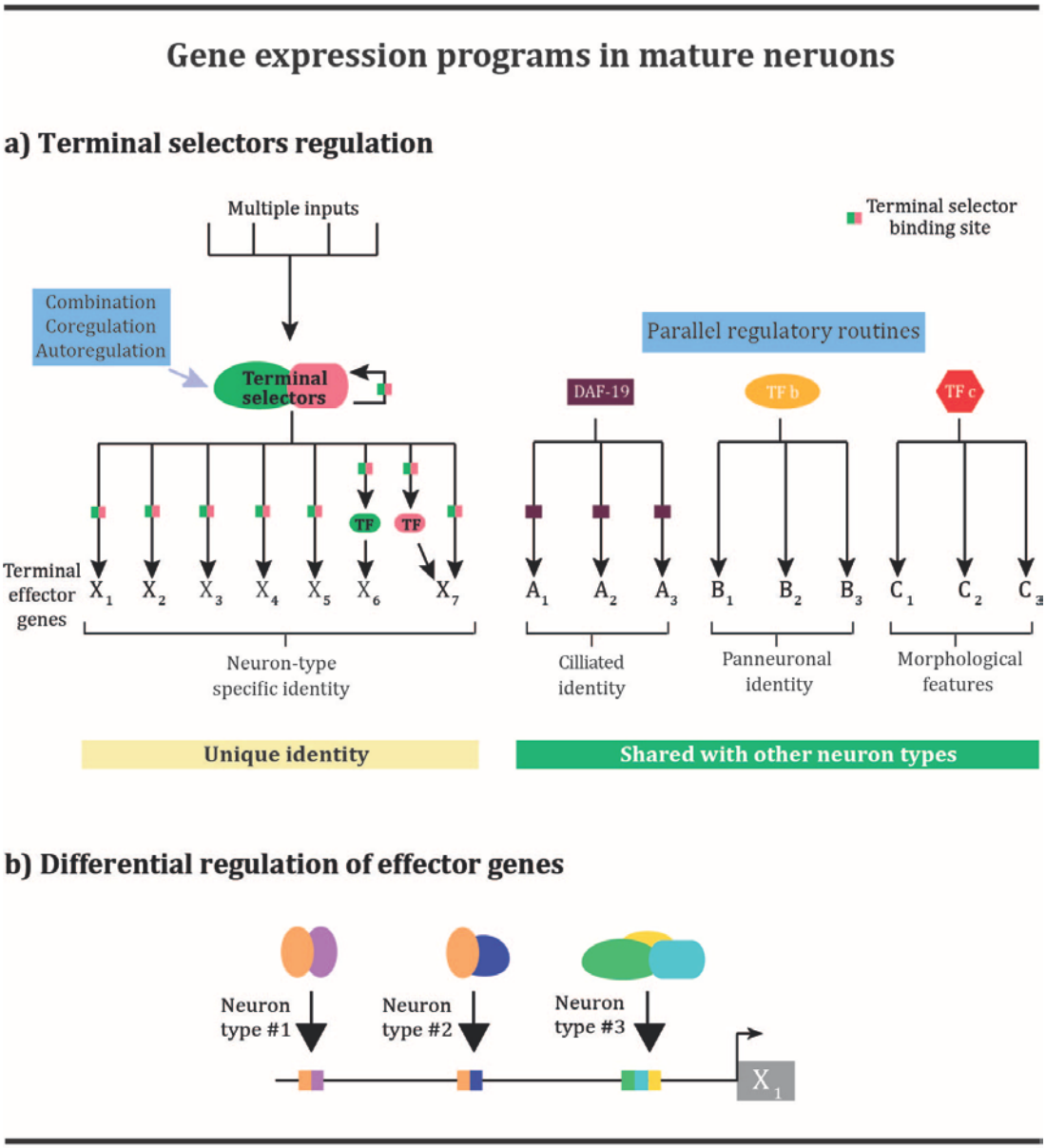

Figure I.8. Terminal selector mode of action. a) Parallel routines integrate the gene regulation of neuronal features. The colored rectangles illustrate the binding of terminal selectors to *cis*-regulatory regions of effector genes. b) Terminal selector codes are organized by modules that receive the specific signature of the combination of TFs. This example presents a common effector gene, X_1, differentially regulated by distinct combinations of terminal selectors in three neuron types. Adapted from *Hobert 2016*.

Importantly, the concept of terminal selectors is not exclusive of neuronal cell types. For instance the TF *pha-4* is the terminal selector of *C. elegans* pharynx (Horner et al. 1998) or *elt-1*, a GATA factor, is required for epidermal fate (Page et al. 1997). However, it is indubitable that large efforts have been done to describe terminal selectors of distinct neuron categories, especially in *C. elegans* (Annex A.1 shows a list of neuronal terminal selectors in the worm). Moreover, terminal selector codes in neurons highlight the breadth of features regulated by these TFs (Hobert 2011), providing insights about the function and execution of gene regulatory programs in this cell type.

Part II. The study of neuron subtype specification using *C. elegans*

In the second part of this Introduction we will review some characteristics of the model *Caenorhabditis elegans* relevant to this Thesis. This nematode was established as an animal model by Sydney Brenner in the 70s and has been deeply studied since then. Thanks to its amenability to carry out genetic screens, transgenesis, RNAi, imaging, behavioral assays, etc; it has become an incredibly useful tool for neuronal development studies.

1. *C. elegans* as a model system

The extraordinary potential of this worm relies on its small size (~1mm long) but still rather complex system and the easiness of maintenance and manipulation. The wild type strain, Bristol N2, was isolated from a mushroom compost in 1959. In the laboratory, worms are kept in petri dishes where animals are fed on an *E. coli* bacterial lawn. Moreover, *C. elegans* can be frozen allowing building big collections of different strains without the need of continuous maintenance.

Other biological features that support the establishment of *C. elegans* as a model is its short life cycle of only 3,5 days. *C. elegans* self-fertilizes and lays eggs, after hatching the worms undergo four larval stages until they reach the adulthood (Figure I.9a, b). This is a great advantage compared to other models such as mouse, where the embryonic development lasts around three weeks and animals reach adulthood at two months. A single *C. elegans* hermaphrodite can produce a progeny of about 300 clonally identical descendants. This, together with the short life cycle provides large populations of animals in a few days. *C. elegans* also has a male form that allows gene transfer by cross-fertilization. The appearance of males is a low frequency event (estimated 0.2%) caused by rare meiotic non-disjunction of the X chromosome, that generates X0 animals that develop as males. *C. elegans* genome is quite compact, with 100 Mb in size compared to the more than 3000 Mb in humans. Importantly, 83% of the proteome of *C. elegans* has an orthologue in humans and, vice versa, around 70% of human genes contain a homologue in the worm genome (Lai et al. 2000).

The first experiments with *C. elegans* were aimed to assess gene function through mutant analysis (forward genetic screen) (Brenner 1974). This phenotypic analysis through mutant strains provided the first link between genes and biological functions. Another two milestones in *C. elegans* research was the description of its complete cell lineage (Sulston and Horvitz 1977; Sulston et al. 1983) and the reconstruction of the nervous system and its connectivity by electron microscopy (Figure I.9c) (White et al. 1986). Due to the transparency of *C. elegans* the expression of green fluorescent protein

C. elegans main features

a) Development and larval stages

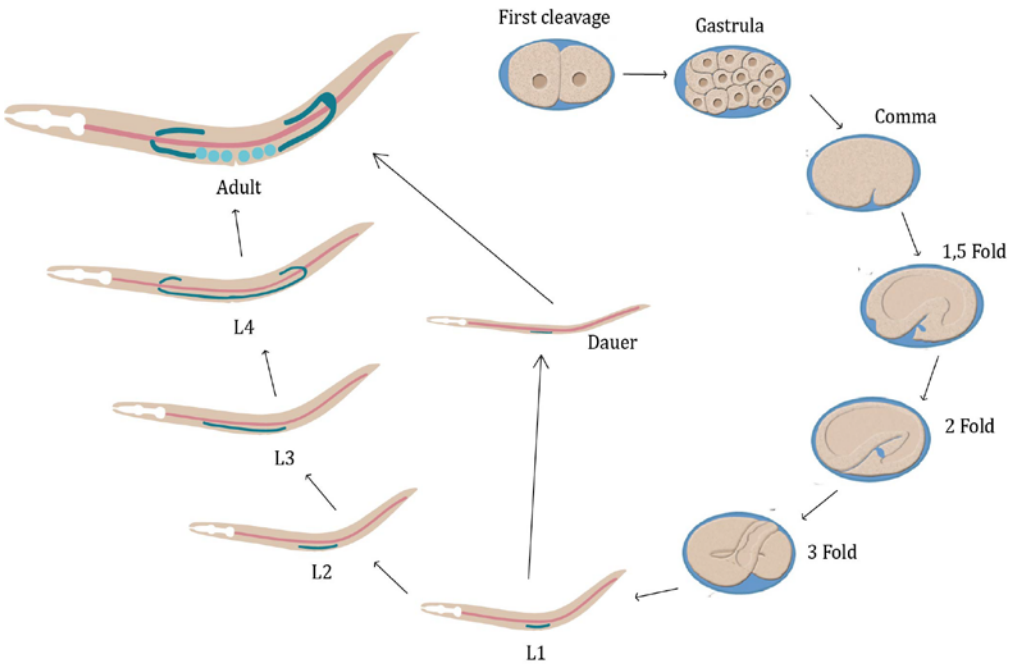

b) Anatomy in adults

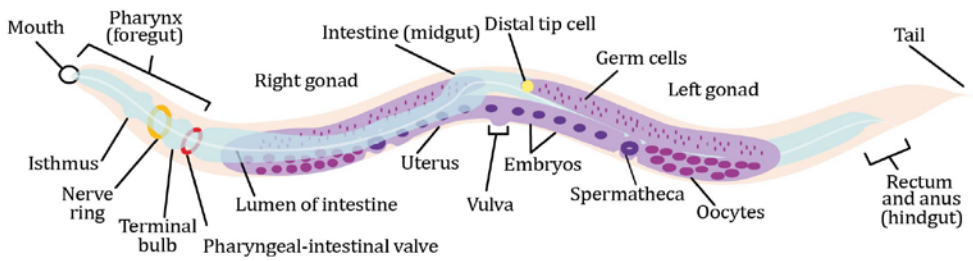

c) Nervous system

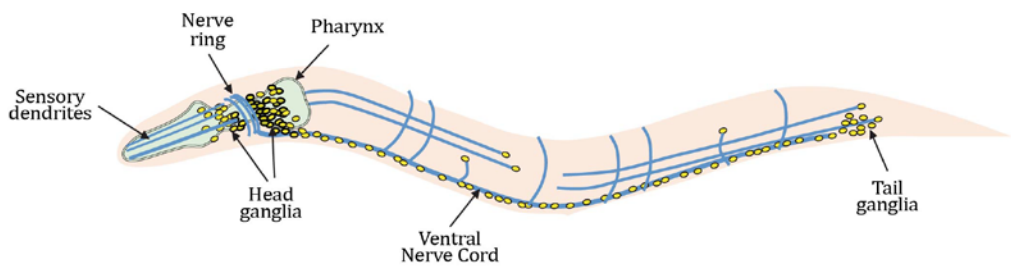

Figure I.9 *C. elegans* main features. a) The life cycle of *C. elegans* last 3.5 days from embryo to reach the adulthood. In extreme conditions or absence of food, L1 animals enter into a resistance form, *dauer*, which will continue until adult stage with benign conditions. b) The features of the anatomy of *C. elegans* are observed through a microscope due to its transparency. Adult hermaphrodites present two gonads where oocytes mature before fecundation from spermatozoids and move towards uterus until embryos will be laid through the vulva. c) The nervous system of *C. elegans* consist of 302 neurons in hermaphrodites (yellow), which are mainly located in head and tail ganglia and along the ventral nerve cord. The axon projections are represented with blue lines. Adapted from *WormAtlas* and *Fang-Yeng et al 2015*.

in the worm allows detailed analysis of expression patterns in living animals (Chalfie and Sulston 1981). Nowadays, classical forward genetic screens take advantage of fluorescent reporter strains for the isolation of specific mutants; this, combined with the use of next generation sequencing techniques to identify the mutations has facilitated the use of *C. elegans* for this kind of experiments (Jorgensen and Mango 2002). Reverse genetics are also commonly used in *C. elegans*, one common way of doing reverse genetic screens is by interference RNAi, as the strategy followed in this Thesis. We explain RNAi in a separate section below.

2. The nervous system of *C. elegans*

Although *C. elegans* nervous system is rather simple compared to other organisms, it still maintains a high cellular and molecular diversity that allows to perform elaborate behaviors. The adult hermaphrodite contains 302 neurons and 56 glial cells, while males contain 385 neurons plus 88 glial cells, which is around a third part of total cells in the worm body. Neurons are classified into 118 morphologically different categories, according to their topology and synaptic connection patterns (White et al. 1986), this classification also correlates to its molecular diversity (Hobert 2016b).

The anatomic organization of *C. elegans* nervous system presents clustered structures of neuronal cell bodies in ganglia, which are the usual structures of invertebrate nervous systems (Figure I.9c) (White et al. 1986; Hall and Russell 1991). The majority of the neurons are distributed in the head and tail ganglia, and their processes go along bundles like the ventral nerve cord. As happens in higher organisms, *C. elengans* has commissures, as the nerve ring in the head. Commissures are processes passing structures where neurites can make contacts with the contralateral part of the body. Two of the main commissures in the head, the amphid and the deirid, serve to classify anatomically distinct neuronal categories (Hall, Lints, and Altun 2005).

C. elegans nervous system presents common features with more complex nervous systems. For instance, some neurons in the worm play similar functional roles as in higher organisms, such as the motorneurons that stimulates muscles; sensory neurons that perceive changes in environment through their sensory endings; interneurons that connect different cells to build neuronal networks and polimodal neurons that perform various roles (Chen, Hall, and Chklovskii 2006; Fang-Yen, Alkema, and Samuel 2015). On the other hand, the main neurotransmitters are present in *C. elegans* nervous system, as is the case of acetylcholine, glutamate, GABA and monoaminergic neurotransmitters (Gendrel, Atlas, and Hobert 2016; Pereira et al. 2015; Serrano-Saiz et al. 2013; Flames and Hobert 2011). The simple structures of neuronal organization and the reiterative positioning among individuals allowed for the description of the whole connectome of the worm nervous system both in hermaphrodites and males. This information is a great tool to improve our understanding of signaling integration and elaboration of complex behavioral responses (White et al. 1986; Haspel and O'Donovan 2012; Jarrell et al. 2012).

The generation of the nervous system in *C. elegans* takes place in three developmental stages. First, in embryogenesis 222 neurons are generated, then a second wave of neurogenesis takes place at late fist larval stage (L1), where many ventral nerve cord (VNC) motor neurons (homologous to motorneurons of the spinal cord in vertebrates) are generated. Finally, a few neurons are born in late L2, as is the case of PDE dopaminergic cells (Sulston et al. 1983; Sulston and Horvitz 1977). In *C. elegans* development, programmed cell death is also important and affects 113 cells. Apoptosis is required for sexual dimorphic features such as removal of the male cephalic neurons (CEM) in hermaphrodites and the specific hermaphrodite neuron (HSN) in males; and it is also necessary for the refining of VNC structure among others (Sulston and Horvitz 1981).

The analysis of *C. elegans* lineage revealed that, in contrast to the vertebrate system, neurons and glial cells derive form very distinct lineages (Sulston et al. 1983). It has been shown that there is no correlation between lineage history with specific terminal features of the neurons and the other way around is also certain; neurons with the same neurotransmitter usually do not exhibit any lineage relationship (Sulston et al. 1983; Sulston and Horvitz 1977). Actually most *C. elegans* neurons are left/right bilaterally symmetric, although they come from distinct branches in the lineage, but those branches are also bilaterally symmetric, and they end up acquiring the same cell fate. Albeit there are some rare exceptions, for example, the RIH serotonergic neuron, AQR and PQR glutamatergic neurons do not have left/right counterparts. On the other hand, some pairs of left/right morphologically symmetric neurons are molecularly and functionally different, as is the case of ASE or AWC neurons (Taylor et al. 2010; Chang, Johnston, and Hobert 2003).

3. Reverse genetic screens in *C. elegans*: Interference RNA

Interference RNA was first described in the worm (Fire et al. 1998) and soon became a suitable tool to perform reverse genetic experiments in many systems.

RNAi processing mechanism was first described though the elicited response of dsRNA injection into gonads (Montgomery, Xu, and Fire 1998). The double stranded RNA molecules enter inside the cell through SID-1 transporter. This exogenous dsRNA is process by Dicer complex, which consists of a RNAse III-like nuclease, DCR-1, that acts together with the helicase DRH-1 and dsRNA binding protein, RDE-4. As a result, initial dsRNA is fragmented into 20-25 nucleotide molecules that will bind RDE-1 dsRNA binding protein that degrades the passenger strand and leads the siRNA generated to its complementary mRNA to activate either the degradation of the messenger or an additional step of amplification (Figure I.10) (Pak et al. 2012).

This amplification is performed by an RNA-dependent RNA polymerase (RdRP) and takes place form 3' to 5' (Sijen et al. 2001). This additional amplification in RNA processing pathway has also been observed in other invertebrates like *Drosophila*, and also in fungi and plants (Grishok 2005). *C. elegans* has four putative RdRPs but only three have demonstrated activity amplifying RNA: *rrf-1*, *ego-1* and *rrf-3*. In response to exogenous dsRNA, *rrf-1* and *ego-1* generate newly dsRNA molecules using mRNA as a template and complementary siRNA as a primer. Those dsRNA are again cleavage by Dicer complex to generate secondary siRNAs that members of worm argonaute proteins (WAGO) bind. WAGOs guide secondary siRNA towards its target messenger to activate RISC complex, whose core is an argonaute protein and which finally degrades the mRNA. The degradation of the messenger occurs in the cytoplasm, but secondary siRNAs can be recruited inside the nucleus through import by NRDE-3, which elicits silencing of nascent transcripts, as of nuclear RISC complex, or heterochromatin formation (Dalzell et al. 2011) (Figure I.10a).

Importantly, not only exogenous dsRNA can elicit interference machinery, in *C. elegans* but also endo-siRNA or miRNA activate an endogenous pathway. This mechanism undergoes the same steps as the exogenous one, but there some components of the machinery are different. Endogenous dsRNA molecules generated commonly by hairpin structures are recognized by ERI-1 (Kennedy, Wang, and Ruvkun 2004). This exonuclease cleavages target dsRNA into primary siRNA molecules that will serve as primers for the amplification step that, in this pathway, is carried out by RRF-3 RdRP. The new dsRNA generated is processes by Dicer complex which is composed by DRH-1 nuclease and DRH-3 helicase (Duchaine et al. 2006). Finally, the secondary siRNA generated will bind argonaute proteins to activate RISC degradation complex or to be transported inside the nucleus, similarly to exogenous pathway (Figure I.10b).

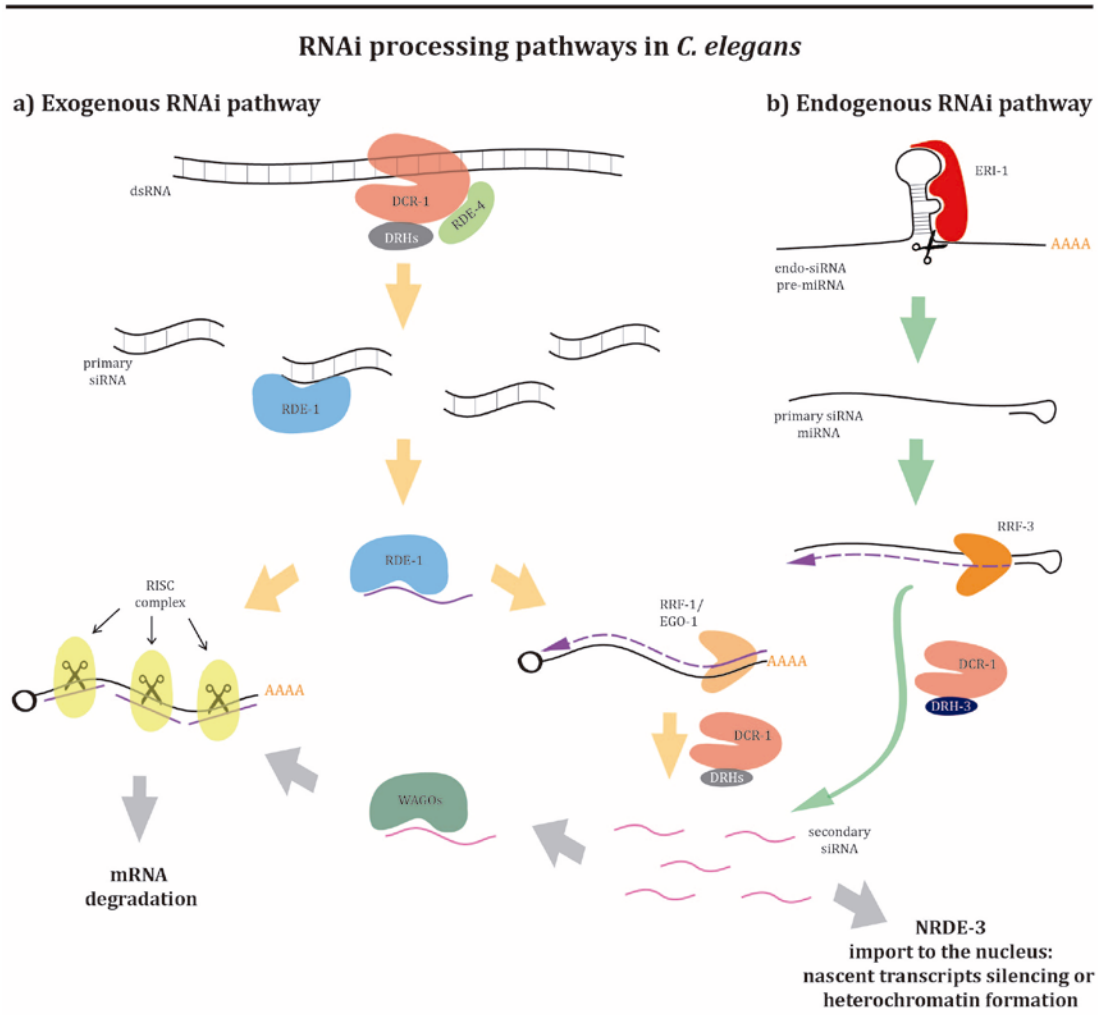

Figure I.10. RNAi processing pathways in *C. elegans*. a) The exogenous pathway (orange arrows) is elicited by dsRNA coming from bacteria, viruses or transposons or can be forced through dsRNA injection inside worm gonads. b) The endogenous pathway (green arrows) is induced through endo-siRNA or pre-miRNA whose double stranded regions are recognized and processed by ERI-1 exonuclease. See main text for further details. Adapted from *Duchaine et al 2006*.

In *C. elegans* germline has been also described that some heterochronic miRNAs, such as *let-7*, are recognized by two *C. elegans* specific argonaute proteins ALG-1/2 due to specific structural features of these miRNAs and promote their cleavage through DCR-1 (Jannot et al. 2008); however, this mechanism is still poorly understood.

Researchers can benefit of exogenous RNAi pathway to achieve silencing of a given transcript. There are four different ways to deliver dsRNA inside animals. The first method and the most effective is direct microinjection of dsRNA in young adult worms (Figure I.11a), phenotypes are observed in the next generation (Fire et al. 1998). Another strategy, also based on microinjection consists on generating transgenic lines that express two inverted repeats of the target gene under the control of a specific promoter (Figure I.11b). The paired sequences produce a hairpin structure that starts the RNAi response to induce mRNA degradation of the target gene (Tavernarakis et al. 2000).

Depending on the selected promoter hairpin expression is induced at specific cell types or times in development. However, it is important to mention that due to the existence of dsRNA transporters in the worm, cell specific expression of RNAi does not ensure cell specific effects. Alternatively, a population of L1 worms can be plunged in a concentrated solution of dsRNA where they remain at least 24 hours so that their cells can acquire the dsRNA by soaking (Figure I.11c); after that period, worms are recovered in normal culture plates to observe possible phenotypes in them and in their progeny (Tabara, Grishok, and Mello 1998; Kuroyanagi et al. 2000). Finally, the most widespread method is based on feeding worms with bacteria that produce dsRNA to achieve the down regulation of the target gene (Figure I.11d) (Timmons, Court, and Fire 2001).

This method employs a genetically engineered *E. coli* strain, HT115 (DE3), which expresses T7 phage RNA-polymerase and is defective for RNase III. To achieve the down regulation of target genes, a small fragment of them (~1kb) is cloned inside the L4440 backbone plasmid, where the multicloning site is flanked by two T7 promoters, and transformed inside the bacteria. The T7 polymerase is induced with IPTG and some hours after induction the synthesis of RNA from both T7 promoters starts. When worms are fed on HT115 bacteria the dsRNA is released in the intestine and systemically transported to the whole organism by the RNA-interference deficient 1 transporter (*sid-1*) (Winston, Molodowitch, and Hunter 2002).

RNAi by feeding is the most commonly used strategy. Unlike microinjection, feeding allows working with large animal population and it is not as expensive as soaking can be, where the synthetic RNA production drives up the costs (Sugimoto 2004). Moreover, the generation of whole genome RNAi libraries by the Ahringer and Vidal laboratories (Kamath and Ahringer 2003; Rual et al. 2004) have allowed to perform whole genome screenings to address many different questions in biology (Webster et al. 2017; Sinha and Rae 2016; Ueno et al. 2012; Poole et al. 2011).

RNAi feeding experiments enables to obtain different types of information depending on the time the is population analyzed (Figure I.11e). Normally, an initial L1 synchronized worm population (P0) is transferred to seeded plates with induced

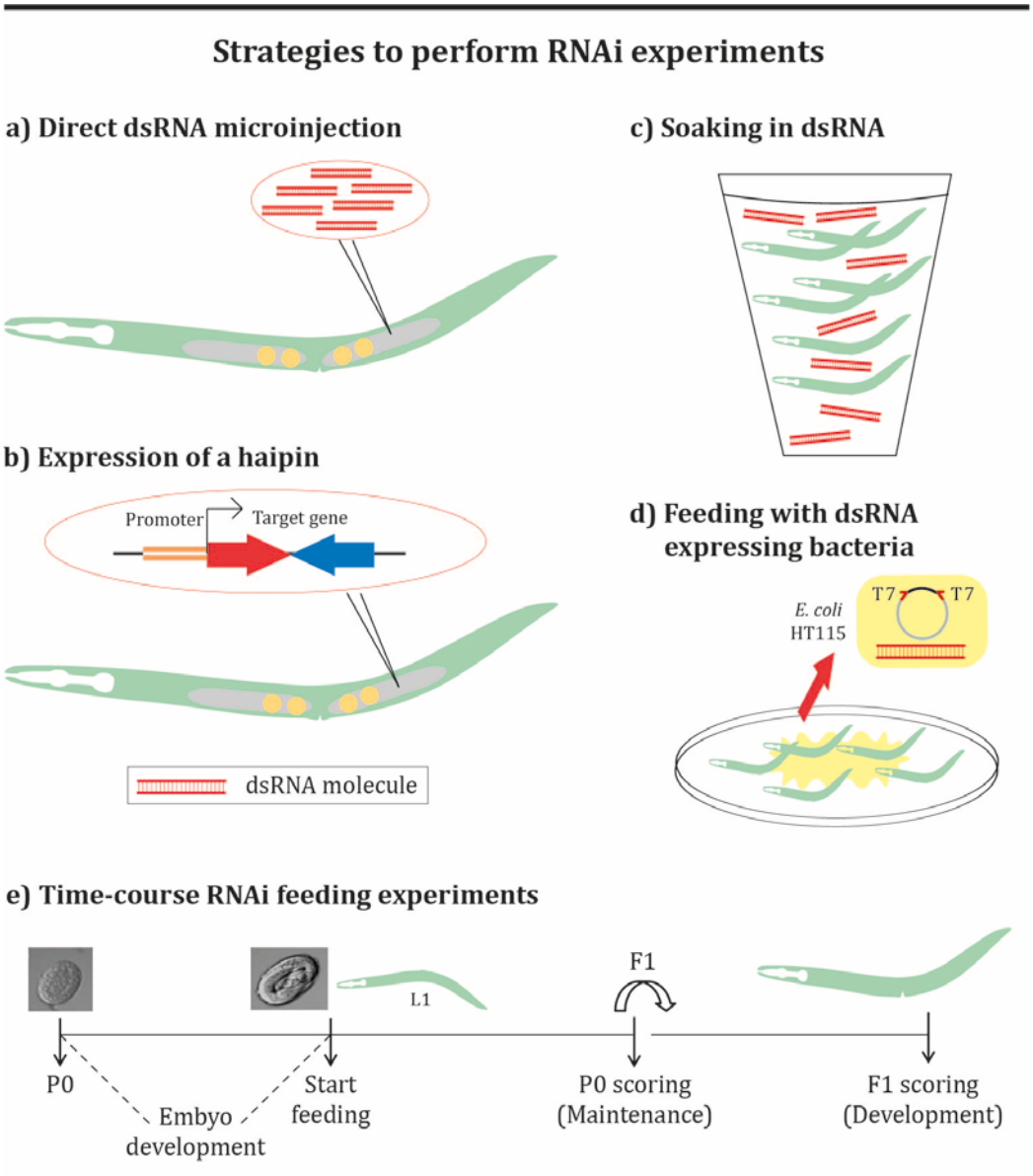

Figure I.11. Strategies to perform RNAi experiments. To initiate the RNAi response, the dsRNA can be delivered inside the worm organism by different methods: direct microinjection inside the gonads (a); through expression of a hairpin that induce RNAi mechanism (b); by soaking in a solution of high concentration of dsRNA (c) or by feeding them with bacteria that produce dsRNA (d). (e) Time course of the feeding method: worms (P0) starts feeding on bacteria after hatching. When they reach young adult state they can be used to analyze the role of the down regulated gene in maintenance of a phenotype, but also animals can be left to generate progeny (F1), where the RNAi effects take place from early developmental stages.

bacterial clones. When these L1 animals start feeding on dsRNA, their body development is complete; in the case of neuronal system, the majority of their neurons have been generated, are mature and functional. If we examine these same worms three days after treatment we will evaluate the role in the maintenance of expression of the studied reporter. On the other hand, if animals remain feeding on RNAi bacteria and produce progeny (F1), those animals will be affected by RNAi since their embryonic development; thus, this generation will report information about the role of that gene in development.

Although RNAi experiments are fast and easy, there are some aspects of the technique that require being cautious. For instance, some gene sequences are extremely similar, as happens in the case of *med-1/med-2* or *end-1/end-3* (Maduro et al. 2001; Maduro et al. 2005), so that the designed dsRNA will target both genes simultaneously. For this reason, to avoid false positives (or OFF target effects), RNAi effects must be validated with mutant alleles in order to confirm that the phenotypes observed can be assigned to a particular gene.

On the other hand, the efficiency of gene silencing fluctuates among different tissues but also is different among clones or even in different experiments. These caveats produce false negatives. The incubation time of the bacteria in IPTG, the use of freshly seeded plates and constant temperature are some of the elements to take into account to reduce variability (Simmer et al. 2003; Sugimoto 2004). Tissue sensitivity is specially problematic regarding neuronal cells, which are very resistant to RNAi effects (Timmons, Court, and Fire 2001). To deal with this issue, some mutations, isolated by genetic screens, have been shown to enhance interference effects in neurons; this sensitized mutants are called *Eri* mutants (Table I.2) (Zhuang and Hunter 2011). One of the first mutant described was the exonuclease *eri-1* whose activity degrades endogenous interference RNA molecules (Kennedy, Wang, and Ruvkun 2004) and competes against the exogenous RNAi pathway (Duchaine et al. 2006). Subsequently, pull-down experiments with Dicer, the ribonuclease that degrades dsRNA, showed a cohort of proteins (*eri-1*, *eri-3 eri-5*, *rrf-3*) that interact with it and whose mutations modify RNAi sensitivity (Duchaine et al. 2006).

Table I.2 Enhanced RNAi Mutations

Gene name	Protein function	Reference
eri-1 (mg366)	Exonuclease. Processing molecules of endo-RNAi through its interaction with Dicer.	(Kennedy, Wang, and Ruvkun 2004)
rrf-3 (pk1426)	RNA-dependent RNA polymerase of endo-RNAi pathway	(Simmer et al. 2002)
eri-3 (tm1361)	Component of Dicer endo-RNAi complex	(Duchaine et al. 2006)
eri-5 (tm1705)	Tandem tudor protein. Contributes to Dicer functions in endo-RNAi	(Duchaine et al. 2006; Thivierge et al. 2012)

eri-6/7 (tm1917)	Helicase. Requiered for short RNAi production in somatic tissues	(Fischer et al. 2008)
ergo-1/eri-8 (gg100)	Endo-RNAi argonaute protein	(Pavelec et al. 2009)
eri-9 (gg106)	Stabilizes endo-RNAi production	(Pavelec et al. 2009)
eri-11 (gg99)	Unknown	(Zhuang and Hunter 2011)
lin-15b (n744)	Homologue of tumor suppressor Rb	(Wang et al. 2005)
nre-1 (hd20)	Unknown	(Schmitz, Kinge, and Hutter 2007)

As can be observed in Table I.2, eri mutants are related to proteins that participate in endogenous RNAi pathway that compete with the exogenous one (Figure I.10). For example, DCR-1 cleaves the dsRNA molecules through a complex formed with helicases (DHRs) and other RNA processing and recognition proteins that vary between endo and exo-RNAi pathways. Particularly, *eri-1, eri-3* and *eri-5* only bind to Dicer to process endogenous RNAi; for this reason, these proteins compete for binding to Dicer against exogenous-RNAi and their mutants enhance RNAi response.

One particular feature of RNAi pathways is that *C. elegans rrf-3* RdRP seems to compete against *rrf-1*, *ego-1* for recruiting Dicer to process the dsRNA molecules that amplify (Sijen et al. 2001; Grishok 2005; Pak et al. 2012). That antagonism can reduce the efficiency of the interference, for that reason *rrf-3* mutants enhance exogenous RNAi effects (Simmer et al. 2002; Thivierge et al. 2012).

Apart from RNA interference pathway proteins, other mutations have been described, despite being unrelated to RNA processing, to also enhance the silencing effect. Some examples are *lin-15b*, a zinc-finger THAP transcription factor (Wang et al. 2005) or *nre-1*, a gene involved in axon pathfinding (Schmitz, Kinge, and Hutter 2007). Usually, *lin-15b* mutation is present in sensitized backgrounds in combination with *nre-1* or *eri-1* mutant alleles, which have proved to show increased RNAi enhancement (Lehner et al. 2006).

Part III. Monoaminergic system

1. Monoaminergic neurotransmitter synthesis

Biogenic amines or monoamines are neurotransmitters synthesized from aromatic amino acids that contain one nitrogen atom, such as tyrosine, tryptophan or histidine. This group of neurotransmitters comprises dopamine (DA), serotonin (5-HT), adrenaline (A), noradrenaline (NA), tyramine (TA), octopamine (OA) and histamine (Figure I.12). Tyramine and octopamine are only present in invertebrates and had been postulated to be the counterparts of vertebrates adrenaline and noradrenaline (Roeder 2005). They are involved in a plethora of behaviors form movement coordination, appetite and addictions to learning and emotions. In humans, deficits in the level of these neurotransmitters are related to diseases like Parkinson (Willis 1987), schizophrenia (Carlsson et al. 2001) and many other neuropsychiatric syndromes as obsessive compulsive disorder, bipolar disorder, anxiety and depression (Wang and Pereira 2016; Otte et al. 2016).

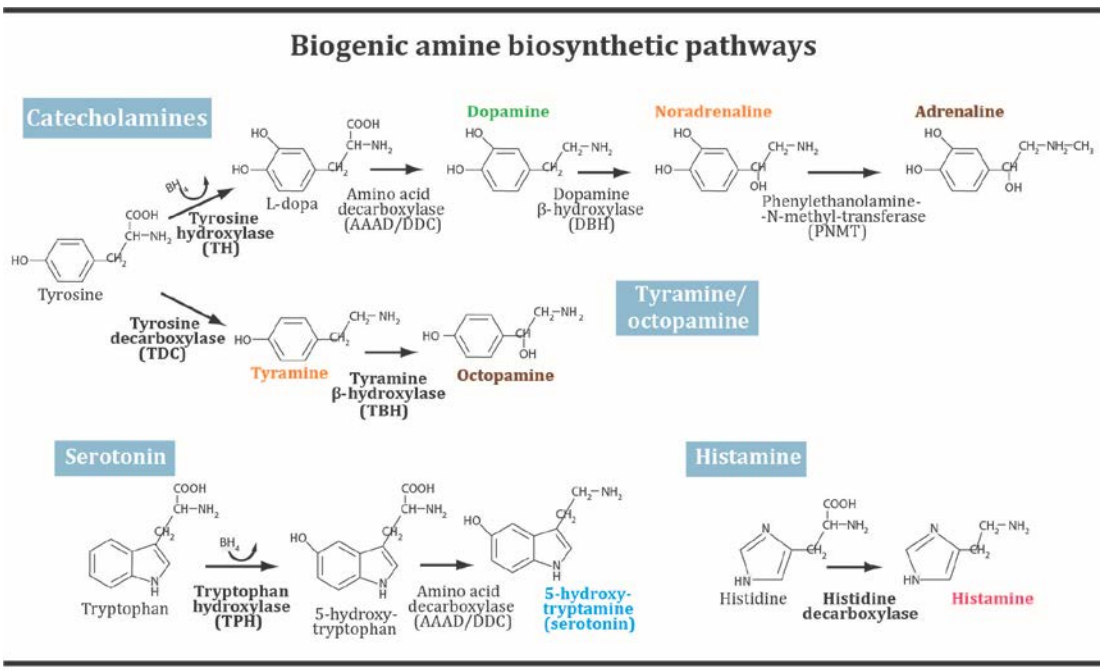

Figure I.12 Biogenic amine biosynthetic pathways. The image shows the distinct routes for MA production. Tyrosine is the aminoacid required both for catecholamines and tyramine/octopamine synthesis. The rate limiting enzymes of each pathway are in bold and the different MA neurotransmitters are labeled in colors. Adapted from *Flames and Hobert 2011*.

Monoamine neurotransmitters are well conserved throughout evolution. This can be observed with the sequence analysis of serotonin (SERT), dopamine (DAT) and general monoamine transporters (MAT). In the different species from nematodes, arthropods and vertebrates, the presence of these transporters evidence their common origin from the same ancestor (Caveney et al. 2006).

To synthesize these neurotransmitters, it is required the expression of a battery of genes that encode for enzymes and transporters that control the production, package, transport, release and reuptake of the neurotransmitter into the synaptic cleft. These gene battery in monoaminergic neurons receives the name of *monoaminergic pathway genes* as an overall appellative (Figure I.13).

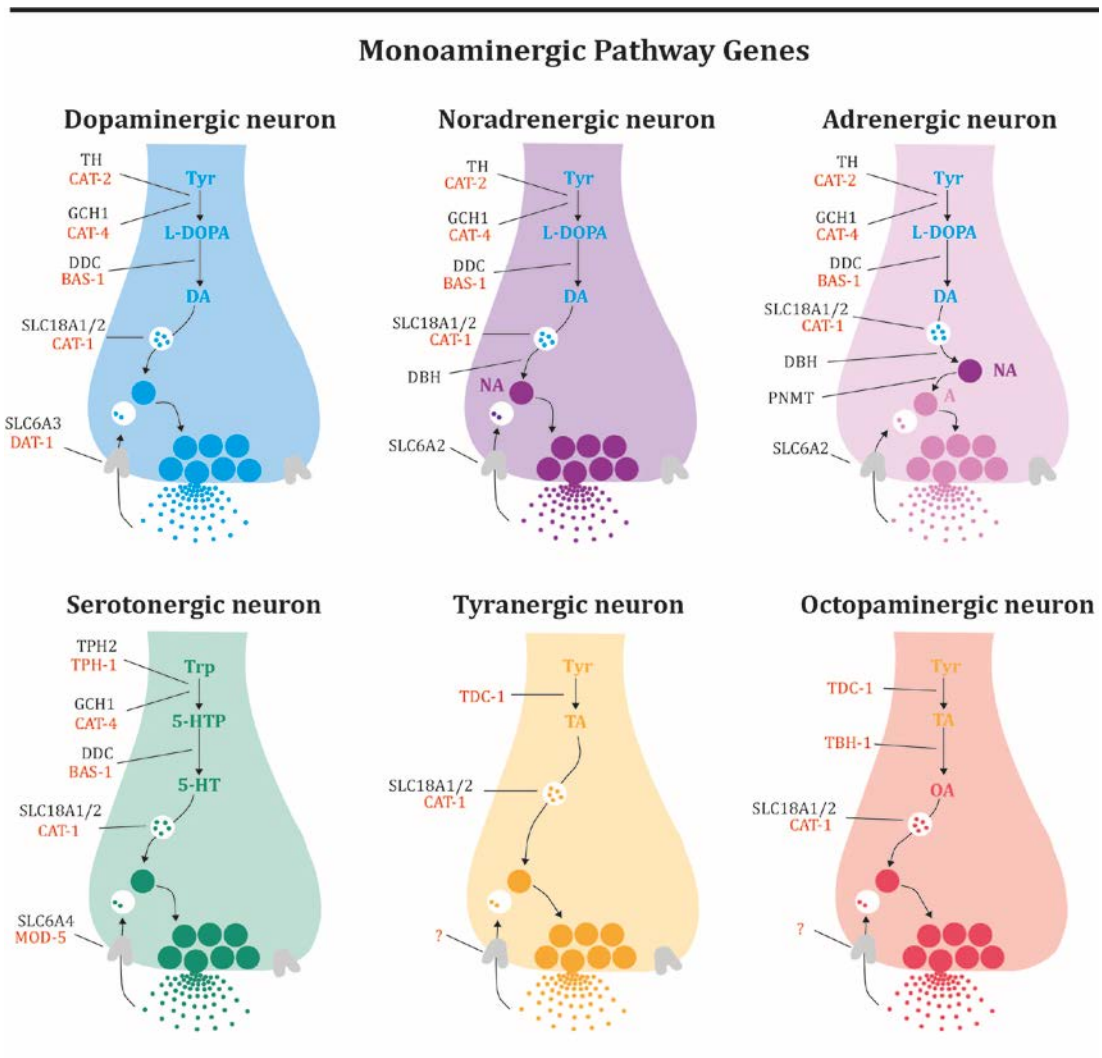

Figure I.14. Dopaminergic systems across phylogeny. a) Mouse DA system: A8-A10 nuclei located in the mibrain correspond to retrorubral field, substantia nigra and ventral tegmental area, respectively. Diencephalic nuclei comprise A11-A15. Moreover, A15 and A16 (located in olfactory bulb, OB) are part of olfactory system. Finally, A17 alludes amacrine neurons from retina. b, c) Zebrafish DA system from different views. DA neurons are distributed among retina, telencephalon and diencephalon. d) *Drosophila* DA system is distributed in brain and along ventral ganglion. e) *C. elegans* DA system, in hermaphrodites comprises four pair of bilateral neurons (for male system see Fig. I18). P/SP, pallial/subpallial system; PO, preoptic area; PR, pretectum; PT, posterior tuberculum; PVO, paraventricular area. Adapted from *Flames and Hobert, 2011.*

Moreover, monoaminergic systems in different animal groups control similar behaviors; for instance, feeding behavior is ruled by serotonin and the stress response in regulated by octopamine or its counterpart adrenaline from arthropods to mammals (Kamhi et al. 2017; Roeder 2005). In the following sections we will review the monoaminergic systems across different animal groups and how MA neurons are specified.

2. Monoaminergic systems specification across phylogeny

2.1. Dopaminergic systems

Dopaminergic neurons (DA), in mammals, such as mouse, are present in telencephalic, diencephalic and mesencephalic structures. Mesencephalic dopaminergic neurons of the substantia nigra (SN) coordinate locomotion and this population is lost in Parkinson's disease. Additionally, dopaminergic neurons of the ventral tegmental area control reward, addiction and cognition (Kandel, Schwartz, and Jessell 1991) (Figure I.14a). In zebrafish DA neurons are located in the telencephalon and diencephalon but are absent from mesencephalon (Matsui and Sugie 2017) suggesting mesencephalic neurons are a recent acquisition only present in tetrapods (Figure I.14b, c).

In *Drosophila*, dopaminergic populations are found in the brain and ventral ganglia and is composed by around 80 neurons that arise from different progenitors and lineages (Figure I.14d). They control arousal, sex behavior, learning and memory (Vömel and Wegener 2008). Finally, *C. elegans* contains four pairs of dopaminergic neurons; three of them CEPV, CEPD and ADE are located in the head ganglia and the last one, PDE, in the mid body (Figure I.14e). As in *Drosophila*, DA neurons of the worm come from different progenitors, but they acquire almost the same terminal features. All of them are mechanosensory ciliated neurons that control locomotion, learning or male mating (Bozorgmehr et al. 2013; Voglis and Tavernarakis 2008; Sawin, Ranganathan, and Horvitz 2000). One well characterized behavioral program of *C. elegans* that is controlled

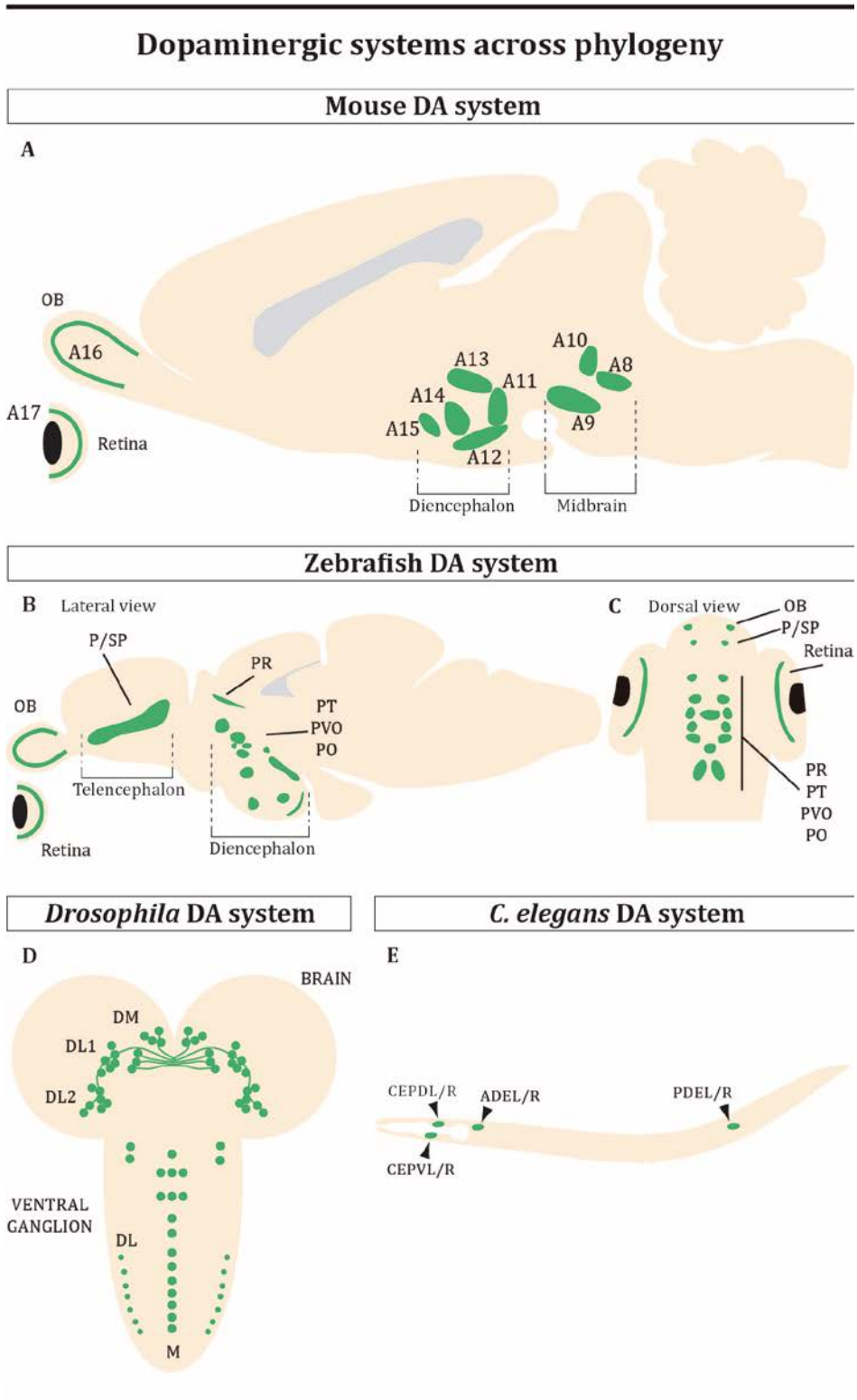
Dopaminergic systems across phylogeny
Mouse DA system
A
OB
A16
A17
Retina
A13
A11
A14
A15
A12
A10
A8
A9
Diencephalon
Midbrain
Zebrafish DA system
B
Lateral view
P/SP
OB
Telencephalon
Retina
PR
PT
PVO
PO
Diencephalon
C
Dorsal view
OB
P/SP
Retina
PR
PT
PVO
PO
Drosophila DA system
D
BRAIN
DM
DL1
DL2
VENTRAL GANGLION
DL
M
C. elegans DA system
E
CEPDL/R
ADEL/R
CEPVL/R
PDEL/R

Figure I.14. Dopaminergic systems across phylogeny. a) Mouse DA system: A8-A10 nuclei located in the mibrain correspond to retrorubral field, substantia nigra and ventral tegmental area, respectively. Diencephalic nuclei comprise A11-A15. Moreover, A15 and A16 (located in olfactory bulb, OB) are part of olfactory system. Finally, A17 alludes amacrine neurons from retina. b, c) Zebrafish DA system from different views. DA neurons are distributed among retina, telencephalon and diencephalon. All nuclei are present in six-day-old animals (c). P/SP, pallial/subpallial system; PO, preoptic area; PR, pretectum; PT, posterior tuberculum; PVO, paraventricular area. d) *Drosophila* DA system is distributed in brain and along ventral ganglion. e) *C. elegans* DA system, in hermaphrodites comprises four pair of bilateral neurons. Adapted from *Flames and Hobert, 2011.*

by DA neurons is the basal slowing response (BSR), which is the slowdown that worms experience when they encounter a source of food and that is essential for their survival in nature (Sawin, Ranganathan, and Horvitz 2000). Another behavior where DA population also intervenes is the area restricted search (ARS), a foraging program used by worms to locate resources and that is also regulated by glutamate (Hills, Brockie, and Maricq 2004).

2.2. Serotonergic systems

Mouse serotonergic neurons are located in the raphe nuclei of the hindbrain, where they control sleep, mood, and feeding behavior among others (Kandel, Schwartz, and Jessell 1991) (Figure I.15a). Moreover, it has also been reported the presence of neurons in the peripheral nervous system of the mouse, where some enteric neurons also release serotonin (Blaugrund et al. 1996). In zebrafish, serotonergic neurons are also found in raphe nuclei and an additional population is located in the diencephalon (Kaslin and Panula 2001) (Figure I.15b, c). Similar to the dopaminergic population, in *Drosophila* serotonergic neurons are present in brain and ventral ganglia and modulate locomotion, learning, memory, circadian rhythms and feeding (Neckameyer et al. 2007) (Figure I.15d).

C. elegans serotonergic neurons also govern a plethora of behaviors, such as feeding, egg laying and chemosensation (Song and Avery 2012; Gürel et al. 2012; Horvitz et al. 1982). There are five different serotonergic neuron subclasses in *C. elegans*: the neurosecretory NSM, the chemosensory ADF, the motorneurons HSN and the interneurons AIM and RIH (Figure I.15e). All of them, with the exception of NSM, also use acetylcholine as neurotransmitter and glutamate in the case of AIM (Sze et al. 2000; Pereira et al. 2015; Serrano-Saiz et al. 2013).

In contrast to dopaminergic neurons which all are functionally equivalent, the different serotonergic subtypes coordinate distinct behavioral programs. For instance, egg laying is governed by HSN (Horvitz et al. 1982) while, NSM and ADF regulate the

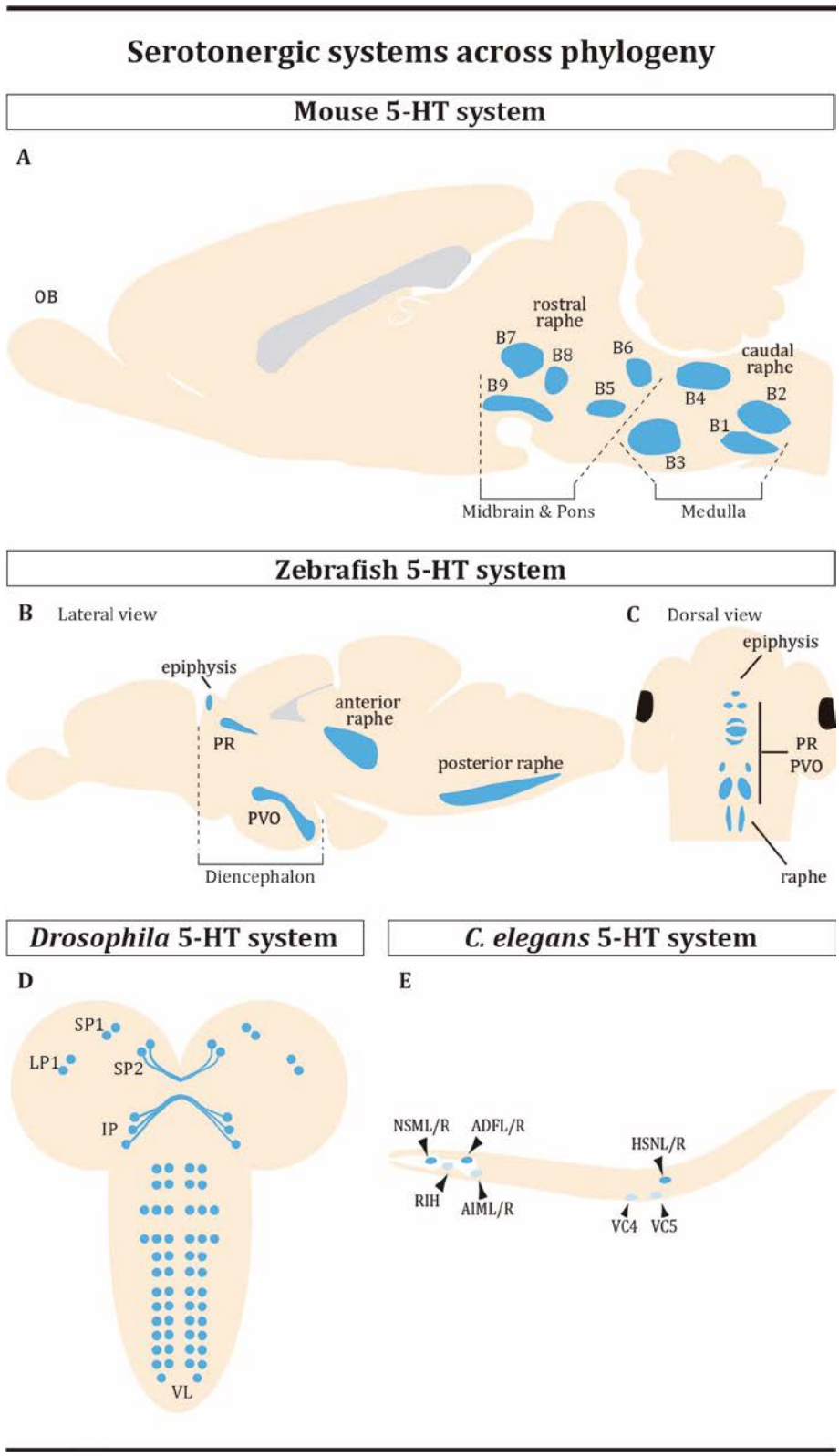
Serotonergic systems across phylogeny
Mouse 5-HT system
A
OB
rostral raphe
B7
B8
B6
caudal raphe
B9
B5
B4
B2
B1
B3
Midbrain & Pons
Medulla
Zebrafish 5-HT system
B Lateral view
C Dorsal view
epiphysis
anterior raphe
PR
posterior raphe
PVO
Diencephalon
epiphysis
PR
PVO
raphe
Drosophila 5-HT system
C. elegans 5-HT system
D
SP1
LP1
SP2
IP
VL
E
NSML/R
ADFL/R
HSNL/R
RIH
AIML/R
VC4
VC5

Figure I.15. Serotonergic systems across phylogeny. a) Mouse 5-HT system is distributed among raphe nuclei, where B1-B4 are settle in caudal part, in medulla, and B5-B9 constitute the rostral area and are located in pons. b, c) Zebrafish 5-HT system form different views. 5-HT neurons are located in raphe nuclei but also in pretectum (PR) and paraventricular area (PVO). All nuclei are present in six-day-old animals (c). d) *Drosophila* 5-HT system is distributed in brain and along ventral ganglion. e) *C. elegans* 5-HT system, in hermaphrodites, comprises three serotonin producer neurons, NSM, ADF and HSN. Besides, AIM, RIH are able to use serotonin as a neurotransmitter although they do not produce it and VC4/5 unreliably stain for 5-HT. Adapted from *Flames and Hobert, 2011.*

enhanced slowing response (ESR), which is the slowdown observed when fasting worms approach to a source of food (Sawin, Ranganathan, and Horvitz 2000; Gürel et al. 2012). Regarding feeding behavior, serotonin increases pharyngeal pumping and it is mainly released by NSM and ADF but with distinct goals: while ADF promotes roaming behavior to localize food resources, NSM favors dwelling (Churgin et al. 2017). Moreover, AIM and RIH also contribute to modulate feeding, in this case through the mediation of other biogenic amines (Fu et al. 2018). Finally, ADF also present some odor-like sensing activities that lead the worm to recognize a previously experienced source of food or reject pathogenic bacteria through the regulation of innate immune response (Song and Avery 2012; Anderson et al. 2013).

2.3. Adrenergic, noradrenergic, tyraminergic and octopaminergic systems

Vertebrates monoaminergic system contains two other catecholamines: adrenaline (A) and noradrenaline (NA). In mouse central nervous system, the noradrenergic neurons are located in the medulla, and they control cardiovascular and endocrine functions. Other group is found in the pons, part of the locus coerulus, which modulates reflexes, pain sensation and responses to sudden stimulation (Kandel, Schwartz, and Jessell 1991) (Figure I.16a). The distribution in zebrafish is similar to mouse (Figure I.16b, c). All vertebrates also contain noradrenergic neurons in the peripheral nervous system, where they innervate the myenteric plexus together with adrenergic neurons (Hartenstein et al. 2017; Wullimann and Rink 2002).

Invertebrates lack the ability to synthesize adrenaline and noradrenaline due to the lack of dopamine beta hydroxylase enzyme. In turn, invertebrates use two other additional monoamines, also synthesized from tyrosine: octopamine and tyramine (Bauknecht and Jékely 2017; Roeder 2005). They are functionally considered the invertebrate equivalent to noradrenaline and adrenaline based on the similar behaviors that those monoamines govern. For instance, in *Drosophila* octopamine mediates in "fight or flight" response likewise adrenergic system in vertebrates (Watanabe et al. 2017). Moreover, octopamine and tyramine are involved in memory and learning (Roeder 2005). Anatomically, in fruit fly octopamine and tyramine neurons are found in

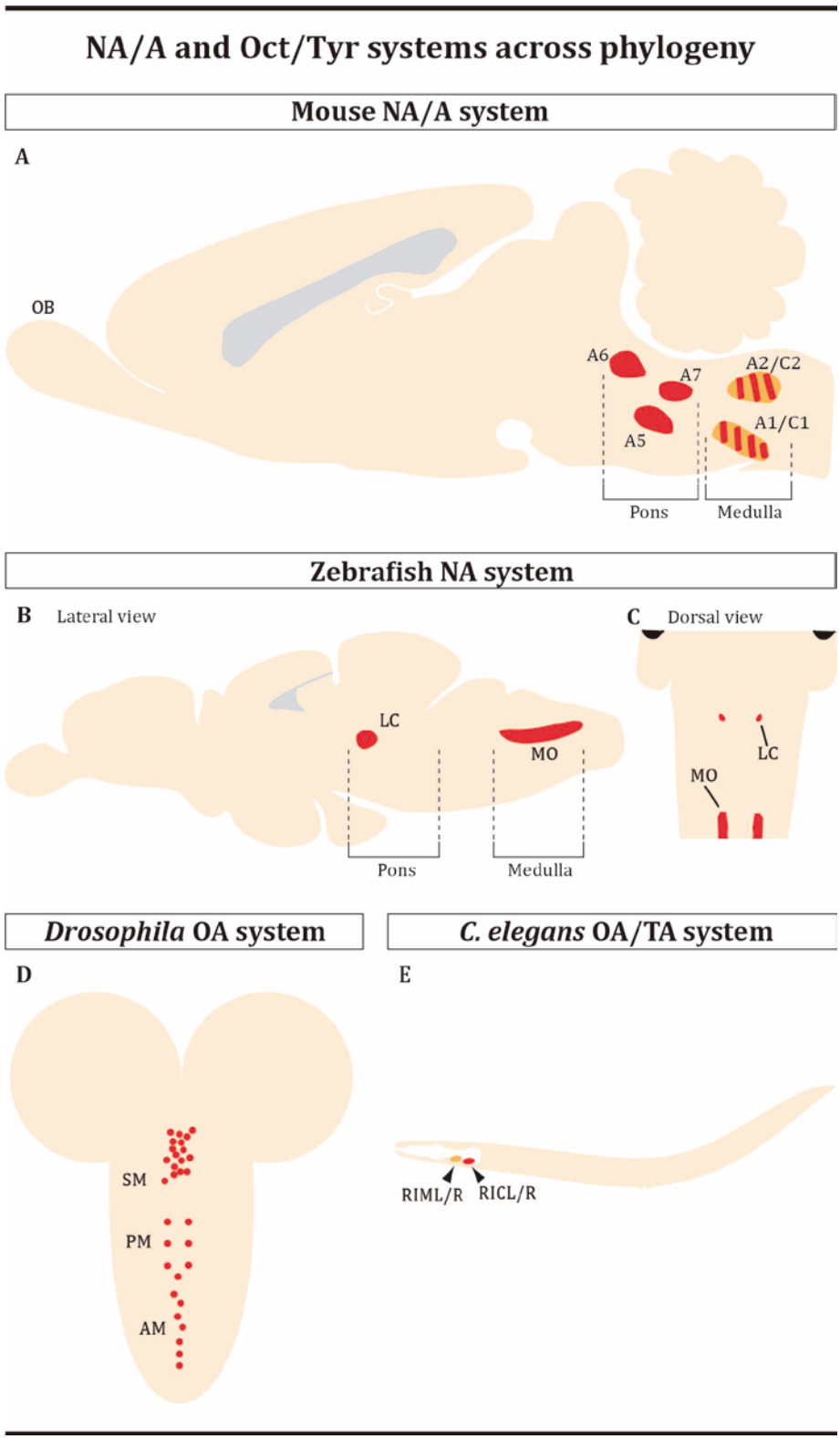
NA/A and Oct/Tyr systems across phylogeny
Mouse NA/A system
A
OB
A6
A7
A2/C2
A1/C1
A5
Pons
Medulla
Zebrafish NA system
B
Lateral view
C
Dorsal view
LC
MO
Pons
Medulla
LC
MO
Drosophila OA system
C. elegans OA/TA system
D
E
SM
PM
AM
RIML/R
RICL/R

Figure I.16. NA/A and Oct/Tyr systems across phylogeny. a) Mouse noradrenergic (red) nuclei are located in pons (A5-7; A6 forms part of locus coerulus) and in medulla A1/C1, A2/C2, which are also adrenergic (orange). b) Zebrafish 5-HT system is also found in locus coerulus and medulla oblongata (MO). All nuclei are present in six-day-old animals (c). d,e) In invertebrates, octopamine and tyramine substitute noradrenaline and adrenaline. d) *Drosophila* OA neurons system is distributed exclusively along ventral ganglion. e) *C. elegans* has one pair of OA and TA neurons, either in hermaphrodites and males. Adapted from *Flames and Hobert 2011.*

the brain and ventral ganglia (Figure I.16d); whereas in *C. elegans* octopaminergic system is composed by only one pair of neurons (RIC) and an additional pair are tyraminergic neurons (RIM) (Alkema et al. 2005) (Figure I.16e). Regarding the behaviors they control, octopamine regulates egg laying and pharyngeal pumping (Horvitz et al. 1982). Additionally, tyramine is also involved in egg laying, tap habituation and scape response (Lau et al. 2012; Pirri et al. 2009; Alkema et al. 2005). A modulatory effect between these neurotransmitters has been described and dopamine and serotonin have opposing roles to octopamine and tyramine in egg laying or feeding behavior (Churgin et al. 2017; Noble, Stieglitz, and Srinivasan 2013; Suo and Ishiura 2013; Suo, Culotti, and Van Tol 2009; Wragg et al. 2007).

An additional monoaminergic neurotransmitter, histamine, is employed by vertebrates and invertebrates. This monoamine is involved in arousal, hormonal secretion and cardiovascular control. In mammals, a small nucleus of histaminergic neurons is located in the posterior hypothalamus and sends its projections to several areas of the brain (Roeder 2003). In *Drosophila* and other arthropods is the only neurotransmitter used by photoreceptors (Sarthy 1991).

3.4. Specific features of C. elegans monoaminergic neurons

A milestone in *C. elegans* research was the description of the whole lineage of *C. elegans* during development. Neurons that synthesize the same neurotransmitter do not necessarily share branches of cell development, even more dramatically, a single terminal division can generate simultaneously a neuron and a not neuronal cell (Sulston et al. 1983). This sparse generation of neuronal types is also observed for monoaminergic neurons (Figure I.17). The closest in lineage are AIM and CEPV, where AIM is the aunt of CEPV. RIC and RIM are also near, they share the same grand-grandmother.

It is important to mention that *C. elegans* male monoaminergic system presents some differences to hermaphrodites. In the male tail, there are three additional pairs of DA neurons, R5A, R7A and R9A, which participate in male ejaculation (Figure I.18a) (LeBoeuf et al. 2014; Sulston, Dew, and Brenner 1975).

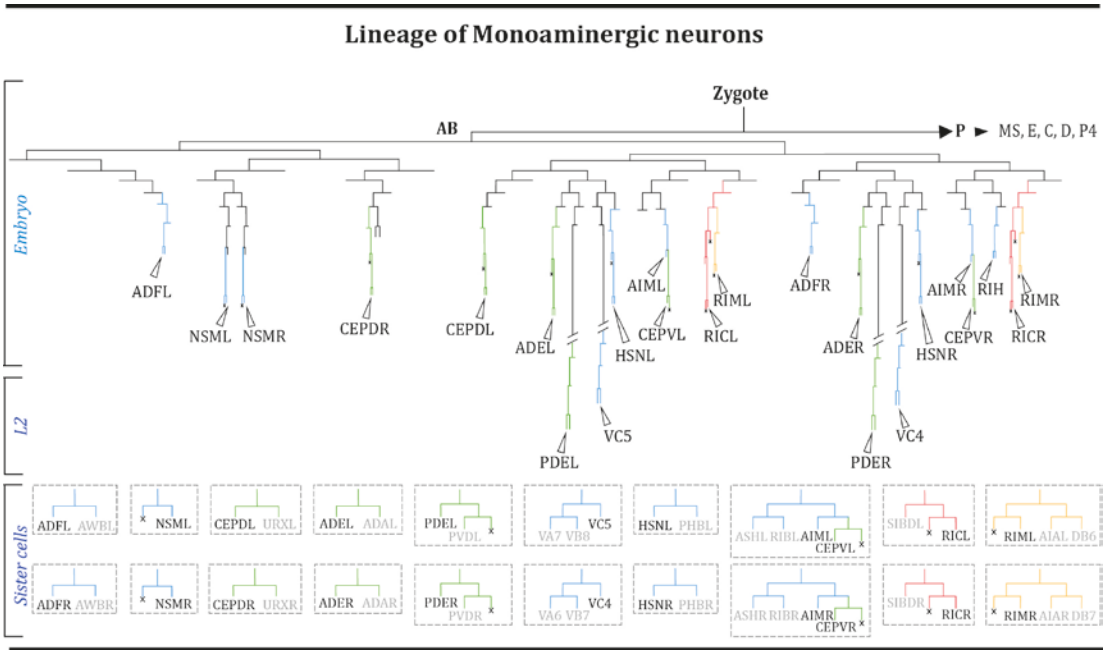

Figure I.17. Lineage of monoaminergic neurons. The scheme represents lineage branches of monoaminergic neurons labeled in different colors (DA, green; 5-HT, blue; RIC, red; RIM, yellow) and how they develop through embryonic stages. All MA neurons come from AB cell and most of them are born in embryonically, except for VC4/5 and PDE, that are born at L2. Although HSN is born at hatching, it does not become fully mature until late L4. At the bottom sister neurons of MA cells are indicated.

Regarding serotonergic neurons, males have six serotonergic unpaired neurons in VNC, CP1-6, one unpaired neuron in the tail, RPAG, and three pairs located in ray sensory structures of male tail, R1B, R3B, R9B (Figure I.18b) (Loer and Kenyon 1993). Additionally, the serotonergic neurons HSN and VC4/5, that in are mainly involved in egg-laying circuit, are absent in males (Horvitz et al. 1982). Interestingly other serotonergic neurons, although shared in both sexes present some dimorphic features. Specifically, ADF response to ascaroside pheromones generates different output depending on the sex of the animal (Fagan et al. 2018). Furthermore, in hermaphrodites AIMs are glutamatergic and serotonergic. In males, they are also glutamatergic and serotonergic until L3 and at L4 they become cholinergic and serotonergic (Pereira et al. 2015; Portman 2017).

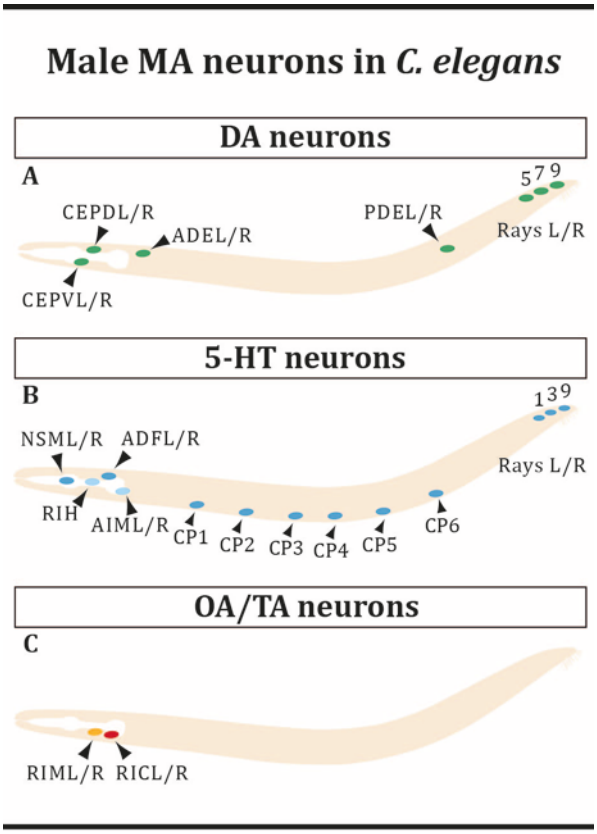

Comparatively, tyraminergic and octopaminergic neurons are equal in hermaphrodites and males and to date, sexual dimorphic features in *C. elegans* RIC or RIM has not been described (Figure I.18c). However, in *Drosophila* some sexual related behaviors depend on differential signaling of these neurons, precisely, octopamine is involved in female protection of the progeny while in males regulate aggressive behavior (Watanabe et al. 2017; Rezával et al. 2014).

Figure I.18. Male MA neurons in *C. elegans*. The pictures illustrate the approximate location of MA neurons along the body of *C. elegans* males. Neurons are labeled in distinct colors: DA in green, 5-HT in blue (RIH and AIM in light blue due to they only use but do not produce serotonin); OA in red and TA in orange.

3. Known regulators of monoaminergic neuron terminal fate

Several TFs are known to be required for the correct generation and/or specification of monoaminergic neurons in different animal models. In this section we provide a brief summary of what is known to date.

3.1. Dopaminergic systems

Mouse mesencephalic dopaminergic specification has been deeply studied due to its clinical relevance. Nurr1, an orphan nuclear hormone receptor, *Pitx3,* an homeodomain TF, and *Lmx1b*, a Lim HD TF, directly control expression of DA pathway genes and other effector genes of DA neurons. Accordingly, they can be considered mammalian terminal selectors for mesencephalic DA neurons. Mutants for *Nurr1*, *Pitx3* and *Lmx1b* present a decreased in the number of *Th* expressing neurons (Jacobs et al. 2009; Smidt, Smits, and Burbach 2003; Hoekstra et al. 2013). Other factors have been also involved in mesencephalic DA specification, such as *Otx2, Pax2, Pax5 or En1/En2*; however, it remains unclear if these factors act terminally on effector genes or if they main role is on the correct specification of DA progenitors (Simon Horst et al. 2006).

Although other DA populations have been less studied, there are some known regulators of OB DA neurons. *Er81* (ETS TF) and *Dlx2* (homeodomain TF) are involved in proper *Th* expression (Flames and Hobert 2009; Brill et al. 2008; Cave et al. 2010). Moreover, DLX2 needs the presence of PAX6 as both interact (Brill et al. 2008). PAX6 in turn also interacts with MEIS2 to drive neurogenesis and specification in OB DA neurons (Agoston et al. 2014). Finally, *Coup-tf1* also regulates *Th* expression in the OB (Bovetti et al. 2013). Interestingly, *Nurr1*, terminal selector for the mesencephalic DA neurons is also expressed in OB and retinal amacrine DA neurons (de Melo et al. 2003), which suggest that *Nurr1* could have a broad role on DA neurons specification. Finally, mutants for the homeodomain TF *orthopiedia (Otp)* show reduced numbers of TH positive cells in the diencephalon (Ryu et al. 2007).

In zebrafish, the regulatory program seems to be conserved as both *Nurr1* and *Otp* are required for diencephalic DA specification (Luo et al. 2008; Ryu et al. 2007). Other TFs are also required such as the transcription elongation factor *Spt5* or the bHLH *Artn2* (Löhr, Ryu, and Driever 2009). Another important DA population in zebrafish is located in the preoptic and optic areas, where the TFs *foxg1a* and *dlx2a* are needed for DA fate (Fontaine et al. 2015).

In *Drosophila,* the analysis of the *cis*-regulatory motifs necessary for dopa-decarboxylase (DDC) expression lead to the identification of two TFs, *Cf1a,* POU homeodomain, and *Islet*, a LIM homeodomain. These two TFs are required for DDC expression and for the correct specification of DA neurons of the ventral region (Johnson and Hirsh 1990; Thor and Thomas 1997).

Finally, *C. elegans* terminal differentiation of dopaminergic neurons has been studied following a bottom-up approach. A combination of three TFs, *ast-1* the ETS ortholog to mammalian *Er81*; *ceh-43*, an homeodomain TF ortholog of mammalian *Dlx2*, and *ceh-20* a PBX homeodomain TF is responsible for the activation of the transcriptome of the four pairs of DA neurons in the worm (Doitsidou et al. 2013; Flames and Hobert 2009). Additionally, other TFs have also been suggested to play a role in DA differentiation such *vab-3* or *ztf-6* (Doitsidou et al. 2018; Doitsidou et al. 2008).

3.2. Serotonergic systems

In mammals, serotonergic progenitors are located in the ventral hindbrain and several TFs are required at different developmental time points to instruct serotonergic fate. In progenitors *Mash1 (a.k.a Ascl1)*, *Foxa2* and *Nkx2.2* are early regulators acting upstream of other factors such as *Gata2-3*, *Lmx1b* and *Pet1* that are expressed in postmitotic neuroblasts (Pattyn et al. 2004; Cheng et al. 2003; Haugas et al. 2016). *Lmx1b* and *Pet1* mutants show defects in 5-HT pathway genes expression and their action is direct on those genes, this is similar to what was observed in the case of *Nurr1* and *Pitx3*

in DA neurons. Accordingly, they have also been considered terminal selectors for 5HT fate. Moreover, their expression is maintained in adult stages, and adult removal of the factors also lead to expression defects.

In zebrafish, *Pet1* is also expressed in raphe serotonergic neurons, where it regulates *Tph* expression. Another factor, *Irx1a*, a TALE homeodomain, also contributes to 5-HT specification in this model organism (Lillesaar et al. 2007; Cheng Chi et al. 2007).

In *Drosophila* serotonergic neurons of the ventral ganglia are specified by three TFs, two zinc fingers *Eagle* (*Ea*) and *Huckebein* (*Hkb*) and the homeodomain *Engrailed* (*En*) (Lundell et al. 1996; Dittrich et al. 1997). Mutants for all three show defects in the number of serotonergic neurons but the step of differentiation where they act remains unknown. For instance, the expression of *Eg* is not maintained in in mature cells but it is required for the acquisition of its terminal fate (Lee and Lundell 2007).

In *C. elegans,* NSM, ADF and HSN are the most studied. Both NSM and HSN require the terminal selector *unc-86*, a POU homeodomain TF (Desai et al. 1988; Zhang et al. 2014). In the case of NSM, *unc-86* works together with the LIM/homeodomain *ttx-3*. They seem to act redundantly in the direct regulation of several effector genes, as only double mutants show significant defects of genes expression (Zhang et al. 2014). Our group recently published the characterization of the HSN regulatory logic. We found that six TFs, *unc-86*, *sem-4* (C2H2 - zinc finger), *hlh-3* (bHLH), *ast-1* (ETS), *egl-46* (C2H2 - zinc finger) and *egl-18* (GATA) work as a TF collective to select the HSN transcriptome (Lloret-Fernández et al. 2018). Interestingly, similar to the DA terminal selector combination (*ast-1/Er81; ceh-43/Dlx2 and ceh-20/Pbx1*) the HSN TF collective is homologous to the TF combination involved in serotonergic differentiation of the mouse raphe neurons. This homology between both programs suggest a phylogenetic conservation between HSN and raphe neurons transcriptional programs (Lloret-Fernández et al. 2018). Finally, terminal selectors controlling ADF fate are still unknown; however, some TFs have been described to be involved in a possible regulation of 5-HT genes in this neuron but their action seem to be indirect. *lim-4* which is the terminal selector of AWB, the sister neuron of ADF, is required for ADF specification but its expression is only seen in the mother cell of ADF (Zheng et al. 2005). On the other hand, the cilia terminal selector, *daf-19*, is also required for *tph-1* expression, although it seems to act indirectly (Xie et al. 2013).

3.3. Adrenergic, Noradrenergic, Tyraminergic and Octopaminergic systems.

In the mouse brain, the NA population is mainly located in locus coerulus. *Phox2a* and *Phox2b*, from the homeodomain family, are expressed and essential for *Th* and *Dbh* expression (Coppola et al. 2010; Pattyn et al. 1997). Their functions are slightly different, both bind to upstream regions of *Th* and *Dbh,* however *Phox2a* is not sufficient to induce

NA differentiation in the absence of *Phox2b*, and *Phox2b* is not expressed at adult stages; therefore, this regulatory program suggests that *Phox2b* may establish NA differentiation while *Phox2a* might be required for its maintenance. This relay between the two TFs is also observed in zebrafish, mutations in *Soulless/Phox2a* drives a reduction in NA population; however, contrary to mouse, in zebrafish *Phox2a* is upstream *Phox2b* (Guo et al. 1999).

The majority of noradrenergic neurons are located in peripheral nervous system as a part of sympathetic system. In mouse, sympathetic neuron specification also requires *Phox2a/b* to regulate its terminal differentiated fate (Ernsberger et al. 2000; Coppola et al. 2010). Additionally, other TFs participate specifically in sympathetic NA fate determination, such as the bHLH member *Hand2*, and *Ap-2β. Hand2* interacts with *Phox2b* and whose mutation also leads to defects to induce and maintain *Th* and *Dbh* expression (Vincentz et al. 2012). The mutants of *Hand2* reveal that panneuronal features are less affected than NA pathway genes, what suggest its role as terminal selector (Schmidt et al. 2009). *Ap-2β* mutants, show reduced numbers of NA neurons both from the brain and the sympathetic system (Hong et al. 2008). Similarly, in zebrafish sympathetic neurons fail to differentiate in *Hand2* and *Ap-2* mutants (Schmidt et al. 2009).

OA and TA neuron specification has not been studied in detail and no TFs are known to be involved in their specification either in *Drosophila* nor in *C. elegans.*

3.4. In vitro strategies to induce MA neuron differentiation

Finally, due to the clinical importance of both serotonergic and dopaminergic neurons, great efforts have been made to induce these monoaminergic fates *in vitro*. The strategies are based either in reproducing the concentration and timing of the morphogens required to specify these progenitors or directly to induce the expression of key TF combinations. The combination of *Ascl1, Lmx1a* and *Nurr1* has been successfully used to induce mouse midbrain DA fate (Caiazzo et al. 2011). In other studies, the combination is integrated by *Ascl1, Lmx1b* and *Nurr1* (Addis et al. 2011), what suggests that both genes, *Lmx1a* and *Lmx1b*, exert important effects in reprogramming. Moreover, due to the complexity of transcriptional network involved in midbrain DA neurons specification, other TFs have been assayed with variable results, such as *Pixt3*, *Brn2* or *Myt1l* (Kim et al. 2011; Vierbuchen et al. 2010; Arenas, Denham, and Villaescusa 2015).

On the other hand, the *in vitro* induction of mouse serotonergic neurons from fibroblast requires the presence of morphogens like *Shh*, FGF-8 and FGF-4 in culture medium. The combination of these morphogens and the TFs *Foxa2*, *Gata-2* and *Ascl1* are enough to induce 5-HT fate (Nefzger, Haynes, and Pouton 2011). But also, the

combination of *Nkx2.2*, *Lmx1b* and *Pet1* has proved to effectively induce 5-HT specification (Cheng et al. 2003).

Regarding other monoamines, very little is known to induce their fate through direct transcriptional reprogramming; however, it has been described that *Phox2b* forced expression, under properly medium conditions, enriches noradrenergic cells in the culture (Mong et al. 2013).

Table I.3 summarize the TFs involved in MA specification in different animal models. As described above, the action of some TFs is conserved across phylogeny. Also, it reflects that different neuronal populations in the same organism, although using the same neurotransmitter are regulated by different combinations of TFs, like DA subpopulations in mousee or serotonergic regulation in *C. elegans*.

Table I.3 TFs involved in MA terminal differentiation

Organism	DA neurons	5-HT neurons	NA/OA
Mouse	-Midbrain: *Nurr1* (NHR), *Pitx3* (HD), *Lmx1b* (HD). -Olfactory bulb: *Er81* (ETS), *Dlx2* (HD), *Pax6* (HD)	-Hindbrain (Raphe nucleus): *Pet1* (ETS), *Lmx1b* (HD), *Nkx2.2* (HD), *Mash1/Ascl1* (HD), *Gata2/3* (GATA), *Brn2* (POU-HD), *Sall2* (C2H2)	-L. coerulus: *Phox2a/b* (HD) -Sympathetic neurons: *Phox2a/b* (HD), *Hand2*, *AP-2β*
Zebra fish	-Diencephalon: *Nurr1* (NHR), *Otp* (HD), *Spt5* (TEF), *Artn2.* -Optic and preoptic area: *Nurr1* (NHR), Foxg1a (FKH), *Dlx2a* (HD)	-Raphe nucleus: *Pet1* (ETS), *Irx1a* (HD)	-L. coerulus: *Phox2a/b* (HD) -Sympathetic neurons: *Phox2a* (HD), *Hand2*, *AP-2β*
Drosophila	-Ventral ganglion: *Cf1a* (Pou-HD), *Islet* (Lim-HD)	-Ventral ganglion: *En* (HD), *Eg* (C2H2), *Hkb* (C2H2)	unknown
C. elegans	- CEPs, ADE, PDE: *ast-1* (ETS), *ceh-43* (HD), *ceh-20* (HD), *vab-3* (HD), *ztf-6* (C2H2)	-HSN: *unc-86* (HD), *ast-1* (ETS), *sem-4*, *hlh-3*, *egl-46*, *egl-18* -NSM: *unc-86* (HD), *ttx-3* (HD) -ADF: *lim-4* (HD), *daf-19* (RFX)	unknown

OBJECTIVES

OBJECTIVES

Monoaminergic neurons control a great variety of behaviors and their dysfunction is linked to several pathological conditions. The identification of the TFs required for MA specification can help understanding the molecular basis of some of these pathologies. Interestingly, TF involved in dopaminergic and serotonergic specification are conserved throughout evolution: *ceh-20/Pbx1, ceh-43/Dlx2* and *ast-1/Er81* in dopaminergic olfactory bulb neurons and *ast-1/Pet1, unc-86/Brn2, sem-4/Sall2*, *egl-46*/*Insm1, egl-18/Gata2/3* and *hlh-3*/*Ascl1* in serotonergic neurons from raphe nuclei.

Phylogenetic conservation of regulatory transcriptional programs supports the use of *C. elegans* as a model to achieve further insights into transcriptional regulatory logic in more complex organisms.

From this perspective, the main goal of this Thesis is to unravel the transcriptional regulatory logic that governs monoaminergic neurons specification using *Caenorhabditis elegans* as an animal model.

To accomplish this aim, we stablished the following objectives:

1. To optimize interference RNA strategy to perform a highly efficient RNAi screen by feeding against all the transcription factors of *C. elegans*.
2. To build a complete and fully verified TF RNAi feeding library to knockdown the expression of all TFs of *C. elegans* in order to detect which of them play a role in monoaminergic specification.
3. To validate and precisely determine the function of the candidates that retrieved the strongest phenotype for each monoaminergic neuron subtype.

MATERIALS & METHODS

MATERIALS AND METHODS

In this section we will review the materials and the experimental procedures used in this Thesis.

1. Experimental procedures

1.1. *C. elegans* strains and maintenance

C. elegans was culture following standard methods (Brenner 1974). Briefly, animals were maintained in NGM (Nematode Growth Medium, composition detailed later in Materials) agar plates (55 mm × 16 mm, non-vented) and fed with *E. coli* OP50 strain (from Caenorhabditis Genetics Center). OP50 bacterial strain is an uracil-requiring mutant with a limited growing rate. Wild type *C. elegans* strain used was N2 Bristol and transgenic lines generated were built from this background. Unless otherwise indicated animals were culture at 20ºC.

Animals were manipulated under the dissection scope (Zeiss Stemi 2000). To cross different strains, the amount of food over the plate was reduced to 30 µL to favor interactions between hermaphrodites and males. N2 males were induced by heat-shock (Lints and Hall 2009) and then maintained by backcross. Newly generated strains were conserved by freezing as currently established (Brenner 1974). A list of strains used for this Thesis is included in Table A.2 in the Annex.

1.2. RNAi clone generation

To generate new RNAi clones we PCR amplified genomic DNA fragments of target genes, cloned them inside L4440plasmid and transformed them into *E. coli* HT115 (ED3) strain (from Caenorhabditis Genetics Center). For PCR amplification of the genomic fragment we designed specific 20-25 nt primers mainly directed towards 3' to maximize the amplification step of secondary RNAi pathway and to avoid targeting only specific isoforms due to differential transcription start site, fragment size was from 300bp to 1500 bp. The polymerase used, Q5® HotStart High-Fidelity 2X Master Mix (NEB, #M049S), is a high-fidelity proof reading polymerase that generates blunt ends. As a template genomic N2 *C. elegans* DNA was used; it was extracted with DNeasy Blood & Tissue Kit (QIAGEN, #69504). See Table M.1 for reagents and M.2 for PCR conditions. PCR products were purified with QIAquick PCR Purification Kit (QIAGEN,#28106).

Table M.1 RNAi PCR reagents

Component	Volume (µL)	Concentration
Q5® HotStart 2X master mix	12.5	1X
Forward Primer	0.5	0.5 µM
Reverse Primer	0.5	0.5 µM

Template DNA	1		8-10 ng/µL
Nuclease-Free Water	10.5		-
Table M.2. Colony PCR conditions			
Step	**Temperature (°C)**	**Time (s)**	**n° of cycles**
Initial denaturation	98	30	1
Denaturation	98	15	25
Annealing	55-70	15	
Extension	72	30 /kilobase	
Final extension	72	120	1
Hold	10	∞	1

After amplification, fragments were cloned into L4440 plasmid (Figure M.1) (Addgene, #1654). This plasmid contains two T7 promoters flanking the multi cloning site (MCS) to which T7 RNA polymerase will bind to produce dsRNA. The vector was digested with *EcoRV*, which generates blunt ends and presents two sites in the MCS and thus, the cut released a small fragment of ~200bp between both T7 promoters. Blunt end ligation requires phosphorylation step of the inserts using T4 PNK (Thermo Sicentific, #EK0031) and, to increase ligation efficiency, the ratio between plasmid and insert was 1:6 (Ligase 40 U/µL) (NEB, #M0208L).

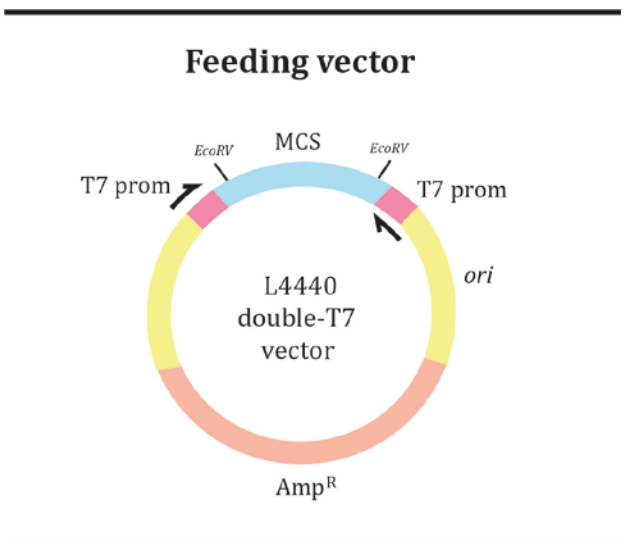

Figure M.1. RNAi feeding vector. L4440 plasmid is currently used in RNAi feeding experiments due to the T7 promoters (pink) in opposite directions, flanking the multi cloning site (MCS, blue). The MCS is cleaved through digestion with *EcoRV* to insert the PCR fragment of a target gene (Amp^R). The plasmid contains an ampicillin resistance selection gene. The vector is transformed into HT115 (DE3) bacteria, that expresses T7 polymerase to synthesize dsRNA upon IPTG induction. Adapted from *Kamath et al. 2000*.

Finally, *E. coli* HT115 (DE3) bacteria were transformed with the ligation product. This strain is RNase-III deficient (*rnc14* mutant), thus, dsRNA is more stable. Furthermore, it expresses T7 polymerase inducible by iso-propyl-β-D-1-thiogalactopyranoside-inducible (IPTG) (Acros Organics, #BP1755-100) and is resistant to tetracycline because the Tn10 transposon insertion that disrupts *rnc14* gene carries a

tetracycline resistant gene. As L4440 carries an ampicillin resistance, to select transformed cells bacteria are seeded in agar plates with both antibiotics. Seeded plates are placed at 37ºC overnight (13-15 h) to get positive colonies. Eight colonies were selected to perform colony PCR to test if the plasmid carried by bacteria had incorporated the insert. In order to preserve some bacteria for further culture, each colony was diluted in 10 µL of ddH_2O from which 3 µL were used as a template for the PCR mix (Table M.3). The primers used anneal in each one of T7 promoters and the polymerase used was GoTaq (Promega, #M7806) (Table M.4 for conditions).

Table M.3. Colony PCR reagents		
Component	**Volume (µL)**	**Concentration**
5X GoTaq® Reaction Buffer	5	1X
$MgCl_2$	2.5	1.5 mM
Nucleotide Mix	0.5	0.2 mM
Forward Primer (mh139, 5'-GAGGAAGCAACCTGGC-3')	0.5	0.5 µM
Reverse Primer (mh140, 5'-GACGGCCAGTGAGCGC-3')	0.5	0.5 µM
GoTaq® DNA polymerase (5U/µL)	0.2	0.21 U/25 µL
Template DNA	3	0.2 – 0.3 µg/µL
Nuclease-Free Water	12.8	-

Table M.4. Colony PCR conditions			
Step	Temperature (°C)	Time (min)	n° of cycles
Initial denaturation	95	2	1
Denaturation	95	0.5	27
Annealing	55	0.5	
Extension	72	1 /kilobase	
Final extension	72	10	1
Hold	10	∞	1

For each cloning construct, two PCR-confirmed colonies were let growing in 5 mL of LB medium (Sigma, #L3522) with ampicillin (50 µg/mL) and tetracycline (15 µg/mL) overnight in order to amplify the plasmid. After plasmid extraction and purification with QIAprep Spin Miniprep Kit (QIAGEN, # 27106), enough material was obtained to analyze the construction by sequencing. Samples were analyzed by Sanger sequencing (Macrogen Spain, Madrid). Correct clones were frozen in cryotubes adding 600 µL of the growth cultures and 400 µL of glycerol (50% diluted in ddH_2O) and conserved at -80 °C. The complete list of RNAi feeding clones generated for this Thesis is included in Table A.3 in the Annex.

1.3. Generation of the Transcription factor RNAi library

To generate the TF RNAi feeding library we followed the next steps:

1. RNAi bacterial clones corresponding to TF were selected from Dr. Ahringer library (Kamath and Ahringer 2003) distributed by Source BioScience LifeSciences. The clones were let grow in LB medium to extract plasmids and confirm their content by sequencing (as explained above).
2. The remaining TF without the corresponding Ahringer clones or that were wrong were selected from Dr. Vidal library (Rual et al. 2004), also distributed by Source BioScience LifeSciences. The accuracy of clones was tested by sequencing and incorrect or missing clones were listed to build in our laboratory.
3. Finally, the TF RNAi library was completed with the cloning protocol detailed in previous section.

The detailed composition of TF RNAi library is contained in Table A.4 in the Annex.

1.4. Protocol for RNAi feeding experiments

To conduct these experiments, RNAi plates were prepared adding IPTG (0,6M) to their normal NGM composition. These plates were seeded with bacterial clones from the TF RNAi library. These bacteria were cultured overnight (15-13 h) in LB medium (Sigma, #L3522) with ampicillin (50 μg/mL) at 37 °C with shaking 180 rpm. The medium did not include tetracycline because it reduces the dsRNA production rate. Three hours before seeding, the cultures were inoculated with an IPTG solution (0.6 M), in order to induce the production of double strand (dsRNA). As IPTG is degraded by light, tubes were covered with aluminum foil. After that three hours, 200 μL of each bacterial clone was seeded per plate. Three plates per clone were used.

Once plates were dried, adult gravid worms of the desired sensitized strain were transferred to one of every different seeded IPTG plates and deposited within a drop of alkaline hypochlorite solution (*Drop Bleach,* see Materials section). Larvae that survived the treatment become the parental generation (P0), which experience the post embryonic effects of the RNAi. When P0 animals reached L4 stage (2-3 days after incubation), between 10-15 animals were transferred to two fresh IPTG plates, with the same bacterial clone to feed on, to avoid animals starvation. Their progeny (F1) develops under the embryonic effects of the RNAi (F1 scoring). We scored F1 generation (approximately 7 days after drop bleach) but whenever the RNAi was lethal at F1, we performed P0 scoring. A minimum of 30 worms per clone, coming from three distinct plates was scored. The statistical analysis applied was Fisher exact test.

Given that the sensitized strains used to perform the experiments is infertile at 25°C due to embryonic lethality, all experiments were performed at 20 °C (Zhuang and Hunter 2011; Simmer et al. 2002). For each clone the same process was done twice, whenever the results from the first and second replicate did not match, we performed a third replicate.

1.5. Generation of mutant strains and genotyping

Mutant strains used to validate the results of the screen were cross with reporter lines of interest. As indicated in Table A.2 in the Annex, most of the strains used were obtained from the Caenorhabditis Genetics Center (CGC). The nature of all used alleles is known; thus, we used that information to genotype and confirm by PCR or sequencing the presence of the mutant allele in the newly generated strains.

To genotype strains, DNA was extracted following a standard worm lysis protocol. PCR Eppendorf tubes (200µl) were filled with 30 µL of lysis buffer (see Materials below) with 1% of Proteinase K (Roche Life Science, #3115879001). 15-20 adult animals per plate were picked and transferred to individual Eppendorf tubes. Tubes and lysis buffer were chilled on ice to let worms settle and once finish, tubes were place inside thermocycler at 65 °C for 1h and at 95 °C for 30 minutes to inactivate Proteinase K. After that period, the DNA is ready to be used, without additional purification or quantification (with an obtained yield of approximately 300 ng/µL). Samples can be stored frozen at –20 °C. The polymerase used for genotype PCRs was GoTaq® (Promega, #M7806) and the rest of reagents and their volume for each PCR reaction are listed below in Table M.5 and reaction conditions in Table M.6.

Table M.5 Mutant genotyping PCR reagents

Component	Volume (µL)	Concentration
5X GoTaq® Reaction Buffer	5	1X
$MgCl_2$	2.5	1.5 mM
Nucleotide Mix	0.5	0.2 mM
Forward Primer	0.5	0.5 µM
Reverse Primer	0.5	0.5 µM
GoTaq® DNA polymerase (5U/µL)	0.2	0.21 U/25 µL
Template DNA	x	0.2 – 0.3 µg/µL
Nuclease-Free Water	Up to 25	

Table M.6 Mutant genotyping PCR conditions

Step	Temperature (°C)	Time (min)	n° of cycles
Initial denaturation	95	2	1
Denaturation	95	0.5	25-30
Annealing	50-65	0.5	
Extension	72	1 /kilobase	
Final extension	72	10	1
Soak	10	∞	1

Deletion alleles were genotyped by PCR fragment size with a combination of three primers in most of the cases: a common forward and two reverse that align out (reverse wild type) and inside the deleted region (reverse mutant). For point mutations, we purified the PCR product of three candidates and confirm their genotype by sequencing

(Table M.7). Regarding alleles *vab-3 (ot346)* and *unc-62 (e644)* it was not necessary genotype them by PCR due to their evident visual phenotype. In the case of *ot346* the worms exhibited abnormal head morphology and *e644* animals were highly dumpy. On the other hand, the allele *unc-62 (mu232)* has integrated in the same chromosome a fluorescent comarker *muIs35* [*mec-7::gfp, lin-15b* (+)] by which the mutant allele could be followed. Additional details and nature of mutations are described in Results.

Once the homozygous mutant background was confirmed, the new strains were maintained at 20 °C, at least two generations, before scoring. This temperature was selected in order to compare RNAi scoring results with the ones from mutants.

Table M.7. Mutant alleles and primers to genotype

Gene	Allele	Type of Mutation	Forward primer	Reverse primer (WT)	Reverse primer (Mutant)
rrf-3	*pk1426*	Deletion	tccgagttcgcatcaagtttcac	agacgaaatccggcatgatcc	cactcccgcgtgtttcaaattcttc
eri-1	*mg366*	23 nt insertion	tccaacaaacgacagatccag	ttgcccaagaaacagtcgatg	cgaatttcgataaagtgcctg
lin-15b	*n744*	Point mutation	tcaggaccatcacaggatc	atgacatccaccgatgctc	-
unc-55	*e1170*	Single nucleotide insertion	ttcggtcacagatcgctcg	ttcttcgtcgtcttcctggctc	-
unc-62	*e917*	Deletion	gtaattcgccgtttagcatagctg	tgacaagcgacaacggattc	tcaattttgagccaactacacagc
cep-1	*ep347*	Deletion	cggcaaataattccgatggaac	agctttgtgggaagcaatcg	tcgatcatccaaatcaaggcac
mef-2	*gv1*	Deletion	aagagagccagagagcacatag	tgagttgaagacgatgagtgc	aattgctgtggtctccactc
mef-2	*gk633*	Deletion	gctcgtgtaattcgtaccttcg	gggctttagggaagaagagag	caagattggtgagagaaatgaacg
zip-5	*gk646*	Deletion	gagacctatgtcattcgagaacc	acaggaaattggatggatgtgc	tccacttgatgtgtgtacgtgtc
pqm-1	*ok487*	Deletion	aatccagctttcgtgcctac	aggaggcatcaaatcaagtgag	ttctcgtaaaccctcgtttcg
dro-1	*tm4722*	Deletion	agatgggtcttccaacgtctg	cagcttcttctcggcttcaac	-

1.6. Generation of *C. elegans* transgenic lines

Constructs for either new transcriptional reporters or for *cis*-regulatory analysis were built into ppD95.75 (Addgene Plasmid #1494) expression plasmid through a standard cloning process. This vector contains the MCS right in front of the *gfp* coding region that is optimized for *C. elegans* and the 3' UTR of the myosin gene, *unc-54*. To enhanced *gfp* expression the plasmid contains a Kozak sequence ahead of the gene and an artificial intron (Figure M.2). Constructs were transform in *E. coli* TOP10 electrocompetent bacteria (Invitrogen, #C404010) generated constructs were confirmed first by enzymatic digestion and then by sequencing.

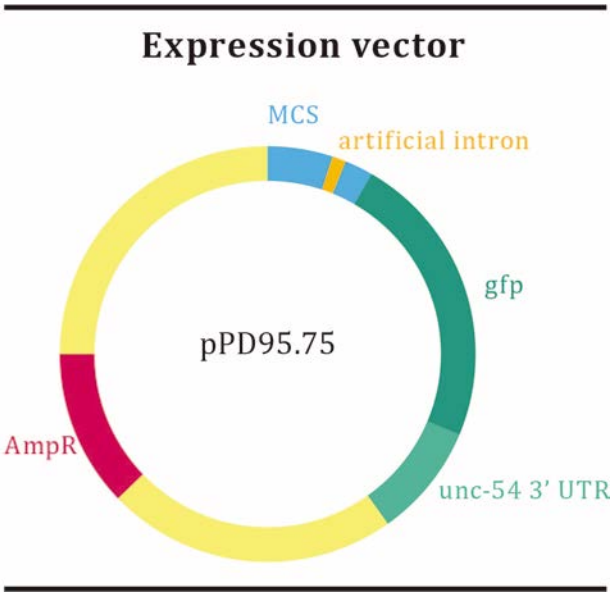

Figure M.2. Expression vector ppD95.75. This plasmid is currently used to generate fluorescent reporters. Multi cloning site (MCS) is ahead of *gfp* coding sequenced codon optimized for *C. elegans*.

After that, the constructs were microinjected to generate transgenic lines that express the plasmid as an extrachromosomal array. Injection mix contained the plasmid of interest (50 ng/µL) and a comarker (100 ng/ µL). Usually, the comarker used was pRF4 *(rol-6(su1006))* (Mello et al. 1991), which encodes a dominant negative mutation of a collagen gene that confers a rolling phenotype to the animals carrying the array. This phenotype is visually detected under dissecting scope because worms crawl twisting (Kramer et al. 1990). For fosmid injections the DNA mix contained fosmid (40 ng/µL) and two comarkers were added, *rol-6(su1006)* (50 ng/µL) and pNF101 *(ttx-3prom::mCherry)* (50 ng/µL).

Prior to microinject, the DNA mix is centrifuged 10 minutes at maximum speed to avoid needle plugging. Needles were homemade with 0,5 µm diameter capillary tips and after load them with 1 µL of injection mix, the needle is adjusted in a micromanipulator adapted to an inverted microscope (Axio Vert.A1 Zeiss) that brings a correct angle for the needle to penetrate worms (15°-45°); the tip is connected to an air compressor system to propel the DNA mix inside animals. Well-fed young adult worms were selected for injections. Animals were placed on 2% agarose pads that hold animals static and allowed clearly visualize the gonads. To avoid that the worms get dehydrated and died, they were covered with Halocarbon oil 700 (Sigma, #H-8898). Once animals were properly still over the pad, they were visualized under the microscope and injected in both gonads where DNA was released. To let animals recover, they were placed in a drop of M9 1X solution (see Materials for composition) on an NGM plate; after they come back crawling, worms were transfer to individual plates.

Approximately three days later, the F1 progeny of injected animals was observed to select which among them had inherited the array, easily detected due to the roller phenotype. We selected a maximum of 150 worms per injection. Single animals were transferred to individual plates to let them produce descendants, F2. The plates that three days after presented a high number of roller animals were considered stable lines due to the ability to transmit the microinjected array. For each construction, normally two independent lines were conserved and named for further scoring and maintenance. Details about generated expression reporters (for *unc-55* and *dro-1*) are described in Results and transgenic lines for *cis*-regulatory studies are detailed in the following section.

1.7. Mutagenesis analysis of *cis*-regulatory modules (CRM)

To unravel functional binding sites of examined TFs, site directed mutagenesis was performed. The specific sequences of TFBS were searched in databases like Transcription Factor encyclopedia (eTF), Cis-BP or JASPAR. To predict putative binding motifs in the analyzed CRMs, those sequences were scanned with the position weight matrixes (PWM) of TFBS, either in 5'-3' or 3'-5' orientations. Once a motive was found, we opted to mutate those nucleotides more conserved, however if the nucleotides were similarly conserved, we mutated the three nucleotides of the core motif (Table M.8). To carry out these experiments we employed Quickchange II XL site-directed mutagenesis kit, Agilent Technologies #200522).

Mutated constructs were confirmed by sequencing and injected as extrachromosomal arrays as described above. For each construct three independent lines were analyzed. A construct was considered to show normal expression when its penetrance for GFP expression was 100-70% of average expression of the corresponding wildtype contruct ("+" phenotype). 70-30% reduction compared to wildtype was considered a partial phenotype "+/-". And, finally, if the percentage of GFP scored neurons was below 30%, it was considered as loss of expression ("-" phenotype).

Table M.8 Primers used for mutagenesis experiments

Strain	Genotype	L	Forward primer	Reverse primer	Site
NFB 610	vlcEx325(bas-1prom74::gfp (50ng/ul),rol-6)	1	cctaccttcgatctctgtcaatTTTgggaaatcttttgctccagc	gctggagcaaaaagatttcccAAAattgacagagatcgaaggtagg	E-box
NFB 611	vlcEx326(bas-1prom74::gfp (50ng/ul),rol-6)	2			
NFB 420	vlcEx239(cat-1prom72::gfp (50ng/ul),rol-6)	1	ccaccaaatttttcaatgttttcccctgCcgAAagaaaaatatgaaaatatcaacg	cgttgatattttcatatttctTTcgGcagggaaaacattgaaaaatttggtgg	E-box
NFB 421	vlcEx240(cat-1prom72::gfp (50ng/ul),rol-6)	2			
NFB 620	vlcEx331(cat-1prom77::gfp (50ng/ul),rol-6)	1			CSL

NFB 631	vlcEx341(cat-1prom77::gfp (50ng/ul),rol-6)	2	gcaaggggcacgtttta gattcccTTTgtctga aaaattgatttg	caaatcaatttttcagac AAAgggaatctaaaac gtgccccttgc	
NFB 737	vlcEx395(cat-1prom81::gfp (50ng/ul),rol-6)	2	gaataagcgagcaagg ggTTcgAtttagattcc cacggtct	agaccgtgggaatctaa aTcgAAccccttgctcg cttattc	E-box
NFB 739	vlcEx397(cat-1prom81::gfp (50ng/ul),rol-6)	1			
NFB 740	vlcEx398(cat-1prom80::gfp (50ng/ul),rol-6)	1	gtgtatgtatagttccT Ttatataatcatttttat gcttcaacttgcagtctc	gagactgcaagttgaag cataaaaatgattatata AAggaactatacataca c	CSL
NFB 741	vlcEx399(cat-1prom80::gfp (50ng/ul),rol-6)	2			
NFB 1322	vlcEx784(cat-1prom90::gfp (50ng/ul),rol-6)	1	ctgagagaaaaatgaa aggaaaatCCCgaga aatgtgataacaaaact gagagtc	gactctcagttttgttatc acatttctcGGGattttcc tttcatttttctctcag	CSL
NFB 1323	vlcEx785(cat-1prom90::gfp (50ng/ul),rol-6)	2			
NFB 1101	vlcEx607(cat-4prom71::gfp (50ng/ul),rol-6)	1	ccagaataccttcata atacatgCcgAAttgt acctttttttttcgtaattt cttc	gaagaaattacgaaaaa aaaaggtacaaTTcgG catgtattatgaaaggtat tctgg	E-box
NFB 1102	vlcEx608(cat-4prom71::gfp (50ng/ul),rol-6)	2			
NFB 1320	vlcEx782(cat-4prom73::gfp (50ng/ul),rol-6)	1	cttattctttttttctcatt ttttcacataaTTTgga aaagatgatgaagtcta tccattcg	cgaatggatagacttcat catcttttccAAAttatgt gaaaaaatgagaaaaaa agaataag	CSL
NFB 1321	vlcEx783(cat-4prom73::gfp (50ng/ul),rol-6)	2			
NFB 621	vlcEx332(cat-4prom69::gfp (50ng/ul),rol-6)	1	gctttctcagctttcttaa gatttacTTacggctca ttttcaatatcacc	ggtgatattgaaaatgag ccgtAAgtaaatcttaag aaagctgagaaagc	CSL
NFB 622	vlcEx333(cat-4prom69::gfp (50ng/ul),rol-6)	2			
NFB 1360	vlcEx807(bas-1prom90::gfp (50ng/ul, rol-6))	1	ctgagagaaaaatgaa aggaaaatCCCgaga aatgtgataacaaaact gagagtc	actctcagttttgttatcac atttctcGGGattttcctt tcatttttctctcag	E-box
NFB 1361	vlcEx808(bas-1prom90::gfp (50ng/ul, rol-6))	2			
NFB 396	vlcEx224(tph-1prom42::gfp (50ng/ul),rol-6)	1	gcagggctcatttattct cTTacggaaaccatga cagca	tgctgtcatggttccgtA Agagaataaatgagccc tgc	CSL
NFB 397	vlcEx225(tph-1prom42::gfp (50ng/ul),rol-6)	2			
NFB 777	vlcEx414(Mdat-1prom1::gfp (50ng/ul),rol-6)	1	cggataaatgtagaaa aagaagaaaagaCCC ataCCCagatagatgc tttccggc	gccggaaagcatctatct GGGtatGGGtcttttctt ctttttctacatttatccg	COUP-TF
NFB 778	vlcEx415(Mdat-1prom1::gfp (50ng/ul),rol-6)	2			
NFB 820	vlcEx454(Mdat-1prom2::gfp (50ng/ul),rol-6)	1	cgttaggagacgccTa catgattcagaagcaga atttgg	ccaaattctgcttctgaat catgtAggcgtctcctaa cg	MEIS
NFB 821	vlcEx455(Mdat-1prom2::gfp (50ng/ul),rol-6)	2			
NFB 822	vlcEx456(Mdat-1prom3::gfp (50ng/ul),rol-6)	1	cacacatacaccggaat attcTacatgccaccac atctag	ctagatgtggtggcatgt Agaatattccggtgtatg tgtg	MEIS
NFB 823	vlcEx457(Mdat-1prom3::gfp (50ng/ul),rol-6)	2			
NFB 833	vlcEx461(Mcat-2prom2::gfp (50ng/ul),rol-6)	1			MEIS

NFB 1093	vlcEx602 (Mcat-2prom-2::gfp; (50ng/ul), rol-6)	2	cggaaggaaatgtggtgtatctctttcagagtactccat	atggagtactctgaaagagatacaccacatttccttccg	
NFB 904	vlcEx49 (Mcat-2prom-1::gfp, rol-6 (50 ng/microL))	2	ggaaatgaaataagcttcaaCCCatgcaatgatgatttgatacggaagg	ccttccgtatcaaatcatcattgcatGGGttgaagcttatttcatttcc	COUP-TF
NFB 903	vlcEx490 (Mcat-2prom-1::gfp, rol-6 (50ng/microL))	1			
NFB 905	vlcEx492 (Mcat-2prom-3::gfp, rol-6 (50 ng/microL))	1	ccataacacagcaacaggCTTaacaattatctcttctagaggatcc	ggatcctctagaagagataattgtTAAgcctgttgctgtgttatgg	PAX
NFB 906	vlcEx493 (Mcat-2prom-3::gfp, rol-6 (50 ng/microL))	2			
NFB 1007	vlcEx539 (Mdat-1prom4::gfp (50ng/ul),rol-6)	1	cgttaggagacgccTacatgattcagaagcagaatttgg	ccaaattctgcttctgaatcaTgtaggcgtctcctaacg	MEIS
NFB 1008	vlcEx540 (Mdat-1prom4::gfp (50ng/ul),rol-6)	2			
NFB 1009	vlcEx541 (Mdat-1prom5::gfp (50ng/ul),rol-6)	1	cggataaatgTagaaaaagaagaaaagaCCCataCCCagatagatgctttccggc	gccggaaagcatctatctgggtatgggtcttttcttcttttctAcatttatccg	COUP-TF and HD
NFB 1010	vlcEx542 (Mdat-1prom5::gfp (50ng/ul),rol-6)	2			
OH8 356	otIs621 (dat-1prom2::gfp (50ng/ul),rol-6)	1	cggataaatgTagaaaaagaagaaaagaagtataagtagatagatgctttccggc	gccggaaagcatctatctacttatacttcttttcttcttttctAcatttatccg	HD
OH8 357	otIs622 otIs621 (dat-1prom2::gfp (50ng/ul),rol-6)	2			
NFB 1011	vlcEx543 (Mdat-1prom6::gfp (50ng/ul),rol-6)	1	gaagaaaagaCCCataCCCagTtagatgcttccggcaattatccaccg	cggtggataattgccggaaagcatctaActGGGtatGGGtcttttcttc	COUP-TF and PBX
NFB 1012	vlcEx544 (Mdat-1prom6::gfp (50ng/ul),rol-6)	2			
NFB 1019	vlcEx549 (Mdat-1prom7::gfp (50ng/ul),rol-6)	1	gaagaaaagaagtataagtagTtagatgctttccggcaattatccaccg	cggtggataattgccggaaagcatctaActacttatacttcttttcttc	PBX
NFB 1020	vlcEx550 (Mdat-1prom7::gfp (50ng/ul),rol-6)	2			
NFB 1021	vlcEx551 (Mdat-1prom8::gfp (50ng/ul),rol-6)	1	gcctattccagtatgTTTccttgaagcagatataatcgcacaaacatat	atatgtttgtgcgattatatctgcttcaaaggAAAcatactggaataggc	COUP-TF
NFB 1022	vlcEx552 (Mdat-1prom8::gfp (50ng/ul),rol-6)	2			
NFB 1023	vlcEx553 (Mdat-1prom9::gfp (50ng/ul),rol-6)	1	gctcggataaatgtagaaaaaTCCgaaaagaagtataagtagatagatgctttccgg	ccggaaagcatctatctacttatacttctttcGGAttttctacatttatccgagc	PAX
NFB 1024	vlcEx554 (Mdat-1prom9::gfp (50ng/ul),rol-6)	2			

Table M.8. Primers used for mutagenesis experiments. In colors are labeled the consensus we search for our candidates and in capital letters are indicated the changes made in the DNA.

1.8. Scoring method and criteria

The protocol followed to score is the same for RNAi experiments, mutants and *cis*-regulatory analysis. Animals were maintained at 20 °C prior to scoring, with the exception of lines from *cis*-analysis that were kept at 25 °C to reinforce GFP expression.

For RNAi screening experiments and *cis*-analysis, 30 young adult animals per line or per RNAi clone and replicate were selected; in the case of mutant analysis 50 young adult worms per strain were analyzed.

4% agarose pads were prepared over crystal slides (Rogo Sampaic #11854782). Worms were placed over the agarose and immobilize with 12 µL of sodium azide 100 µM (Sigma, #26628-22-8). Finally, slides were sealed with conventional coverslips (22 × 22 mm) (VWR #631-1570). Scoring was performed using 40X objective in a Zeiss Axioplan 2 microscope. For each neuron class, three possible states were considered: the neuron was 'ON' when the fluorescent reporter was detected and 'OFF' in the opposite case, under some circumstances, if the ON expression was substantially weak, a category of 'FAINT' was also considered.

The percentage of expression in each neuron was plotted as contingency graphs and compared with the control of each experiment using Fisher exact test, two tailed, for statistical analysis and Standard Error of the Proportion (SEP) was also calculated with GraphPad QuickCalcs online software (www.graphpad.com/quickcalcs/).

1.9. Expression pattern analysis and image acquisition

To detect the expression of transcription factors of interest in monoaminergic neurons, reporter strains were ordered to CGC or build and injected in our laboratory as previously explained. For generated reporters, the best two lines were analyzed in order assess the expression pattern. To detect colocalization of those reporters in MA population, we crossed all strains with distinct *mCherry* reporters, such as *cat-1::mCherry*, *dat-1::mCherry, tdc-1::mCherry*, etc. Animals were maintained at 25 °C to ensure robust GFP expression. Between 15-30 animals, of distinct developmental stages, were mounted in coverslips as explained in the section above.

Images were taken with confocal TCS-SP8 Leica microscope or Zen System 2011 (Zeiss) and then processed with the free software ImageJ 1.50i (Rasband, W.S., https://imagej.nih.gov/ij/), but also with Adobe Photoshop CC and Adobe Illustrator CC.

1.10. Enhanced slowing response protocol

To assess the role of *lag-1* and *hlh-14* in ESR regarding ADF activity, animals fed with RNAi against both TFs were analyzed at P0. Null mutant strains for both genes present L1 lethality and molt defects, that is the reason why P0 RNAi was preferred. Moreover, P0 RNAi avoids lineage defects in ADF produce in *hlh-14* mutants (Poole et al. 2011). *rrf-3(pk1426)* sensitized background was selected to increase RNAi efficiency (Simmer et al. 2002), and this background is also present in the strain which expressed tetanus toxin specifically in ADF, to prevent any bias resulting from different backgrounds.

The RNAi protocol followed is the same as explained above. After three days of feeding in RNAi P0 population reached young adult stage and ~100 young adult animals were selected to record their movement response. First, worms were transfer to 1,5 mL Eppendorf with 500 µL of M9 1X buffer (see Materials for composition) and washed for 5 times. Then animals were release for freely crawl for 2 h in normal unseeded IPTG plates whose agar perimeter was delimited with a 4 M fructose ring to avoid worms to scape (White et al. 1986). After that period of fasting, animals were recovered washing the plate with M9 1X medium.

To analyze the locomotion of worms approaching a source of food, animals were recorded, at room temperature (22 °C), with a multi worm tracker device from Dr. Alkema's laboratory. Plates for the assay were also IPTG plates seeded with 25 µL of bacteria 5X concentrated. Bacteria occupied an area from 100 to 150 mm^2 on one side of the plate and once seeded, they were maintained at 4°C prior to experiments. Plates for each assay were seeded with the same bacterial clone as animals were previously fed to promote animals recognize the food. Worms were transfer to assay plates by pipetting. Usually, 4 groups of 8-15 worms were recorded per RNAi clone, approximately 50 worms per condition. The empty vector, L4440, was considered the control group.

Once the liquid droplet where animals were transferred in one side of the plate dried out, worms start crawling and the recording began. Usually a period of 5 minutes was enough for animals to reach the bacterial lawn and remain there. Animals that did not encounter food after that time were rejected due to possible damage caused by pipetting. On the other hand, animals that reached bacteria less than 1 minute after start crawling were also rejected to minimize transferring effect over records. Each RNAi was assayed in at least three different days and controls were recorded each day in parallel. The variability observed between days was negligible, accordingly, all obtained data was analyzed together.

Images were captured with CCD camera (Prosilica GC2450, Allied Vision Technologies, Stadtroda, Germany) at 4 frames per second and a 1.1× magnification for posture-based analysis. Under those circumstances, the area of a single worm was 70-75 pixels. The records were performed with the free Kerr Lab software Multi-Worm Tracker (http://sourceforge.net/projects/mwt/) and locomotion parameters were analyzed with custom MATLAB scripts (MathWorks Inc., Natick, MA, USA). Those animals that got touched each other while recording were removed from analysis.

Once values of speed were obtained data was treated with Microsoft Excel®. Time 0 s corresponds to the moment when worm's nose touches the edge of bacterial lawn. That adjust was executed for all individual analyzed animals in order to compare their speed values prior the encounter of food.

Statistical analysis was performed with GraphPad software. First, normality distributions were assessed with Shapiro-Wilk test for samples n ≤ 50 animals. In case of non-parametric distribution or small size of the samples, Kruskal-Wallis test was applied for multiple comparisons with Dunn's correction. On the other hand, to compare only two independent groups, control and one RNAi, in this case we used the non-parametric Mann-Whitney test. Linear regression analysis was used to compare slowdown interval, where the goodness of the fit (r^2) was always higher than 0.8, and both slope and elevation were contrasted to detect differences among groups. Significant differences (*) were considered under a p-value < 0.05 and highly significant differences (**) with a p-value < 0.01.

1.11. Calcium imaging recordings

The activation of ADF by chemical stimuli present was analyzed through calcium imaging recordings. As in ESR, the ultimate goal was to compare the role of *lag-1* and *hlh-14* regarding ADF ability to sense changes in the environment. In this case, P0 RNAi approached was also used for the same reason as in ESR experiments. However, in these experiments, the sensitized RNAi strain also carried a genetical engineered protein, GCaMP3, expressed only in ADF that exhibits an increased GFP emission when calcium enters inside the cell (Tian et al. 2009).

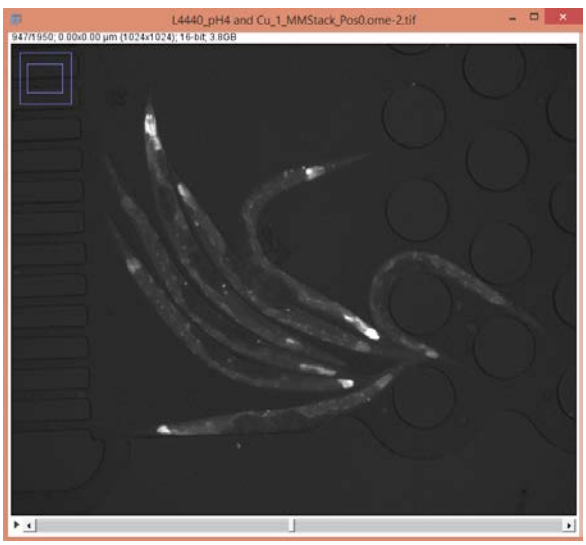

Figure M.3. Animals inside the microfluidics chamber.

Calcium recordings where performed when RNAi fed animals reached young adult stage. Animals were washed with M9 1X and treated for 30 minutes with 1 mM tetramisole hydrochloride (Sigma, #L9756) to paralyze their movements. Importantly, this drug did not affect neuronal activity. After that period, worms were transferred inside a methacrylate microfluidics chamber (self-custom at Worcester Polytechnic Institute, MA, USA). The chamber was settle on an inverted fluorescence microscope (Axio VertA.1, Zeiss) and connected to a liquid flow system. The flow system was controlled through an Arduino platform (D'Ausilio 2012) and MATLAB custom scripts (MathWorks Inc., Natick, MA, USA) to regulate the input inside the chamber of M13 buffer as basal solution (see Materials for composition) or the stimulation solution. In these experiments the stimulation solution

was prepared adding $CuSO_4$ (10 mM) to M13 buffer and adjusting to pH4. Both basal buffer or stimulation buffer contained also tetramisole (1mM) to avoid worm movement. Images were captured with a CCD camera (Prosilica GC2450, Allied Vision Technologies, Stadtroda, Germany) with 20X objective and 2 frames per second taken with Micro-Manager software (Edelstein et al. 2010) (Figure M.3).

Animals were delivered inside the microchamber and let adapt to flowing conditions for 5 minutes. To start each experiment, Arduino system was activated to regulate the flow of distinct solutions and, at the same time, Micro-Manager software was taking images of worms. After 30 s since experiment started, the first stimulation pulse took place, where worms in the chamber were exposed to stimulation solution for 30 s before flow changed again to basal buffer. Animals recovered for 3 minutes and 30 seconds in basal solution before the second stimulation pulse of 30 seconds. The process was repeated to record in total four pulses and recovery periods, what provided a final duration of the experiment of 16 minutes. 15-20 animals were recorded for each experiment. Assays were performed at least in three different days and control animals, L4440 as in ESR protocol, were recorded in every session.

Image files were analyzed with free Fiji software (Fiji.sc). As worms remained paralyzed throughout the experiment, occupying the same position, it was possible to determine the area corresponding to each ADF neuron and integrate the fluorescent emission along the time the experiment was running. Same areas were traced for all neurons to avoid bias due to surface size. Once measures were obtained, statistics were performed with GraphPad software. The percentage of changes in fluorescence intensity relative to the initial intensity F_0, $\Delta F = (F-F_0)/F_0 \times 100\%$, were plotted as a function of time for all curves. The mean values of calcium signals were plotted in various colors also as a function of time. To compare the maximum fluorescent emission in first stimulation between different groups, the same procedure as in ESR analysis was followed. First, normality test Shapiro-Wilk was performed to conclude that the results distribution was non-parametric; then, Kruskal-Wallis test was used for multiple comparisons with Dunn's correction and Mann-Whitney test was address to compare two distinct groups.

2. Materials

This section includes specific composition of media used for protocols detailed in past section.

Nematode Growth Media and IPTG plates

The NGM agar contains, in 1 L medium: NaCl (3 g), agar (17 g), peptone (2.5 g), CaC_2 (1M, 1 mL), $MgSO_4$ (1M, 1 mL), KH_2PO_4 buffer (1M, pH=6.0, 25 mL), cholesterol (5 mg

m in ethanol 95%, 1mL), Milli-Qwater (Merck Millipore) water and nystatin (Sigma), to prevent fungal and bacterial contamination. The composition of IPTG plates is the same of NGM plates but substituting nystatin for ampicillin (50 mg/ml) and adding IPTG (0,6 M).

M9 Buffer

The M9 buffer is used at 1X to collect worms from agar plates and to grow worms without food. M9 10X is prepared with the following components (in 1L): $Na_2HPO_4 \times 12H_2O$ (146 g), KH_2PO_4 (30 g), NaCl (5 g) and NH_4Cl (10 g).

Worm Lysis Solution

This solution, after the addition of Proteinase K, is used to disaggregate the worms and obtain genomic DNA. It is stored at 4 °C and its components are: KCl (50 mM), Tris-HCl (10 mM, pH 8.3), $MgCl_2$ (2.5 mM), Triton X-100 (0.45% (v/v), Sigma), Tween 20 (0.45% (v/v), Sigma).

Drop bleach

The Drop Bleach solution is used to kill sensible bacteria or fungi that frequently contaminate worm plates and also to synchronize a small animal population. It is prepared with 500 µL NaClO (commercial bleach), 200 µL NaOH (5 M) and 300 µL ddH_2O.

M13 Buffer

This solution is prepared as in (Guo et al. 2015) and contains: 30 mM Tris, 100 mM NaCl and 10 mM KCl. This solution was considered the basal buffer for calcium imaging experiments, flowing through the chamber with the exception of 30 s pulses of stimulation. To generate stimulation buffer, M13 was modified to also contained 10 mM $CuSO_4$ at pH4.

Fructose solution

To prepare fructose avoidance solution (4 M) was needed: D-Fructose (Merck Millipore, #104007), 1% Red Congo dying and ddH_2O.

RESULTS

RESULTS

1. Establishing an RNAi screen against all *C. elegans* TFs to study monoaminergic specification

1.1. Screen design: Determining the best sensitized background and reporters to study monoaminergic neuron specification

The main aim of this Thesis is to identify *C. elegans* TFs involved in the specification of the different subpopulations of monoaminergic neurons. The strategy we have followed it to perform an RNAi screen against all 876 TFs of *C. elegans* genome (Narasimhan et al. 2015). The RNAi strategy provided us an amenable and effective way to evaluate functional requirement for all these genes.

As described in the introduction, among the different methodologies employed to perform RNAi experiments in *C. elegans*, RNAi by feeding is the best way to analyze a large number of clones. There are two available genome wide RNAi feeding libraries, one generated by Ahringer's laboratory and another by the Vidal's group (Kamath and Ahringer 2003; Rual et al. 2004). As we wanted to perform a complete and fully verified TF RNAi screen we started our work from these two libraries, extracted all TF clones, verified them by sequencing and completed the missing RNAi clones by our own cloning (See section 1.2 for further detail).

The second important feature to consider when performing RNAi experiments in *C. elegans* is that some tissues, especially the nervous system, are refractory to the RNAi effects (Kamath et al. 2000). To circumvent this problem, it has been described that some mutated genes increase the susceptibility of the tissues to RNAi. These mutants are called "enhanced RNAi mutants" (eri) (Zhuang and Hunter 2011). Not all reported eri mutants are equally effective in neurons or even between different neuronal types. Thus, before starting the screen we determined which of the described enhanced RNAi mutants would be best to detect phenotypes in the monoaminergic population.

Previous experiments in the lab were focused on searching a sensitized background that increased the RNAi effect in the DA population. In those experiments, three enhanced RNAi mutants were compared: *nre-1 (hd20), lin-15b (hd126); eri-1 (mg366), lin-15b (n744);* and *rrf-3 (pk1426).* All these genes participate in the RNAi metabolism as described in the introduction. To assess the effect of these mutations in the RNAi effectiveness in DA cells, these mutants were cross with the reporter *otIs199 (cat-2::gfp)*. The gene *cat-2* encodes for tyrosine hydroxylase, the rate limiting enzyme for dopamine synthesis. Thus, *otIs199* reporter specifically labels the DA population. We tested all the strains with RNAi against *gfp* and scored the number of dopaminergic neurons that

remain labeled with GFP. The results showed that the best sensitized background to perform RNAi experiments in the dopaminergic population was *eri-1 (mg366)*, *lin-15b (n744)*, although in the other two strains we also observed a significant reduction in the number of GFP positive neurons (Figure R.1).

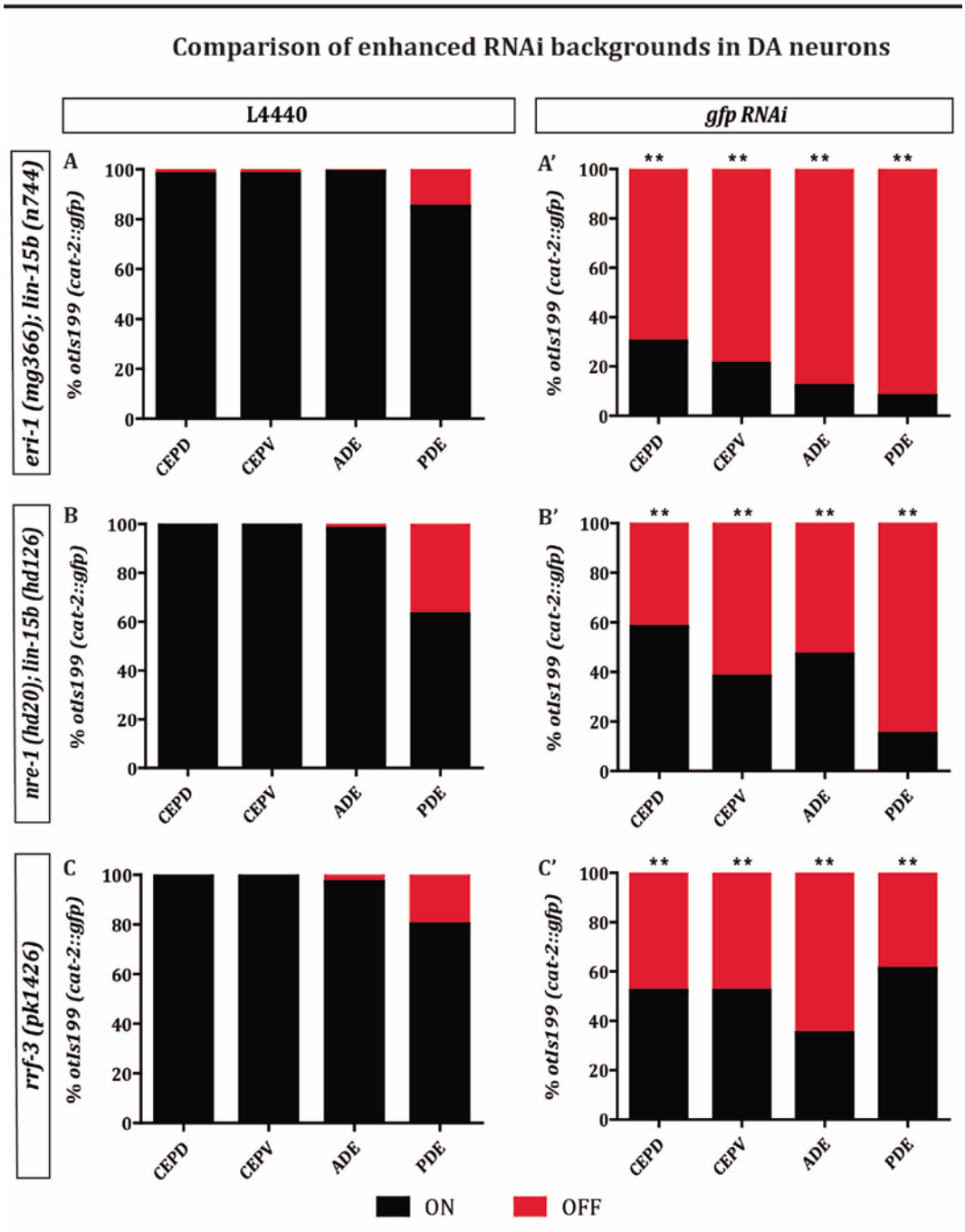

Figure R.1. Comparison of enhanced RNAi backgrounds in DA neurons. All the graphs represent the percentage of DA neurons expressing the *otIs199 (cat-2::gfp)* reporter in three different RNAi enhanced backgrounds: *eri-1 (mg366); lin-15b* (a, a'), *nre-1 (hd20); lin-15b (hd126)* (b, b') and *rrf-3 (pk1426)* (c, c'). Left column graphs correspond to negative control where worms are fed with L4440 empty vector, and right column to *gfp* RNAi scores. Significance was assessed through Fisher exact test two tailed (*) = ($p<0.05$), (**) = ($p<0.01$). n.s. = no significant. n=30 worms.

Next, these backgrounds were tested to evaluate its efficiency in the serotonergic population, the other main MA population in *C. elegans*. In this case we used the reporter strain *zdIs13(tph-1::gfp)* in which the fluorescent protein is expressed only in serotonergic neurons NSM, ADF and HSN. However, *tph-1* gene is located in the same chromosome as *eri-1*, and we excluded the *eri-1 (mg366), lin-15b (n744)* strain from this analysis. The tested RNAi was also against *gfp* and the results showed that the background *rrf-3 (pk1426)* was significantly better than the *nre-1, lin-15b* strain (Figure R.2a', b').

To see if we could further increase the penetrance of the RNAi, we also tested *rrf-3 (pk1426)* in combination with the array *uIs69(unc-119::SID-1)* that drives expression of the transmembrane nucleic acids transporter *sid*-1 in all neurons. SID-1 allows the passive cellular uptake of RNAi and has been described to increase the RNAi effects (Calixto et al. 2010). For that purpose, we built a strain combining both, the *rrf-3* mutation and the array, and we examined the effect of RNAi against *gfp* in the serotonergic population. To score the serotonergic neurons, we used again the *tph-1::gfp* reporter. Unexpectedly, the data indicates that, SID-1 expression did not enhaced RNAi effects. Indeed, panneuronal *sid-1* expression seemed to decrease the efficiency of the RNAi against *gfp* in NSM and ADF, while in HSN we observed no difference between the two backgrounds (Figure R.3c'). Although we do not have a clear explanation for this negative effect, it could be that exacerbated transport of RNAi into non-serotonergic neurons ends up decreasing the availability of RNAi in the serotonergic neurons.

Although the use of RNAi against gfp is a fast way to assess differential effects of RNAi, in the real screen we aim to target TFs that might have direct or indirect role in GFP expression. Thus, to reproduce more faithfully the conditions of the screen we decided to use RNAi clones against some of the TFs already known to be required for 5-HT fate. For the NSM we employed RNAi against *unc-86* (Sze et al. 2002); for ADF we selected as targets *daf-19* and *lim-4* (Xie et al. 2013; Zheng et al. 2005); and for HSN, *unc-86* and *ast-1* (Lloret-Fernández et al. 2018) (Figure R.2 d-f). We used this RNAi clones to compare again the *rrf-3* mutant strain with the combined *rrf-3* mutant with *sid-1* neuronal expression. Our results were similar and we corroborated that *sid-1* expression

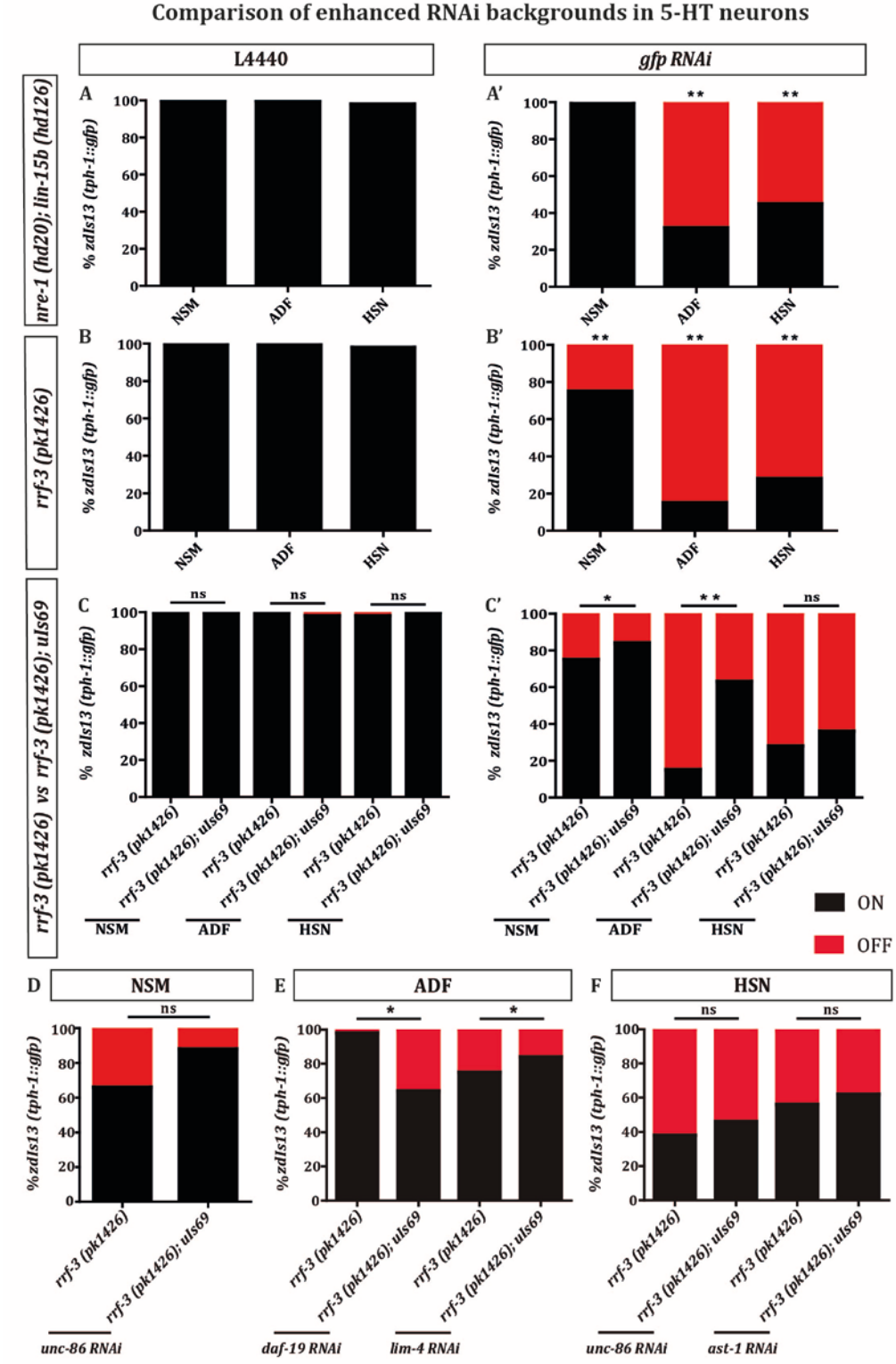
Comparison of enhanced RNAi backgrounds in 5-HT neurons
L4440
gfp RNAi
nre-1 (hd20); lin-15b (hd126)
rrf-3 (pk1426)
rrf-3 (pk1426) vs rrf-3 (pk1426); uIs69
A
A'
B
B'
C
C'
% zdIs13 (tph-1::gfp)
NSM
ADF
HSN
rrf-3 (pk1426)
rrf-3 (pk1426); uIs69
ns
*
**
ON
OFF
D
E
F
%zdIs13 (tph-1::gfp)
unc-86 RNAi
daf-19 RNAi
lim-4 RNAi
ast-1 RNAi

Figure R.2. Comparison of enhanced RNAi backgrounds in 5-HT neurons. All the graphs represent the percentage of 5-HT neurons expressing the *zdIs13 (tph-1::gfp)* reporter in two different RNAi enhanced backgrounds, *nre-1 (hd20); lin-15b (hd126)* (a-a') and *rrf-3 (pk1426)* (b-b'). Left column graphs correspond to negative control, L4440, and right column to *gfp* RNAi scores. Comparison of *rrf-3* mutant background with and without neuronal expression of *sid-1* transporter (*uIs69*) with RNAi against GFP (c-c'). d-f) Comparison of *rrf-3* mutant background with and without neuronal expression of *sid-1* transporter (*uIs69*) with RNAi against known regulators of 5-HT fate. Significance was assessed through Fisher exact test two tailed (*) = ($p<0.05$), (**) = ($p<0.01$). n.s. = no significant. n=30 worms.

does not enhance RNAi effects, with the exception of the *daf-19* phenotype in ADF that is only observed when *sid-1* expression is also in the background (Fig. R.2e). For the rest of the clones analyzed either there was no difference between strains or the expression of *sid-1* in all neurons blocks RNAi effects (such as the effect of *lim-4* RNAi on GFP expression in ADF or *unc-86* RNAi effect on GFP expression in NSM). Thus, in view of these results, we discarded the use of the *sid-1* array for our screening.

As explained in the introduction, our working paradigm proposes that terminal selectors act in combinations, working as TF collectives to directly regulate the expression of neuron-type specific effector genes. We have observed that TF collectives often work in a redundant manner (Lloret-Fernández et al. 2018; Zhang et al. 2014), meaning that when analyzing the expression of specific effector genes in different mutant backgrounds, each gene is more dependent on a specific TF but not on others. For example, *bas-1* (aromatic decarboxylase) expression in HSN is completely gone in *unc-86* mutants while unaffected in *ast-1* mutants while tph-1 expression is lost in both mutant backgrounds (Lloret-Fernández et al. 2018). Thus, it is important that, in our screen, for each neuronal type, we are able to analyze the effect of each RNAi clone in the expression of more than one single gene. In accordance, apart from using fluorescent reporters specific for DA and 5-HT neurons we decided to add in the same sensitized reporter strain a pan-monoaminergic reporter that allowed us to score the whole MA population. Thus, we decided to use *cat-1::gfp*, as *cat-1* is the vesicular monoamine transporter and is expressed by all monoaminergic neurons (Duerr et al. 1999). The use of *cat-1* has the additional advantage of allowing us to study not only DA and 5-HT populations but also tyraminergic and octopaminergic neurons (RIC and RIM) plus the cholinergic neurons VC4/5 that also express *cat-1*.

First, we confirmed that RNAi against *gfp* works well in *rrf-3(pk1426)*, *otIs224 (cat-1::gfp)* strain. All 11 MA neuron types show significant decrease of *gfp* expression being the CEP dopaminergic neurons and the NSM serotonergic neurons the less affected (Figure R.3a, b). Finally, we also tested this strain with TFs known to affect the specification of the MA neurons. For this purpose, apart from the candidates presented

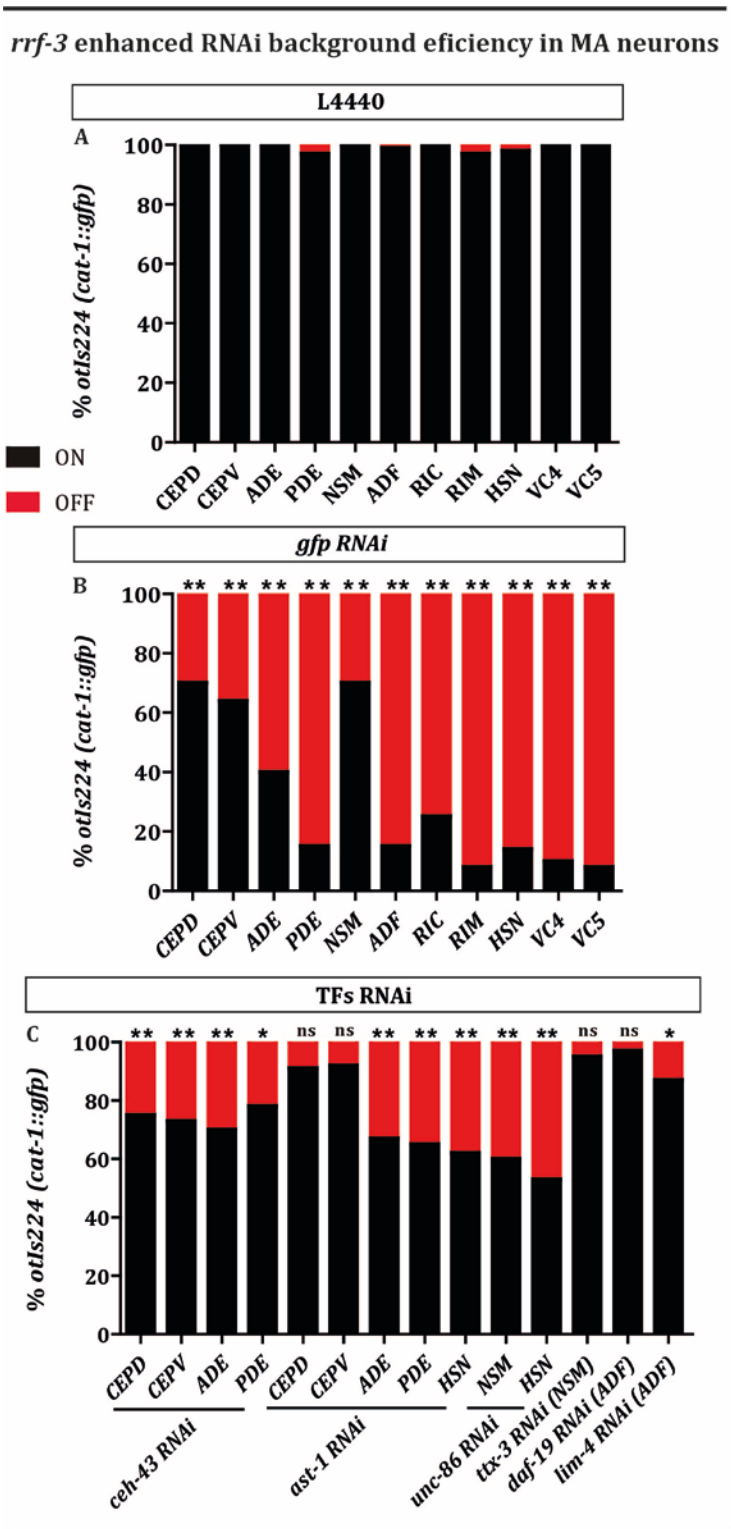

Figure R.3 *rrf-3* enhanced RNAi background eficiency in MA neurons. All the graphs represent the percentage of MA neurons expressing *otIs224 (cat-1::gfp)* reporter (black) and the percentage of undetected fluorescent neurons (red) in a population of 30 worms with *rrf-3 (pk1426)* background. Negative control L4440 (a) and *gfp* RNAi (b) and TFs involved in the specification in MA neurons (c) were compared. Results were analyzed though Fisher exact test two tailed (*) = ($p<0.05$), (**) = ($p<0.01$). n.s. = no significant.

before for the serotonergic neurons, we chose *ast-1* and *ceh-43* for the dopaminergic population (Flames and Hobert 2009; Doitsidou et al. 2013) (Figure R.3c). We did not

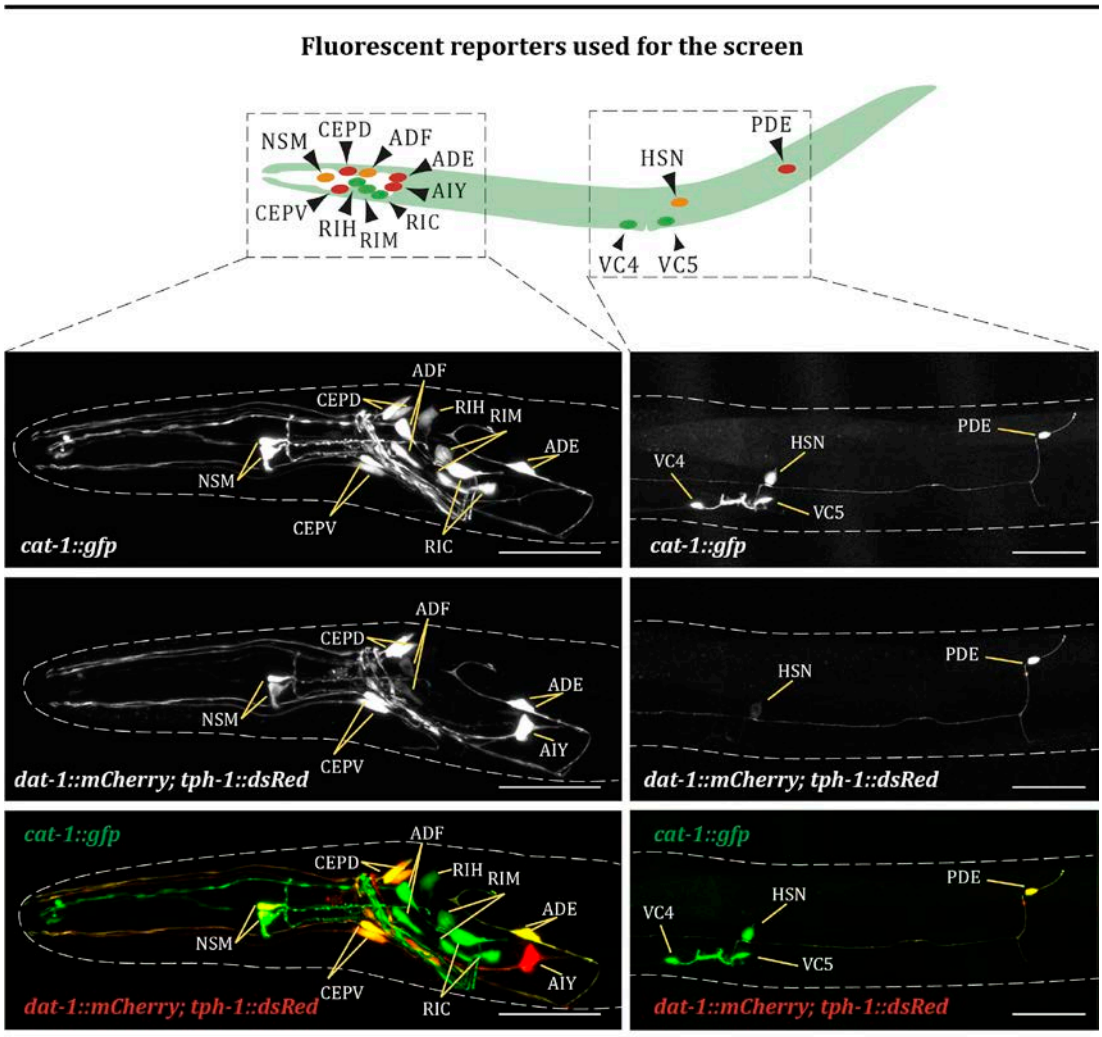

Figure R.4. Fluorescent reporters in the screening strain. The cartoon in top of the panel illustrates the location of MA neurons inside the worm. Neurons labeled in red express *otIs181 (dat-1::mCherry)*; the ones colored in orange express *vsIs97 (tph-1::dsRed)*; and, finally, although all MA neurons express *otIs224 (cat-1::gfp)*, neurons that only express this reporter and not the other two are labeled in green. The real images in the columns correspond with the two squared drawn in the cartoon over the head and the mid body of the worm. The merge of the three reporters can be noticed in images at the bottom. As the *mCherry* fluorescence is stronger than *dsRed*, the yellow color indicating confluence of reporters is more easily detected in dopaminergic neurons. Given *otIs181* reporter was integrated with *ttx-3::mCherry* comarker, AIY neuron is also labeled, only in red, but it was not analyzed in the screen due to its cholinergic nature. Scalebars, 10 µm.

assay any TF for RIC or RIM because there was none previously described for them.

All RNAi against evaluated candidates produced a significant reduction in the percentage of GFP positive neurons in serotonergic and dopaminergic populations with the exception *ast-1* in CEPs. *ast-1* mutants show *cat-1* expression defects in CEPs (Flames and Hobert 2009), thus, it is possible that the partial loss of function produced by RNAi is not sufficient to induce the phenotypes observed with the mutants.

Altogether, to achieve a good balance for our TF RNAi screen that gives sensitivity to detect phenotypes in all MA populations we decided to use the *rrf-3 (pk1426)* allele in the background. Additionally, to maximize the information retrieved from the screen we included three fluorescent reporter constructs in the same strain: *otIs181*, which labels the dopaminergic neurons expressing *mCherry* under the *dat-1* (dopamine reuptaker) promoter; *vsIs97 (tph-1::dsred)*, that identifies serotonergic population; and *otIs224* (*cat-1::gfp*), as a pan-MA marker (Figure R.4).

1.2. Building up a complete and fully verified TF RNAi library

As our goal was to perform an RNAi screen for all TFs in the *C. elegans* genome we first aimed to build a complete and fully verified TF RNAi libraty. Our starting point was the whole genome RNAi libraies built from the Ahringer's and Vidal's laboratories. Both libraries are against the whole genome, the difference being that Ahringer's used genomic DNA whereas Vidal's employed cDNA to build RNAi clones (Kamath and Ahringer 2003; Rual et al. 2004).

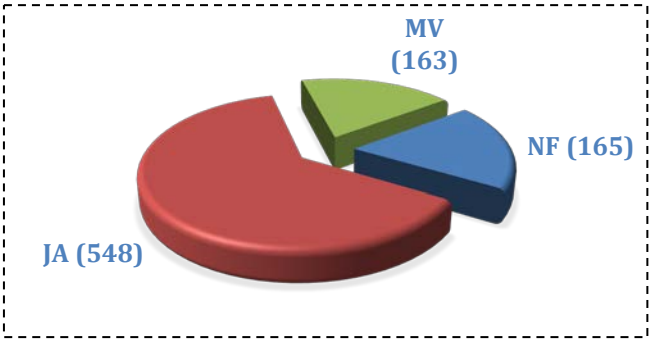

Figure R.5 Composition of our TF RNAi library. The 69.6% of the clones come from Ahringer's library (red), the 18.6% from Vidal's library (green) and finally the 18.8% of the clones were built in our laboratory (blue).

Our first approach was to extract the majority of RNAi clones targeting TFs from Ahringer's library. We sequenced all of them and discarded the ones that were incorrect. TF RNAi clones that were either missing or incorrect from Ahringer's library were selected and sequenced from Vidal's library. Finally, missing clones were done at the laboratory by our own cloning process. In summary our library consists of 876 verified clones targeting all *C.*

elegans TFs: 548 clones from Ahringer, 163 clones from Vidal and 165 cloned in our laboratory (Figure R.5 and A.3 and A.4 for a list of RNAi clones, targets and primers used).

2. Results of the RNAi screen: quantification, observed phenotypes and statistics

2.1. Visible phenotypes

According to their DNA binding domains, *C. elegans* TFs can be divided in 48 TF families (Narasimhan et al. 2015; Reece-Hoyes et al. 2005). To carry out the screen we decided to group our analysis by TF families.

For each clone, 30 worms were mounted in slides and scored under the microscope. We scored every experiment seven days after the worms started feeding on the RNAi bacteria, corresponding to young adult (YA) animals of the first filial generation (F1). It was important to score YA and not younger stages because some monoaminergic neurons, such as HSN, differentiate at this late stage. With the RNAi clones that gave lethal or sterile phenotypes, that precluded us from scoring F1 generation, we scored three days after feeding corresponding to the first generation of fed worms (P0). In both cases, for each RNAi clone we repeated the scores twice in different technical replicates. In each set of experiments both the empty vector (L4440) and the RNAi against *ast-1* were scored as negative and positive controls to verify RNAi plates were in good conditions.

A TF was considered a hit when its RNAi phenotype was present at least in 10% of the population and when it was found in both replicates. In cases where the RNAi clone showed effect only once, we carried out a third replicate and considered a positive hit when two out of three experiments produced the phenotype.

The phenotypes detected were mainly the following: 1) the most obvious was the absence of some or all the fluorescent reporters in one or more monoaminergic neuron subtypes indicating the target TF of the RNAi clone is required for the generation, specification or survival of that neuron type, we call this phenotype "MISSING" (Figure R.6a). 2) In some cases, fluorescent expression was still detected but it was clearly reduced. This phenotype was considered “FAINT”. 3) We also found examples of miss-location and abnormal migration of cells, we termed this phenotype "MIGRATION" (Figure R.6b). 4) Regarding morphology, we also noticed that some RNAi gave aberrant dendrite branching or axon pathfinding defects (Figure R.6c), proper formation of synapytic connections is fundamental for the correct functions of the neurons, we termed this phenotype "MORPHOLOGY". 5) We also found in some cases increased

number of fluorescently labeled cells, we named this phenotype "ECTOPIC" (Figure R.6d).

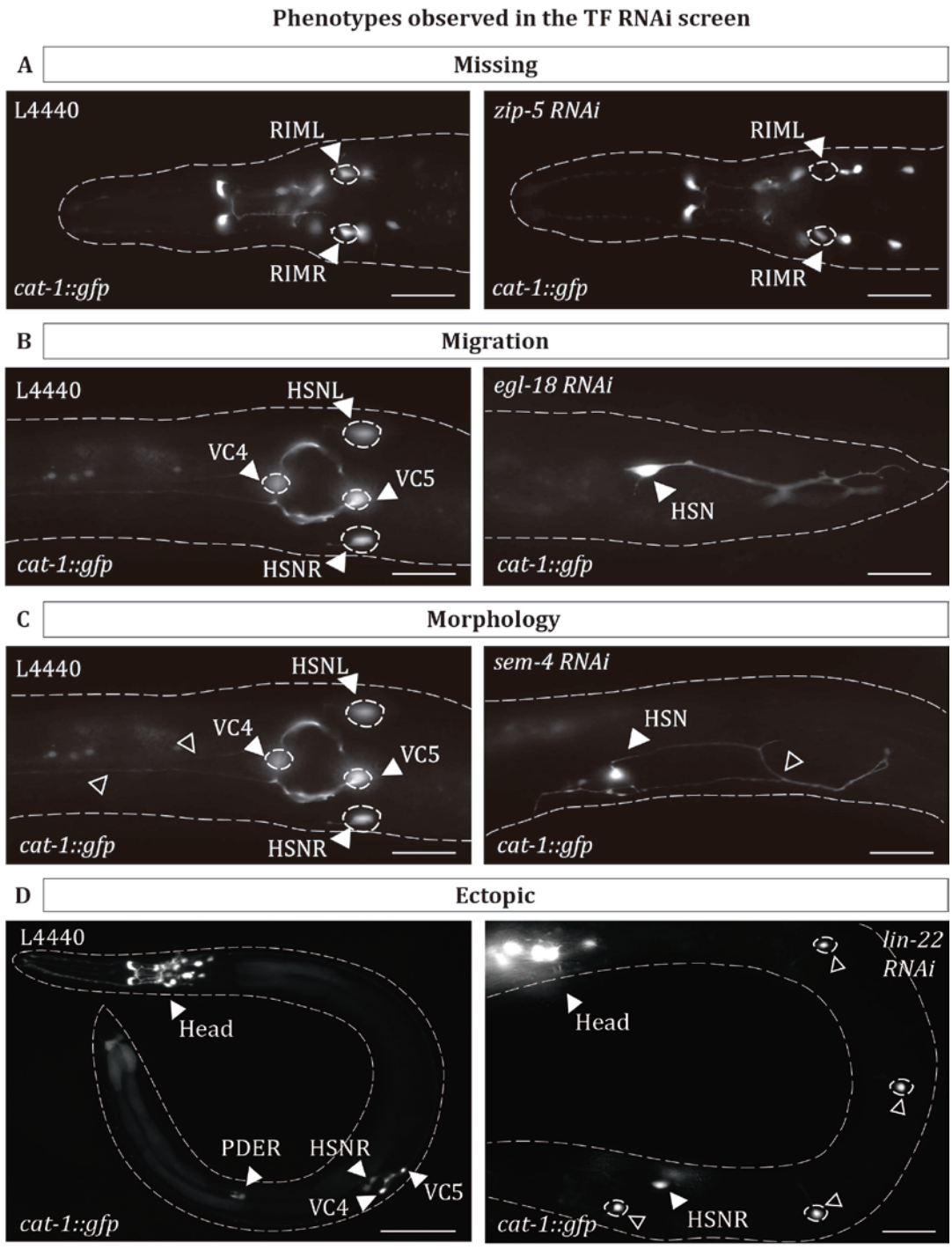

Figure R6. Phenotypes observed in our TF RNAi screen. a) Example of missing fluorescence phenotype in RIML neuron (arrowhead) observed with *zip-5 RNAi*. b) Abnormal migration of the HSN neuron, the picture in the left shows the normal location of the neuron near the vulva and next to VC4/5s neurons. The picture in the right presents the neuron located in the tip of the tail, with abnormal axonal projections produced by *egl-18* RNAi. c) Example of defective HSN morphology. Normal HSN projects the dendrite to the head (black arrowhead, left picture), in contrast *sem-4* RNAi leads to projections towards the tail and branching defects (right picture). d) Ectopic phenotype: *lin-22* RNAi leads to fluorescent reporter expression in four extra neurons (pointed by black arrowheads Scale bars a-c, 20 µm; d, 50 µm.

Additionally, other phenotypes, not necessarily linked to MA fate can be observed without the need of specific fluorescent markers. These "easy-to-spot" phenotypes have been reported in different RNAi screens. In our screen we also detected a variety of classical visible phenotypes (Schindelman et al. 2011) such as uncoordinated animals, dumpy, smaller in size, lethal, egg laying defective, etc (Table R.1). Visible phenotypes observed in our screen matched those already reported and validate the setup of our RNAi screen.

Table R.1. Visible Phenotypes

Gene Name	DBD	Phenotype	Previously Reported
swsn-7	ARID - RFX	Emb	Yes
let-526	ARID/BRIGHT	Let	Yes
attf-6	AT Hook x2	Let	Yes
lin-15B	AT Hook x2, ZF - THAP	Muv, Gro, Pvl	Yes
hmg-11	AT Hook x3	Unc, Prz	Yes
hmg-12	AT Hook x7	Gro	Yes
bar-1	β-catenin/ARmadillo	Increased male ratio	Yes
wrm-1	β-catenin/ARmadillo	Emb	Yes
hlh-1	bHLH	Egl	Yes
hlh-8	bHLH	Egl	Yes
atf-5	bZIP	Bmd, Sma	Yes
fos-1	bZIP	Emb	Yes
zip-10	bZIP	Emb, Ste	No
atf-2	bZIP - 2 domains	Bmd	Yes
let-607	bZIP (CREB)	Let	Yes
grh-1	CP2	Gro	Yes
lag-1	CSL	Emb	Yes
lin-54	CxC	Emb	Yes

pal-1	HD - HOX	Emb	Yes
php-3	HD - HOX	Emb	Yes
lin-11	HD - LIM	Muv	Yes
ceh-6	HD - POU	Prz	Yes
unc-86	HD - POU	Unc	Yes
unc-30	HD - PRD, bHLH	Unc	Yes
pax-3	HD - PRD - FULL	Emb, Unc	Yes
unc-39	HD - SIX	Unc	Yes
ceh-20	HD - TALE	Emb, Egl	Yes
unc-62	HD - TALE	Dpy*	Yes
pop-1	HMG box	Emb	Yes
sem-2	HMG box	Egl	Yes
sox-2	HMG box	Emb, Egl	Yes
swsn-3	HMG box	Emb, Lon	Yes
hmg-1.2	HMG box - 2 domains	Emb	Yes
hmg-5	HMG box - 2 domains	Let	Yes
ekl-4	MYB	Emb	Yes
swsn-1	MYB	Emb	Yes
cdc-5L	MYB - 2 domains	Emb	Yes
snpc-4	MYB - 5 domains	Emb	Yes
npax-1	Paired Domain - NPAX	Gro	No
npax-2	Paired Domain - NPAX	Gro, Unc	No
npax-3	Paired Domain - NPAX	Gro	Yes
npax-4	Paired Domain - NPAX	Gro	No
gmeb-2	SAND	Muv	No
F19F10.9	SART-1	Emb	Yes
tbp-1	TBP	Emb	Yes
let-381	WH - Fork Head	Dpy	Yes
bed-3	ZF - BED	Emb	Yes
lect-2	ZF - C2H2 - 1 finger	Lon	Yes
lir-1	ZF - C2H2 - 1 finger	Emb	Yes
lir-2	ZF - C2H2 - 1 finger	Sma	No
lir-3	ZF - C2H2 - 1 finger	Sma	No
repo-1	ZF - C2H2 - 1 finger	Emb	Yes
somi-1	ZF - C2H2 - 1 finger	Emb, Egl	Yes
W04D2.4	ZF - C2H2 - 1 finger	Emb	Yes
Y56A3A.18	ZF - C2H2 - 1 finger	Emb	Yes
lin-13	ZF - C2H2 - 15 fingers	Let	Yes
R10E4.11	ZF - C2H2 - 2 fingers	Unc	No

sdz-38	ZF - C2H2 - 2 fingers	Unc	No
C16A3.4	ZF - C2H2 - 3 fingers	Emb	Yes
die-1	ZF - C2H2 - 3 fingers	Emb	Yes
pat-9	ZF - C2H2 - 3 fingers	Emb	Yes
sptf-3	ZF - C2H2 - 3 fingers	Emb	Yes
blmp-1	ZF - C2H2 - 4 fingers	Dpy	Yes
egl-43	ZF - C2H2 - 4 fingers	Bmd, Muv	Yes
ztf-7	ZF - C2H2 - 4 fingers	Sma	Yes
zag-1	ZF - C2H2 - 4 fingers, HD - ZFHD	Emb	Yes
lsl-1	ZF - C2H2 - 5 fingers	Gro	Yes
mep-1	ZF - C2H2 - 5 fingers	Lva	Yes
tra-1	ZF - C2H2 - 5 fingers	Unc	Yes
C27A12.2	ZF - C2H2 - 6 fingers	Unc	No
F26F4.8	ZF - C2H2 - 6 fingers	Rup	No
let-391	ZF - C2H2 - 6 fingers	Let, Muv	Yes
sup-37	ZF - C2H2 - 6 fingers	Muv	No
sem-4	ZF - C2H2 - 7 fingers	Egl, Pvl	Yes
sma-9	ZF - C2H2 - 7 fingers	Sma	Yes
spr-3	ZF - C2H2 - 7 fingers	Sma	Yes
hbl-1	ZF - C2H2 - 9 fingers	Dpy	Yes
dmd-5	ZF - DM	Emb	Yes
egl-18	ZF - GATA	Egl, Ste	Yes
elt-2	ZF - GATA	Emb	Yes
elt-4	ZF - GATA	Egl, Unc	No
elt-6	ZF - GATA	Egl, Unc	Yes
elt-1	ZF - GATA - 2 domains	Emb	Yes
egl-27	ZF - GATA, MYB	Egl, Pvl	Yes
lin-40	ZF - GATA, MYB	Dpy	Yes
nhr-141	ZF - NHR	Emb	No
nhr-204	ZF - NHR	Lon	No
nhr-23	ZF - NHR	Let, Dpy	Yes
nhr-25	ZF - NHR	Sma, Gro	Yes
nhr-31	ZF - NHR	Let, Gro	Yes
nhr-48	ZF - NHR	Sma	Yes
nhr-52	ZF - NHR	Unc	No
nhr-58	ZF - NHR	Unc, Egl	No
nhr-67	ZF - NHR	Egl, Unc	Yes
nhr-97	ZF - NHR	Muv	Yes
odr-7	ZF - NHR	Unc	Yes

sex-1	ZF - NHR	Unc	Yes
unc-55	ZF - NHR	Unc	Yes
nhr-219	ZF – NHR – 2 domains	Gro	No

Table R.1 Visible phenotypes observed in the TFs RNAi screen. TFs are grouped by their DNA-binding domain (DBD). Abbreviations: Emb (embryonic lethal), Ste (sterile), Gro (slow postembryonic growth), Lva (larval arrest), Let (larval lethal), Bmd (body morphological defects), Dpy (dumply), Egl (egg-laying defective), Lon (long), Mlt (molt defects), Muv (multivulva), Prz (paralyzed), Pvl (protruding vulva), Unc (uncoordinated).

We compared our result of 97 TFs with visual phenotypes with previous RNAi screenings whose results were available. Simmer et al. 2003 and Kamath et al 2003 performed whole genome RNAi screens (Kamath and Ahringer 2003) (Simmer et al. 2003). The first used in their screen *rrf-3 (pk1426)* background, whereas the second was conducted in N2 background. We extracted from all of their hits the transcription factors from which they detected any visual phenotype. We noticed that Simmer and colleges described phenotype for up to 114 TFs, 17 genes more than our list of 97 visual phenotypes; whereas Kamath and colleges detected 79 TFs whose RNAi produced any visual phenotype. Surprisingly, the number of our 97 TFs that overlapped with the other two data sets was 51 TFs, this is 40 TFs in common with Simmer screen and 37 with Kamath screen (52.6% of the total phenotypes we reported) (Figure R.7). However, the percentage of overlapping results in the two-by-two comparison is low: our results have 31% in common with Simmer results and 26% with Kamath; meanwhile, Simmer and Kamath overlap in 51%. This difference could be due to RNAi library differences. While we have previously verified our library, they employed the Ahringer's library with no previous verification and it has been determined that in Ahringer's library 17.54% need to be reannotated (Qu et al. 2011). On the other hand, it is possible that our number of visible phenotypes is lower because the detection of them was not the main goal of our screen and thus, if these phenotypes were not very obvious, we might have missed them. Moreover, the difference could also be a matter of the variability among RNAi experiments. This is a common issue and will be described in more detail in the discussion.

Next, we also decided to consult in WormBase (W257 version) for comparison. We downloaded the RNAi phenotypes of our list of 97 TFs with SimpleMine tool and interestingly, only 16 of them were never pinpointed with any visual phenotype (Table R.1). The fact that 83% of our detected visual phenotypes had been previously described through RNAi experiments is an indication that the conditions of our screen were correct.

Perhaps the 16 newly described phenotypes could be the first step towards the characterization of new roles for those TFs.

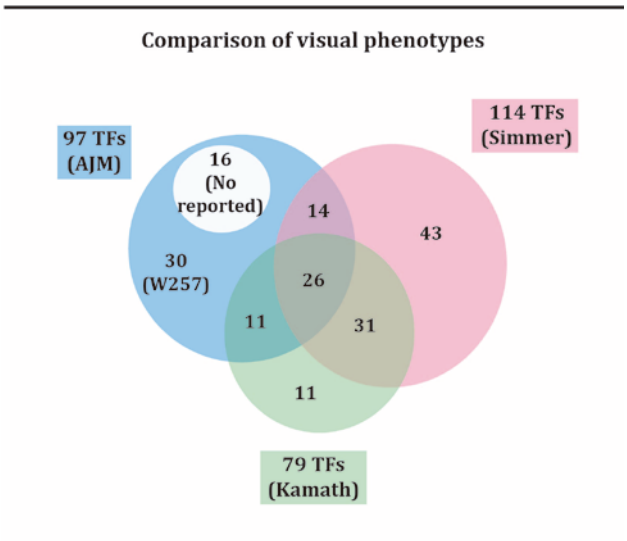

Figure R.7 Comparison of visible phenotypes detected in different RNAi screens. 97 RNAi clones with visible phenotypes from our screen are represented by the blue circle (AJM). Data of TFs from Simmer and Kamath RNAi screens are represented in pink and green circles respectively (extracted from Simmer et al 2003 and Kamath et al 2003). All data sets share 26 overlapping clones. Our screen shares 40 clones with Simmer and 37 with Kamath. There are 30 clones from our screen whose phenotype is confirmed from WormBase (W257 version). The white circle represents visible phenotypes form our screen not previously

2.2. Validation of the RNAi screen strategy with known modulators of MA fate

Apart from the previously reported visual phenotypes, we observed more specific phenotypes under the fluorescent microscope (as described in Figure R.6). Table R.2 is the collection of all the information we obtained for the RNAi clones for TFs in regard to their role in the monoaminergic neuron specification. Some of them generate more than one phenotype or in more than one monoaminergic neuron subpopulation.

Table R.2. TF RNAi screen results

Gene Name	DBD	Neuron affected	Phenotype	Fluorescent expression		
				cat-1 ::gfp	***dat-1:: mCherry***	***tph-1 ::dsred***
wrm-1	β-catenin /Armadillo	VCs	Missing fluorescence	48/60	n.e.	n.e.
aha-1	bHLH	n.a.	Ectopic cells	+	+	-

aha-1	bHLH	PDE	Morphology	+	+	n.e.
ahr-1	bHLH	n.a.	Ectopic cells	+	-	-
hlh-14	bHLH	ADF	Missing fluorescence	18/60	n.e.	13/60
hlh-14	bHLH	HSN	Migration	+	n.e.	+
hlh-3	bHLH	HSN	Missing fluorescence	45/60	n.e.	40/60
lin-22	bHLH	n.a.	Ectopic cells	+	-	-
lin-32	bHLH	PDE	Missing fluorescence	5/60	5/60	n.e.
ref-1	bHLH - 2 domains	n.a.	Ectopic cells	+	-	-
C32E8.1	bZIP	CEPV, CEPD, ADE, PDE	Missing fluorescence	49/60	41/60	n.e.
fos-1	bZIP	n.a.	Ectopics in tail	+	-	-
xbp-1	bZIP	HSN	Aberrant axon	+	n.e.	+
zip-10	bZIP	ADF	Missing fluorescence	42/60	n.e.	42/60
zip-5	bZIP	RIC/RIM	Missing fluorescence	82/120	n.e.	n.e.
zip-6	bZIP	RIC/RIM	Missing fluorescence	100/120	n.e.	n.e.
dro-1	CBF	CEPV, CEPD, ADE	Missing fluorescence	49/60	49/60	n.e.
nfyb-1	CBF	RIC/RIM	Missing fluorescence	104/120	n.e.	n.e.
cey-1	COLD BOX	RIC/RIM	Missing fluorescence	106/120	n.e.	n.e.
lin-28	COLD BOX	HSN	Missing fluorescence	42/60	n.e.	42/60
lin-28	COLD BOX	PDE	Missing fluorescence	10/60	10/60	n.e.
lin-28	COLD BOX	VCs	Missing fluorescence	50/60	n.e.	n.e.
lag-1	CSL	ADF	Missing fluorescence	12/60	n.e.	5/60
ceh-44	HD - CUT	PDE	Missing fluorescence	40/60	40/60	n.e.
ceh-12	HD - HOX	RIC/RIM	Missing fluorescence	96/120	n.e.	n.e.
ceh-13	HD - HOX	RIC/RIM	Missing fluorescence	92/120	n.e.	n.e.
ceh-16	HD - HOX	n.a.	Ectopic cells*	+	-	-
ceh-16	HD - HOX	PDE	Missing fluorescence	47/60	47/60	n.e.

lin-39	HD - HOX	VCs	Missing fluorescence	10/60	n.e.	n.e.
egl-5	HD - HOX	HSN	Missing fluorescence	32/60	n.e.	32/60
nob-1	HD - HOX	HSN	Missing fluorescence	24/60	n.e.	24/60
nob-1	HD - HOX	n.a.	Ectopics in tail	+	+	-
vab-7	HD - HOX	RIC/RIM	Missing fluorescence	100/120	n.e.	n.e.
lim-4	HD - LIM	ADF	Missing fluorescence	45/60	n.e.	40/60
lim-7	HD - LIM	NSM	Aberrant axon	+	n.e.	+
ceh-27	HD - NK	ADF	Missing fluorescence	52/60	n.e.	51/60
ceh-27	HD - NK	RIC/RIM	Missing fluorescence	96/120	n.e.	n.e.
ceh-31	HD - NK	n.a.	Ectopic cells	+	+	-
ceh-43	HD - NK	CEPV, CEPD, ADE, PDE	Missing fluorescence	45/60	39/60	n.e.
mls-2	HD - NK	PDE	Missing fluorescence	50/60	50/60	n.e.
vab-15	HD - NK	PDE	Missing fluorescence	32/60	32/60	n.e.
unc-86	HD - POU	HSN	Missing fluorescence	18/60	n.e.	12/60
unc-86	HD - POU	NSM	Missing fluorescence	40/60	n.e.	40/60
unc-86	HD - POU	PDE, ADE	Ectopic cells	+	+	-
ceh-36	HD - PRD	RIC/RIM	Missing fluorescence	96/120	n.e.	n.e.
ceh-37	HD - PRD	ADF	Missing fluorescence	50/60	n.e.	50/60
unc-4	HD - PRD	VCs	Missing fluorescence	10/60	n.e.	n.e.
pax-3	HD - PRD - FULL	ADF	Missing fluorescence	50/60	n.e.	50/60
pax-3	HD - PRD - FULL	HSN	Aberrant axon	+	n.e.	+
pax-3	HD - PRD - FULL	VCs	Missing fluorescence	10/60	n.e.	n.e.
vab-3	HD - PRD - FULL	n.a.	Ectopics in head	+	+	-
vab-3	HD - PRD - FULL	CEPV, ADE, PDE	Missing fluorescence	47/60	49/60	n.e.

ceh-32	HD - SIX	n.a.	Ectopics in head	-	+	-
ceh-20	HD - TALE	ADE, PDE	Missing fluorescence	43/60	44/60	n.e.
ceh-20	HD - TALE	n.a.	Ectopics in head	+	+	-
ceh-20	HD - TALE	VCs	Missing fluorescence	16/60	n.e.	n.e.
unc-62	HD - TALE	ADE, PDE	Missing fluorescence	40/60	40/60	n.e.
unc-62	HD - TALE	CEPV, CEPD	Missing fluorescence	50/60	51/60	n.e.
unc-62	HD - TALE	n.a.	Ectopics in head and tail	+	-	-
sem-2	HMG	HSN	Missing fluorescence	26/60	n.e.	22/60
mef-2	MADS BOX	CEPV, CEPD, ADE	Missing fluorescence	53/60	53/60	n.e.
sma-3	MH1 - SMAD	RIC/RIM	Missing fluorescence	98/120	n.e.	n.e.
cep-1	p53	CEPV, CEPD, ADE	Missing fluorescence	52/60	52/60	n.e.
sta-1	STAT	RIC/RIM	Missing fluorescence	102/120	n.e.	n.e.
tbx-11	T - box	n.a.	Ectopics in head	+	-	-
tbx-30	T - box	RIC/RIM	Missing fluorescence	98/120	n.e.	n.e.
lin-14	unknown	HSN	Missing fluorescence	6/60	n.e.	6/60
lin-14	unknown	NSM	Missing fluorescence	48/60	n.e.	48/60
lin-14	unknown	VCs	Missing fluorescence	40/60	n.e.	n.e.
ham-1	WH	CEPV, CEPD	Missing fluorescence	25/60	25/60	n.e.
ast-1	WH - ETS	ADE, PDE	Missing fluorescence	40/60	34/60	n.e.
ast-1	WH - ETS	HSN	Missing fluorescence	32/60	n.e.	29/60
let-381	WH - Fork Head	NSM	Aberrant axon	+	n.e.	+
unc-130	WH – Fork Head	ADF	Missing fluorescence	49/60	n.e.	46/60
bed-3	ZF - BED	PDE	Missing fluorescence	40/60	40/60	n.e.
egl-46	ZF - C2H2 – 1 finger	HSN	Missing fluorescence	50/60	n.e.	50/60

dxbp-1	ZF - C2H2 – 1 finger	CEPV	Missing fluorescence	50/60	50/60	n.e.
lin-26	ZF - C2H2 – 1 finger	PDE	Missing fluorescence	47/60	47/60	n.e.
pqn-21	ZF - C2H2 – 1 finger	ADF	Missing fluorescence	49/60	n.e.	49/60
R05D3.3	ZF - C2H2 – 1 finger	ADF	Missing fluorescence	52/60	n.e.	52/60
R05D3.3	ZF - C2H2 – 1 finger	RIC/RIM	Missing fluorescence	104/120	n.e.	n.e.
sup-35	ZF - C2H2 – 1 finger	CEPV	Missing fluorescence	54/60	54/60	n.e.
dnj-17	ZF - C2H2 – 2 fingers	CEPV, CEPD	Missing fluorescence	50/60	50/60	n.e.
scrt-1	ZF - C2H2 – 2 fingers	RIC/RIM	Missing fluorescence	100/120	n.e.	n.e.
sdc-1	ZF - C2H2 – 2 fingers	RIC/RIM	Missing fluorescence	102/120	n.e.	n.e.
odd-2	ZF - C2H2 – 3 fingers	ADF	Missing fluorescence	54/60	n.e.	54/60
pqm-1	ZF - C2H2 – 3 fingers	RIC/RIM	Missing fluorescence	92/120	n.e.	n.e.
ref-2	ZF - C2H2 – 3 fingers	VCs	Missing fluorescence	40/60	n.e.	n.e.
ztf-8	ZF - C2H2 – 3 fingers	CEPV	Missing fluorescence	50/60	50/60	n.e.
egl-43	ZF - C2H2 – 4 fingers	RIC/RIM	Missing fluorescence	100/120	n.e.	n.e.
lin-48	ZF - C2H2 – 4 fingers	CEPD	Missing fluorescence	54/60	54/60	n.e.
row-1	ZF - C2H2 – 5 fingers	CEPV	Missing fluorescence	49/60	49/60	n.e.
tra-1	ZF - C2H2 – 5 fingers	VCs	Missing fluorescence	20/60	n.e.	n.e.
C27A12.2	ZF - C2H2 – 6 fingers	RIC/RIM	Missing fluorescence	102/120	n.e.	n.e.
sem-4	ZF - C2H2 - 7 fingers	HSN	Missing fluorescence	39/60	n.e.	37/60
spr-3	ZF - C2H2 - 7 fingers	HSN	Aberrant axon	+	n.e.	+
hbl-1	ZF - C2H2 – 9 fingers	HSN	Missing fluorescence	35/60	n.e.	35/60
hbl-1	ZF - C2H2 - 9 fingers	PDE	Aberrant axon	+	+	n.e.
hbl-1	ZF - C2H2 – 9 fingers	PDE	Missing fluorescence	23/60	23/60	n.e.
flh-2	ZF - FLYWCH	ADF	Missing fluorescence	53/60	n.e.	50/60
flh-1	ZF - FLYWCH	ADF	Missing fluorescence	48/60	n.e.	48/60

egl-18	ZF - GATA	HSN	Migration	+	n.e.	+
egl-18	ZF - GATA	HSN	Missing fluorescence	48/60	n.e.	50/60
pha-4	ZF - GATA	HSN	Missing fluorescence	50/60	n.e.	50/60
egl-27	ZF - GATA, MYB	CEPV, CEPD	Aberrant axon	+	+	n.e.
egl-27	ZF - GATA, MYB	HSN	Aberrant axon	+	n.e.	+
lin-40	ZF - GATA, MYB	ADE, PDE	Aberrant axon	+	+	n.e.
lin-40	ZF - GATA, MYB	HSN	Aberrant axon	+	n.e.	+
lin-40	ZF – GATA, MYB	VCs	Missing fluorescence	14/60	n.e.	n.e.
nfx-1	ZF - NF - X1	RIC/RIM	Missing fluorescence	102/120	n.e.	n.e.
nrh-148	ZF - NHR	RIC/RIM	Missing fluorescence	102/120	n.e.	n.e.
nhr-157	ZF- NHR	RIC/RIM	Missing flurescence	104/120	n.e.	n.e.
nhr-2	ZF - NHR	RIC/RIM	Missing fluorescence	98/120	n.e.	n.e.
nhr-223	ZF- NHR	CEPV, CEPD	Missing fluorescence	50/60	50/60	n.e.
nhr-61	ZF - NHR	VCs	Missing fluorescence	46/60	n.e.	n.e.
sex-1	ZF - NHR	ADF	Missing fluorescence	44/60	n.e.	44/60
sex-1	ZF - NHR	HSN	Missing fluorescence	33/60	n.e.	33/60
unc-55	ZF- NHR	CEPV, CEPD	Missing fluorescence	54/60	54/60	n.e.

Table R.2. TFs RNAi screening results. TF RNAi clones with significant phenotype. Table is grouped by DBD. The last three columns from the right represent the proportion of neurons that remain with each reporter after RNAi treatment. For technical reasons, RIC and RIM neurons were scored together and also VC4 and VC5 are in the same category as "VCs". n = 30 animals/clone. n.a. = not asigned. n.e. = not expressed. "+" = positive expression. "-" = negative expression.

After the screen was completed, we obtained 91 candidates that play a role in monoaminergic specification. This number represents around 10% of all *C. elegans* TFs (that could be involved in the control MA neurons that represent around 7% of the total number of neurons in *C. elegans* hermaphrodite). The first and most obvious conclusion is that none of the RNAi TF clones affected the expression of the reporter genes in all MA subtypes. This was expected, as we have determined from our previous studies that DA

and 5-HT neuronal classes are regulated through different terminal selector codes (Doitsidou et al. 2013; Lloret-Fernández et al. 2018; Zhang et al. 2014). The second conclusion we made is that, in most of the cases, when the expression of one gene is affected in a specific neuronal type, (e.g *cat-1::gfp* gone) the other reporter gene is also affected (e.g concomitant *dat-1::mcherry* expression affected). This observation supports our model of co-regulation of effector genes by terminal selectors (see introduction). Alternatively, it might also indicate that the RNAi produces lineage or survival defects and cell is not present. To distinguish between these two possibilities, we will perform further experiments on selected candidates (see sections 3 and 4 of the results).

Next, we analyzed how many of the TFs already reported to have a role in MA specification were retrieved from our screen. As explained in the introduction DA terminal differentiation requires the combination of *ceh-20*, *ceh-43* and *ast-1* TFs (Doitsidou et al. 2013; Flames and Hobert 2009). Additionally, other TFs produce either defects or excess of DA neurons due to lineage defects (e.g *unc-86*, *lin-32*, *ham-1*, *vab-3*) (Doitsidou et al. 2008). Regarding 5-HT specification, a role for *daf*-19 and *lim-4* TFs has been reported for ADF (Zheng et al. 2005; Xie et al. 2013), *unc-86* for NSM (Zhang et al. 2014) and *unc-86, sem-4, ast-1, egl-46, hlh-3* and *egl-18* among other for HSN (Lloret-Fernández et al. 2018).

Table R.3 summarizes TFs known to have a role in MA specification and the phenotypes observed in our screen. The number of false negatives is 17%, which is relatively low compared to other RNAi screens where this rate can reach from 25% to 45% (Rual et al. 2004). Although our number of false negatives is lower than other screens, it is still high; it indicates that we are losing important information with this strategy. The source of this problem is mainly that the RNAi is a downregulation of gene expression that might not be sufficient to generate a phenotype. In the future, alternative strategies such as forward genetic screens could be undertaken to complement our results.

Table R.3 TFs with previous known phenotype

Gene Name	DBD	Neuron affected	Phenotype	Confirmed	Reference
hlh-2	bHLH	HSN	Missing flurescence	No	(Portman and Emmons 2000)
hlh-3	bHLH	HSN	Missing fluorescence	Yes	(Lloret-Fernández et al. 2018)
lin-32	bHLH	PDE	Missing fluorescence	Yes	(Portman and Emmons 2000)
egl-5	HD - HOX	HSN	Missing fluorescence	Yes	(Singhvi, Frank, and Garriga 2008)
lin-39	HD - HOX	VCs	Missing fluorescence	Yes	(Potts, Wang, and Cameron 2009)

lim-4	HD - LIM	ADF	Missing fluorescence	Yes	(Zheng et al. 2005)
ceh-43	HD - NK	ADE, CEPV, PDE	Missing fluorescence	Yes	(Doitsidou et al. 2013)
unc-4	HD - POU	VCs	Missing fluorescence	Yes	(Zheng et al. 2013)
unc-86	HD - POU	HSN, NSM	Missing fluorescence	Yes	(Lloret-Fernández et al. 2018)
ceh-20	HD - TALE	CEPs, ADE, PDE, VCs	Missing fluorescence	Yes	(Doitsidou et al. 2013; Potts, Wang, and Cameron 2009)
tbx-2	T - box	HSN	Missing fluorescence	No	(Singhvi, Frank, and Garriga 2008)
ham-1	WH	CEPs	Missing fluorescence	Yes	(Doitsidou et al. 2008)
ast-1	WH - ETS	CEPs, ADE, PDE, HSN	Missing fluorescence	Yes	(Lloret-Fernández et al. 2018; Flames and Hobert 2009)
daf-19	WH - RFX	ADF	Missing fluorescence	No	(Xie et al. 2013)
egl-46	ZF - C2H2 - 1 finger	HSN	Missing fluorescence	Yes	(Lloret-Fernández et al. 2018)
zag-1	ZF - C2H2 - HD	HSN	Missing fluorescence	No	(Clark and Chiu 2003)
sem-4	ZF - C2H2 - 7 fingers	HSN	Missing fluorescence	Yes	(Lloret-Fernández et al. 2018)
egl-18	ZF - GATA	HSN	Missing fluorescence	Yes	(Lloret-Fernández et al. 2018)

Table R.3. RNAi clones with known MA phenotypes. The column "Confirmed" indicates if we obtained the same observation or not as previously reported. According to this table we could estimate a 22% false negative rate in our screen (4/18).

The relative low rate of false negatives as well as the number of candidates obtained, such us our 97 visible phenotypes and 91 TFs involved in MA development, validate our strategy. Thus, we next aimed to globally analyze the results of our screen. First, we provide a description of retrieved phenotypes by TF families and then we explain the most common phenotypes detected.

2.3. Global analysis of TF famillies involved in MA specification

The TF families more represented in our results are: Homeodomain (HD) with 24 TFs with an associated RNAi phenotype (23.76% of HD family); basic helix loop helix (bHLH) 7 TFs with an associated RNAi phenotype (16.66% of the family); bZip 6 TFs with an associated RNAi phenotype (16.66% of the family); Zinc Finger (ZF-C2H2) 21 TFs

with an associated RNAi phenotype (10.82% of the family) and Zinc finger nuclear hormone receptor (ZF-NHR) 7 TFs with an associated RNAi phenotype (2.57% of the family) (Figure R.8).

Figure R.8 Results by TF family

TF Family	Nº members	TF Family	Nº members
β-catenin /Armadillo	1	**T - box**	2
bHLH	7	**unknown**	1
bZIP	6	**WH**	1
CBF	2	**WH - ETS**	1
COLD BOX	2	**WH – Fork Head**	2
CSL	1	**ZF - BED**	1
HD	24	**ZF - C2H2**	21
HMG	1	**ZF - NF - X1**	1
MADS BOX	1	**ZF - NHR**	7
MH1 - SMAD	1	**ZF - FLYWCH**	2
p53	1	**ZF - GATA**	4
STAT	1		

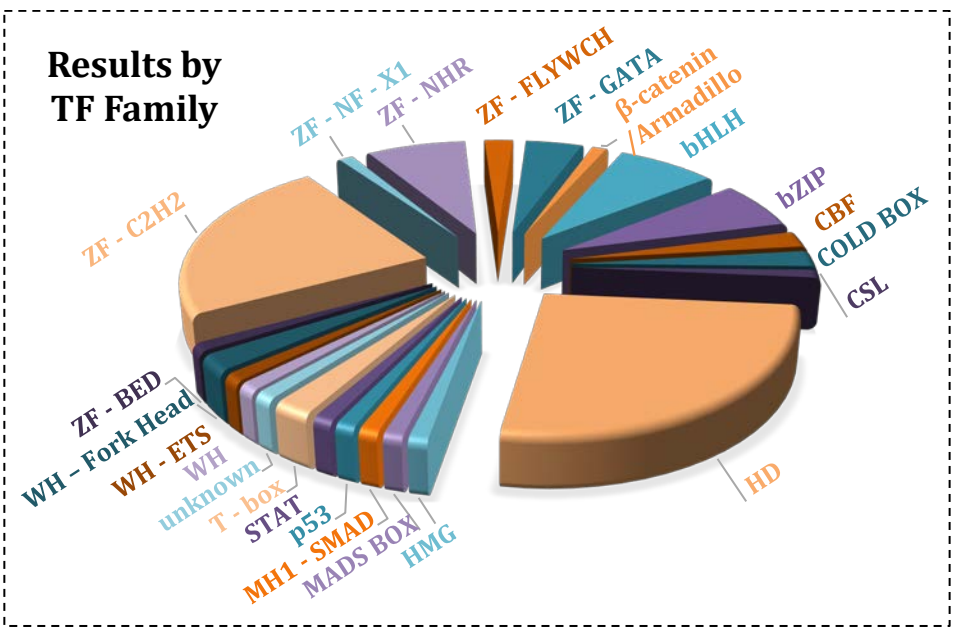

Figure R.8. Distribution by families of TFs with phenotype in MA neurons in our RNAi screen. All the families from Table R.2 are here represented.

In HD family, RNAi clones against 23 out of the total 101 HD members show a phenotype (23%). In this group we find the highest variety in observed phenotypes and

in several cases each TF performed functions in different monoaminergic neurons (see Table R.2). Some HD TFs act upon the lineages that generate the different monoaminergic subpopulations, such us *lin-28*, *nob-1*, *ceh-44* and *pax-3*, etc (Tsialikas et al. 2017; Zacharias et al. 2015). Most of these TFs involved in lineage determination execute their function in the posterior half of the body of *C. elegans*, from the vulva to the tail, and thus the most affected monoaminergic neurons are HSN, VCs and PDE. Following with this observation, these neurons are the ones most affected by TFs from other families also involved in lineage specification, as it is detailed in Table R.4 and discussed in the following section. Other HD TFs are known terminal regulators of MA fate (such as *ceh-20*, *ceh-43* or *unc-86*) while others have not been previously reported to be involved in MA differentiation. HD TFs seem also to be predominant in the specification of other neuron types (Hobert 2016b; Serrano-Saiz et al. 2013).

Regarding ZF-C2H2 family, this is one of the largest in *C. elegans*, with 192 members, 22% of all the TFs in the worm. Thus, it is not surprising that we obtained many candidates from this family. ZF-C2H2 family regulates a plethora of pathways from metabolism to development. RNAi candidates from this family generate mainly missing phenotype, with the only exception of *hbl-1* and *spr-3* that produce axon guidance defects in HSN and PDE respectively. As in the case of HD TFs, other ZF-C2H2 have been previously described to be involved in neuron subtype specification (Hobert 2016b).

The next families with more TFs among our results are bHLH and bZIP. Some bHLH, are known to regulate cell lineage, like *ref-1* or *lin-22* (Lanjuin et al. 2006; Wrischnik and Kenyon 1997). Lineage defects are most likely the explanation for the ectopic GFP observed in four out of the seven bHLH TF RNAi experiments. Other bHLH members, such as the subfamily *Achaete-Scute*, are proneuronal genes, as is the case of *lin-32*, *hlh-3*, *hlh-14* (Frank, Baum, and Garriga 2003; Portman and Emmons 2000). Given that RNAi against these three TFs produces a missing phenotype in our scores, they might be affecting generation of MA neurons. In cat, we recently showed evidence for the proneuronal action of *hlh-3* in HSN serotonergic neurons (Lloret-Fernández et al. 2018). In section 4 of this Results we will further explore the role of *hlh-14.*

In our results, bZIP family is represented by six TFs, four of them reported missing phenotype in any of MA neurons; the other two exhibited morphology defects or ectopic cells. Curiously, this family of TF perform several functions mainly related to metabolism (CREB TF belongs to this family), but no member has been related yet to neuronal differentiation (Rodríguez-Martínez et al. 2017; Xu et al. 2007).

Finally, the ZF-NHR family, which is the largest TF family in elegans 272 members, and it is striking that is very underrepresented in our hit list (only 7 with any phenotype, less than 3% of the total NHR TFs). The NHR family has been described to be involve in

differentiation and developmental processes, including neuron subtype specification, as is the case of *nhr-67* in GABAergic neurons (Sarin et al. 2009) (Arda et al. 2010), however according to our screen they do not seem to play a major role in monoaminergic specification. However, we cannot discard that NHR TFs act very redundantly and thus RNAi knockdown would not be sufficient to unravel their role in MA specification.

2.4. Global analysis of MA phenotypes

According to our results, from the 91 distinct TFs obtained in our RNAi screen, we observed that most them (83 TFs) presented missing fluorescence phenotype. But also, we detected ectopic pattern (13 TFs), defects in morphology (8 TFs) and migration (2 TFs). The total number of observed phenotypes exceeds the number of 91 TFs because a single TF can originate more than one type of defect and in more than one MA neuron type (Figure R.9).

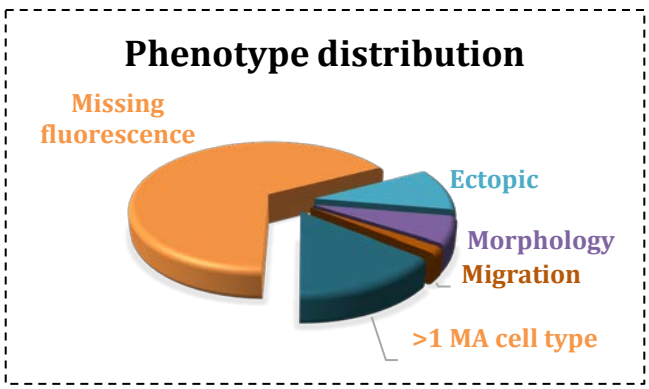

Nº of TFs	Phenotype
83	Missing fluorescence
13	Ectopic
8	Morphology
2	Migration
18	>1 MA celll type

Figure R.9. Distribution of phenotypes observed in our RNAi results. The phenotypes correspond to the different 91 TFs that we obtained from the screen.

Considering TFs that lead to GFP expression defects, those affecting RIC/RIM neuron expression are the most abundant, followed by TFs affecting CEP expression (Figure R.10). We retrieved more than ten candidates for each neuron type with the exception of NSM, where we only find two. It is worth mentioning that RNAi against GFP produces the weakest phenotype in NSM compared to the rest of MA neurons, thus, it is possible that NSM is particularly refractory to RNAi even in our *rrf-3* sensitized background. Alternatively, TFs involved in NSM specification could be acting in a very redundant manner, thus RNAi against single TFs would not produce significant phenotypes.

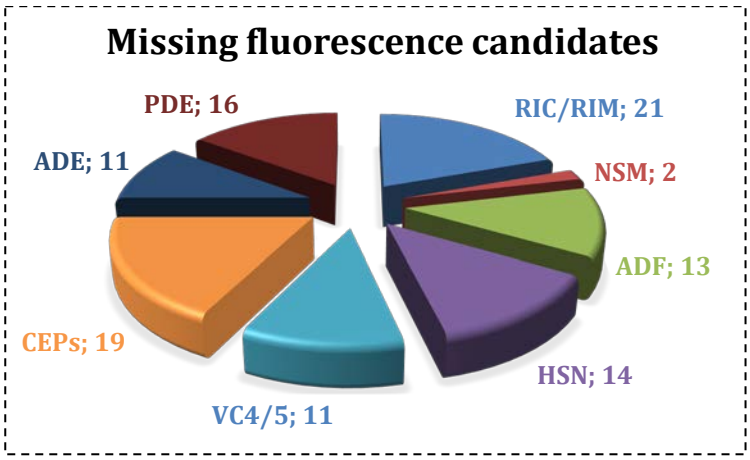

Figure R.10. Number of TFs with missing GFP RNAi phenotype for each MA neuron.

2.3.1. Analysis of lineage defects

Lineage defects can generate either ectopic of missing GFP depending on how the lineage is modified. A missing phenotype could also indicate an effect on reporter expression (either directly or indirectly). This distinction is especially relevant for us because we are most interested in determining the TFs that act in the last steps of differentiation of monoaminergic neurons and not so much in lineage determinants. In Table R.4 we collected the TFs already known to be required for lineage specification. For instance, RNAi against bHLH family members in our screen originate 25% of ectopic phenotypes likely due to lineage defects. Apart from bHLHs other TFs from other families also have known roles in lineage specification and produce either missing or ectopic phenotypes (Table R.4). Albeit their roles in lineage specification, this does not exclude a possible role in differentiation as could be the case of *hlh-14* (see results section 4.3).

Table R.4. TFs affecting cell lineage

Gene Name	DBD	Neuron affected	Phenotype	Reference
lin-22	bHLH	PDE	Missing fluorescence	(Wrischnik and Kenyon 1997)
lin-32	bHLH	PDE	Missing fluorescence	(Portman and Emmons 2000)
hlh-14	bHLH	ADF	Missing fluorescence	(Poole et al. 2011)
ceh-16	HD - HOX	PDE	Missing fluorescence	(Huang et al. 2009)
egl-5	HD - HOX	HSN	Missing fluorescence	(Chisholm 1991)
lin-39	HD - HOX	VC4/5	Missing fluorescence	(Clark, Chisholm, and Horvitz 1993)

nob-1	HD - HOX	HSN	Missing fluorescence and ectopic cells	(Malin et al. 2016)
mls-2	HD - NK	PDE	Missing fluorescence	(Jiang, Horner, and Liu 2005)
vab-15	HD - NK	PDE	Missing fluorescence	(Du and Chalfie 2001)
pax-3	HD - PRD	VCs	Missing fluorescence	(Thompson et al. 2016)
vab-3	HD - PRD	VCs	Missing fluorescence	(Chamberlin and Sternberg 1995)
unc-86	HD - PRD	ADE, PDE	Ectopic cells	(Baumeister, Liu, and Ruvkun 1996)
ceh-20	HD - TALE	ADE, PDE, VC4/5	Missing fluorescence	(Van Auken et al. 2002)
unc-62	HD - TALE	All DA	Ectopic cells	(Van Auken et al. 2002)
sem-2	HMG	HSN	Missing fluorescence	(Tian et al. 2011)
ham-1	WH	CEPs	Missing fluorescence	(Singhvi, Frank, and Garriga 2008)
bed-3	ZF - BED	PDE	Missing fluorescence	(Inoue and Sternberg 2010)
lin-26	ZF - C2H2	PDE	Missing fluorescence	(Quintin et al. 2001)
lin-48	ZF - C2H2	CEPD	Missing fluorescence	(Chamberlin et al. 1999)
ref-2	ZF - C2H2	VC4/5	Missing fluorescence	(Alper and Kenyon 2002)
lin-40	ZF - GATA - MYB	VC4/5	Missing fluorescence	(Chen and Han 2001)

2.4.2. Analysis of heterochronic genes

Our screen also retrieved three heterochronic genes as candidates for MA specification: *hbl-1*, *lin-28* and *lin-14*. Heterochronic genes regulate the timing of some developmental processes such as molting transitions (Moss 2007). RNAi against these three genes affect expression of fluorescent reporters in HSN and additionally, removing *hbl-1* and *lin*-28 affects expression in PDE and *lin-28* and *lin-14 RNAi* affects VC4/5. In these three neurons the control of molting transitions is essential because, contrary to the rest of monoaminergic neurons that are fully mature at hatching, these neurons mature at different larval stages: PDE neurons are born and mature at L3 while VC4/5 and HSN differentiate at late L4 stage. This could explain why heterochronic genes play a role in the differentiation of these neurons. It could be very interesting, for future projects, to study how the heterochronic pathway is integrated in the terminal fate of HSN, PDE and VC4/5.

2.4.3. Analysis of TFs controlling sexual dimorphism of MA neurons

In the last years *C. elegans* has emerged as a good model to study molecular mechanisms controlling sexual dimorphism of the nervous system (Portman 2017, 2007). Some neurons are specifically found in males or hermaphrodites while others,

although present in both sexes, show morphological, synaptic and molecular differences between sexes. Among the *cat-1::gfp* positive neurons two neuronal types are sexually dimorphic: HSN is only found in hermaphrodites, while in males it suffers programed cell death and VC4/5 are only present in hermaphrodites due to lineage differences in the male. Additionally, ADF, which is present in both sexes has been recently reported to be functionally dimorphic among sexes (Fagan et al. 2018).

Interestingly, among the RNAi clones producing missing phenotypes we observed several TF candidates related to sex dimorphism (Portman 2007). RNAi against *tra-1* (transformer, XX animals converted into males)–leads to *cat-1* reporter expression defects in VC4/5. This TF acts cell autonomously positively regulating all aspects of hermaphrodite somatic sexual differentiation and has an already reported role in HSN specification as well (Portman 2007). However, a specific role in MA effector gene expression in VC4/5 has not been reported before. Additionally, we find that RNAi against *sex-1* (signal element on X chromosome) produces reporter expression defects both in HSN and ADF. Finally, RNAi against *sdc-1* (sex dosage compensation) leads to expression defects in RIC/RIM neurons, this phenotype is particularly interesting as RIC/RIM neurons have not been previously reported to be dimorphic. The characterization of the link between genes controlling sex dimorphism and the development of monoaminergic neurons could be very interesting as it is still poorly understood.

2.4.4. Pleiotropic functions of TFs in several populations of MA neurons

As already mentioned, TFs are pleiotropic, a single TF can be expressed in several neuronal types or tissues and fulfill different functions depending on the cellular context. We also found in our TF RNAi screen candidates that some are required for cell fate specification of several MA neuronal types (Figure R.11).

The dopaminergic subpopulation is the one that shares more candidates among the four neuron subtypes that integrate this group (CEPV, CEPD, ADE, PDE). All dopaminergic neuronal classes are mechanosensory and share the expression of many effector genes, thus, it is not surprising that they also share the TFs required for their specification. CEPs and ADE regulators are more similar than PDE; maybe because, as we have just explained, this neuron matures late in development and requires a different program.

In contrast to DA neurons, serotonergic population are functionally very diverse (as explained in the introduction), accordingly, they barely express common effector genes with the exception of the serotonergic pathway. Thus, it is not surprising that common TF candidates are less frequent among 5HT populations. As explained in the previous section, HSN and ADF are sexually dimorphic and share the requirement of *sex-1*.

Additionally, *unc-86* has an already reported role for NSM and HSN terminal specification (Sze et al. 2002). NSM and HSN also share the requirement of *lin-14*. This is interesting as *lin-14* is an heterochronic gene, it would be interesting to analyze if *lin-14* regulates the expression of *unc-86* in both neurons and thus, the expression of *cat-1* and *tph-1* reporters.

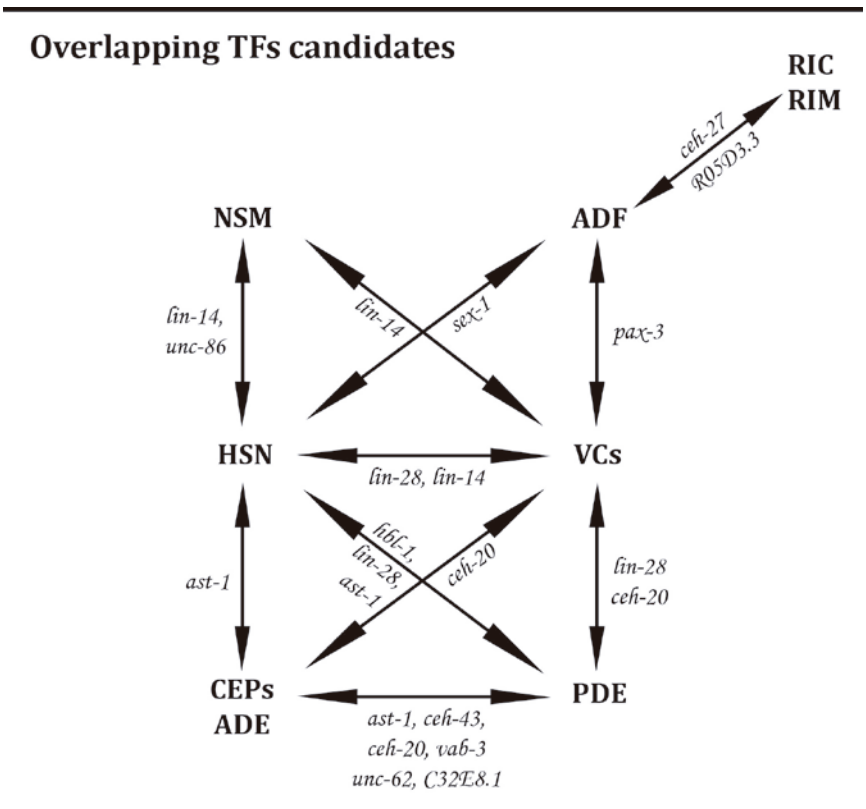

Figure R.11 Overlapping candidates between distinct MA classes. The scheme illustrates the relations between neurons that share TFs candidates with missing phenotype.

Importantly, TF candidates are not only shared among neuron subclasses with the same neurotransmitter. For example, *ast-1* has reported roles as a terminal selector for specification of all DA neuron classes as well as for HSN serotonergic fate (Lloret-Fernández et al. 2018; Flames and Hobert 2009).

Finally, for tyramine and octopaminergic neurons RIM and RIC, as these two neurons are very close to each other and morphologically very similar, we did not distinguish them in our screen. Further experiments should determine if our TF candidates affect RIM fate, RIC fate or both. RIC and RIM arise from the same lineage (Figure I.17) thus it is conceivable that they also share their terminal selectors.

2.4.5. Candidate TFs to play a role in MA terminal specification

Several of our TF candidates could have a previously uncharacterized role in MA terminal specification. As mentioned in introduction (Part I, section 5), the mature fate of a given neuron is characterized by the expression of a battery of genes that allow the cell to receive inputs and generate a response. Some TFs retrieved from our screen could be candidates to act at a terminal level. However, as mentioned above in section 2.4.1, deficit in expression of our reporters could be also related to lineage defects or other indirect effects. Nevertheless, several cases have been described of TFs essential for lineage establishment and also, in later steps of neuronal development, for terminal differentiation. Just to mention a few examples, *ceh-20* for DA neurons (Doitsidou et al. 2013), *mls-2* for AWC (Kim, Kim, and Sengupta 2010) or *unc-86* for NSM and HSN among other neurons (Sze et al. 2002).

Our next step after this general characterization of the results was the validation of some TF candidates through mutant analysis. We have classified the results by MA neuron subtype.

3. Validation of the TF candidates required for the generation of dopaminergic neurons population

3.1. Additional RNAi screen of TF candidates for dopaminergic neuron specification with an alternative sensitized background strain

The regulatory logic of dopaminergic terminal differentiation has been previously studied. Three different TF *ast-1* (ETS), *ceh-43* (HD) and *ceh-20* (PBX HD subfamily) act as terminal selectors for these neurons (Doitsidou et al. 2013; Flames and Hobert 2009). Our RNAi retrieved those TFs validating our approach. In addition, we also found other 14 RNAi clones that showed missing fluorescent expression in these cells (Table R.5).

Table R.5. TF candidates for dopaminergic specification

Gene Name	DBD	Neuron affected	Phenotype	*cat-1 ::gfp*	*dat-1 ::mCherry*
dro-1	CBF	ADE, CEPs, PDE	Missing fluorescence	49/60	49/60
cep-1	p53	ADE, CEPs	Missing fluorescence	52/60	52/60
mef-2	MADS BOX	ADE, CEPs	Missing fluorescence	53/60	53/60
ceh-43	HD - NK	ADE, CEPV, PDE	Missing fluorescence	45/60	39/60
vab-3	HD - PRD - FULL	ADE, CEPV, PDE	Missing fluorescence	47/60	49/60

C32E8.1	bZIP	ADE, CEPV, PDE	Missing fluorescence	49/60	41/60
ast-1	WH - ETS	ADE, PDE	Missing fluorescence	40/60	34/60
unc-62	HD - TALE	ADE, PDE	Missing fluorescence	40/60	40/60
unc-62	HD - TALE	CEPs	Missing fluorescence	50/60	51/60
ceh-20	HD - TALE	ADE, PDE	Missing fluorescence	43/60	44/60
dnj-17	ZF - C2H2	CEPs	Missing fluorescence	50/60	50/60
nhr-223	ZF- NHR	CEPs	Missing fluorescence	50/60	50/60
unc-55	ZF- NHR	CEPs	Missing fluorescence	54/60	54/60
row-1	ZF - C2H2	CEPV	Missing fluorescence	49/60	49/60
dxbp-1	ZF - C2H2	CEPV	Missing fluorescence	50/60	50/60
ztf-8	ZF - C2H2	CEPV	Missing fluorescence	50/60	50/60
sup-35	ZF - C2H2	CEPV	Missing fluorescence	54/60	54/60
ceh-44	HD - CUT	PDE	Missing fluorescence	40/60	40/60

Table R.5. TF candidates involved in dopaminergic specification. The list includes the TFs from the RNAi screen that present significant phenotype in DA population. RNAi clones affecting timing, lineage or asymmetric divisions have been excluded (*lin-48, ham-1, hbl-1, lin-28, vab-15, lin-26 and bed-3*). The scoring results with the reporter *cat-1* and *dat-1* indicate the ratio of remaining neurons after the RNAi feeding, in a population of 30 worms.

Among the new candidates we decided to focus our attention on those that gave the highest phenotype in all or almost all dopaminergic neuron classes: *vab-3, unc-62, dro-1, cep-1* and *mef-2*. The gene *C32E8.1* also presented phenotype in the three out of four different dopaminergic cells. However, we did not go further in its analysis because there are no mutant or reporter strains available. Furthermore, we selected another candidate, *unc-55*, because in mammals the functional orthologue of this candidate, COUP-TF1, plays an important role in the specification of olfactory bulb dopaminergic neurons, which shares the worm's dopaminergic regulatory logic (AST-1/ER81, CEH-43/DLX2 and CEH-20/PBX1) (Bovetti et al. 2013; Zhou et al. 2015).

As stated before, we selected *rrf-3* as RNAi sensitize background for all MA neurons; however, when specifically considering DA cells, the most sensitized background is the one combining the mutant alleles *eri-1 (mg366)* and *lin-15b (n744)*. Accordingly, we

decided to confirm the results from the screen testing our candidates in this additional mutant background and scoring the expression of a different DA reporter, *otIs199 (cat-2::gfp)*, which employs the regulatory region of the rate limiting enzyme for dopamine synthesis, tyrosine hydroxylase, to drive *gfp* expression in DA neurons.

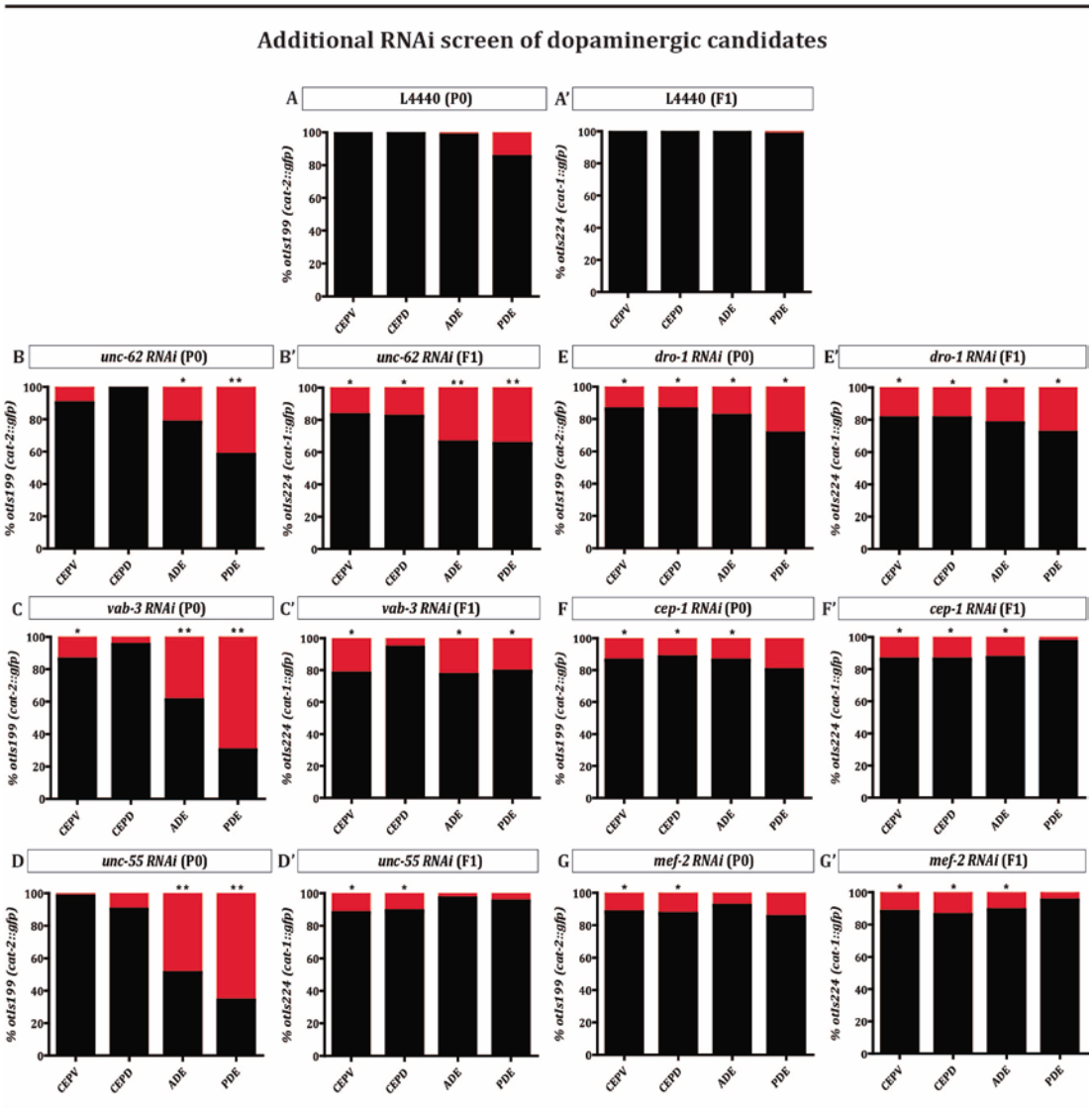

Figure R.12 Additional RNAi screen of dopaminergic candidates. a-g) P0 scoring in the sensitized background *eri-1 (mg366)*, *lin-15b (n744)* with the reporter *cat-2::gfp*. a'-g') F1 scoring of the candidates from the RNAi screen, with the reporter *cat-1::gfp.* Graphs a and a' represent the negative control for each background, L4440. N = 30 worms/clone. Statistical analysis with Fisher exact test (*) = (p<0,05), (**) = (p<0,01).

In most cases, the expression of terminal selectors is maintained throughout the life of the animal and their role is required to maintain the correct fate (Deneris and Hobert 2014). Thus, considering that two of our candidates, *unc-62* and *vab-3* have been described to affect some neuronal lineages and presented ectopic *cat-1* expression in the head we decided to perform these additional RNAi experiments scoring at P0: worms start feeding on RNAi bacteria when they are L1 and CEPs and ADE are already born and then the phenotype is scored at young adult. It is important to highlight that with this P0 strategy we avoid early effects of RNAi on neuronal lineages but we are assessing a role for this TFs in fate maintenance and not in specification (Hobert 2016a).

The two sets of RNAi experiments are very different: they use different reporter strains, different sensitized backgrounds and different generations are scored. However, if we compare the results from both we conclude that all candidates show phenotypes both for the F1 and for P0 screen. In the cases of *dro-1*, *cep-1* and *vab-3,* the neuron subpopulations affected are the same. However, in *mef-2*, *unc-62* and *unc-55* there are some differences. In the case of *mef-2* and *unc-62*, F1 RNAi for *cat-1* expression reveals an effect in additional cells, which might indicate either lineage defects at F1, a role for these factors in specification and not maintenance in some subpopulation of DA cells or a differential effect on *cat-1* compared to *cat-2*. Globally, these results reinforce the hypothesis that these candidates play a role in the dopaminergic population of *C. elegans*. Thus, our next step after the RNAi approach was to evaluate the expression pattern of the candidate TFs and to analyze the phenotype of the corresponding null mutant backgrounds.

3.2. Analysis of the expression pattern and phenotypes of TFs candidates to be required for dopaminergic neuron specification

The RNAi strategy, as we said, it is a fast and affordable way to conduct screens. However, RNAi experiments produce partial loss of function that can lead to partial effects. Moreover, the basis of RNAi is in the complementation of two sequences: the one for the built clone that the worms feed on, and the one of the mRNA inside the cells of the animals. It is known that the homology between sequences can lead to secondary target effects, where another mRNA molecule is degraded because of its similarity to the RNAi clone. Thus, this can lead to attribute a phenotype to a gene that is not really causing it. For both reasons, it is essential to validate RNAi results of the screen with the corresponding mutant analysis of our candidates.

To achieve our purpose, we decided to order mutant strains to the Caenorhabditis Genetics Centre Table A.2 in the Annex and cross them with the reporter *otIs199 (cat-2::gfp)* to assess their role in dopaminergic neurons. We selected the *cat-2::gfp* reporter because is DA specific and because it is the gene whose expression is most affected in the known DA terminal selectors (Doitsidou et al. 2013; Flames and Hobert 2009). In the

cases where the TF candidate is located in chromosome I (*cep-1, mef-2 and unc-55*), as *otIs199* is integrated there, we used another *cat-2::gfp* reporter named *nIs118*.

Complementary to the mutant analysis, we also studied the expression pattern of our DA TF candidates, we expect that, if they act as terminal selector they should be expressed in DA neurons (as is the case for *ast-1, ceh-20* and *ceh-43*) (Doitsidou et al. 2013). Several methods have been developed to assess the expression of a given gene in *C. elegans*. Most techniques are based on visualizing gene expression with a fluorescent protein. To accurately recapitulate temporal and spatial expression it is important to preserve the genomic context of the gene. Thus, the best reporter expression of any gene can be obtained by tagging the endogenous locus (for example by CRISPR). Nevertheless, this is a recent technique, still difficult to perform and few reporter strains built with this method are available. Prior to CRISPR, the gold standard was the use of tagged fosmids (Sarov et al. 2006). Fosmids are large genomic fragments (40 kbp DNA) that can be replicated and modified inside bacteria. When properly selected, a given gene contained in a fosmid is thought to contain all the regulatory regions controlling its expression. Thus, although it does not tag the endogenous locus, fosmid based reporter expression is supposed to give a good approximation for endogenous expression, better than other techniques such as translational or transcriptional reporters that contain only a few kilobases surrounding the gene. Finally, it is important to highlight that unlike CRISPR, where the endogenous locus is tagged though genome editing, the other three strategies consist on injecting the worms to generate transgenics, and usually it generates multicopy array lines.

In this Thesis, as a first step, we decided to use fosmids whenever they were available and translational or transcriptional reporters when there was not availability of those. *unc-62* and *mef-2* reporter fosmid strains were available at CGC. We obtained the recombined *vab-3* fosmid from Source Biosicence and generated our own transgenic lines. We also analyzed an already published *cep-1* translational reporter. Finally, for the last two candidates, *dro-1* and *unc-55*, transcriptional reporters were generated (Table R.6).

Table R.6. Reporters of dopaminergic candidates

Gene	Reporter type	Expression	Source
vab-3	Fosmid reporter	In all DA neurons	SourceBioscience (WRM0628bC03)
unc-62	Fosmid reporter	In ADE and PDE	CGC (Niu et al. 2011)
mef-2	Fosmid reporter	In all DA neurons	CGC (Niu et al. 2011)
cep-1	Translational reporter	Not detected in DA neurons	CGC, (Hofmann et al. 2002)

dro-1	Transcriptional (184 bp upstream 5')	Not detected in DA neurons	This work
unc-55	Transcriptional (3777 bp upstream 5´)	In ADE and PDE	This work

Table R.6 Reporters of dopaminergic candidates. This table summarizes the reporters used, their source and the expression we detected regarding the DA population.

To unequivocally assess if the TF candidates are expressed in DA neurons, we crossed the TF reporter strains (marked with GFP) with the reporter *otIs181*, which drives *mCherry* expression in DA neurons, and we looked for co-localization. In the following sections we explain the results obtained for each analyzed TF.

3.2.1. Characterization of mef-2 role in DA specification

mef-2 is a feeding state-dependent transcriptional regulator for chemoreceptor genes (van der Linden, Nolan, and Sengupta 2007). We examined two alleles: *gk633* and *gv1* (Figure R.13a). Both alleles entail deletions; *gk633* presents a loss of 1075 bp corresponding to the MADS DNA binding domain and was obtained by the Deletion Mutant Consortium 2012. Regarding *gv1*, this 1376 bp deletion affects the MADS and MEF domains, essential for the function of the protein (Dichoso et al. 2000). The two alleles are considered likely null mutants; we decided to cross both with *cat-2* reporter to assess with more confidence the role of *mef-2* in the dopaminergic population.

Surprisingly, despite our reported defects on *cat-1, dat-1* and *cat-2* expression in CEPS and ADE by RNAi (Figure R.12 and Table R.5), we did not observe any defect in *cat-2* expression in neither of both alleles (Figure R.13c, d). Perhaps the RNAi phenotype could be due to off target effects or to compensatory effects specific of the mutant alleles and not of the RNAi. Nevertheless, we will cross *mef-2* mutants to additional DA reporters (*cat-1::gfp* and *dat-1::gfp*) to discard the lack of phenotype is due to the reporter's choice.

Despite the lack of phenotype of *mef-2* alleles we decided to analyze its expression in DA neurons using a fosmid recombineered construct. We found *mef-2* is widely expressed in neurons (Figure R.14a, b) including all DA subtypes (Figure R.14c). *mef-2* is also expressed in not neuronal cells such as neuronal support cells, hypodermal and muscle cells. The expression of this fosmid was detected from embryo, starting at coma stage, and throughout adulthood. Regarding the nervous system, at first sight this gene could be pan-neuronal according to its fosmid expression, but it would be necessary to compare this pattern with a recognized pan-neuronal gene to confirm this observation.

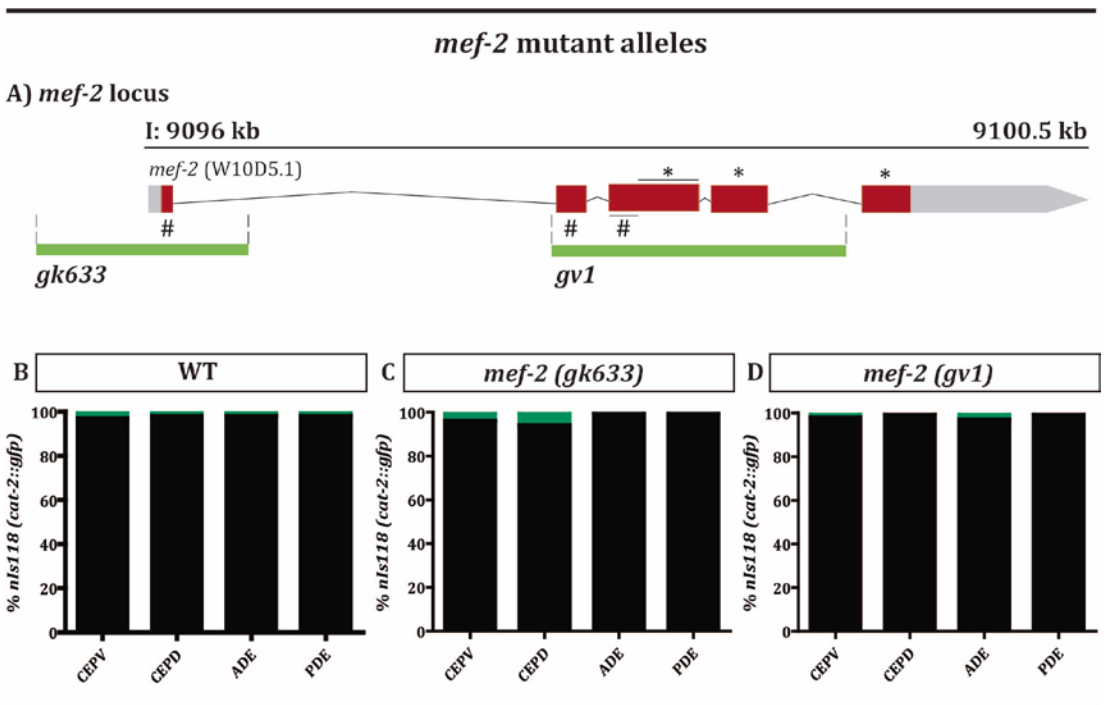

Figure R.13. *mef-2* mutant analysis. Representation of the genomic locus of *mef-2* gene, where red boxes represent exons and connecting lines, introns. Grey boxes represent untranslated regions of the mRNA. a) *mef-2* locus encodes one isoform with two DBDs, (#) indicates the sequence for the MADS domain and (*) for the MEF domain. The deletion of the allele *gk633* affects MADS domain and the transcriptional starting site, whereas the deletion in *gv1* alters both DBDs. b-d) Representation of the scoring results of the reporter *nIs118 (cat-2::gfp)* in control and mutant backgrounds *gk633* and *gv1*. The black color represents the percentage of neurons that continue expressing the fluorescence reporter and in green is shown the percentage of missing neurons. N = 50 worms. Statistical analysis with Fisher exact test.

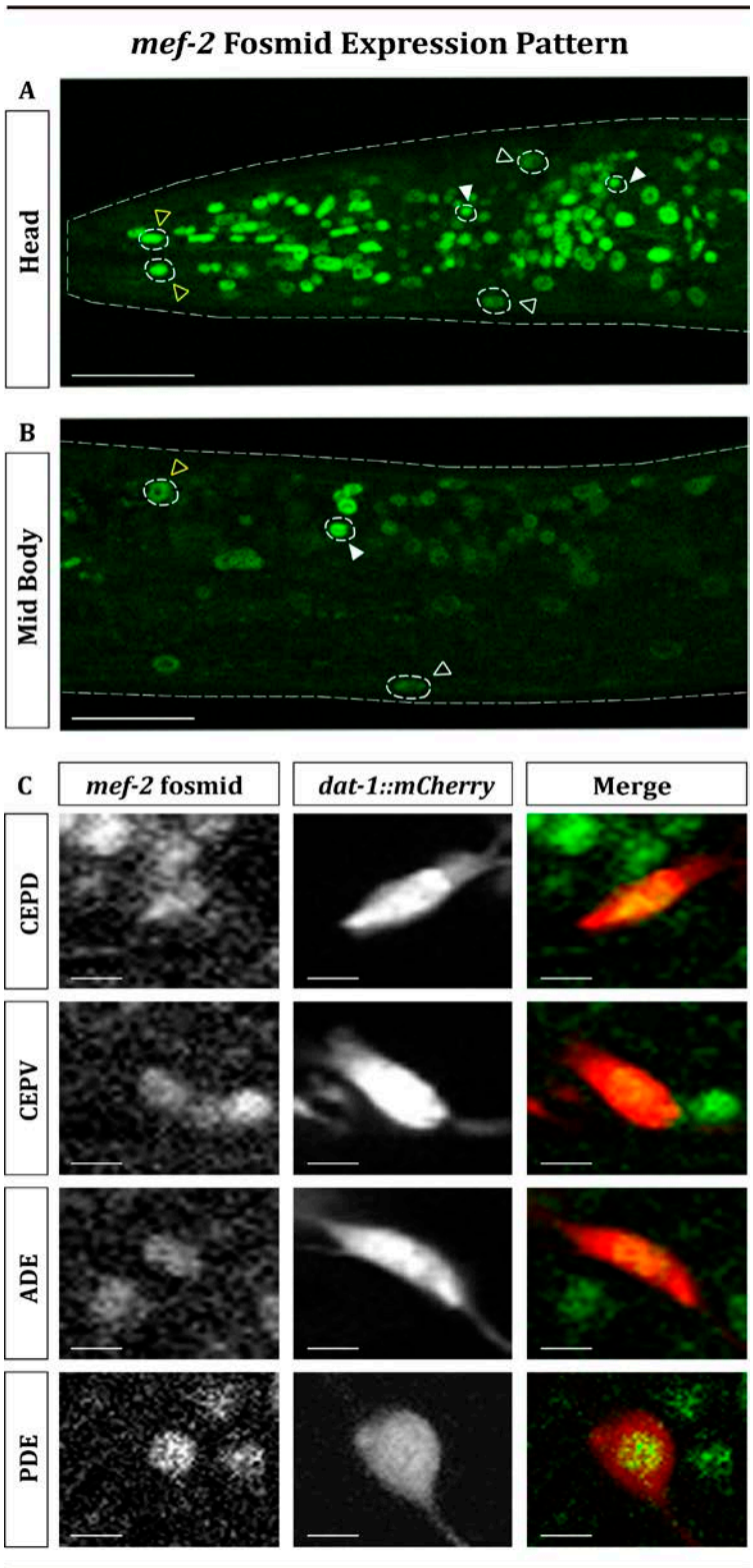

Figure R.14. Expression pattern of *mef-2*. Confocal micrographs of *mef-2* fosmid tagged with GFP from a young adult worm. a) *mef-2* expression in the head, arrowheads point out neurons (white), hypodermal cells (black) and sensory support cells (yellow). b) View of posteorir part of the body, *mef-2* is detected in neurons (white arrowhead), hypothermal cells (black arrowhead) and intestinal cells (yellow arrowhead). Scale bars in a and b, 30 µm. c) *mef-2* is expressed in DA cells, labeled in red with the reporter *otIs181 (dat-1::mCherry)*. Scale bars, 5 µm.

3.2.2. Characterization of cep-1 role in DA specification

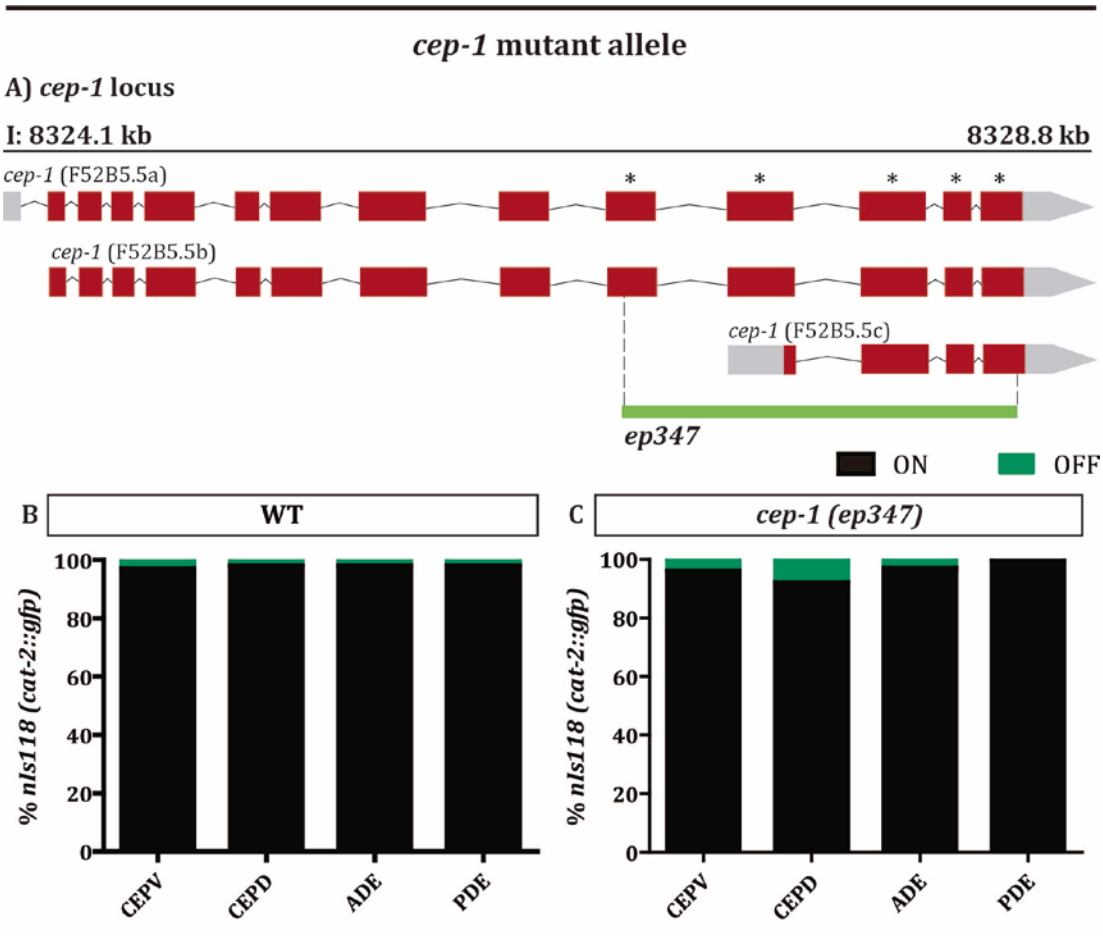

Figure R.15. *cep-1* mutant analysis. Representation of *cep-1* genomic locus, where red boxes represent exons and connecting lines, introns. Grey boxes represent untranslated regions of the mRNA. a) Scheme with the three isoforms of *cep-1*. (*) indicate the coding sequence of the DNA binding domain, which is affected in all the isoforms for the deletion *ep347*. b-c) Representation of the scoring results of the reporter *nIs118 (cat-2::gfp)* in the mutant backgrounds *ep347*. The black color represents the percentage of neurons that remain expressing the fluorescence reporter and in green is shown the percentage of missing neurons. N = 50 worms. Statistical analysis with Fisher exact test.

cep-1 is the worm orthologue of the human tumor suppressor p53. This TF promotes DNA-damage induced apoptosis and is involved in longevity in response to starvation (Hoffman et al. 2014; Yanase et al. 2017), however a role on neuron subtype specification has not been reported. We ordered the allele *ep347* that corresponds to a deletion of 1827 bp that removes exon 9 to 13, a region that includes the domain that induces

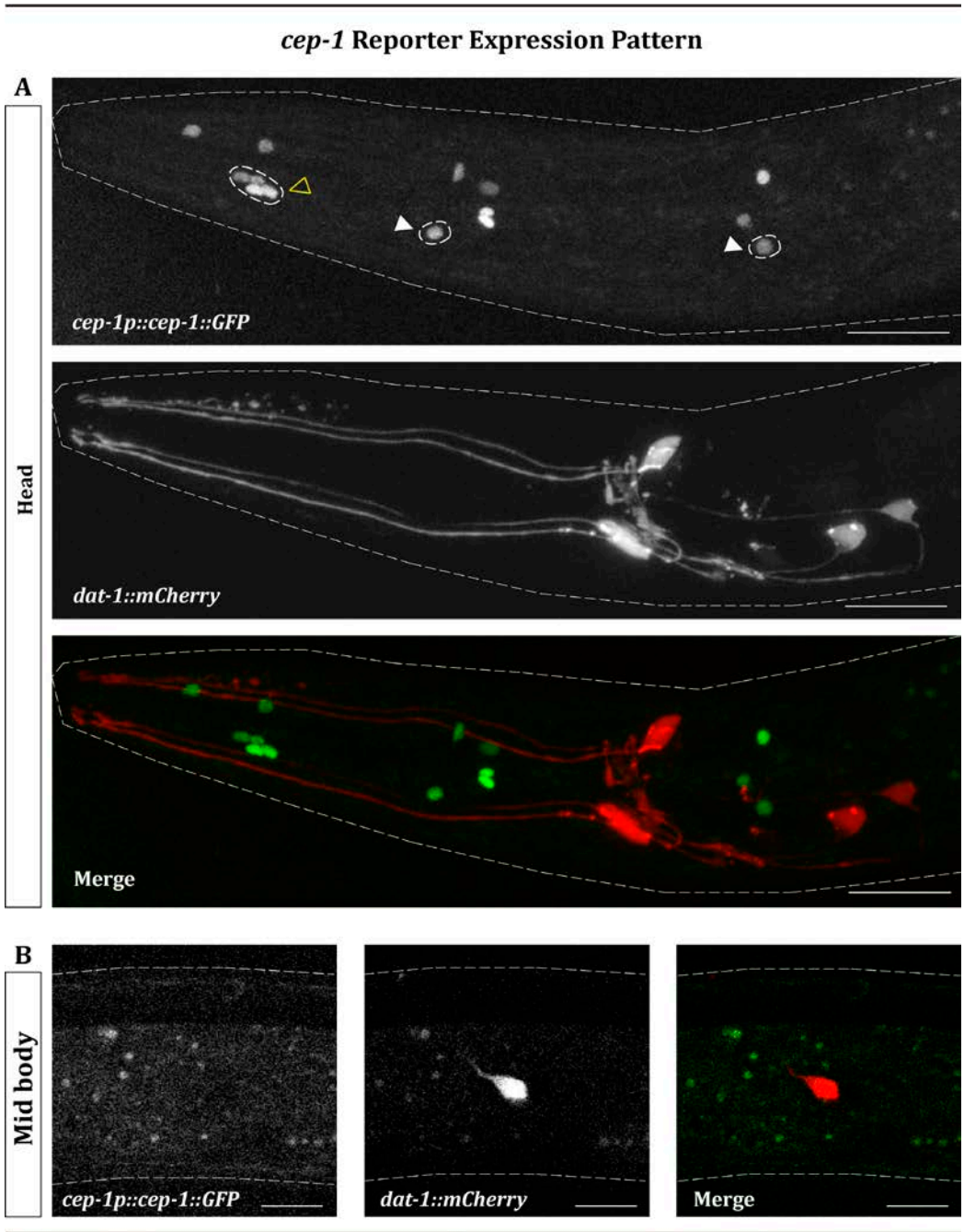

Figure R.16. Expression pattern of *cep-1*. Confocal micrographs of *cep-1* translational reporter tagged with GFP at young adult stages. a) General expression of *cep-1* in head (upper panel), compared with *otIs181 (dat-1::mCherry)* that labels dopaminergic cells. *cep-1* is expressed in neurons (white arrowheads) and pharyngeal nuclei (yellow). Scale bars, 30 µm. b) Mid body, where PDE was detected (red) but with no *cep-1* expression. Scale bars, 5 µm.

apoptosis after DNA damage (Lackner et al. 2005) (Figure R.15a). In contrast to our RNAi screen results, that showed missing cat-1 and dat-1 in ADE and CEPS, *cep-1* mutants show normal *cat-2* expression in DA neurons (Figure R.15c). These results suggest that the effect of *cep-1* RNAi clone might be due to the downregulation of unknown off targets. Alternatively, as RNAi knockdown is an acute process it is conceivable that compensatory effects in *cep-1* mutants are not employed in RNAi and thus the effect is more pronounced. As *cep-1* is involved in longevity, it would be interesting to analyzed if *cep-1* mutants show *cat-2* expression defects in old animals compare to wildtype. additionally, we will check *cat-1* and *dat-1* expression in *cep-1* mutants.

Next, we used a translational reporter to assess the expression pattern of *cep-1* (Figure R.16). We found this construct is expressed in some neurons in the head and also some support cells, but they do not co-localized with dopaminergic neurons. It is possible that our reporter construct, as it is small, does not re-capitulate the endogenous *cep-1* expression. Indeed, the first intron of the isoform c is big in size and contains elements conserved in 5 additional species, suggesting it might contain regulatory information. There is a *cep-1* recombineered fosmid commercially available, in the future we will inject it to generate lines and study its expression.

3.3.3. Characterization of dro-1 role in DA specification

Very little is known about *dro-1*. It is considered the worm orthologue of human *DR1* (down-regulator of transcription). This gene inhibits transcription of RNA polymerase II through its binding to TBP (Kantidakis and White 2010). The null mutant allele of this gene, *tm4702*, is a 314 bp deletion that extents from 40 bp upstream ATG until 275 bp of the first exon (Figure R.21a). This mutation was isolated by the Mitani Deletion Mutant Consortium and described to be lethal and has not been further characterized (of note, *dro-1* RNAi does not produce lethality). To maintain the lethal allele the strain contains a genetic balancer to keep the deletion allele in heterozygosis. We observed that homozygous mutants die at late L1 or L2 stage. Thus, when we crossed this strain with the *cat-2* reporter we only could score CEPs and ADE and not PDE because this neuron is born at L3.

RNAi against *dro-1* leads to *cat-1, dat-1* and *cat-2* expression defects in all DA subpopulations (Figure R.5e) in contrast, our mutant analysis shows a small but significant phenotype only in the ADE (Figure R.17c). As explained for *mef-2* and *cep-1*, stronger *dro-1* RNAi effects could be due to off targets or to compensatory effects taking place in the mutant, additionally, as *dro-1* is lethal, the analyzed balanced strain could produce maternal rescue.

Next to study *dro-1* expression we used a transcriptional reporter spanning 184bp of upstream promoter, which is the intergenic region that separates *dro-1* to *nud-1*. We

observed some GFP expression in some neurons in the head. Although we saw faint expression in CEPs and ADE, it could be due to conversion from the *dat-1::cherry* (a problem we have encountered before) (Figure R.18). Thus, we cannot confirm if *dro-1* is expressed in head DA neurons. Regarding PDE, we did not detect any expression of the reporter. A more detailed examination of the *dro-1* locus revealed it is part of the operon CEOP3784. *dro-1* is the second of five co-transcribed genes (*nud-1*, involved in nuclear migration, *ife-1* an initiation factor, *acaa-2*, an acetyl CoA acyltransferase and *mtm-6* a lipid phosphatase). Thus, it is likely that the regulatory information driving *dro-1* expression is upstream of the start of the operon. In future experiments we will generate a GFP reporter under the regulation of the intergenic region upstream of the operon (approximately 2Kb).

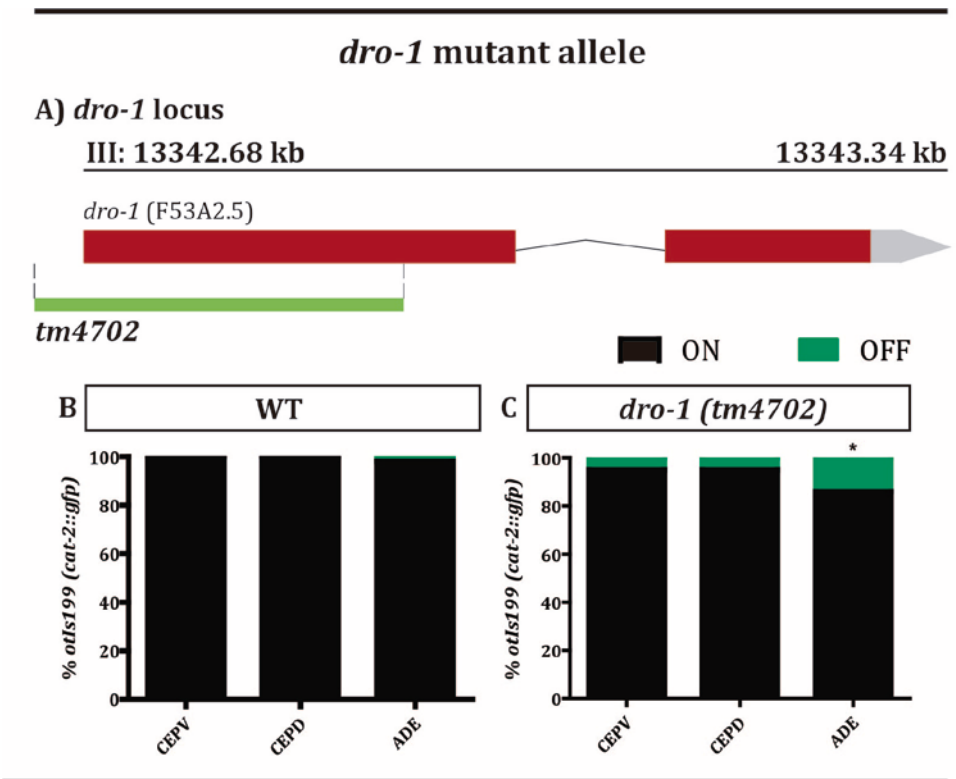

Figure R.17. *dro-1* mutant analysis. a) Representation of the genomic locus of the gene. Red boxes represent exons and connecting lines, introns. Grey boxes represent untranslated regions of the mRNA. The deletion in the allele *tm4702* affects part of the promoter and the first exon of the gene, whose sequence is thought to encode for the DBD. b-c) Representation of the scoring results of the reporter *otIs199 (cat-2::gfp)* in control and mutant background *tm4702*. Black represents the percentage of neurons remaining expressing the fluorescence reporter and in green is shown the percentage of missing neurons. N = 50 worms. (*) = significant result, Fisher exact test ($p < 0.05$).

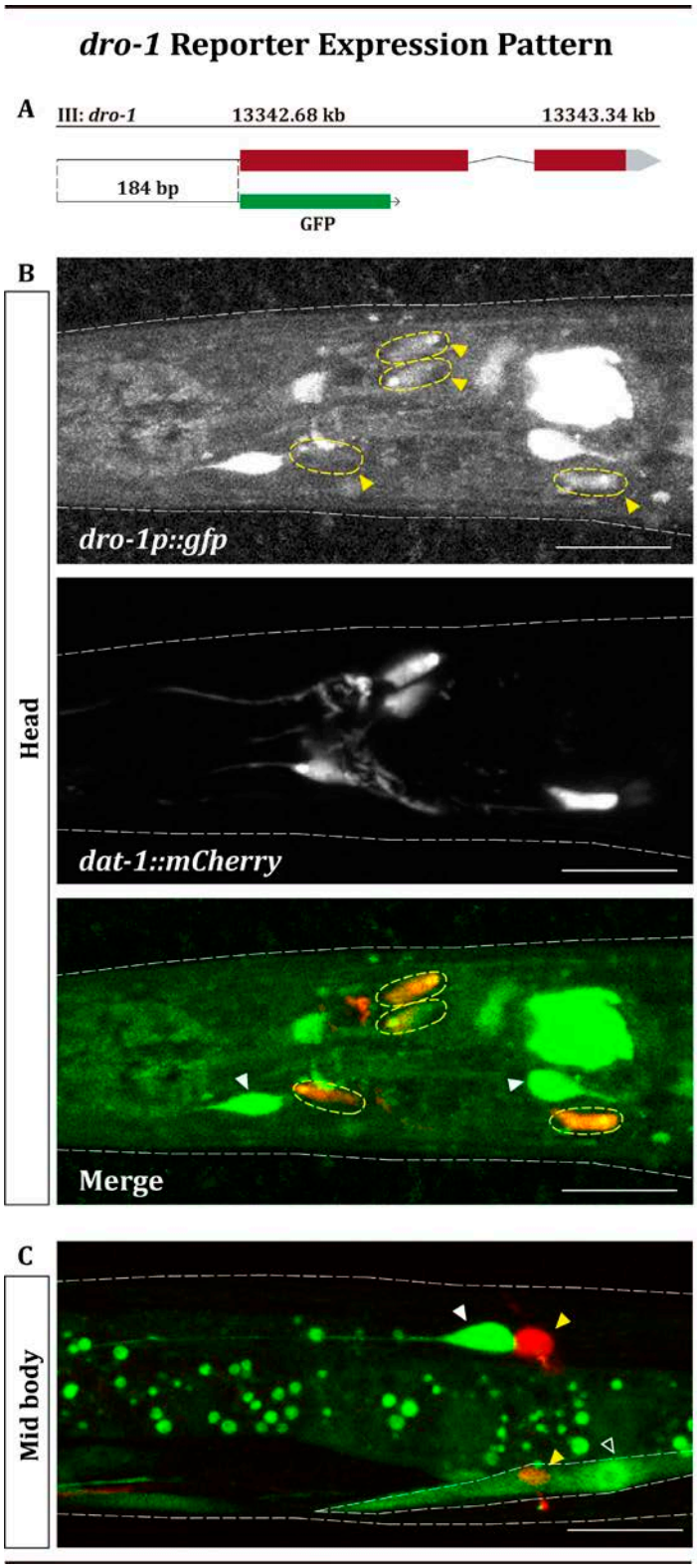

Figure R.18 Expression pattern of *dro-1*. Confocal micrographs of *dro-1* transcriptional GFP reporter from a young adult worm. a) Genomic region of *dro-1* locus where was cloned the promoter of 184 bp in front of GFP (green rectangle) to build *dro-1* transcriptional reporter. b) General expression of *dro-1* in head (upper panel), compared with *otIs181 (dat-1::mCherry)* that labels dopaminergic cells. This TF is expressed in neurons (white arrowheads). Yellow circles point location of DA neurons, but the expression of *dro-1* is too faint to assume colocalization with DA reporter. c) Area from tail. PDE neuron was detected (red channel, yellow arrowheads), next to other neurons (white arrowhead) and muscle cell (black arrowhead). Scale bars in b and c, 20 µm.

3.3.4. Characterization of vab-3 role in DA specification

Next, we examined mutant alleles for *vab-3*, a TF required in multiple processes such us hypodermal specification, head development or gonad cell migration (Dozier et al. 2001). *Pax-6* is the mammalian ortholog of *vab-3* and has broad roles in neuronal specification including cortical neurons, retina and DA neurons of the OB (Brill et al. 2008, Klimova, 2014). We selected the allele *ot346*, which is a viable allele that contains a deletion that affects the paired domain that directly contacts the DNA (Figure R.19a) (Doitsidou et al. 2008). This allele has been reported to show DA defects, however, it is likely not a null as shorter isoforms are probably unaffected (Figure R.19a).

It has been described that *vab-3* mutants have a visual phenotype where the head of the animals presents an abnormal morphology. Due to this disorganized head it was difficult to distinguish between CEPV and CEPD when we scored *cat-2* reporter. Accordingly, we grouped them in the same category. The results showed ectopic neurons in the area next to CEPs and also missing fluorescence in CEPs and ADE (Figure R.19c). Similar extra and missing expression in CEPs has been previously reported for the *dat-1::gfp* reporter strain (Doitsidou et al. 2008). We also noticed very similar results with RNAi (Figure R.5c), however we avoided the ectopic phenotype with a P0 scoring of the RNAi experiment but maintained the missing phenotype (Figure R5.c) suggesting that, apart from its role in lineage specification, *vab-3* has also roles in terminal differentiation. Additionally, the P0 RNAi phenotype in CEPs and ADE tell us that this TF is also essential for the maintenance of the dopaminergic fate. Intriguingly, as happed with *unc-55 (e1170)*, the RNAi of *vab-3* also showed phenotype in PDE, while this defect was not present in the mutant.

Considering the defects of *cat-2::gfp* expression in DA neurons of *vab-3* mutants we also analyzed *dat-1::gfp* expression. We found similar defects with *dat-1* reporter as the ones observed in *cat-2*: missing expression of the reporter and ectopic neurons in the area near CEPs. However, *dat-1* exhibited normal expression in ADE and PDE (Figure R.19e). Normal *cat-2* expression defects and *dat-1* normal expression in ADE corroborate *vab-3* role in terminal differentiation. It would be interesting to analyzed the rest of DA pathway genes however, the fact that the rest of the pathway is expressed in additional cells, such as *cat-4* and *bas-1* in serotonergic population or *cat-1* that labels all monoaminergic neurons, and due to the abnormal morphology of the head of these animals the identification of the neurons of interest becomes challenging.

We next analyzed *vab-3* expression in DA neurons by generating a fosmid GFP reporter strains. *vab-3* fosmid is expressed broadly but not in as many cells as *mef-2* (Figure R.14). It is expressed in head neurons, neural support cells in head and hypodermal cells; its expression in the tail is difficult to detect (Figure R.20a, b). *vab-3* is expressed from embryonic stages to adulthood but with highest intensity in L1 larval

stage. Using the *dat-1::mCherry* reporter we were able to unequivocally determine that *vab-3* is expressed in all DA neuronal types and stages (Figure R.20c).

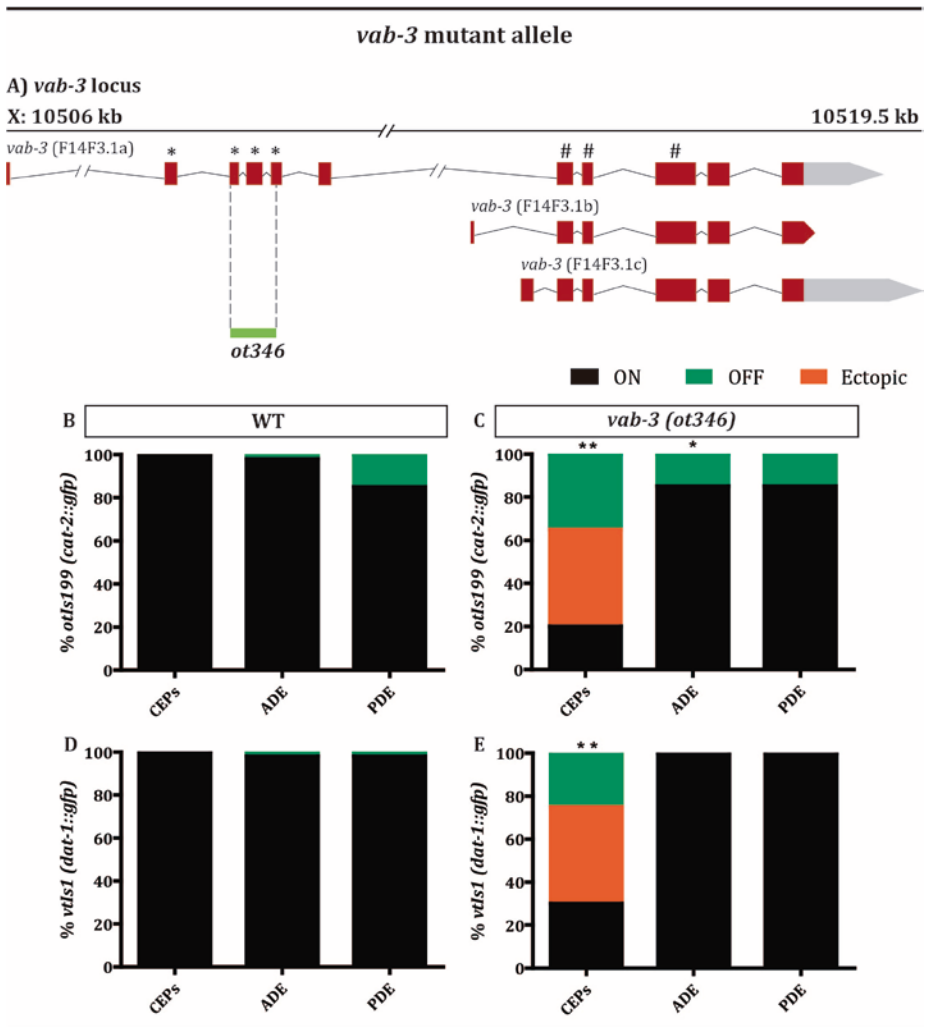

Figure R.19. *vab-3* mutant analysis. a) Representation of *vab-3* genomic locus, red boxes represent exons and connecting lines, introns. Grey boxes represent untranslated regions of the mRNA. *vab-3* locus encodes three isoforms with an Homeodomain (#). Only isoform **a** presents a Paired domain (*). The deletion of the allele *ot346* affects Paired domain. b-c) Representation of the scoring results of the *otIs199 (cat-2::gfp)* and *vtIs1 (dat-1::gfp)* in *ot364* background. The black color represents the percentage of neurons remaining expressing the fluorescence reporter and in green is shown the percentage of missing neurons. In the case of CEPs, black indicates the presence of 4 neurons; orange indicates ectopic neurons in this area and green implies less than 4 neurons. N = 50 worms. Statistical analysis with Fisher exact test: (*) = ($p < 0.05$), (**) = ($p < 0.01$).

The expression of *mef-2* and *vab-3* in DA neurons coincide with the RNAi phenotypes for these two genes that affect *cat-1* and *cat-2* expression in all dopaminergic cells, with the exception of CEPD being unaffected in *vab-3* RNAi and PDE in *mef-2* RNAi. This lack of effect could be due to partial loss of function of RNAi.

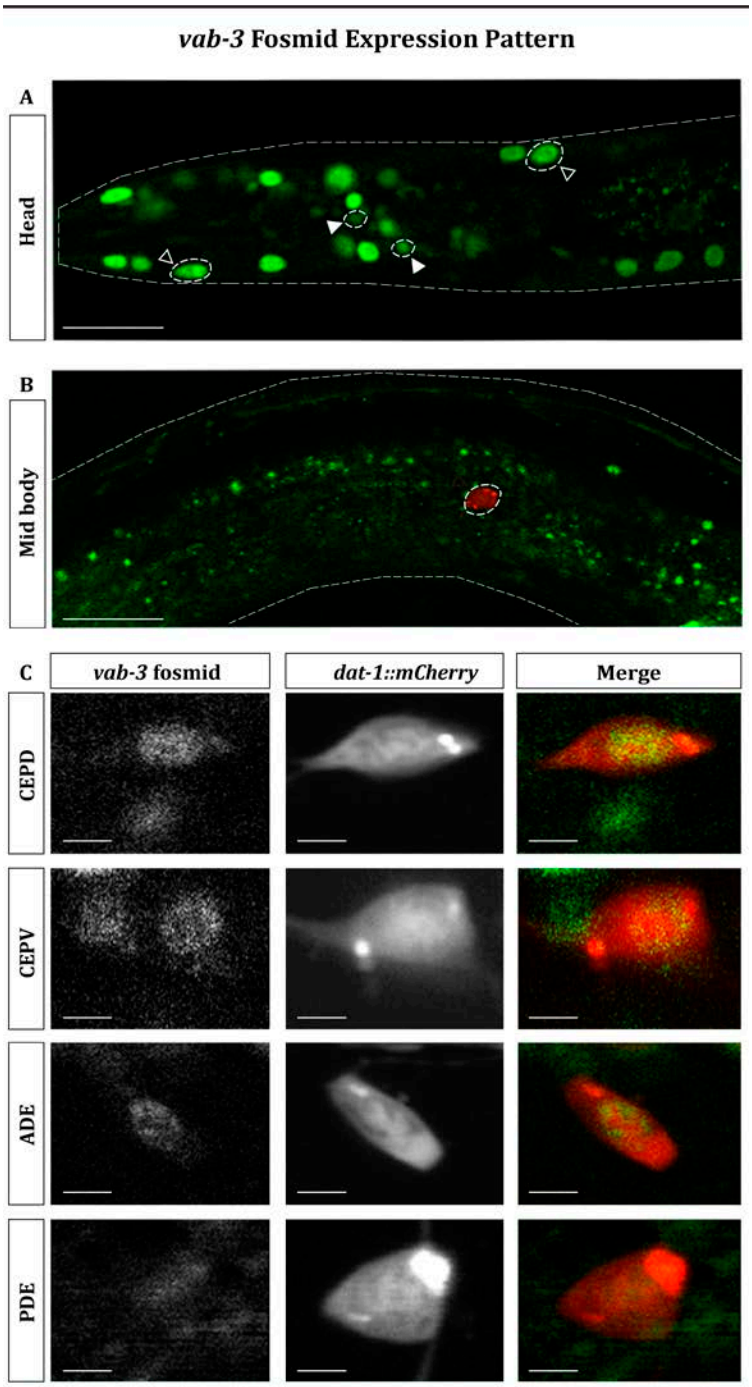

Figure R.20. Expression pattern of *vab-3*. Confocal micrographs of *vab-3* fosmid tagged with GFP from a young adult worm. a) General view of *vab-3* pattern in head, where arrowheads point out neurons (white) and hypodermal cells (black). b) Area from mid body where PDE was detected (red). Scale bars in a and b, 30 µm. c) Expression of *vab-3* fosmid in dopaminergic cells labeled in red with the reporter *otIs181 (dat-1::mCherry)*. Scale bars, 5 µm.

3.3.5. Characterization of unc-62 role in DA specification

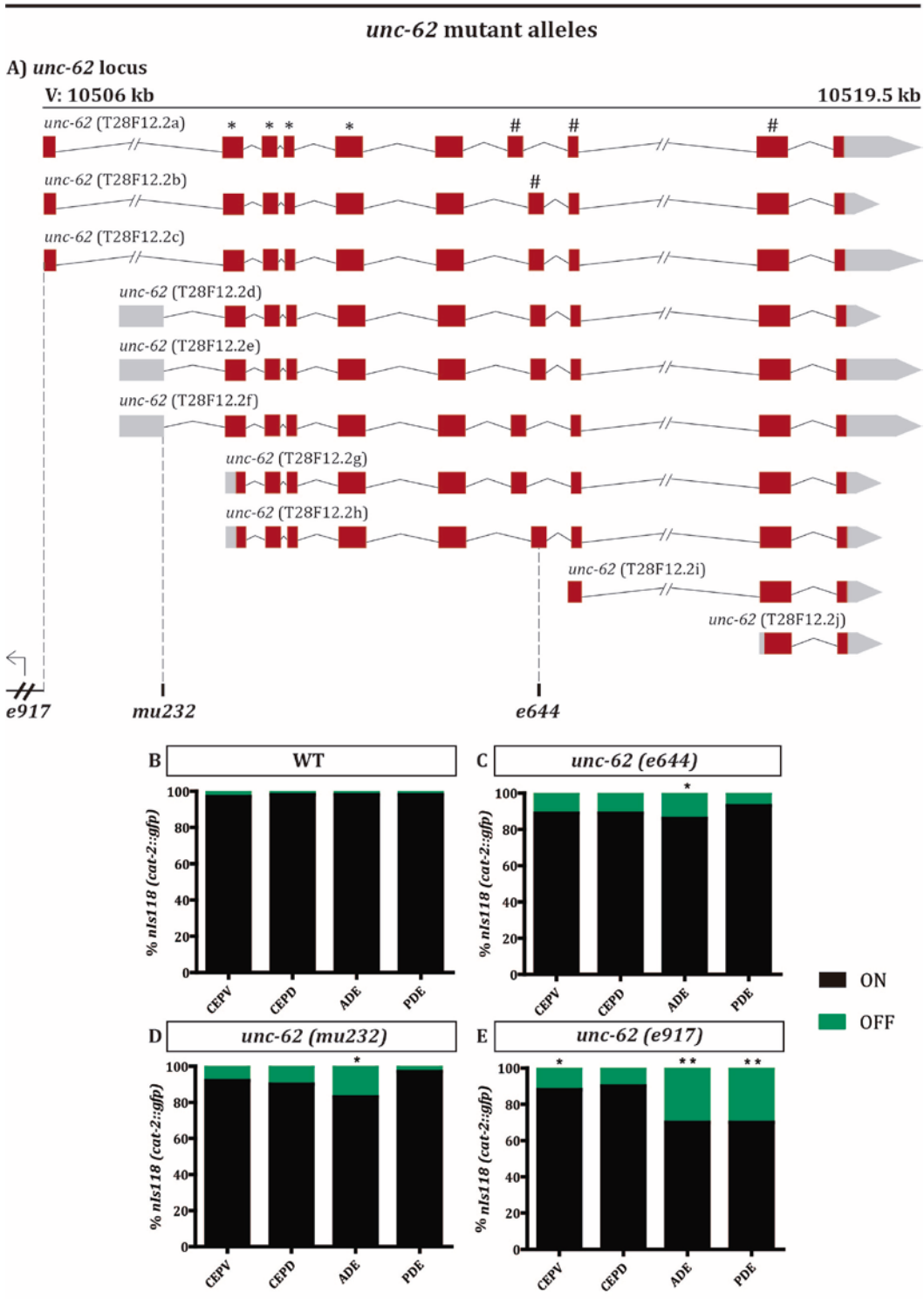

Figure R.21. *unc-62* mutant analysis. Representation of *unc-62* genomic locus, where red boxes represent exons and connecting lines, introns. Grey boxes represent untranslated regions of the mRNA. a) *unc-62* has ten isoforms; (*) indicates the coding sequence of the Homeobox binding domain and (#) points out the TALE domain, where is located the point mutation *e644*, that affects the isoforms b-d and h. On the other hand, isoforms c, d and e are affected by the missense in the splice site provoked for the mutation *mu232*. Finally, the chromosomic inversion *e917* is found in the 5'UTR of the gene. b-e) Representation of the scoring results of the reporter *nIs118 (cat-2::gfp)* in control and the three mutant backgrounds. The black color represents the percentage of neurons remaining expressing the fluorescence reporter and in green is shown the percentage of missing neurons. N = 50 worms. Statistical analysis with Fisher exact test: (*) = ($p < 0.05$), (**) = ($p < 0.01$).

unc-62 has been involved in posterior embryonic morphogenesis and normal locomotion (Van Auken et al. 2002). *unc-62* is the worm ortholog of mouse *Meis1/2* which has classically been studied as a co-factor for Hox genes, however it also acts independently of Hox factors. Interestingly, *Meis2* is required for DA specification of the OB (Agoston et al. 2014).

For our mutant analysis we used several alleles given that the null mutant allele, *s472* is embryonic lethal. Thus, to avoid this lethality we used hypomorphic alleles (Figure R.21). The first analyzed allele was *e644*, a point mutation that affects an exon that is alternatively spliced and codes part of the TALE homeodomain of the protein and leads to a premature stop codon (Van Auken et al. 2002). Thus, this allele only affects specific isoforms (Figure R.21a). When we scored the dopaminergic population with *cat-2* reporter in this background, we notice missing expression of the reporter in ADE neuron but not in other DA populations (Figure R.21c). This phenotype is lower than what we noticed with RNAi, which affected all DA populations (Figure R.5b).

The next allele analyzed, *mu232*, is a missense mutation that disrupts the initiation codon (Met) in exon 1b thus, it specifically affects isoforms that include this exon (Campbell and Walthall 2016) (Figure R.21a). Interestingly, the phenotype of *mu232* is different from the *e644* allele. *mu232* allele show ectopic GFP positive neurons in head, although dopaminergic cells were perfectly distinguishable by location and morphology. Moreover, we confirm missing phenotype again in ADE neuron (Figure R.21d).

Finally, we studied a third allele, *e917*. This allele is part of a chromosomic inversion that disrupts promoter and transcription start site of exon 1a therefore, this allele also affects a different subset of *unc-62* isoforms (Van Auken et al. 2002). The worms with this mutant background were morphologically very affected and exhibited high rate of lethality and a slower growing rate. Interestingly, this allele shows *cat-2* expression defects in CEPV, ADE and PDE (Figure R.21e), similar to what we observed with RNAi

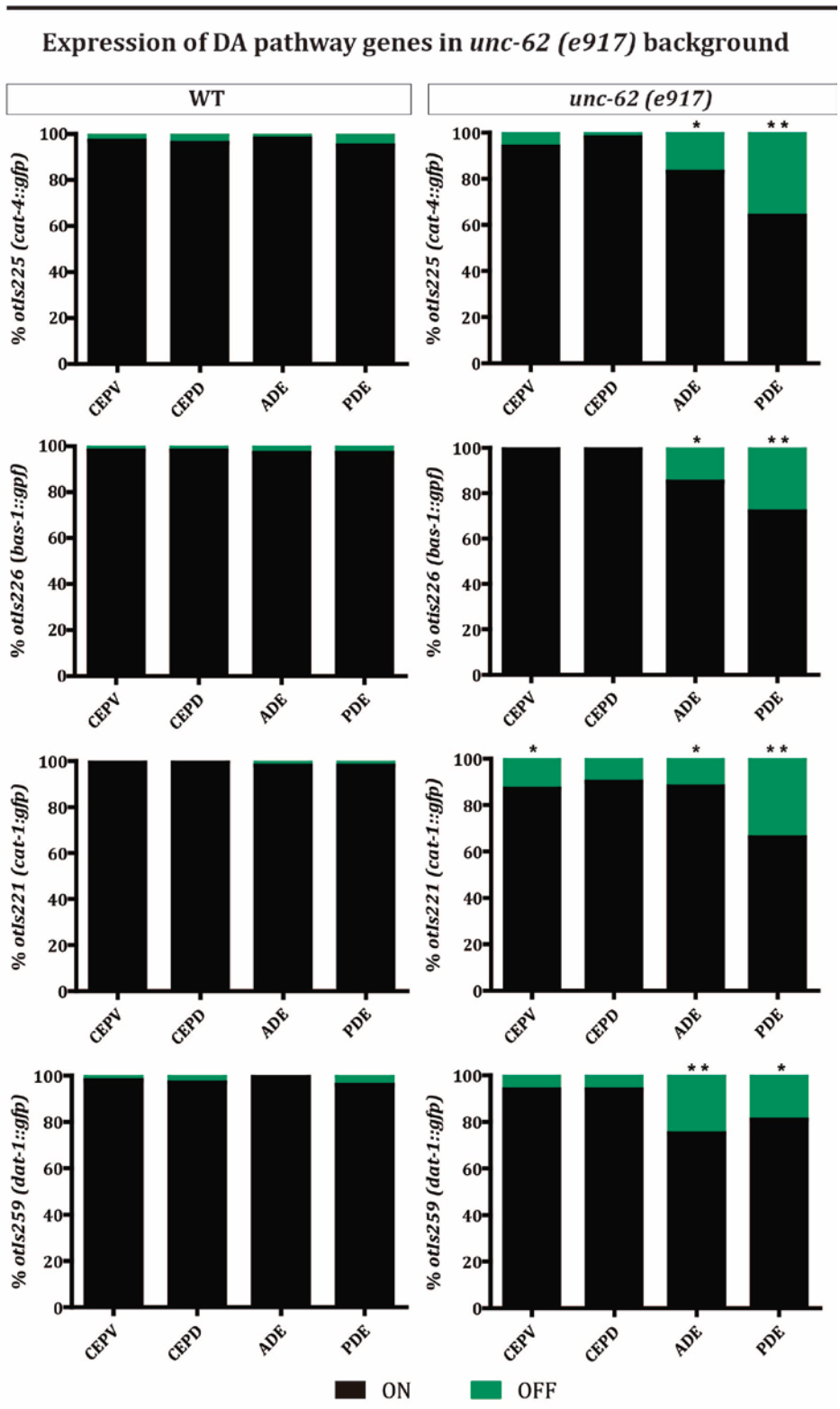
Expression of DA pathway genes in unc-62 (e917) background
WT
unc-62 (e917)
% otIs225 (cat-4::gfp)
% otIs226 (bas-1::gpf)
% otIs221 (cat-1::gfp)
% otIs259 (dat-1::gfp)
0
20
40
60
80
100
CEPV
CEPD
ADE
PDE
*
**
ON
OFF

Figure R.22. Expression of the dopaminergic pathway genes in *unc-62 (e917)* background. Left column represents the scores of the reporters analyzed (*cat-4, bas-1, cat-1* and *dat-1*, in this order) in a wild type background. Right column contains the scores of those reporters in the mutant background of *unc-62*. Black bars indicate the percentage of neurons expressing the fluorescent reporter. Green represents the percentage of neurons with undetected fluorescent. N = 50 worms/condition. Statistical analysis with Fisher exact test: (*) = ($p < 0.05$), (**) = ($p < 0.01$).

(Figure R.5b). Thus, in order to keep validating the function of this TF in the dopaminergic specification, we continued the experiments only with this allele.

In our analysis of additional DA pathway genes, we found that *unc-62 (e917)* animals show defects of expression of *dat-1*, *bas-1* and *cat-4* in ADE and PDE neurons while *cat-1* expression was affected in ADE, PDE and also CEPD (Figure R.22). Given the important role of *unc-62* regulating the dopaminergic pathway genes, we wanted to know if this gene is involved in the regulation of other terminal features of these neurons. In order to answer this question, we crossed the fluorescent reporters of *asic-1* with the mutant background *unc-62 (e917)*. The gene *asic-1* encodes for a sodium channel that contributes to the sustained neurotransmission of dopaminergic neurons (Topalidou and Chalfie 2011). Interestingly, the results showed a significant reduction in *asic-1::gfp* expression in ADE and PDE neurons (Figure R.23), proving that *unc-62* is necessary in

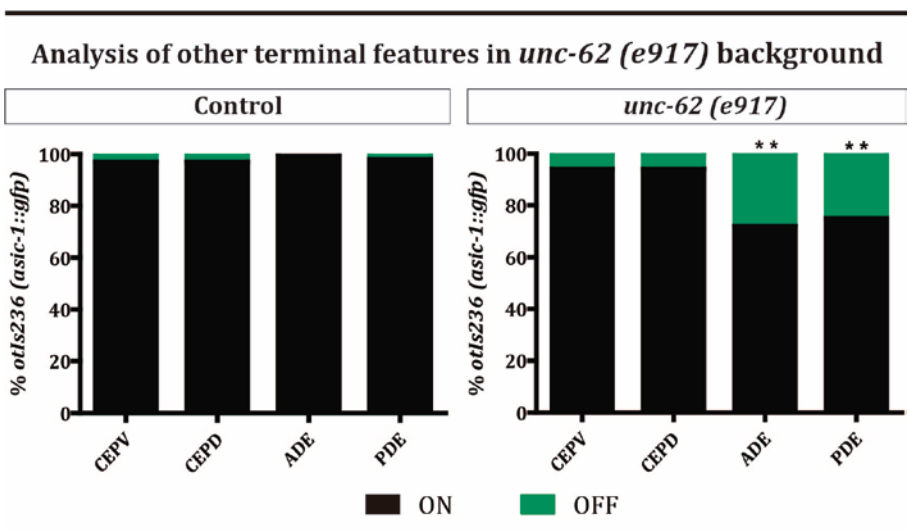

Figure R.23. Terminal features. Evaluation of *asic-1::gfp* reporter expression in control and mutant *unc-62 (e917)* background. Black bars point out the percentage of neurons expression the reporter, while green indicates missing fluorescence percentage. N= 50 worms. Statistical analysis with Fisher exact test: (**) = ($p < 0.01$).

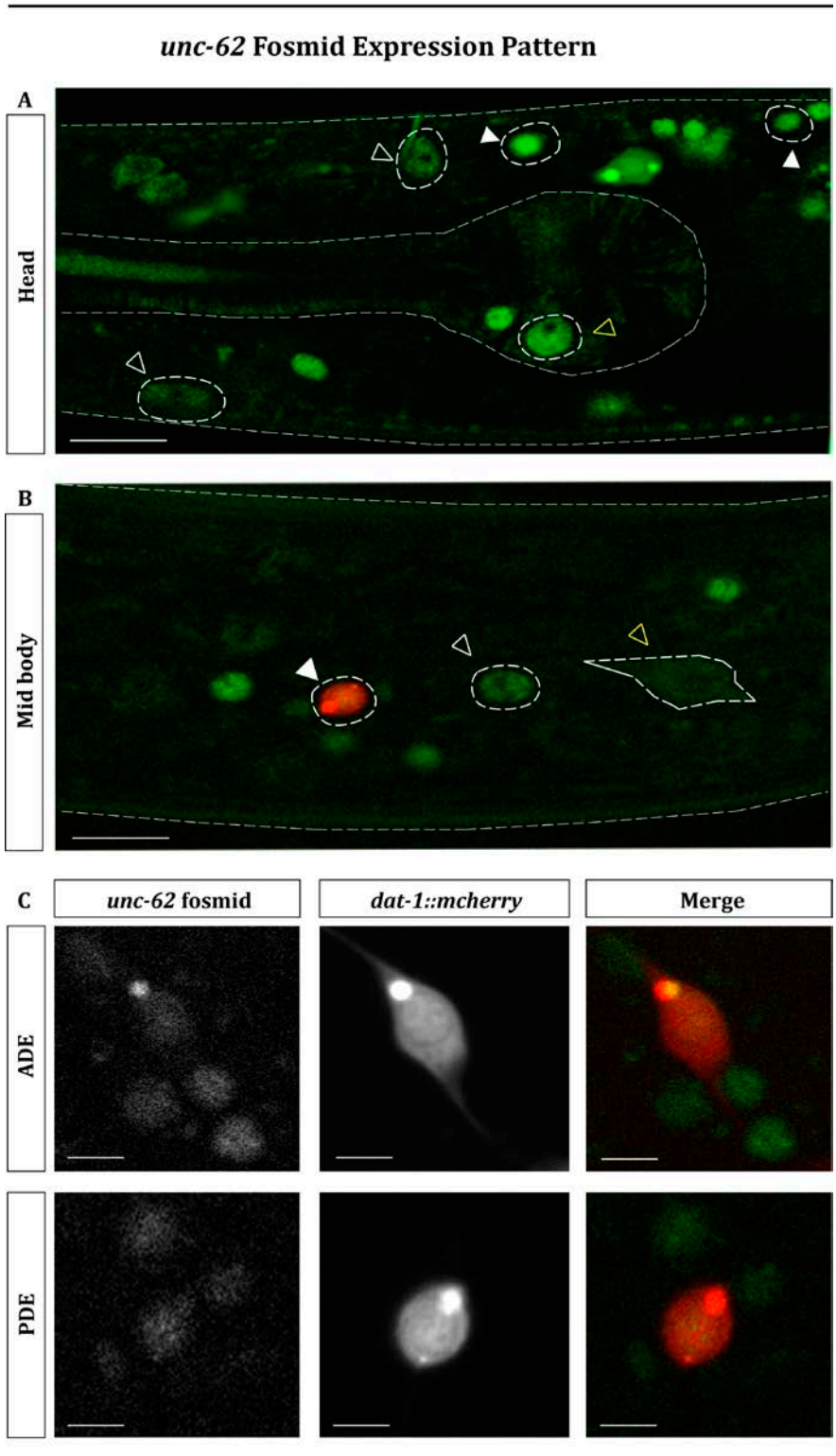
unc-62 Fosmid Expression Pattern
A
Head
B
Mid body
C
unc-62 fosmid
dat-1::mcherry
Merge
ADE
PDE

Figure R.24. Expression pattern of *unc-62*. Confocal micrographs of *unc-62* fosmid tagged with GFP form a young adult worm. a) Example of expression of *unc-62* in head, the second bulb of the pharynx is located in the center. Arrowheads point out neurons (white), hypodermal cells (black) and pharyngeal cell (yellow). b) Area from mid body, PDE neuron was detected (red) among hypodermal (black arrowhead) and intestinal cells (yellow arrowhead). Scale bars in a and b, 20 µm. c) Localized *unc-62* fosmid expression in dopaminergic cells labeled in red with the reporter *otIs181 (dat-1::mCherry)*. Scale bars, 5 µm.

these cells to regulate the expression of other terminal features apart from dopaminergic pathway genes. Thus, this TF could be essential to select the transcriptome of these dopaminergic neurons.

However, due to the fact that the expression of all analyzed reporters is affected in ADE and PDE in similar percentages it is possible that the ADE and PDE neurons in this allele is not generated or dies, in future experiments we will analyze if, on one hand, fate of sister cells of ADE and PDE are affected in *unc-62 (e917)* allele. Defects in sister cells of the lineage will indicate that *unc-62* has a role in lineage determination. On the other hand, we will also analyze expression of pan-neuronal and ciliated features in ADE and PDE. Pan-neuronal gene expression and cilia components are normally independent of terminal selector activity, thus, if *unc-62* is acting terminally we would not expect defects in expression of pan-neuronal genes, conversely, if pan-neuronal or cilia genes are affected will support a role of *unc-62* in lineage determination.

We next analyzed the expression pattern of *unc-62* fosmid (Figure R.24). We detected expression in the ADE and PDE but not in CEPs even at L1 stage, where fosmid shows the strongest expression. We also observed expression in other neurons, hypodermal and intestinal cells. This transgene starts to be detected at coma stage and continues in the adult. The lack of detectable *unc-62* in CEPs at adult stages coincides with the lack of maintenance requirements of *unc-62* in this DA population in contrast to ADE and PDE, were RNAi effects are also observed in P0 screens. It is possible that *unc-62* is required for CEP specification but not for maintenance, *unc-62* could be expressed in the embryo when CEPs are differentiating but its expression is not maintained in the adult. Alternatively, the fosmid strain we analyzed might not be an accurate representation of *unc-62* expression, indeed, previous results from our lab have determined differences between fosmids and CRISPR strains for the same gene. Finally, the effects of *unc-62* in CEPs could be because it is expressed early in the lineage that generates these neurons or due to non-cell autonomous effects. The lack of maintenance defects in the CEPs would be in agreement with the fact that *unc-62* is required either for CEP lineage or for early differentiation and not maintenance.

3.3.6. Characterization of unc-55 role in DA specification

unc-55 is involved in the specification of synaptic connections of VD motorneurons. The mouse ortholog of *unc-55*, COUP-TF1 is required for neuronal specification, including cortical neurons as well as dopaminergic neurons of the olfactory bulb (Bovetti et al. 2013). The allele we selected, *e1170*, presents an insertion of a C nucleotide in the position 47 of the first exon (Walthall and Plunkett 1995) (Figure R.25a). The insertion produces a frameshift that generates a non-functional protein. This mutation triggers a coiled-coil behavior which promotes the worms to coil backwards ventrally with a gentle touch. *unc-55(e1170)* shows *cat-2* transgene expression defects in the ADE neuron (Figure R.25c). This correlates with the results from the RNAi (Figure R.5d) although we did not detect any phenotype in PDE contrary to the results of the RNAi.

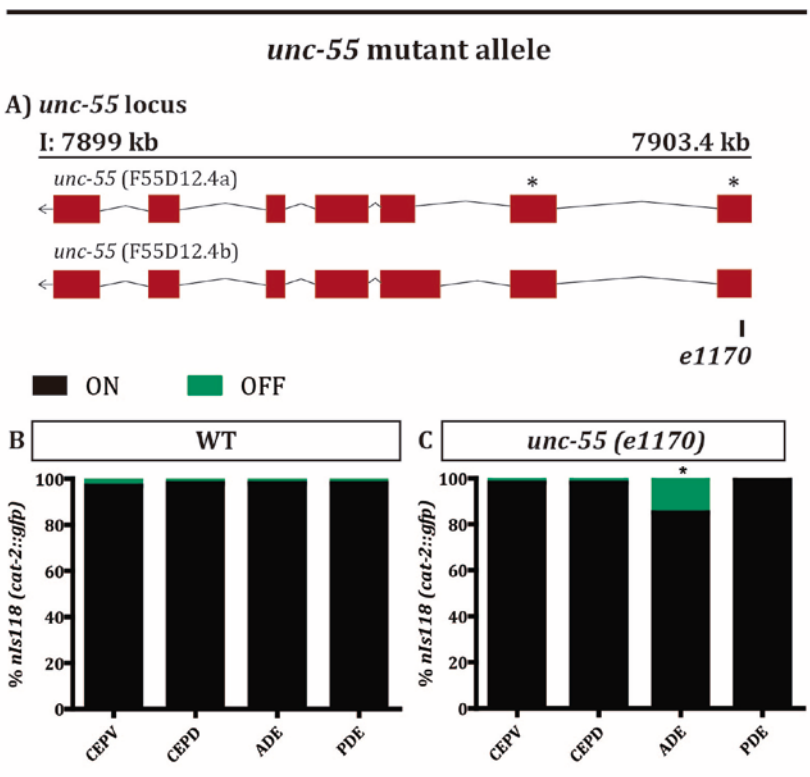

Figure R.25. *unc-55* mutant allele. Representation of *unc-55* genomic locus, where red boxes represent exons and connecting lines introns. Grey boxes represent untranslated regions of the mRNA. A) Scheme with the two isoforms of *unc-55*. (*) indicate the coding sequence of the NHR binding domain, which is affected in both isoforms for the insertion *e1170*. B-C) Representation of the scoring results of the reporter *nIs118 (cat-2::gfp)* in control and *e1170* backgrounds. The black color represents the percentage of neurons expressing the fluorescence reporter and in green is shown the percentage of missing neurons. N = 50 worms. (*) = significant result, Fisher exact test ($p < 0.05$).

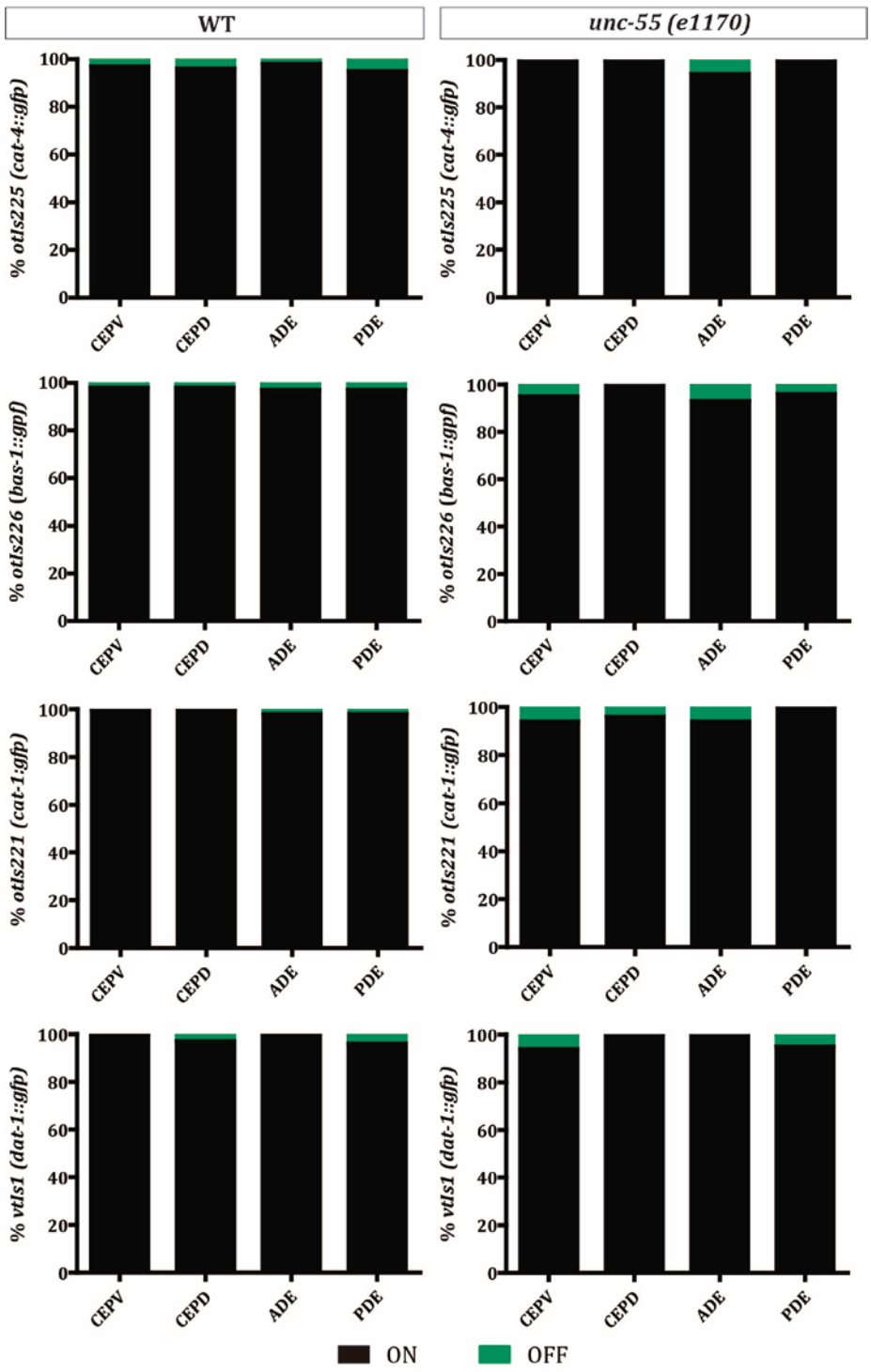
Expression of DA pathway genes in unc-55 (e1170) background
WT
unc-55 (e1170)
% otIs225 (cat-4::gfp)
% otIs226 (bas-1::gpf)
% otIs221 (cat-1::gfp)
% vtIs1 (dat-1::gfp)
0
20
40
60
80
100
CEPV
CEPD
ADE
PDE
ON
OFF

Figure R.26. Expression of the dopaminergic pathway genes in *unc-55 (e1170)* background. Left column represents the scores of the reporters analyzed (*cat-4, bas-1, cat-1* and *dat-1*, in this order) in a wild type background. Right column contains the scores of those reporters in the mutant background of *unc-55*. Black bars indicate the percentage of neurons expressing the fluorescent reporter. Green represents the percentage of neurons with undetected fluorescent. N = 50 worms/condition. Statistical analysis with Fisher exact test, any significant result was found.

Next, we crossed the *unc-55* mutant with reporters for the rest of the DA pathway genes. Surprisingly, *cat-4*, *bas-1* and *cat-1* expression is normal in the DA neurons of *unc-55* mutants (Figure R.26) and only *cat-2* expression is affected in ADE (Figure R.25c).

The specific effects of *unc-55* mutant on *cat-2* expression were surprising as our RNAi results showed expression defects also for *cat-1* and *dat-1* reporters (Table R.2). We were also surprised by the specific effects in ADE, as RNAi affects expression in all DA neurons. Previous work from the lab has shown that terminal selectors can act redundantly in some cases, meaning loss of function of one mutant does not produce any phenotype and only TF double mutants show expression defects (Lloret-Fernández et al. 2018; Doitsidou et al. 2013). Thus, we hypothesized that, if *unc-55* is acting as a terminal selector for DA fate it could be acting redundantly with other DA terminal selectors. Interestingly, although *ast-1,* a terminal selector for DA fate, is required for the expression of all DA pathway genes, the hypomorphic allele *ast-1 (hd1)* only affects *cat-2* expression, similar to *unc-55* mutant. Thus, we decided to cross both mutant backgrounds and check the expression of two other reporters of the dopaminergic pathway genes, *bas-1* and *dat-1*, to see if they could show synergistic and compensatory effects in the regulation of these genes.

Although both single mutants showed normal expression of *bas-1*, *ast-1(hd1)* and *unc-55(e1170)* double mutants show CEPD expression defects (Figure R.27c). Similarly, dat-1 expression shows PDE expression defects in PDE (Figure R.27f). These results prove that *unc-55* has an extended role in dopaminergic specification (both in DA subpopulations and DA pathway genes) than the one reported with single mutant background (Figure R.26), which is in agreement to what we observed through RNAi (Figure R.5d, d').

Next, to study *unc-55* expression we used a transcriptional reporter that contains 4kb upstream unc-55 starting site. We detected GFP in a few cells in the head and tail including ADE and PDE (Figure R.28). However, we did not observed expression where it was described: in VD motorneurons along the ventral nerve cord (Shan et al. 2005). Additionally, we did not see expression until L1 larval stage. This could indicate that our transcriptional reporter is not big enough to recapitulate the endogenous expression of

this TF. Similar to *unc-62*, *unc-55* is required to maintain expression of *cat-2* in ADE and PDE, the two neuronal populations in which we see the reporter expressed in adults. The phenotype in CEPD, both for RNAi and also in double mutants, contrasts with the undetected expression of *unc-55* in this neuron at adult stages. It is possible that *unc-55* is only expressed at embryonic stages or, alternatively, that the transcriptional reporter we used is not accurately reproducing the endogenous expression of the gene. It would be interesting, in future experiments to try to tag the locus of *unc-55* by CRISPR.

In summary, from our mutant characterization of TF candidates for DA specification we find that, generally, mutants phenotypes are less penetrant compared to the RNAi or, in the cases of *cep-1* and *mef-2*, we could not detect any defect in the dopaminergic

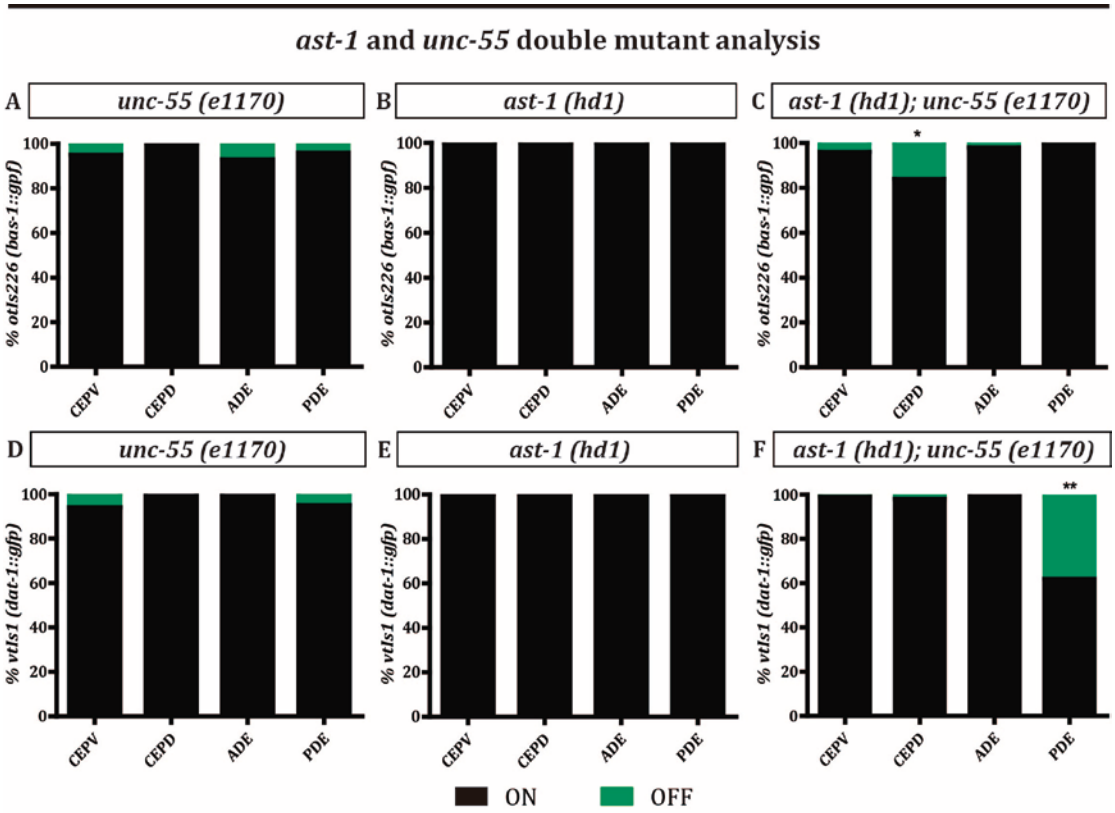

Figure R.27. *ast-1* and *unc-55* double mutant analysis. Double mutant analysis to assess cooperativity between *unc-55* and *ast-1*. Upper graphs (a-c) correspond to *bas-1* reporter scorings and lower graphs (d-f) correspond to *dat-1*. Double mutant scorings are indicated in right graphs (c and f). The single mutant results of *unc-55* (a and d) and *ast-1* (b and e) are also shown. In both double mutants we observe cooperativity between both TFs, represented by green bars, indicating loss of expression of the reporter. Black bars represent percentage of fluorescent remaining neurons. Statistics by Fisher test (*) = $p<0.05$; (**) = $p<0.01$.

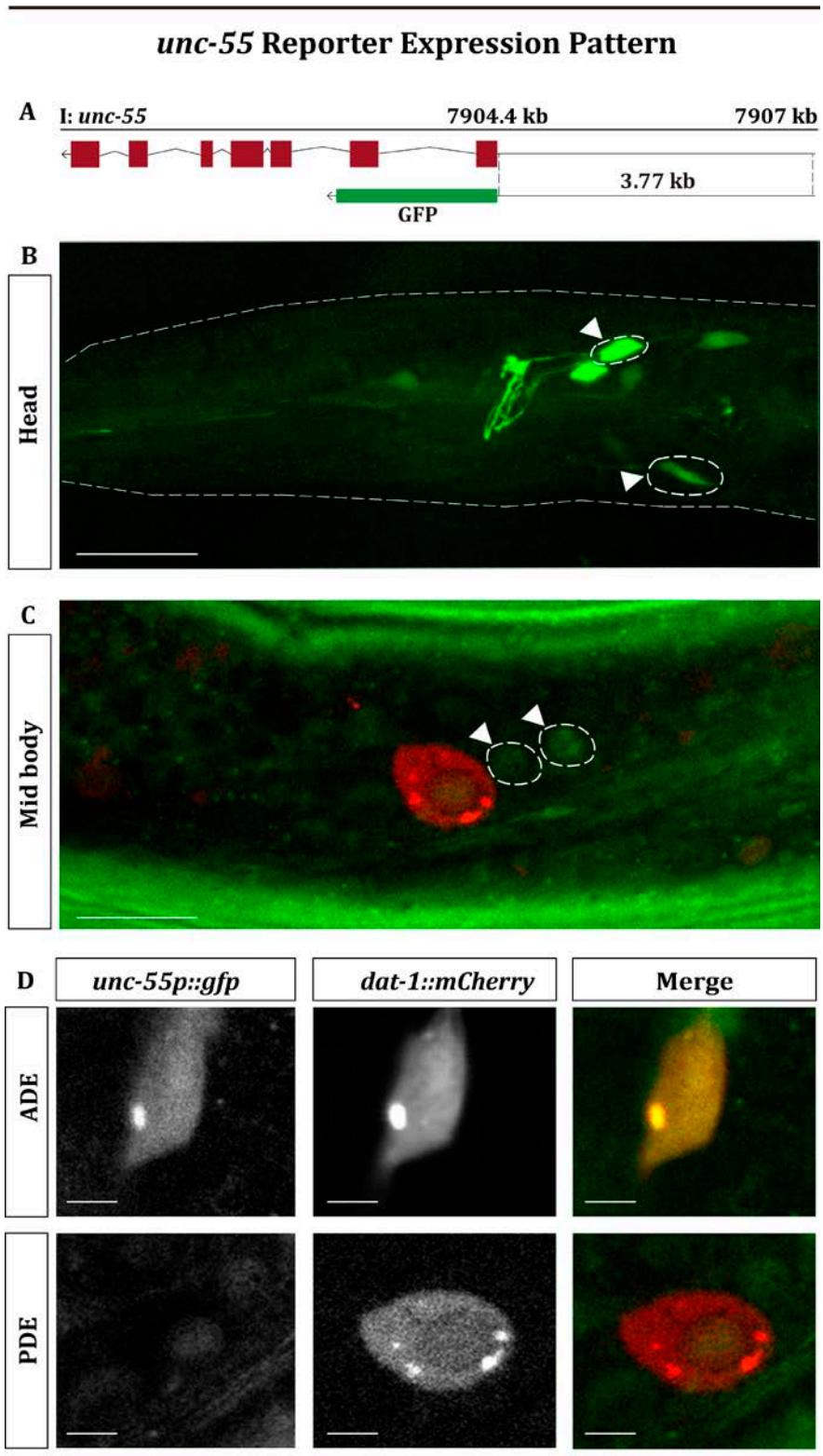
unc-55 Reporter Expression Pattern
A
I: unc-55
7904.4 kb
7907 kb
3.77 kb
GFP
B
Head
C
Mid body
D
unc-55p::gfp
dat-1::mCherry
Merge
ADE
PDE

Figure R.28. Expression pattern of *unc-55*. Confocal micrographs of *unc-55* transcriptional GFP reporter from a young adult worm. a) Genomic region of *unc-55* locus where was cloned the promoter of 3.77 kb in front of GFP (green rectangle) to build *unc-55* transcriptional reporter. a) Expression patter of *unc-55::gfp* in head. White arrowheads point out neurons. a) Area from mid body, PDE neuron was detected (red), next to other neurons (white arrowhead). Scale bars in B and C, 30 μm. d) Colocalization of the TF reporter with dopaminergic, *otIs181 (dat-1::mCherry)* (red). Scale bars, 5 μm.

neurons. As we previously mentioned, one explanation for this phenomenon could be that RNAi clones had secondary targets that generate the observed phenotypes. Other possibility is that there are compensatory effects in the mutant alleles that are not present in the RNAi experiments. We detected phenotypes in DA neurons for four out of the total six mutant candidates analyzed.

3.3. *cis*-regulatory analysis of dopaminergic pathway genes

TF collectives act together to bind and activate their target genes (Khoueiry et al. 2017). In our laboratory, we have previously isolated the CRMs of the dopamine pathway genes and we identified functional binding sites for AST-1, CEH-43 and CEH-20 (Doitsidou et al 2013). From our RNAi screen and our mutant allele validation we have identified four new TFs that are required for DA specification: *dro-1*, *unc-62, vab-3* and *unc-55*. To study if our candidates play a direct role in the expression of the DA pathway genes we performed cis regulatory analysis of DA pathway genes CRMs to look for functional binding sites, we focused on *unc-62, vab-3* and *unc-55* as these are the mutants with stronger phenotypes and whose expression is detected in DA neurons. *unc-62*, belongs to the TALE/MEIS homeodomain family, with a consensus binding sites corresponding to GACA. *vab-3*, is a Paired/Pax homeodomain, with a reported consensus site YAATTW. Finally, *unc-55* is a nuclear hormone receptor from the group Coup-tf (chicken ovalbumin upstream promoter transcription factor), with a consensus site TGACCW or AAGTW. All consensus sequences for each TF class were obtained from the data bases CisBP (Weirauch et al. 2014) and Jaspar (Khan et al. 2018).

The consensus of *unc-62* and *vab-3* are located in the binding domain corresponding to their homeodomain sequence (Table R.7). In case of *unc-62* there is a direct evidence of this consensus, whereas for *vab-3*, the motif was inferred from its mouse homologue *Pax6*. Moreover, *vab-3* also has a paired domain, but the bibliography attributes the binding to the homeodomain. On the other hand, the DNA binding domain of *unc-55* is located in its nuclear hormone receptor domain. However, there was no direct evidence of this binding in *C.elegans* but there was for their counterparts in mouse: the direct vertebrate orthologue of *unc-55*, which is *Nr2f1* or COUP-TF1, presents a direct binding

site, TGACCW, that we also seek in the CRM of dopamine pathway (Table R.7). It is important to highlight that consensus binding sites for TFs of the same family are very well conserved, even among members belonging to different species (Inukai, Kock, and Bulyk 2017).

Table R.7 TF binding consensus		
Transcription Factor	**DBD sequence**	**Source**
unc-62/Meis	GACA	(Campbell and Walthall 2016)
vab-3/Pax	YAATTW	(Berger et al. 2008)
unc-55/Coup-tf	AAGTW/TGACCW	(Qu et al. 2010; Badis et al. 2009)

We focused our analysis on *dat-1* and *cat-2* genes, both exclusively expressed in DA neurons. We found predicted binding sites for *unc-62*, *vab-3* and *unc-55* in *cat-2* and *dat-1*. However, consensus sites are small and degenerate and thus they are extensively found in the genome. The presence of a predicted binding site does not imply that they are functional. To assess their functionality, we performed site directed mutagenesis (Table R.8) and *in vivo* transgene analysis.

Table R.8 Consensus mutations		
Site	**Sequence**	**Change**
COUP-TF	AAGTA	AcccA
MEIS	GACA	tACA
PAX	GAAGAA	tccGAA
PBX	GATAGA	GtTAGA
DLX	ATAAT	ATccT

The CRM of *cat-2* contains predicted binding site for *unc-55* (COUP-TF), *vab-3* (PAX) and *unc-62* (MEIS) (Figure R.29). Point mutation of PAX and MEIS leads to a dramatic loss of expression in CEPD, ADE and PDE neurons in both cases (Figure R.29), whereas GFP expression in CEPV neurons remain unaffected. On the other hand, COUP-TF mutation affects partially to ADE and, to a less extend, CEPD GFP expression (Figure R.29).

If we compare these results to that of the mutant backgrounds with the *cat-2* reporter, we observed some differences. For example, *unc-55(e1170)* show *cat-2* expression defects in ADE but not in CEPD (Figure R.25c). In case of *unc-62(e917)*, ADE, PDE and CEPV show *cat-2* expression defects (Figure R.21e), while mutations in MEIS binding site affect ADE and PDE but not CEPV expression (Figure R.29). Moreover, MEIS binding site mutation affects GFP expression in CEPD, which is unaffected in *unc-62* mutant animals (Figure R.21). Finally, *vab-3 (ot346)* mutants show defects in ADE and CEPs expression (Figure R.19), while PAX mutation affects ADE, CEPs and also PDE expression (Figure R.29).

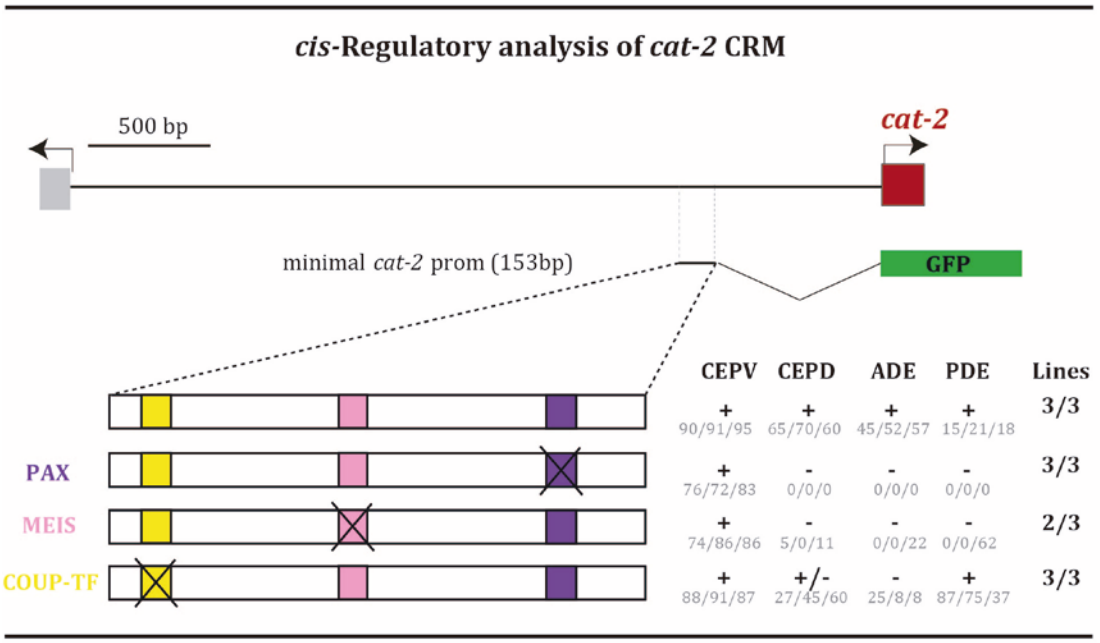

Figure R.29. *cis*-regulatory analysis of *cat-2* CRM. The color boxes represent the predicted binding sites for *unc-55* (COUP-TF site, yellow), *unc-62* (MEIS site, pink) and *vab-3* (PAX site, purple). The black crosses indicate a mutation to disrupt the binding motif. "+" ≥ 70% of transgene expression; "+/-" = 70-30% partial expression; "-" ≤ 30%, loss of expression. The percentages, also included (grey), are referred to the average expression of WT construct. The column "lines" alludes the number of worm lines scored where we observe the indicated phenotype. N = 30 worms/line.

Similar discrepancies between regulatory mutations in CRMs and mutant allele phenotypes have been previously reported (Lloret-Fernández et al. 2018). This discrepancy can be explained because, on one hand, the length of the promoter region is different in the CRM analysis and in the reporter mutant analysis. Thus, compensatory effects in longer reporters might not exist in smaller CRMs. This could be the case for the CEPD expression defect in COUP-TF and MEIS mutation compared to *unc-55* and *unc-62* mutants or the PDE expression defect of PAX mutation that is not present in *vab-3* mutants. To assess if the compensatory effects are the cause of this discrepancy, we will analyze expression of *cat-2* minimal CRM in the mutant backgrounds of *unc-55*, *unc-62* and *vab-3* and compare the phenotypes with the full reporters.

On the other hand, although we were very careful mutating the putative binding sites of the TF, the possibility still exists that we are disrupting the binding of another transcription factor or creating a binding for another protein that could repress the expression of the transgene.

We have also previously described the converse effect in which, while the mutant allele shows expression defects, the mutation of the corresponding TF binding site does not produce any significant defect in expression (Lloret-Fernández et al. 2018). This can be explained because, as TFs act as a collective with extensive TF-TF interactions, in some occasions TFs can be recruited to the CRM even in the absence of a functional TF binding sites (Khoueiry et al. 2017).

We also analyzed *dat-1* CRM that also bares putative binding sites for all three candidate TFs (Figure R.30). PAX binding site mutation leads to GFP expression defects in the PDE. This is in contrast to *vab-3* mutant analysis that shows *dat-1* expression defects in CEPs but not in PDE. Next, we performed point mutation analysis of MEIS sites. The CRM of *dat-1* contains two predicted MEIS binding sites and the mutation of them individually resulted in a partial missing phenotype in PDE. Combined mutation of both sites produces GFP expression defects also in ADE neurons. If we compare these results with the mutant background analysis, in this case, both strategies show similar phenotypes.

Finally, there are three COUP-TF BS in dat-1 CRM, as two of them are close to each other we mutated both simultaneously. However, this mutated construct does not show expression defects (Figure R.30), thus we simultaneously mutated the three COUP-TF sites in the same construct. This combined triple mutation produced a lack of GFP expression in the PDE, what proves that this third binding site for COUP-TF, or the combination of the three sites, is functional. As in the case of the *cat-2* CRM analysis, COUP-TF mutation in *dat-1* CRM produces a greater effect than *dat-1* reporter expression in *unc-55* mutants, which is unaffected. However, we actually observed a phenotype in PDE in the double mutant of *un-55 (e1170)* and *ast-1 (hd1)* (Figure R.24c and e), this double mutant analysis, together with our CRM mutational analysis strongly suggests *unc-55* is terminally required to control DA fate in several DA subpopulations.

Considering *unc-55* synergistic effects with *ast-1,* we decided to explore other genetic interactions through combinations of TF binding site mutations. Mutation of the ETS/*ast-1* site from the *dat-1* CRM result in a complete loss of fluorescence in all dopaminergic neurons (Doitsidou et al. 2013), thus we cannot use this binding site mutation in our combinatorial analysis. Alternatively, we decided to evaluate combined binding site mutation of unc-55/COUP-TF site with *ceh-20*/PBX and *ceh-43*/DLX, two TFs already described to be involved in dopaminergic development and whose binding site mutations cause partial *dat-1* expression defects. Combined *unc-55*/COUP-TF and ceh-20/PBX mutation does not increase the *dat-1* expression defects observed with single mutations (Figure R.30). In contrast, while *ceh-43*/DLX binding site mutation only affects *dat-1* expression in CEPs, the combination with *unc-55*/COUP-TF mutation (that does not

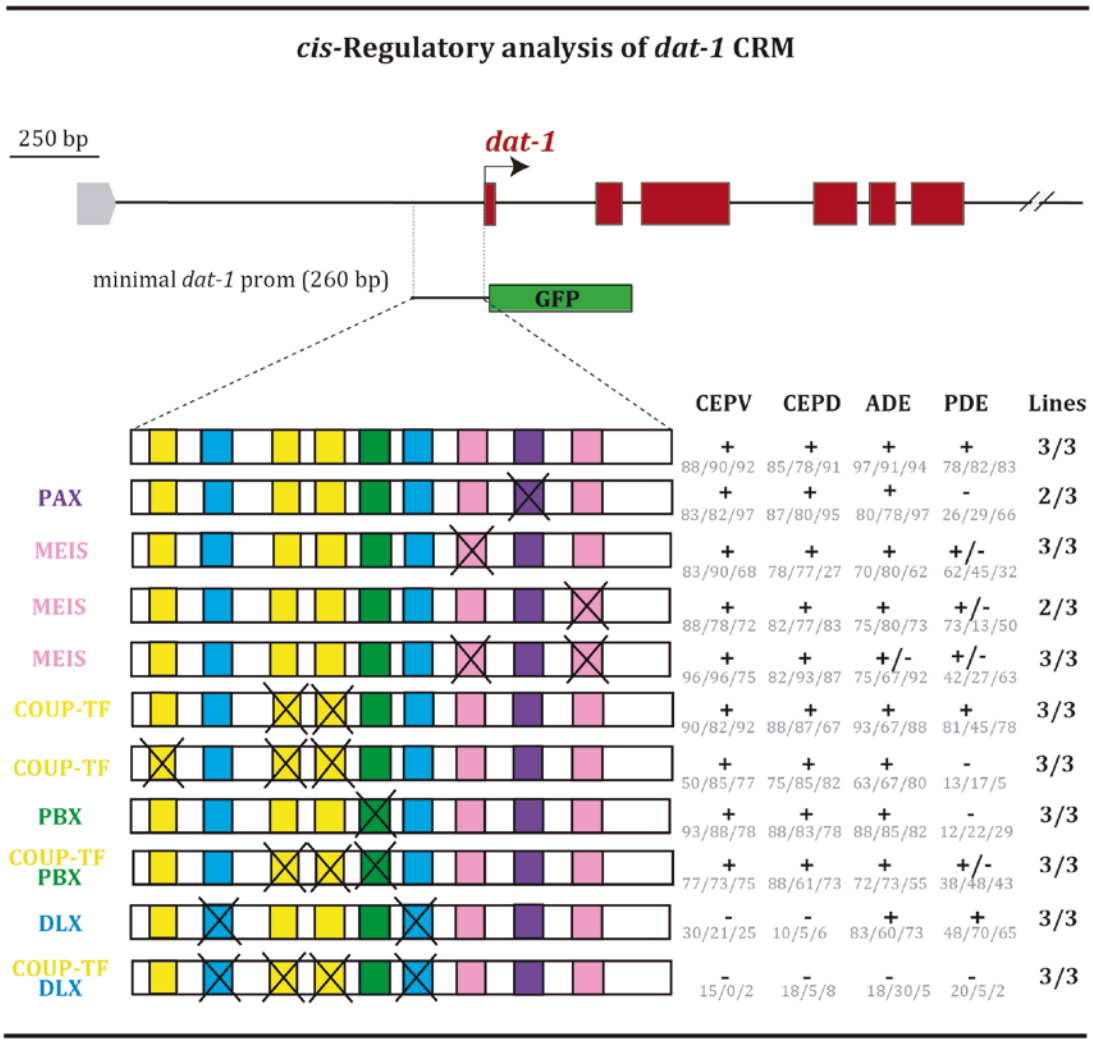

Figure R.30. *cis*-regulatory analysis of *dat-1* CRM. The color boxes represent the predicted binding sites for *unc-55* (COUP-TF, yellow), *unc-62* (MEIS site, pink), *vab-3* (PAX site, purple), *ceh-20* (PBX, green) and *ceh-43* (DLX, blue). The black crosses indicate a mutation to disrupt the binding motive. "+" ≥ 70% of transgene expression; "+/-" = 70-30% partial expression; "-" ≤ 30%, loss of expression. The percentages, also included (grey), are referred to the average expression of WT construct. The column "lines" alludes the number of worm lines scored where we observe the indicated phenotype. N = 30 worms/line.

have an effect on its own) leads to complete loss of GFP in all DA cells. These results prove that both TF cooperate to directly regulate the expression of *dat-1* CRM.

The conclusion from this this part of the work is that through the RNAi screen we identified new TFs involved in dopaminergic neurons differentiation that we have validated through mutant and *cis*-regulatory analysis (see Table R.9 for summary). It

seems that *unc-62*, *vab-3* and *unc-55,* together with the already characterized *ast-1*, *ceh-20* and *ceh-43* factors act to regulate DA terminal fate. Importantly, single mutant phenotypes for most of these factors show weak and partial defects suggesting extensive compensatory effects among the DA TF collective, this redundancy is probably required to drive robust expression of DA effector genes.

Table R.9 Summary of results from DA candidates

TF	Reporter	RNAi		Mutant		*cis*-Analysis	
		Stage	Neuron affected	Allele	Neuron affected	Mutated Motif	Neuron affected
cep-1	*cat-2*	P0	CEPV, CEPD, ADE	*ep347*	none		
	cat-1	F1	CEPV, CEPD, ADE				
mef-2	*cat-2*	P0	CEPV, CEPD	*gk633, gv1*	none		
	cat-1	F1	CEPV, CEPD, ADE				
dro-1	*cat-2*	P0	CEPV, CEPD, ADE, PDE	*tm4702*	ADE		
	cat-1	F1	CEPV, CEPD, ADE, PDE				
unc-55	*cat-2*	P0	ADE, PDE	*e1170*	ADE	COUP-TF	CEPD, ADE
	cat-1	F1	CEPV, CEPD	*e1170*	none		
	cat-4			*e1170*	none		
	bas-1			*e1170*	none		
				e1170; hd1	ADE		
	dat-1			*e1170*	none	COUP-TF (2X)	none
						COUP-TF (3X)	PDE
				e1170; hd1	PDE	COUP-TF (2X); PBX	PDE
						COUP-TF (2X); DLX (2X)	CEPV, CEPD, ADE, PDE
vab-3	*cat-2*	P0	CEPV, ADE, PDE	*ot346*	CEPs, ADE	PAX	CEPD, ADE, PDE
	cat-1	F1	CEPV, ADE, PDE				
	dat-1			*ot346*	CEPs	PAX	PDE
unc-62	*cat-2*	P0	ADE, PDE	*e644*	ADE	MEIS	CEPD, ADE, PDE
				mu232	ADE		

				e917	CEPV, ADE, PDE		
	cat-1	F1	CEPV, CEPD, ADE, PDE	*e917*	CEPV, CEPD, ADE		
	cat-4			*e917*	ADE, PDE		
	bas-1			*e917*	ADE, PDE		
	dat-1			*e917*	ADE, PDE	MEIS	PDE
						MEIS (2X)	ADE, PDE

Table R.9 Summary of results from DA candidates. This table contains results from RNAi, mutant *cis*-analysis about the six TF (*cep-1, mef-2, dro-1, unc-55, vab-3* and *unc-62*) whose role in DA pathway genes expression was analyzed. Grey squares indicate results did not achieve. See table A.5 in the Annex for detailed scores of RNAi and mutant DA candidates.

4. Validation of the TF candidates required for the generation of different serotonergic neuron subtypes

4.1. The different serotonergic neurons do not share TF candidates from the screen

The nematode *C. elegans* contains three subtypes of bilaterally symmetric serotonergic neurons: NSM, ADF and HSN. These neurons share the expression of the enzymes and transporters required to synthesize and release serotonin, however they originate from different lineages in development (see Intro Figure I.13) and they perform distinct functions: neurosecretory, chemosensory and motorneuron, respectively. Apart from these bona fide serotonergic neurons, the worm also contains other group of neurons that do not produce serotonin but they are able to reuptake this neurotransmitter from the medium and use it as their own. These neurons are the AIM (bilateral neuron) and RIH (unilateral). All serotonergic neurons (bona-fide or re-uptakers) express the vesicular monoamine transporter, *cat-1*, to pack and release 5-HT. However, it is important to remind that the *cat-1* reporter we used in the screen is not expressed in the AIMs and RIH at young adult state so we did not retrieve TF candidates required for the specification of these two neuronal types. Additionally, VC4/5 neurons, located near the vulva, although they are cholinergic motorneurons, they express the *cat-1* reporter and are unreliably stained for 5-HT, thus, in our screen we also obtained TF candidates to be required for *cat-1* expression in these two neurons.

As mentioned in section 2.1 of the present Results, our RNAi screen reported phenotype for most of the known regulators of serotonergic fate in the different neuron subtypes. We retrieved RNAi phenotypes for the 6 TFs involved in the terminal

differentiation of HSN neuron (Lloret-Fernández et al. 2018). We also found expression defects of the corresponding RNAi clones for other already reported TFs such us *unc-86* role in NSM or *lim-4* in ADF or *unc-4* for VC4/5 (Zhang et al. 2014; Zheng et al. 2005; Zheng et al. 2013). The only TF reported to have a terminal role in serotonergic fate not retrieved in the RNAi screen was *daf-19*, whose action is necessary for *tph-1* expression in ADF. These results indicate that our RNAi screen should be a good strategy to identify new regulators of serotonergic fate.

Unlike the dopaminergic population, the serotonergic neurons do not share any common TF candidate. This is in agreement with the functional and molecular diversity of each serotonergic subtype. It is reasonable to propose that, as the transcriptomes of each 5-HT subtype are very different, each cell type employs different genetic programs (that is different terminal selector combinations) to regulate their expression. Indeed, in our previous 5-HT pathway gene cis regulatory analysis we isolated different modules active in each serotonergic neuron class (Lloret-Fernández et al. 2018).

In our screen we identified fourteen TF candidates to have a previously unreported role in serotonergic specification (Table R.10). Most of the candidates belong to the homeodomain and Zn-C2H2, as is the case, in general, for other monoaminergic populations. The highest number of TF candidates was obtained for the ADF neuron subtype, this is particularly interesting as the TFs required for ADF terminal fate remain mostly unknown.

Surprisingly, for NSM serotonergic neuron we only retrieved the already known factor *unc-86* and the heterochronic gene *lin-14.* The gene *unc-86* is known to work together with *ttx-3* for NSM specification, where only double *unc-86* and *ttx-3* mutants show prominent synergistic effects regulating several effector genes. Thus, one possible explanation for the lack of NSM candidates is that other TFs are also redundant, with *unc-86* or other factors, and thus, loss of function RNAi experiments can be compensated by the presence of the other factors. Combined used of several RNAi clones does not produce good knockdown effects; however, one possible strategy to retrieve additional NSM clones would be to use the *unc-86 (n846)*, *rrf-3(pk1426) or ttx-3 (ot22)*, *rrf-3(pk1426)* mutant as strain background to perform RNAi.

Regarding VC4 and VC5 we retrieved 11 TF candidates involved in their specification (Table R.2). Some of them affect their lineage, such us *lin-39*, *lin-40* or *pax-3* (Table R.4); others like *lin-28* or *lin-14* are heterochronic genes. Finally, we included in Table R.10 the TF that could be most likely involved in later steps of development for these two neurons. However, as VC4/5 are cholinergic and, although they express the *cat-1* gene, they are not considered to be monoaminergic, thus we did not further characterize those candidate TFs.

Table R.10. TF candidates involved in 5-HT specification

Gene Name	DBD	Neuron affected	Phenotype	*cat-1 ::gfp*	*tph-1 ::dsRed*
hlh-14	bHLH	ADF	Missing fluorescence	18/60	13/60
zip-10	bZIP	ADF	Missing fluorescence	42/60	42/60
lag-1	CSL	ADF	Missing fluorescence	12/60	5/60
lim-4	HD - LIM	ADF	Missing fluorescence	45/60	42/60
ceh-27	HD - NK	ADF	Missing fluorescence	52/60	51/60
pax-3	HD - PRD	ADF	Missing fluorescence	50/60	50/60
ceh-37	HD - PRD	ADF	Missing fluorescence	50/60	50/60
unc-130	WH - ForkHead	ADF	Missing fluorescence	49/60	46/60
pqn-21	ZF - C2H2	ADF	Missing fluorescence	49/60	49/60
odd-2	ZF - C2H2	ADF	Missing fluorescence	54/60	54/60
R05D3.3	ZF - C2H2	ADF	Missing fluorescence	52/60	52/60
flh-2	ZF - FLYWCH	ADF	Missing fluorescence	53/60	53/60
flh-1	ZF - FLYWCH	ADF	Missing fluorescence	48/60	48/60
hlh-3	bHLH	HSN	Missing fluorescence	45/60	40/60
unc-86	HD - POU	HSN	Missing fluorescence	18/60	12/60
lin-14	unknown	HSN	Missing fluorescence	32/60	29/60
ast-1	WH - ETS	HSN	Missing fluorescence	32/60	29/60
hbl-1	ZF - C2H2	HSN	Missing fluorescence	50/60	48/60
egl-46	ZF - C2H2	HSN	Missing fluorescence	50/60	50/60
sem-4	ZF - C2H2	HSN	Missing fluorescence	39/60	37/60
egl-18	ZF - GATA	HSN	Missing fluorescence	48/60	50/60
pha-4	ZF - ForkHead	HSN	Missing fluorescence	50/60	50/60
unc-86	HD - POU	NSM	Missing fluorescence	40/60	40/60
lin-14	unknown	NSM	Missing fluorescence	48/60	48/60
lin-28	COLD BOX	VCs	Missing fluorescence	10/60	n.e.
unc-4	HD - PRD	VCs	Missing fluorescence	10/60	n.e.
ceh-20	HD - TALE	VCs	Missing fluorescence	16/60	n.e.
lin-14	unknown	VCs	Missing fluorescence	40/60	n.e.
tra-1	ZF - C2H2	VCs	Missing fluorescence	40/60	n.e.
nhr-61	ZF - NHR	VCs	Missing fluorescence	46/60	n.e.

Table R.10. TF candidates involved in serotonergic specification. The list includes the TFs from the RNAi screen that present significant missing fluorescence phenotype in 5-HT population, without those reported to clearly affect lineage (*egl-5, nob-1, lin-39, pax-3, sem-2, ref-2, lin-40*). Grey font indicates TFs already reported to have a role in the specification of that neuronal population. The scoring results with the reporters *cat-1* and *tph-1* indicate the ratio of remaining neurons after the RNAi feeding, in a population of 30 worms. n.e. = not expressed.

In summary, as ADF specification is the less characterized and we obtained several interesting candidates for this neuron subtype we decided that for the validation of TF candidates by mutant analysis we would focus on ADF.

4.2. Characterization of *lag-1* as terminal selector for ADF fate

To prioritize in our analysis, we decided to analyze the role of *lag-1*, the TF candidate that gave the highest missing phenotype in this neuron. *lag-1* is the only *C. elegans* member of the CSL (CBF-1, Su(H), Lag-1) TF family. CSL factors are the transcriptional mediators of the Notch signaling pathway. When Notch proteins, that are transmembrane receptors, bind to their ligands, they suffer a proteolytic cleavage giving rise to the Notch intracellular cleavage domain (NICD), which is translocated to the nucleus, where binds a CSL TF to regulate transcription. It has been described that, when CSL binds to DNA it behaves as a repressor and it is the complex formed with NICD which drives an active expression of target genes (Johnson and MacDonald 2011) (Figure R.31).

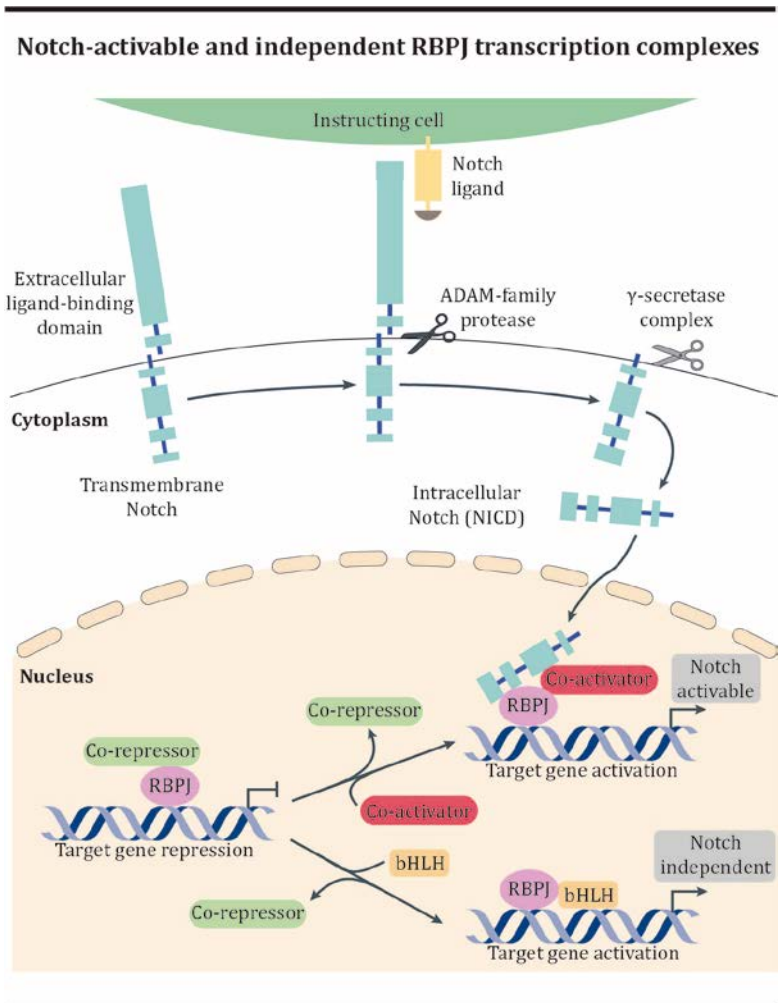

Figure R.31. Notch-activable and independent RBPJ transcription complexes. Representation of canonical Notch pathway and independent activation of RBPJ (mammalian *lag-1* ortholog) transcription. Adapted from *Amsen et al 2009.*

In *C. elegans*, the Notch signaling pathway has been involved in terminal fate. For instance, their expression in the precursors of anchor cell and ventral uterine cell is necessary to select their terminal fate (Park, Choi, and Hwang 2013). However the role of *lag-1* in neuronal terminal fate has never been uncovered, although it has been involved in the specification of some features of neurons, such us left/right asymmetry (Bertrand et al. 2011).

First, we analyzed the expression pattern of *lag-1* to determine if it is expressed in ADF. As commented before, the most accurate reporters are those modifying the endogenous locus. For this purpose, Dr. Maicas from our lab built, through CRISPR technique, a mNeongreen knock in to tag the endogenous locus of *lag-1* (Figure R.32a).

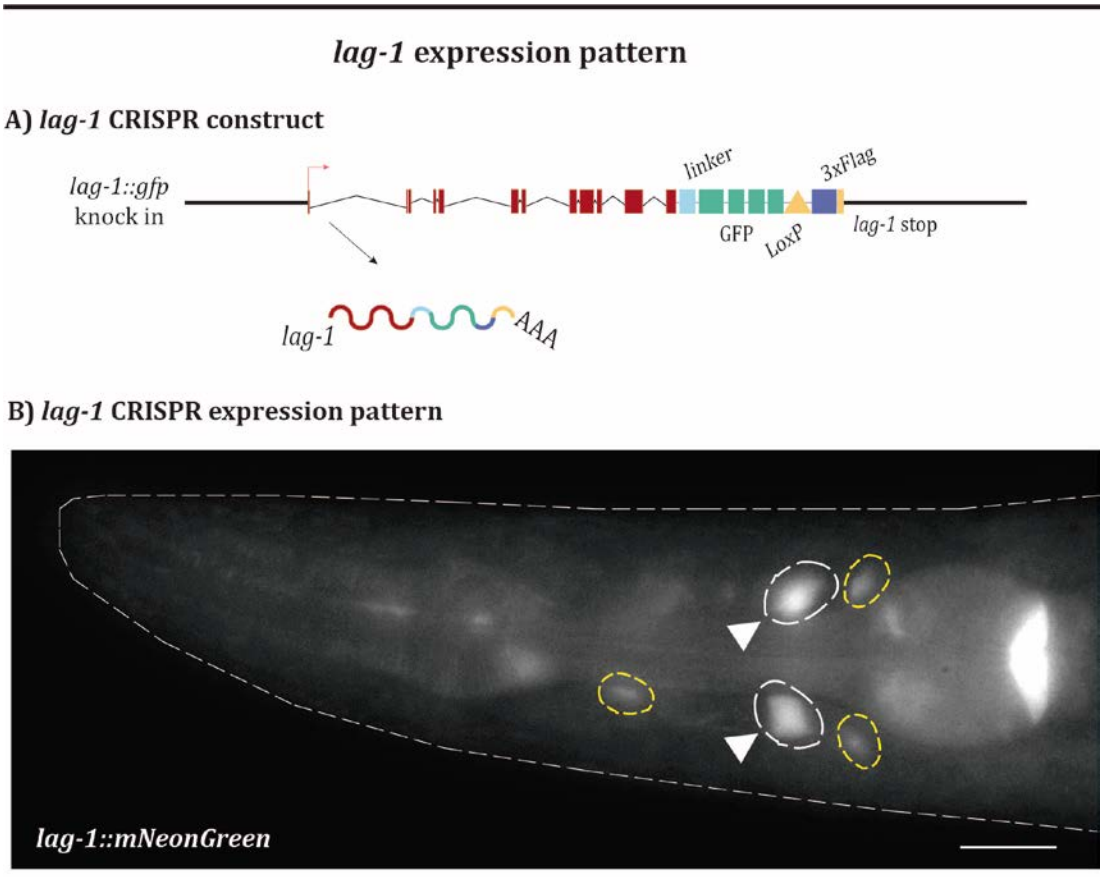

Figure R.32. *lag-1* expression pattern. a) Scheme of CRISPR construct to tag endogenous *lag-1* locus. b) Expression pattern of *lag-1* CRISPR reporter tagged with mNeongreen at young adult stage. Fluorescence expression in ADF is denoted with white arrowheads. Expression in other cells is marked with yellow circles. Scale bar, 25 µm. CRISPR construct and analysis of *lag-1* expression were conducted by Dra. Miren Maicas.

With this method, we could notice a clear expression of this TF in ADF (Figure R.32b), what could point out that its effects over this neuron are cell autonomous. Moreover, the expression of this reporter in adults is restricted to some cells in the head of the animals, approximately 4 pairs of cells, the ADF pair and another pair of unidentified neurons.

After detecting the expression of *lag-1* in ADF, we continue exploring the role of this candidate through its mutant analysis. As happens with RNAi, the null mutant allele of this TF, *q385*, produces early larval lethality; strains with this allele are maintained with a genetic balancer. This allele corresponds to a single nucleotide substitution (G > A) that provokes a premature stop codon, disrupting the last 48 aminoacids of the protein (Lambie and Kimble 1991; Christensen et al. 1996) (Figure R.33a). Another *lag-1* mutant allele, *om13*, also consists of a single nucleotide substitution (G > A) in the same exon as *q385* (Figure R.33a), however this missense mutation generates an aminoacid change (A551T) that do not produce larval lethality at 15ºC; this hypomorphic allele is temperature sensitive and thus, the strain can be maintained at 15 °C allowing animals to survive until adult stages and at 25ºC is lethal (Qiao et al. 1995). Interestingly, neither of these two mutations alter *lag-1* DNA-binding domain, but both affect the four isoforms encoded by *lag-1* locus.

We ordered both mutant alleles and crossed them with the reporters of serotonergic pathway genes to analyze the effect of *lag-1* over this subset of terminal features characteristic of ADF. The results show that both alleles exhibit significant reduction in expression in all 5-HT pathway genes. These defects are especially notable in the null allele, *q385* (Figure R.33b).

Thus, in view of these data *lag-1* seem to be a robust candidate to drive terminal fate in ADF neuron. Consequently, as mentioned above, we wonder if the role of *lag-1* in ADF maturing was coordinated through the Notch signaling pathway, where this TF participates as transcriptional effector, or if, by contrast, the function of *lag-1* in ADF is independent of Notch. It has been described that this CSL TF can exert regulatory roles in a Notch independent pathway: CSL cooperatively binds to other coactivators to assess gene expression. This complex is able to overcome the repressor role of CSL and its formation is dependent on the presence of binding motif in the target sequences for this TF and on the availability of specific cofactors within a tissue. One example of this kind of complex is the pancreatic transcription factor 1 (PTF1). This complex drives the expression of exocrine pancreatic genes and is composed of Rbpj, the mammal orthologue of *lag-1*, or its paralogue Rbpl, and Ptf1a, a member of bHLH TF family (Beres et al. 2006). Moreover, this complex is also found in neurons from spinal cord, cerebellum and retina, where selects the inhibitory GABAergic fate of neurons preventing the excitatory lineages (Hori et al. 2008).

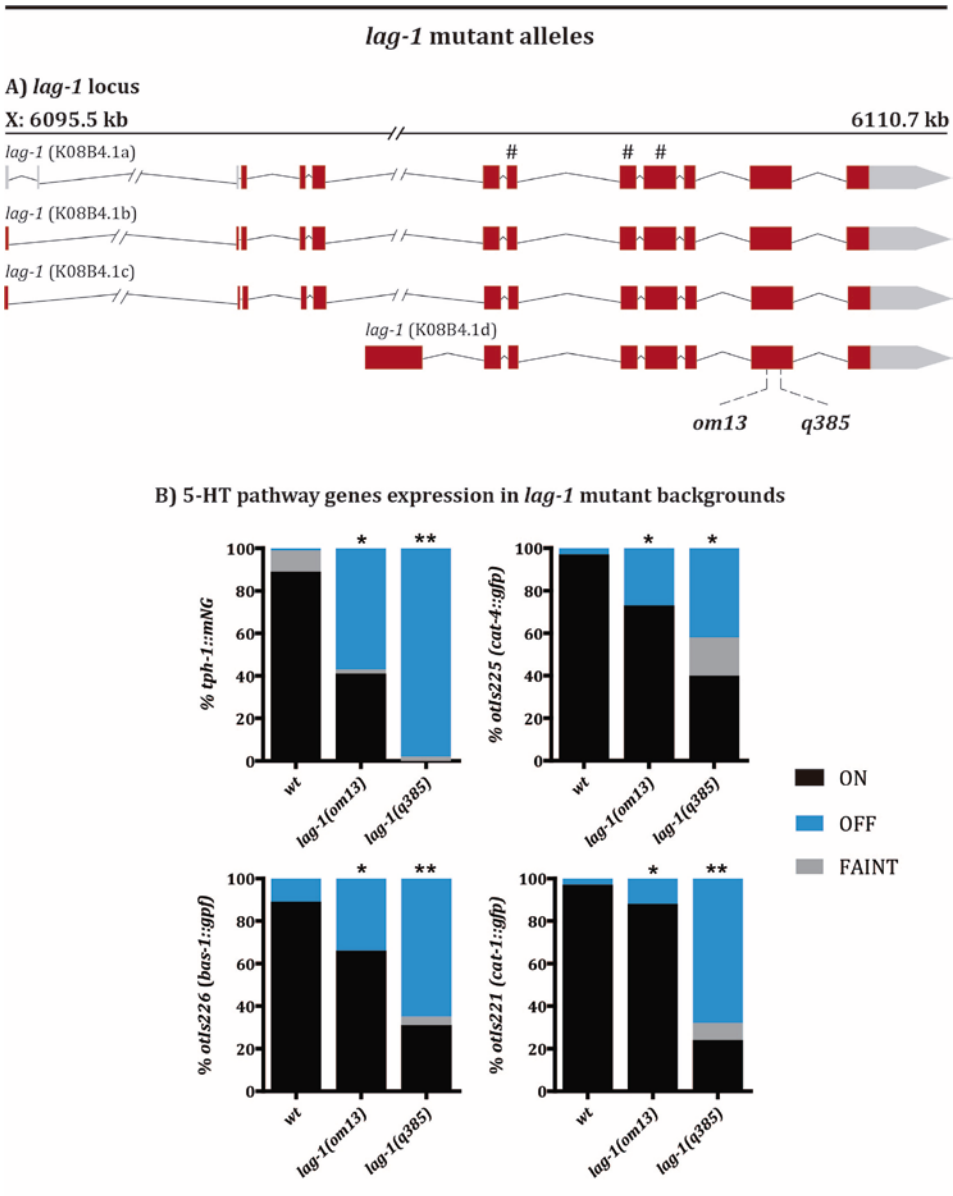

Figure R.33. *lag-1* mutant alleles. Representation of *lag-1* genomic locus, where red boxes represent exons and connecting lines, introns. Grey boxes represent untranslated regions of the mRNA. a) Scheme with the three isoforms of *lag-1*. (#) indicates the coding sequence of the DNA binding domain. Discontinuous lines point where mutations *om13* and *q385* are located. b) Scores of 5-HT pathway genes in *lag-1* mutant backgrounds. Black bars indicate normal expression; gray, faint expression; and blue, represent undetected fluorescence in ADF. N = 50 animals. Statistics with two tail Fisher test showed significant differences compare to wild type control. (*) < p =0,05; (**) = p < 0,01. These results were obtained by Dra. Miren Maicas. See Table A.6 in the Annex for detailed scores of *lag-1*.

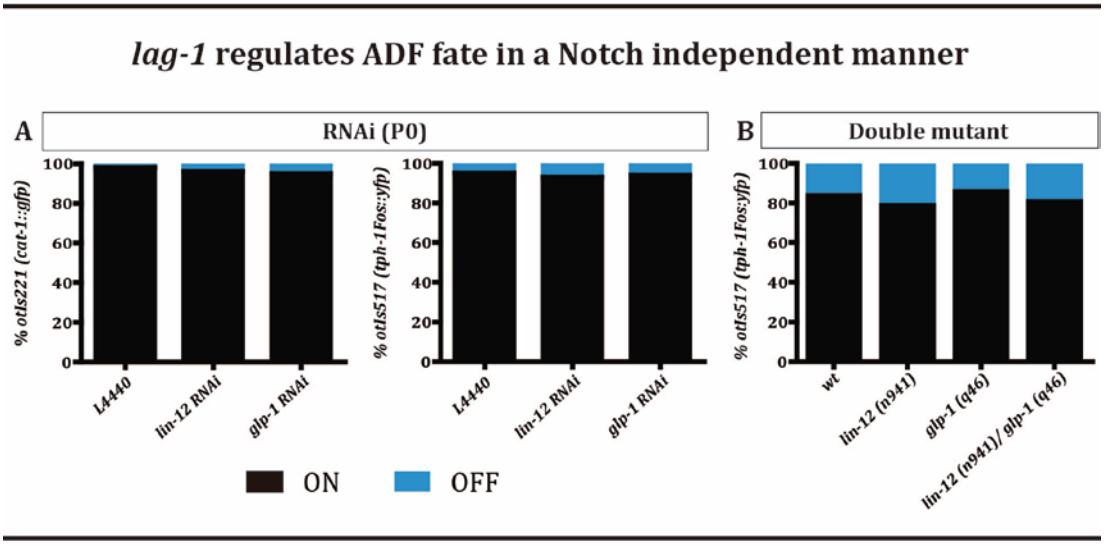

Figure R.34. *lag-1* regulates ADF fate in a Notch independent manner. A) RNAi against *lin-12* and *glp-1*. We scored P0 animals because of RNAi lethality of both clones. The reporters scored in each case were *otIs517 (tph-1fosmid::gfp)* and *otIs221 (cat-1::gfp)*. B) Expression of *otIs517 (tph-1fosmid::gfp)* in ADF in *lin-12* and *glp-1* double mutant background. Black bars represent the percentage of ADF neurons expressing the reporters after the RNAi feeding (N = 30 animals) or in double mutant background (N = 50 animals); blue bars point loss of expression. Statistical analysis was performed with Fisher exact test, none of the results was significant.

In the case of ADF remains unknown if the role of *lag-1* is Notch dependent or independent. To assess this, we performed mutant analysis and RNAi experiments against *lin-12* and *glp-1*, the worm orthologues of Notch.

When we conducted RNAi experiments, we noticed that the expression of *tph-1* and *cat-1* reporters in ADF remain unaltered under *lin-12* and *glp-1* conditions (Figure R.34a). Moreover, we also evaluated the expression of *tph-1* in ADF in *lin-12* and *glp-1* double mutant background but we did not find any significant difference respect to expression in control animals (Figure R.34b). These results showed that neither of both *lin-12* and *glp-1* reported similar phenotype to what we detected through *lag-1* mutant analysis, suggesting that in ADF this TF could function in a Notch independent manner.

As mentioned above, when *lag-1* acts independently of Notch can bind to other partners as bHLH TFs. Interestingly, in our RNAi screen we found that *hlh-14* RNAi reported missing fluorescence phenotype in ADF. Thus, we next explore the possibility that *hlh-14* is also involved in ADF specification.

4.3. *hlh-14* is involved in ADF generation and specification

The TF *hlh-14* is a member of the achaete-scute family of bHLH TFs that has conserved proneural activity in different metazoan groups including *Drosophila*, mammals or molluscs (Frank, Baum, and Garriga 2003). In previous work from our lab, we found that *hlh-3*, a paralog of *hlh-14*, acts as a proneural gene for HSN specification (Doonan et al. 2008) and also as terminal selector directly inducing HSN effector gene expression (Lloret-Fernández et al. 2018). Thus, we hypothesized that *hlh-14* could be acting in a similar way in the ADF neuron.

hlh-14 is expressed in several neuroblasts, not only in the one that that gives rise to the ADF. Among others, this TF has been involved in the specification of ASE neuron (Poole et al. 2011). Interestingly, ASE and ADF come from the same lineage branch

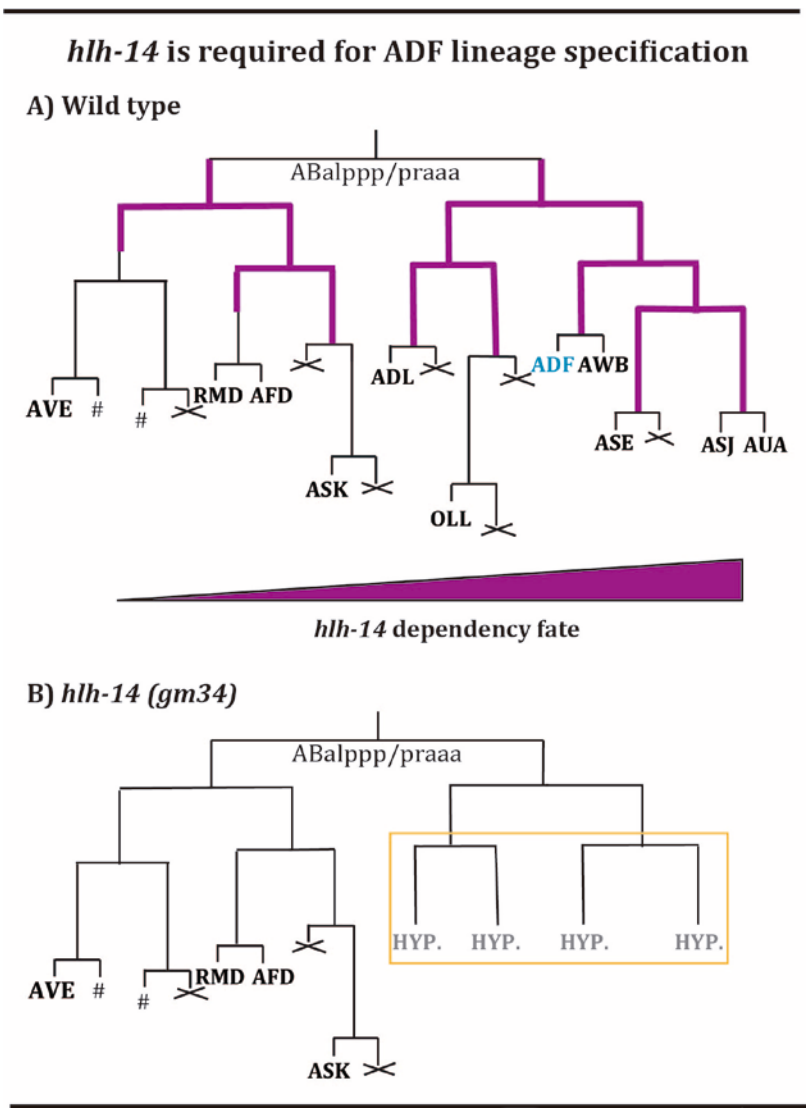

Figure R.35. *hlh-14* is required for ADF lineage specification. The scheme illustrates both ABalppp and ABpraaa branches, corresponding to right and left neurons of the same identity. a) The expression of *hlh-14* in wild type conditions is pointed with purple lines, increasing its presence in a gradient dependent manner as represents the wedge under the scheme. ADF is remarked in light blue. The crosses correspond to cells that undergo a programmed death. (#) marks the generation of non-neuronal cells. b) The null mutant allele of *hlh-14 (gm34)* cause that some branches of the lineage (highlighted by yellow square) undergo hypodermal cell differentiation. Adapted from *Poole et al. 2011.*

(ABalppp/ABpraaa) and this branch expresses *hlh-14* and shows a gradient of dependency upon this TF (Figure R. 35a). In *hlh-14* mutants, the neurons rising from this lineage undergo differentiation into hypodermal cells (Figure R.35b) (Poole et al. 2011). However, it is unknown if *hlh-14* could be operating not only in lineage but also at a more terminal level. In the case of ADF, the expression of this TF is detected embryonically until the mother of ADF but not in ADF itself (Poole et al. 2011).

To assess if *hlh-14* could have a terminal role in ADF specification and thus, acting as a partner of *lag-1*, we conducted P0 RNAi experiment. As we previously mentioned, the RNAi can provide different information depending on the time when the worms start feeding on RNAi. F1 analysis gives insights about the role of a given TF during development, whilst the P0 generation is analyzed to examine possible functions of the TF in maintenance of the observed phenotype (with the exception of the neurons born post embryonically). According to this, we decided to score P0 cohort of animals for the RNAi against *hlh-14,* to observe if these TF participate in the mature fate of ADF neurons and exclude *hlh-14* lineage defects.

We examined the expression three reporters from genes that characterize the mature of ADF. Two of them are members of 5-HT pathway, the fosmid reporter of *tph-1* and the transcriptional reporter *cat-1*; and the last reporter employed labels the expression of *srh-142* a serpentine receptor exclusively expressed in ADF (R.36b). The three reporters were in the sensitized background *rrf-3 (pk1426)* to increase RNAi effects.

We scored the P0 generation and we follow the experiments until F1 to finally compare both stages. Ve did not notice ADF missing *cat-1* expression at P0, only at F1 we observed a significant reduction (Figure R.36a). Interestingly, we detected a significant reduction in *tph-1* fosmid expression in P0 RNAi animals, and also in F1, showing that *hlh-14* could actually be involved in ADF fate maintenance in addition to its function in development and lineage specification (Figure R.36b). Regarding *srh-142*, the results showed that *hlh-14* RNAi did not affect its expression, neither in P0 nor in F1, suggesting that either this gene is not regulated by *hlh-14* or the RNAi effects are not strong enough

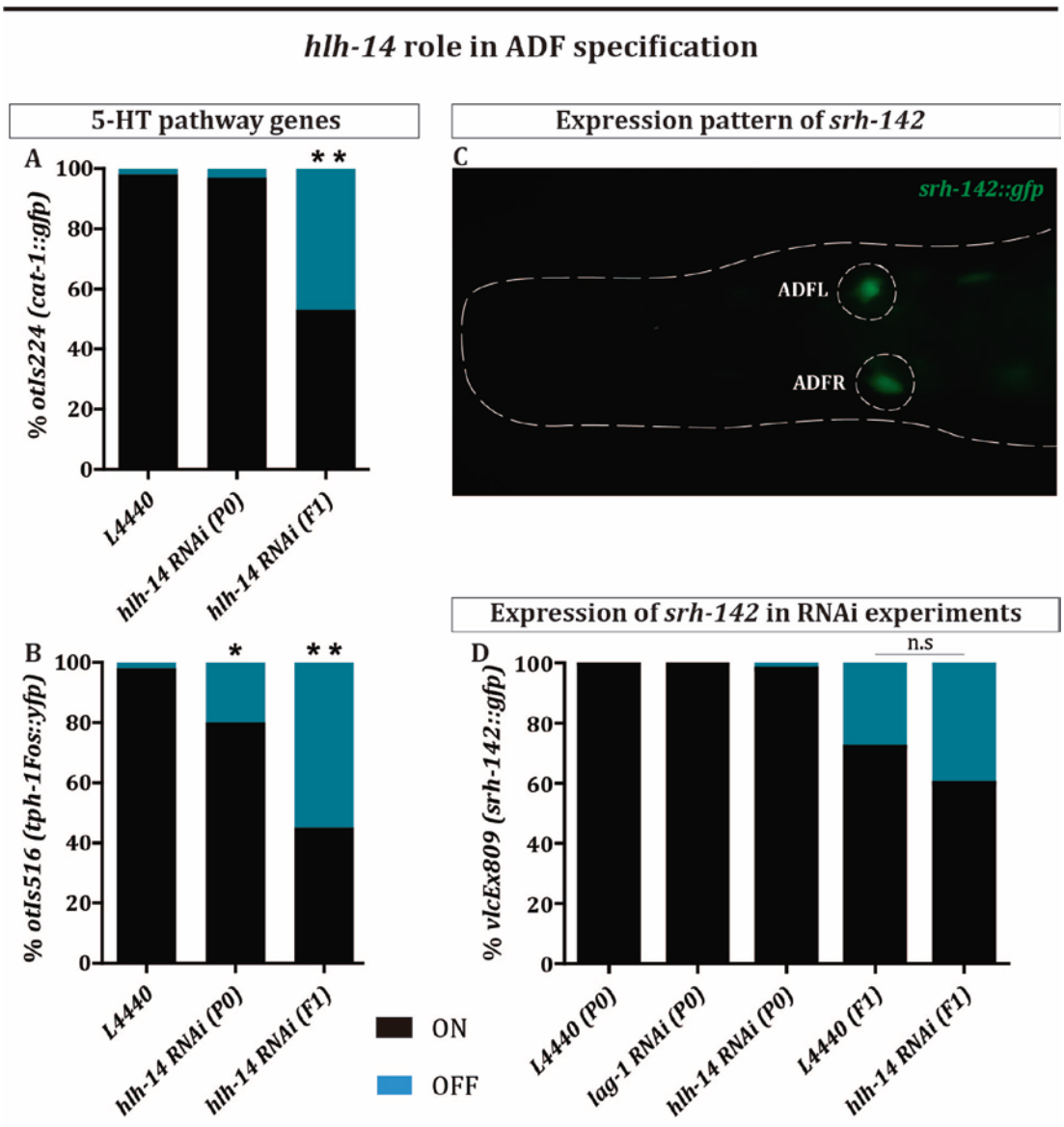

Figure R.36. *hlh-14* role in ADF specification. The graphs represent the scoring results of ADF under the effects of *hlh-14* RNAi at P0 and F1 generations. The bars represent the percentage of expression (black) and missing fluorescence (blue) in a population of 30 worms. a) RNAi results regarding two serotonergic reporters, *cat-1* reporter (up) and *tph-1* fosmid (down); L4440 is the negative control with the empty vector, where both reporters showed the same expression in P0 and F1. b) Overview of *srh-142* expression (green) in head, where is only detected in ADF neurons. c) Scoring of *srh-142* expression in *lag-1* and *hlh-14* RNAi conditions. In this case the expression of the reporter was different in P0 and F1 in control conditions (L4440). Statistics were analyzed by Fisher exact test, (*) = ($p < 0.05$), (**) = ($p < 0.01$). See Table A.6 in the Annex for detailed scores of *hlh-14*.

to induce a phenotype (Figure R.36d). We also assessed that *lag-1* RNAi did not affect *srh-142* expression, what could also suggest that *lag-1* neither regulates the expression of this gene (Figure R.36d)

Importantly, the expression of *srh-142* in the F1 generation of *hlh-14* RNAi proved that ADF is generated. As previously explained, in null *hlh-14* mutants, ADF undergoes hypodermal differentiation (Figure R.35b) and thus, we cannot asses the role of *hlh-14* in mature ADF through mutant analysis. However, RNAi conditions are weaker, as it only downregulates gene expression, and this partial effect allow us to unravel that *hlh-14* is required in ADF terminal fate. We can then conclude *hlh-14* is necessary for *cat-1* and *tph-1* expression in ADF and for *tph-1* maintenance of expression.

This partial loss of function of *hlh-14* affects expression of effector genes of ADF, what suggest that *hlh-14* could be the partner of *lag-1* in ADF specification. However, to determine if *hlh-14* and, also *lag-1*, play a direct role in regulation of 5-HT pathway genes, we performed *cis*-regulatory analysis to find binding sites for both candidates.

In our lab, Dra. Miren Maicas dissected the promoters of serotonergic pathway genes to find the minimal regulatory modules required for the expression of this effector genes in ADF (see(Lloret-Fernández et al. 2018)). Consequently, we search putative binding sites in those CRMs for both candidates looking for their consensus sequences: RTGGGAA in the case of CSL (*lag-1*) (Christensen et al. 1996) and CANNTG as E-BOX motif, the consensus for bHLH TFs (Massari and Murre 2000).

We found CSL and E-BOX binding motifs in all CRMs with the exception of *tph-1* minimal, were no E-BOX was found (Figure R.37). To asses if those sites were functional, we carried out site directed mutagenesis (as we performed for CRM of dopaminergic pathway genes) to find out if mutations in those sites led to a loss of expression in the fluorescent reporters built with these minimal promoter regions of serotonergic pathway genes.

First, mutation in E-BOX motif in *bas-1* produced a partial loss of expression, however this site is so close to a CSL site that we cannot assure that the mutation did not affect also CSL site. Regarding *cat-1*, in this gene the CRM is divided in two regions that go from -1088 to -566 and from -180 to +5 in the 3' UTR region of *cat-1*. The mutation of an E-BOX in the furthest region led to a complete missing expression in contrast to mutations in two sites found in the closest region that did not produced any phenotype. Finally, mutated E-BOX motif in *cat-4* CRM exhibited a wild type phenotype (Figure R.37).

Then, we examined CSL binding motifs. Mutations in *tph-1* and *cat-1* (both regions of this CRM) resulted in a complete loss of expression of the reporter constructs. As mentioned above, in *bas-1* CRM, E-BOX and CSL sites are practically overlapping and the

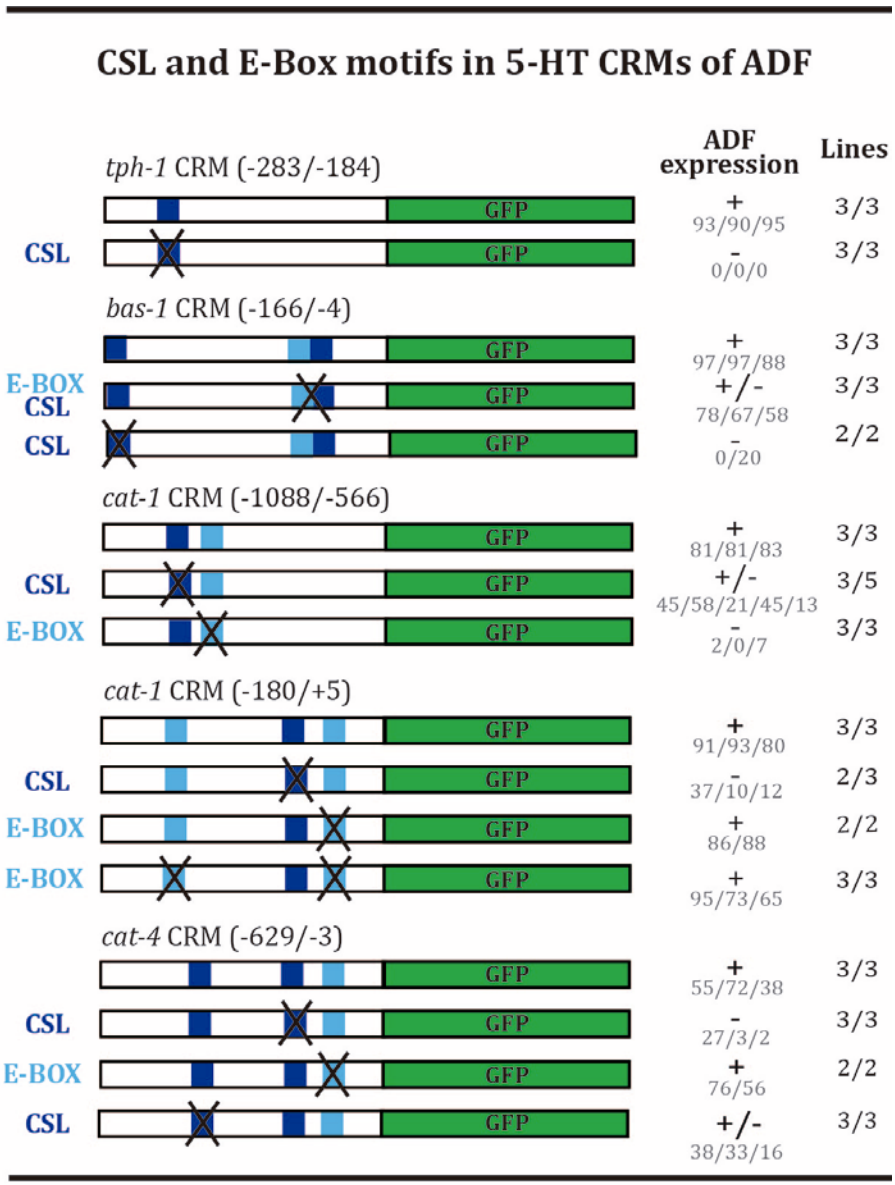

Figure R.37. CSL and E-BOX motifs in 5-HT CRMs of ADF. White boxes represent the CRM promoter regions of each 5-HT pathway genes that drive the expression of *gfp* (green boxes). Inside every CRM, the binding motifs of *lag-1* (CSL, dark blue) and *hlh-14* (E-BOX, light blue) are labeled. The black crosses indicate mutations to disrupt the binding motif. "+" ≥ 70% of transgene expression; "+/-" = 70-30% partial expression; "-" ≤ 30%, loss of expression. The percentages, also included (grey), are referred to the average expression of WT construct. The column "lines" alludes the number of worm lines scored where we observed the indicated phenotype. N = 30 worms/line. Mutagenesis and scorings were performed by Dra. Miren Maicas.

phenotype observed is the consequence of alter both sites. Finally, in *cat-4* we found two distinct CSL motifs and the mutation of one of them produced loss of expression but the other only led to partial loss of expression (Figure R.37).

In view of these results we found strong evidence about *lag-1* role in regulating 5-HT pathway genes in ADF neuron directly binding to their regulatory sequences. However, regarding *hlh-14*, we only found evidence of direct bHLH binding to *cat-1*. It is possible that *hlh-14* interacts with *lag-1* and thus, *hlh-14* could be recruited to these sites in a DNA independent manner; similar indirect recruitments have been reported for TF collectives (Lloret-Fernández et al. 2018; Khoueiry et al. 2017). Alternatively, *hlh-14* action could be indirect, perhaps regulating *lag-1* expression. Future experiments should be aim to better address the role of *hlh-14* in ADF terminal differentiation.

In summary, we have been able to determine that HLH-14, a proneural factor, and LAG-1, a CSL TF, cooperate to initiate ADF terminal fate. Although the null mutants of both TF are lethal, the partial defects that we obtained through RNAi will allow us to continue assessing the role of these two genes in the functionality of ADF.

4.4. *lag-1* and *hlh-14* play a critical role in the responses of ADF to external stimuli

4.4.1. Analysis of the role of lag-1 and hlh-14 in the enhanced slowing response.

As stated before, ADF is a chemosensory neuron that has a sensory cilium in contact with the medium. ADF has been involved in the locomotor behavior of *C. elegans,* participating in the enhanced slowing response (ESR) and also in the detection of averse external conditions for the animals, such us high copper concentration or acidic pH (Guo et al. 2015). Our results indicate that both *lag-1* and *hlh-14* are required for the expression of the serotonin pathway genes in ADF. We are currently assessing if, as would be expected from the terminal selector mode of action, the expression of other terminal features not related to serotonin biosynthesis are also affected. Nevertheless, we wanted to go one step further and evaluate the importance of these TFs for the correct functionality of the neuron. To achieve our purpose, I did a three month stay in the laboratory of Dr. Mark Alkema in University of Massachusetts Medical School. Dr. Alkema works in the behavioral field and he provided to our project the methods and the expertise to answer this question.

First, we evaluated ADF locomotor response of the worm when approaching a source of food. It is known that, after a starvation period, when worms are approaching a source of food, there is a reduction in speed due to the serotonin release from NSM and ADF neurons (Sawin, Ranganathan, and Horvitz 2000). Through its cilium, ADF is able to

detect the chemical cues which arise from the food and starts releasing serotonin to induce the change in speed and, in a second step, NSM is activated further reducing velocity (Iwanir et al. 2016).

In order to elucidate the possible role that *lag-1* and *hlh-14* could have in ADF enhanced slowing response, we decided to perform RNAi experiments against the candidates and record the young adult population with a multi worm tracker (MWT) device. This tool can provide over twenty parameters about the locomotion of the animals and take data simultaneously from fifteen to twenty individuals. We used P0 RNAi to discard lineage defects of *hlh-14* in ADF neuron and because *lag-1* RNAi is embryonic lethal.

To develop this experiment, when P0 RNAi progeny reached young adult stage, we maintained the animals two hours under starvation conditions before transferring ten to twenty animals to a seeded plate and start recording the locomotion parameters of the animals in their way to encounter the source of food. The animals fed with the negative control L4440 displayed the expected behavior (Figure R.38a): the worms start reducing the speed at around 13 seconds before they reach the edge of the bacterial lawn, but it is in the 7 seconds previous were they display the sharpest deceleration (Figure R.38a). Once the animals are surrounded by bacteria, they continue moving forward but slower than prior to encounter the food. According to literature, the initial deceleration (-13 to -7 seconds) is due to ADF action (Iwanir et al. 2016) and the sharpest speed reduction and the quiet state inside food are achieved through NSM and dopaminergic neurons, respectively (Sawin, Ranganathan, and Horvitz 2000).

When we performed the same experiments after the effect of RNAi against *lag-1*, and *hlh-14*, we did not observe the first stage of speed reduction (-13 to -7 seconds) that is dependent on ADF. The speed reduction started at -7/-6 seconds prior to reach the bacterial lawn, the phase that corresponds to NSM action (Figure R.38b). Accordingly, while mean speed is similar between controls and *lag-1* and *hlh-14* RNAi treated animals at -30 ms (Figure R.38c), there are significant differences in speed at the beginning and end of the speed reduction phase controlled by ADF (-13 and -7, Figure R.38b), at the end of which, at -7 s, we found maximal speed differences among three groups (Figure R.38d). Finally, it is known that when worms enter in the bacterial lawn, they change their foraging behavior for dwelling, and almost stop moving. In our experiments we observed that the three groups did not present differences in speed after spending nearly 100 seconds among bacteria (Figure R.38e), suggesting that the role of dopaminergic population remains intact despite the RNAi treatment.

ADF and NSM act at different moments and create distinct rates of speed reduction. To distinguish between the function of both neurons, we performed a linear regression

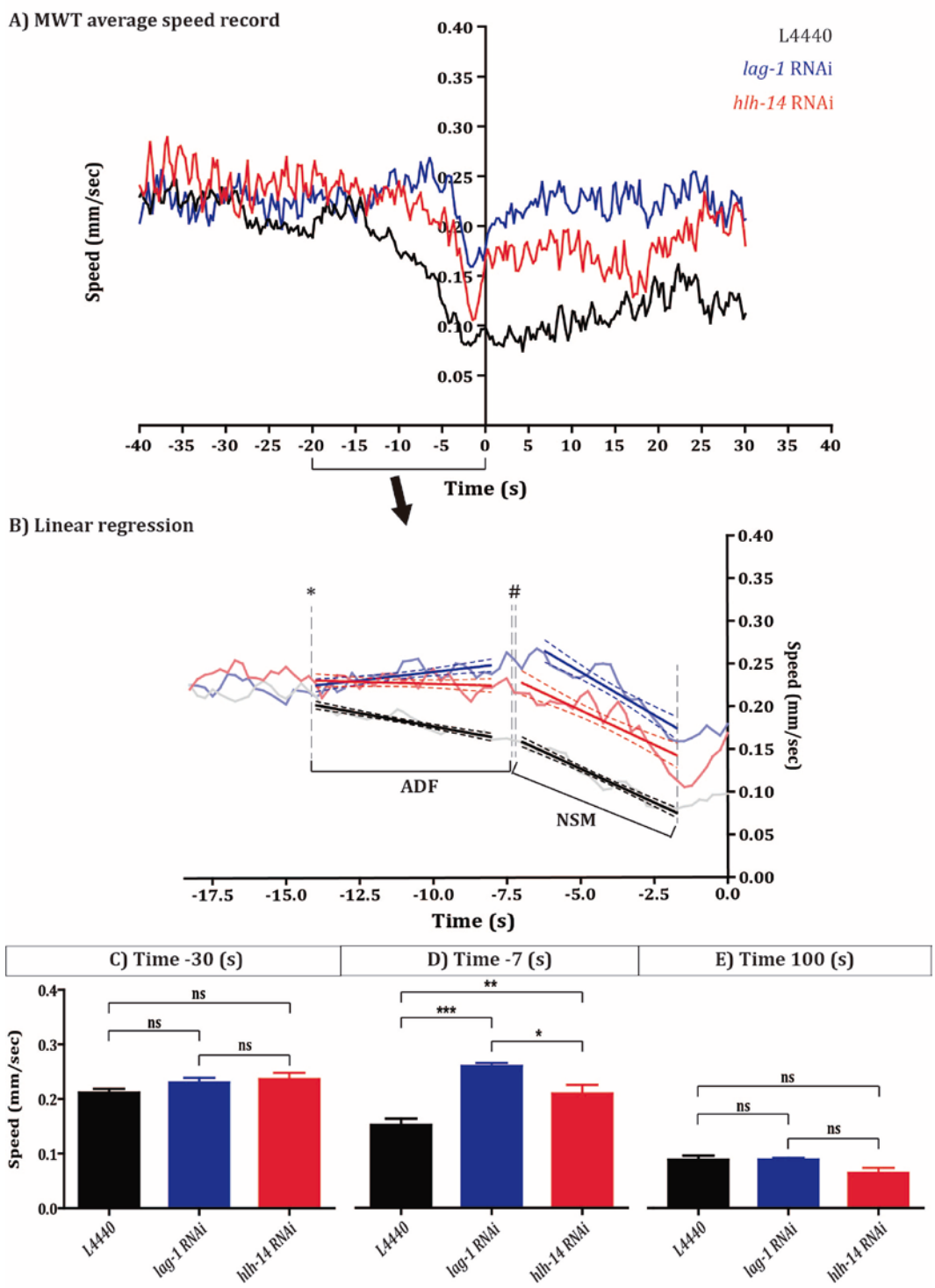
Analysis of lag-1 and hlh-14 requirements for the enhanced slowing response
A) MWT average speed record
L4440
lag-1 RNAi
hlh-14 RNAi
Speed (mm/sec)
Time (s)
B) Linear regression
ADF
NSM
Speed (mm/sec)
Time (s)
C) Time -30 (s)
D) Time -7 (s)
E) Time 100 (s)
Speed (mm/sec)
ns
***
**
*
L4440
lag-1 RNAi
hlh-14 RNAi

Figure R.38. Analysis of *lag-1* and *hlh-14* requirements for the enhanced slowing response. This figure collects the results coming from the multi worm tracker (MWT) recording of locomotor features from worms searching for food after 2h starvation. We considered time = 0s when animals got in touch with the edge of the food. a) Representation from the 40s previous and 30s after worms arrive to the bacterial lawn. b) Analysis of ESR steps controlled by serotonergic neuron (-13 to 0 s). Each linear regression adjusts the slowdown related to ADF and NSM activity. The initial reduction in speed is attributed to ADF (Iwanir et al. 2016). (*) indicates the interval of ADF, starting where the difference between L4440 and both RNAi is significant (Mann Whitney test, $p < 0.05$). (#) starting of NSM interval. c) Speed average 30s before encounter of food. d) Speed average 7s before encounter the bacterial lawn where maximal differences in speed are found. e) Speed average 100s after reaching food. The data of the graphs were analyzed, two-by-two comparisons with Mann Whitney test. n.s. = non-significant; significant levels: (*) = $p < 0.05$, (**) = $p < 0.01$ and (***) = $p < 0.001$ N = 50 animals per group.

analysis to adjust through a straight line the values of the first and second phase of speed reduction (Figure R.38b). We considered a reliable adjust those values observed from the deceleration period that conferred a Pearson correlation coefficient (r^2) greater than 0,8. The adjust showed that in ADF interval, the slopes of the two RNAi groups are significantly different compared to control group, which means that the dynamic of the movement is distinct, what is assignable to ADF dysfunction. Regarding NSM, each experimental group enters the phase controlled by this neuron with a different mean speed; however, the slopes of the three lines in this phase are similar, indicating NSM function is maintained (Figure R.38b).

To find out if the effect we were observing with the two TF was similar to a null ADF function where the neuron cannot release serotonin, we performed the same experiments with another strain expressing the tetanus toxin only in this neuron (by driving its expression through the ADF specific promoter of the *srh-142 gene)*. These animals produce serotonin but they cannot release it to the synaptic cleft. We crossed the strain with the tetanus toxin with the sensitized background for RNAi (*rrf-3* mutant) to avoid putative differences in our results due to distinct genetic backgrounds (R.39a).

When we evaluated the results from the MWT with this strain, we observed defects in speed reduction corresponding to the ADF phase (Figure R.39b), where we found maximal speed difference at the end of ADF interval (at time 7s). We decided to compare this ADF::TeTx time point with the maximal speed of control and RNAi groups (at time 7s) and we found significant differenced not only between control and the other three groups, but also between *lag-1* RNAi and ADF::TeTx (Figure R.39c).

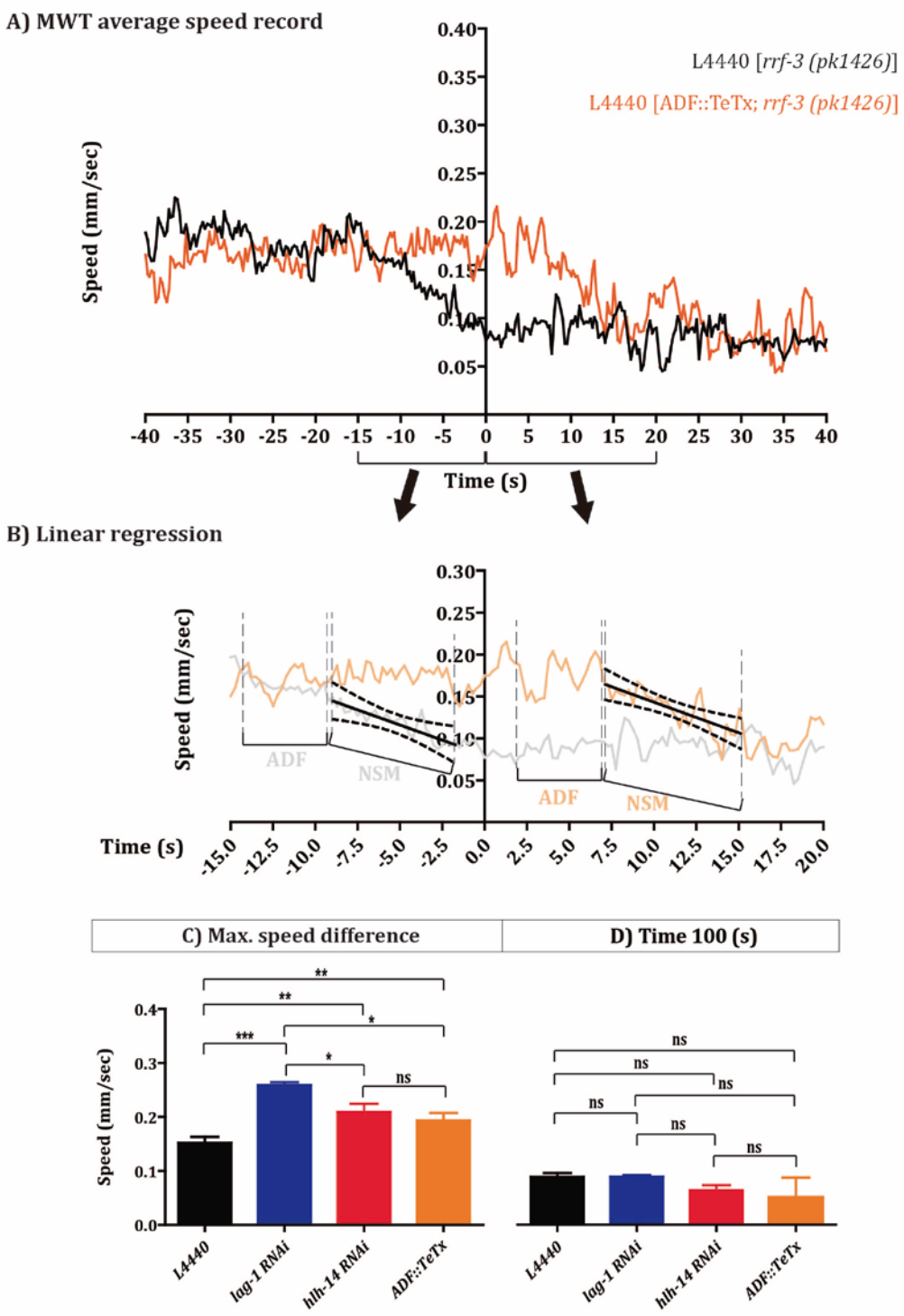
Comparison of lag-1 and hlh-14 RNAi and ADF:TeTx effects on ESR
A) MWT average speed record
L4440 [rrf-3 (pk1426)]
L4440 [ADF::TeTx; rrf-3 (pk1426)]
Speed (mm/sec)
Time (s)
B) Linear regression
Speed (mm/sec)
ADF
NSM
ADF
NSM
Time (s)
C) Max. speed difference
D) Time 100 (s)
Speed (mm/sec)
L4440
lag-1 RNAi
hlh-14 RNAi
ADF::TeTx
ns

Figure R.39. Comparison of *lag-1* and *hlh-14* RNAi and ADF:TeTx effects on ESR. This experiment was carried out with the previous strain to perform RNAi, that includes *rrf-3 (pk1246)* and a new one combining this mutation and the extrachromosomal construction with ADF::TeTx (*srh-142prom::TetanusToxin*), exclusively expressed in ADF. a) Average speed records of animals after 2 hours starvation. b) Magnification of speed records from 15s before and 20s after encounter the bacterial lawn. The regression analysis of L4440 control (left) is the same as in Figure R.37. The linear adjust of ADF::TeTx (right) shows a line whose slope is similar to that of L4440 adjust. c) Comparison of maximal speed difference among control, RNAi (time -7s) and TeTx (time 7s) groups at the end of ADF interval. d) Speed comparison 100s after food encounter. N = 50 animals/group. Two-by-two comparisons were analyzed with Mann Whitney test. n.s. = non-significant; significant levels: (*) = $p < 0.05$, (**) = $p < 0.01$ and (***) = $p < 0.001$ N = 50 animals per group.

Additionally, we noticed that the sharp decrease in speed of the NSM fate was delayed in time, taking place not at -7 to 0 second prior food encounter but at +7 to +12 seconds after food encounter (Figure R.39b). This is in line to what we saw with our candidates, but in those previous experiments delay was not as lag as with the tetanus toxin strain. One possible explanation for this discrepancy is that with the RNAi we are not obtaining such effect because it is only downregulating the expression of our candidates, and thus there might be still some activity of the neuron, that could release serotonin or other neurotransmitters or neuropeptides, as ADF is also cholinergic and expresses several neuropeptides. This hypothetical remaining signaling would not occur in the ADF expressing tetanus toxin strain.

We calculated again the linear adjust attributed to the slowdown produced by NSM (Figure R.38b). Slopes of L4440, *lag-1* RNAi, *hlh-14* RNAi and ADF::TeTx were not significantly different. Of note, while in the RNAi experiments the mean speed is normalized to control levels at 100s after food encounter, in the ADF::TeTx experiments they reach comparable speed to controls much earlier (15 seconds after food encounter). This delay in *lag-1* and *hlh-14* RNAi treated animals suggest they could have defects in other neurons involved in this response.

With these set of experiments, we determine that loss of *lag-1* and *hlh-14* abolishes the correct response elicited by ADF function. This phenotype could be due directly to deficits in 5-HT release but also, as terminal selectors broadly affect the fate of the cell they regulate, it is possible that *lag-1* and *hlh-14* loss of function affects the ability of ADF to respond to external stimuli and be activated. To shed some light into this aspect, we moved onto calcium imaging experiments to evaluate the response of ADF to stimuli in the medium and compare normal conditions with animals fed with RNAi against *lag-1* and *hlh-14*.

4.4.2. Analysis of ADF activation in lag-1 and hlh-14 loss of function experiments.

We used the microfluidics device at Dr Alkema's laboratory to perform calcium imaging experiments. This system is based on a microchamber where the alive worms are located and with basal buffer flowing through it. The basal solution can be substituted for a stimulation solution that triggers the response of the neurons. ADF is a chemosensory neuron that can detect a variety of chemical cues (Bargmann and Horvitz 1991). .For our purpose, we determined to combine two stimuli that activate ADF, pH4 and 10 mM $CuSO_4$, to obtain a clear and high response (Guo et al. 2015). Moreover, we built a specific strain which expressed a sensing calcium GFP fluorescent protein, GCaMP3, only in ADF neuron (using the ADF specific promoter from the *srh-142* gene). We combined the calcium sensor with the RNAi sensitized mutation *rrf-3 (pk1426)* and the allele *lite-1 (ce314)*, that abolish the intrinsic response of the worms to a source of light.

Our protocol consisted of four stimulation pulses, to evaluate both acute response to stimuli and adaptation. Each pulse lasted thirty seconds and between them there was a recovery period for three minutes and thirty seconds to ensure the neuron could have enough time to respond the following stimulation pulse in wild type conditions. Thus, each experiment was sixteen minutes long and while it was running we took two pictures per second to quantify the fluorescence emission. As a positive control we used RNAi against *daf-19*. This TF is required for the correct formation of sensory cilium (Swoboda, Adler, and Thomas 2000). We reasoned that RNAi against *daf-19* should produce defects in ADF cilia formation and thus in its ability to respond to chemical cues.

We started analyzing the calcium imaging results from the L4440 control group (Figure R.40a). We noticed the animals showed a clear response in every stimulation and that this response decreased in time. As expected, animals fed with RNAi against *daf-19* show a significant decrease in their response to the chemical stimuli (Figure R.40b).

When we tested P0 RNAi young adults against *lag-1* and *hlh-14*, we observed a clear reduction in the response to the stimulus, indicating that ADF is not activated in these conditions (Figure R.40c, d). One possible scenario for this behavior is that ADF is not able to detect the stimulus because these TFs are regulating the expression of receptors; alternatively, loss of *lag-1* and *hlh-14* could be affecting expression of different ion channels that elicit the neuron depolarization and calcium entrance inside the cell and allow depolarization. Other possibility is that the loss of normal levels of our candidates leads the neuron to a partial loss of its mature identity, becoming unable to normally respond to stimuli. Although we cannot yet assign the specific molecular identity behind this phenotype we can ensure that *lag-1* and *hlh-14* RNAi affects expression of other effector genes not directly related to 5-HT signaling that are required for ADF activation.

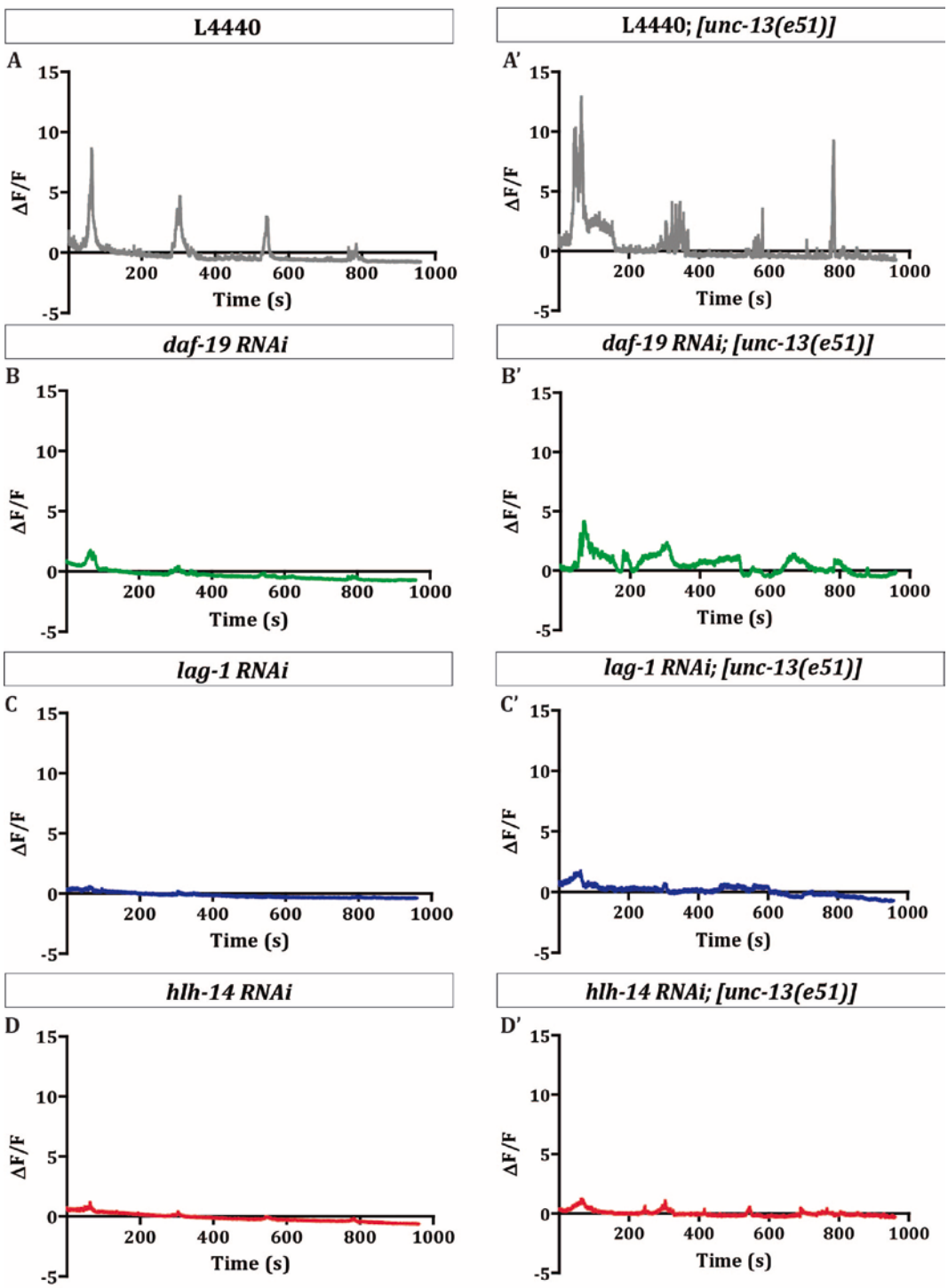
ADF Calcium Imaging Experiments
L4440
A
L4440; [unc-13(e51)]
A'
daf-19 RNAi
B
daf-19 RNAi; [unc-13(e51)]
B'
lag-1 RNAi
C
lag-1 RNAi; [unc-13(e51)]
C'
hlh-14 RNAi
D
hlh-14 RNAi; [unc-13(e51)]
D'
ΔF/F
Time (s)
15
10
5
0
-5
200
400
600
800
1000

Figure R.40. ADF calcium imaging experiments. The graphs represent the emission of fluorescence of the GCaMP3 as a consequence of the activation of ADF neuron in response to a combined stimulus of pH4 and 10 mM Cu_2SO_4. Negative fluorescence values are due to a bleaching effect. Graphs on the left were obtained in the *rrf-3* mutant background, with 50 animals per group, and in the right, *rrf-3* and *unc-13 (e51)* mutant background, 15 animals per group.

The ADF neuron is part of a complicated neuronal network and, apart from being a chemoreceptor, it receives several inputs from other neurons, both excitatory and inhibitory (Figure R.41). Some of the neurons that are presynaptic to ADF, such as ASE, ASH or ASI, also detect changes in pH or the presence of copper in the medium (Guo et al. 2015). Thus, it was possible that the effect seen by the *lag-1* and *hlh-14* RNAi are due to indirect effects of other neurons to the ADF. Therefore, we next aimed to detect the response of ADF itself, discarding any possible contribution from other neurons.

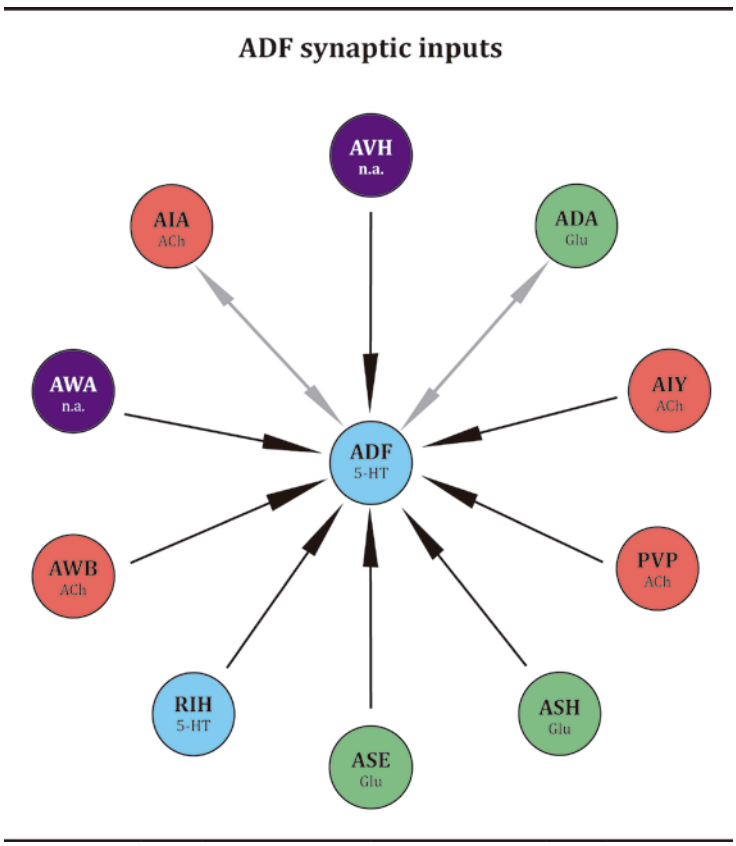

Figure R.41. ADF synaptic inputs. The diagram represents the connections in which ADF is the post synaptic neuron. Grey arrows indicate gap junction links. The colors are characteristic of the neurotransmitter of each neuron: glutamate (Glu), serotonin (5-HT) and acetylcholine (ACh); with the exception of ADF and RIH that also employ acetylcholine. n.a. = unknown neurotransmitter.

To circumvent this problem, we included in the background of the original strain, a null mutant allele of *unc-13 (e51)*. The gene *unc-13* encodes for a protein essential to achieve the fusion of neurotransmitter vesicles with the cell membrane to release their

content into the synaptic cleft (Richmond, Davis, and Jorgensen 1999). The lack of this protein drives an absolute absence of chemical synapsis; that is why the incorporation of this allele in the strain allowed us to specifically record the activity of ADF in response to chemical stimuli without the influence of any synapses of other neurons.

In this genetic background, control animals (L4440 group) show a clear response to the four stimuli pulses (Figure R.40a'). These results corroborate that ADF is able to detect these chemicals by itself. As expected, ADF in *daf-19, lag-1* and *hlh-14* RNAi treated animals failed to show activation upon stimuli (Figure R.40b', c', d'). Interestingly, there is a general tendency in this new set of results: all of them present more noise in the signal, including the control. This could be explained because, for time constrains, we recorded a lower number of animals. In the first set we had fifty worms per group; however, we only analyzed 15 animals for each group in *unc-13* mutant backgrounds. Other possibility is that the mutation of *unc-13* is affecting the health of the worms (these animals cannot move and that conditions their access to the food) and that gave a not robust signal, finally, it could be that the primary ADF response to external stimulus is modulated by other cells to elicit a sharper and more defined response. Therefore, it seems reasonable to think that the loss of those connections may influence in the response we detected. On the other hand, *unc-13* mutation does not affect the communication between cells through gap junctions and that could also bias the final response.

To elucidate if there were significant differences in the responses between each group in the distinct backgrounds, we compared the maximal fluorescent emission that took place with the first stimulation. We found significant differences between the control and the three RNAi both in wildtype or in *unc-13* mutant background (Figure R.42a, b) but not between the candidates comparing with their counterpart in the other strain, with the exception of *lag-1* (Figure R.42c).

In summary our results demonstrate that *lag-1* and *hlh-14* are involved achievement of terminal fate of ADF neuron, not only regulate the expression of the serotonergic pathway genes, but also other terminal features that allow the neuron to respond to stimuli.

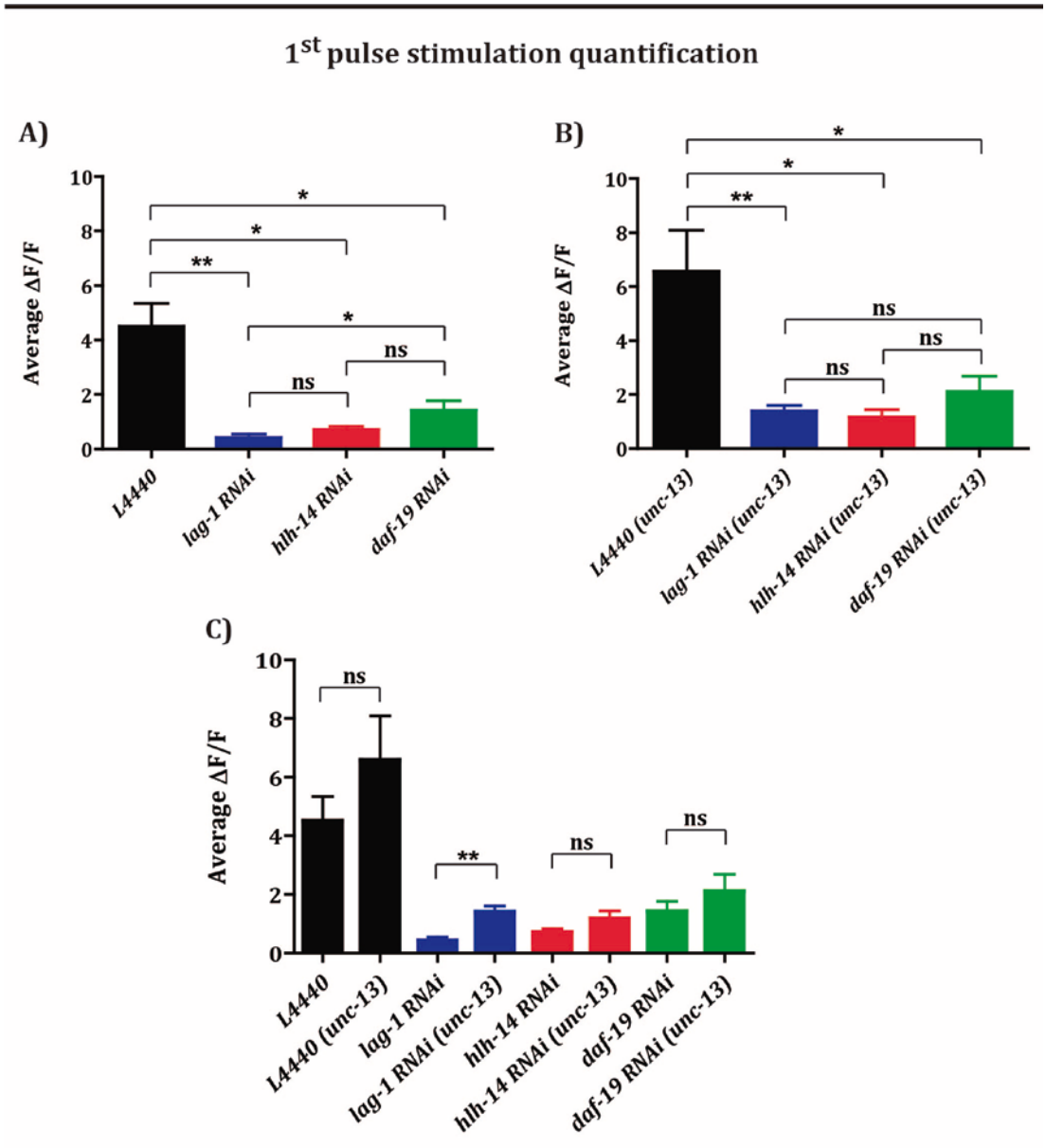

Figure R.42. 1st stimulation quantification. The graphs represent the quantification of fluorescence emission from the GCaMP3 expressed specifically in ADF, at second 60, corresponding to the highest response of the first stimulation. a) Average emission in *rrf-3 (pk1426); lite-1 (ce314)* strain. N = 50 worms/group. b) Average emission in *unc-13 (e51); rrf-3 (pk1426); lite-1 (ce314)* strain. N = 15 worms/group. c) Comparison of the different groups between both strains. Statistical analysis with Mann Whitney test. (*) = $p < 0.05$; (**) = $p < 0.01$.

5. Validation of the TF candidates to be required for the generation of tyraminergic and octopaminergic neurons

5.1. TF candidates involved in specification of tyraminergic and octopaminergic neurons

The third group of neurons analyzed in our screen is the pair of octopaminergic (RIC) and tyraminergic (RIM) neurons. These neurons are involved in complex behaviors, for instance, in the case of RIM, this neuron is essential for the orchestration of backward movement in response to aversive stimuli (Donnelly et al. 2013; Pirri et al. 2009). Additionally, RIC counteracts the effect of 5-HT in feeding behavior and egg lying and is involved in fat metabolism (Horvitz et al. 1982; Wragg et al. 2007). Both share the expression of the vesicular monoamine transporter *cat-1* and the enzyme tyrosine decarboxylase (*tdc-1)* that converts tyrosine into tyramine (Figure I.13). Additionally, RIC neurons express the enzyme tyramine *β*-hydroxylase (*tbh-1)* to convert tyramine into octopamine.

Anatomically, RIC and RIM have similar morphology and are located very close to each other near the second pharynx bulb what makes it difficult to distinguish from each other. Thus, we decided to score them as a single RIC/RIM category in the screen and validate afterwards the candidates to identify which of the two pairs is affected (Table R.11).

Table R.11. TF candidates involved in RIC/RIM specification

Gene Name	DBD	Neuron affected	Phenotype	*cat-1 ::gfp*
zip-5	bZIP	RIC/RIM	Missing fluorescence	82/120
zip-6	bZIP	RIC/RIM	Missing fluorescence	100/120
nfyb-1	CBF	RIC/RIM	Missing fluorescence	104/120
cey-1	COLD BOX	RIC/RIM	Missing fluorescence	106/120
ceh-12	HD - HOX	RIC/RIM	Missing fluorescence	96/120
ceh-13	HD - HOX	RIC/RIM	Missing fluorescence	92/120
vab-7	HD - HOX	RIC/RIM	Missing fluorescence	100/120
ceh-27	HD - NK	RIC/RIM	Missing fluorescence	96/120
ceh-36	HD - POU	RIC/RIM	Missing fluorescence	96/120
sma-3	MH1 - SMAD	RIC/RIM	Missing fluorescence	98/120
sta-1	STAT	RIC/RIM	Missing fluorescence	102/120
tbx-30	T-BOX	RIC/RIM	Missing fluorescence	98/120
C27A12.2	ZF - C2H2	RIC/RIM	Missing fluorescence	104/120
egl-43	ZF - C2H2	RIC/RIM	Missing fluorescence	100/120
pqm-1	ZF - C2H2	RIC/RIM	Missing fluorescence	92/120

R05D3.3	ZF - C2H2	RIC/RIM	Missing fluorescence	104/120
scrt-1	ZF - C2H2	RIC/RIM	Missing fluorescence	100/120
sdc-1	ZF - C2H2	RIC/RIM	Missing fluorescence	104/120
nfx-1	ZF - NF - X1	RIC/RIM	Missing fluorescence	102/120
nhr-2	ZF - NHR	RIC/RIM	Missing fluorescence	98/120
nrh-148	ZF - NHR	RIC/RIM	Missing fluorescence	102/120
nhr-157	ZF - NHR	RIC/RIM	Missing fluorescence	104/120

Table R.11. TF candidates involved in RIC/RIM specification. The list includes the TFs from the RNAi screen that present significant phenotype in this pair of neurons. The scoring results with the reporter *cat-1* indicate the ratio of remaining neurons after the RNAi feeding, in a population of 30 worms.

Transcription factors required for RIC and RIM specification have not been identified to date. Intriguingly, in our RNAi screen RIC and RIM specification retrieved the highest number of candidates (Table R.11).

Among the TF families present in the list of candidates we found mainly Homeodomain and Zf-C2H2, as also happens with dopaminergic and serotonergic populations. Curiously, a group of the candidates obtained for these two neurons, like *ceh-13*, *ceh-36*, *ceh-27* or *vab-7*, are under Wnt signaling regulation (Zacharias et al. 2015), so it could be that the generation of this neuron is mainly influenced by this pathway. It is also remarkable that we have identified two bZIP TFs because it is known that the members of this family can bind to DNA as homo and heterodimers, although the cases of heterodimer complex in lower eukaryotes are more scarce (Rodríguez-Martínez et al. 2017). It is possible that both *zip-5* and *zip-6* could be required for the development of RIC and RIM working as heterodimers. On the other hand, we found two paralogs, *ceh-12* and *ceh-13*, among the candidates. These two Hox genes share some similarities in their sequences, thus, the validation may lead us to distinguish which of them or if both are required for RIC and RIM development.

Another important feature is that from our candidate list we did not identified TFs related to lineage specification (*lin*); however, we cannot rule out that some of the identified TFs have unreported roles on RIC/RIM lineage specification. Finally, we noticed a missing phenotype for *sdc-1*, a TF involved in the regulation of sex dimorphism features (Portman 2007), this is particularly interesting because to date RIC and RIM have not been reported to be sexually dimorphic. In hermaphrodites RIC activity regulates egg laying, thus it would be possible that its function and/or connectivity differs in males that do not display this behavior.

For the validation of the screen candidates we focused on the analysis of *zip-5* and *pqm-1*. These are the two candidates with strongest phenotypes and they have been reported to regulate processes that require Octopamine or Tyramine signaling, for instance *pqm-1* participates in the signaling pathway for fat storage, which is activated by octopamine release (Tepper et al. 2013; Burkewitz et al. 2015). On the other hand and *zip-5* mutants exhibit tap habituation defects, a behavior regulated through tyramine signaling (Swierczek et al. 2011). As we did with the candidates for the other monoaminergic subpopulations, we studied the expression pattern of these genes and the RIC and RIM phenotypes of the corresponding mutant alleles.

5.2. Characterization of RIC and RIM candidates *pqm-1* and *zip-5*

To characterize the expression of *pqm-1* we used an available fosmid reporter strain that we crossed with *tdc-1::mCherry* to assess the expression of the TFs in RIC and RIM neurons. We detected its expression from the end of gastrulation and beam stage until 3-fold stage (Figure R.43a). The cells expressing the reporter were the intestine primordial cells, as has been previously described (Tepper et al. 2013), but we could not observe expression in RIC or RIM neurons when we compare with *tdc-1* reporter (Figure R.43b).

Despite the fact that we did not observed *pqm-1* expression in the RIC or RIM neurons we decided to analyze mutant allele of this TF, because we have previously seen cases in which fosmid expression does not fully recapitulate endogenous gene expression, thus, it is possible that *pqm-1* is in fact expressed in RIC/RIM; second, *pqm-1* could still have a non-cell autonomous effect in RIC/RIM differentiation.

We obtained the *pqm-1* allele *ok485*, that consists in a complex substitution with a 1470 bp deletion and an insertion of two nucleotides (Figure R.43c). This modification affects the Zn-C2H2 domain and it is likely a null allele (Tepper et al. 2013). We did not find expression defects for *tdc-1::mCherry* or *tbh-1::gfp* in *pqm-1* mutants (Figure R.43d, e). This lack of phenotype contrasts with the *cat-1* expression defects observed in our RNAi. One possibility is that *pqm-1* is required for *cat-1* expression but not for *tbh-1* or *tdc-1* expression, alternatively, *pqm-1* might not be required for specification of RIC and or RIM and thus would be a false positive in our screen. To distinguish between these two possibilities, we are currently analyzing *cat-1* expression in *pqm-1*(*ok485)* mutants.

On the other hand, *zip-5* transcriptional reporter also showed early expression but it is maintained throughout adulthood. We were able in this case to clearly assess the expression of this reporter in RIC and RIM neurons (Figure R.44a). We also detected the expression of *zip-5* in other head neurons, head muscles, some neurons in midbody and cells in the tail (Figure R.44a).

pqm-1 expression and mutant analysis

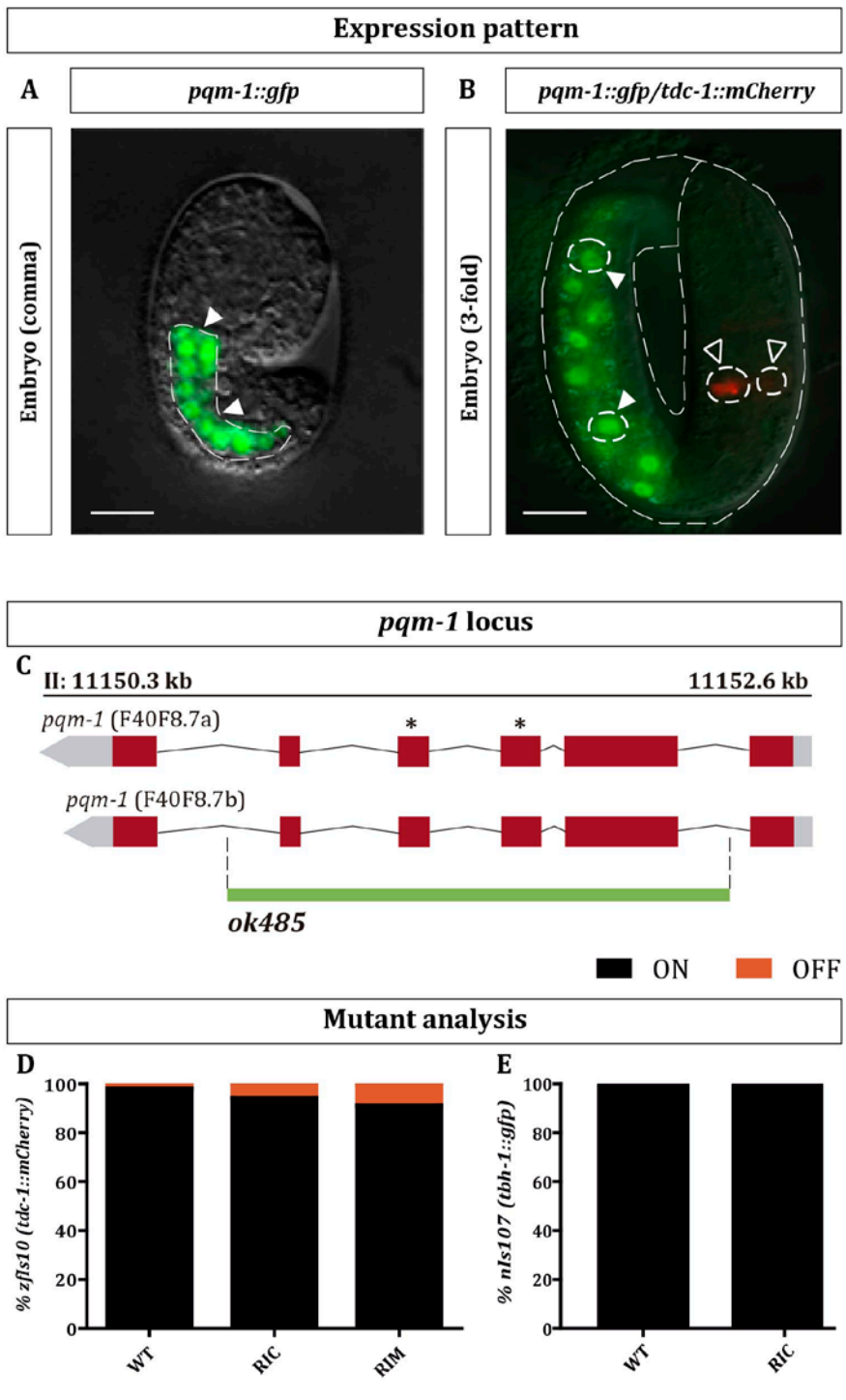

Figure R.43. *pqm-1* expression and mutant analysis. a, b) GFP shows *pqm-1* fosmid expression and RIC and RIM neurons are labeled with *tdc-1* reporter, in red. In comma stage embryo, white arrowhead points the expression of *pqm-1* in primordial intestine cells, whereas in 3-fold embryo *pqm-1* is detected in the intestine (white arrowheads) and do not collocalize with *tdc-1* reporter (black arrowheads). Scalebars, 10 μm. c) Representation of *pqm-1* genomic locus, where red boxes are exons and connecting lines, introns; regions in green are untranslated sequence of the mRNA. This gene encodes for three isoforms and the deletion *ok485* affects all of them. (*) indicates the exons that participate in Zf-C2H2 DBD. d, e) The graphs represent the scoring results of *tdc-1::mCherry* and *tbh-1::gfp* reporter expression in RIC and RIM neurons in *pqm-1 (ok485)* bacground. Black bars indicate WT expression and orange bars, loss of expression. Statistics from Fisher exact test two tailed, (*) = $p < 0.05$; (**) = $p< 0.01$. N = 50 worms/condition.

To study if *zip-5* activity is required for proper RIC and RIM specification we obtained the allele *zip-5*(*gk646)*. The nature of this allele is a deletion of 2008bp long that eliminates the bZip domain of the protein and it is considered a null allele (Figure R.43b). Interestingly, this allele shows defects in "tap habituation" a behavior coordinated by RIM neuron (Lau et al. 2012). *zip-5(gk646)* animals exhibit a lower probability of escape responses (reversal) compared to wildtype animals upon an initial plate tap (Swierczek et al. 2011). When we crossed this mutant allele with *tdc-1::mCherry* and *tbh-1::gfp* reporters, the results indicated that *zip-5* produced loss of expression defects in *tdc-1* in RIC and RIM, but *tbh-1* expression in RIC is unaffected (Figure R.44c). This result, added to the intrinsic expression of this candidate in both neurons, indicates that the role of this TF could be cell autonomous.

We are currently further characterizing the role of *zip-5* in tyraminergic/octopaminergic differentiation by analyzing the expression of other RIC and RIM terminal features in *zip-5 (gk646)* mutants (see Table A.6 in the annex for detailed scores of *pqm-1* and *zip-5*).

Figure R.44. *zip-5* expression and mutant analysis. a) *zip-5* transcriptional reporter is expressed in both RIC and RIM labeled with *tdc-1* reporter (red). *zip-5* reporter is expressed in other neurons in the head (white arrowheads) and also head muscles (black arrowheads). Scalebars: 5 μm and 20 μm. b) Representation of *zip-5* genomic locus where exons are represented as red boxes and introns as connection lines. Grey boxes indicate untranslated sequences of the mRNA. This gene encodes for three isoforms altered by the deletion *gk646*. (#) points out the exon from the bZip DBD. c, d) The graphs represent the scoring results of *tdc-1::mCherry* and *tbh-1::gfp* reporter expression in RIC and RIM neurons in *zip-5 (gk646)* backgrounds. Black bars indicate WT expression and orange bars, loss of expression. Statistics from Fisher exact test two tailed, (*) = $p < 0.05$; (**) = $p< 0.01$. N = 50 worms/condition.

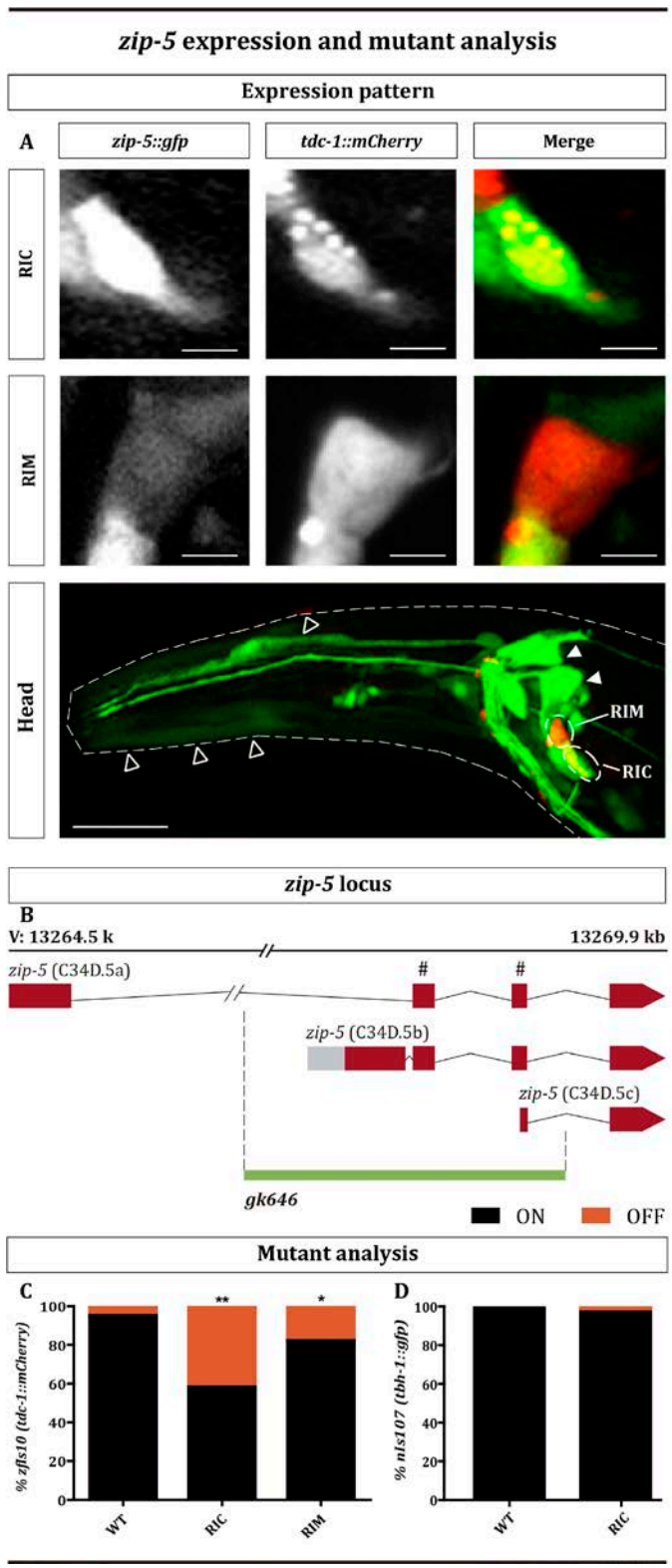
zip-5 expression and mutant analysis
Expression pattern
A
zip-5::gfp
tdc-1::mCherry
Merge
RIC
RIM
Head
RIM
RIC
zip-5 locus
B
V: 13264.5 k
13269.9 kb
zip-5 (C34D.5a)
zip-5 (C34D.5b)
zip-5 (C34D.5c)
gk646
ON
OFF
Mutant analysis
C
% zfIs10 (tdc-1::mCherry)
WT
RIC
RIM
D
% nIs107 (tbh-1::gfp)
WT
RIC

DISCUSSION

DISCUSSION

The processes in which one cell is committed to acquire a specific fate requires a complex and precise spatiotemporal regulation of gene expression. The problem of the correct establishment of cell type diversity is especially prominent in the nervous system that is composed by multitude of neuronal types.

The action of transcription factors has long been in the spotlight of developmental biologists as they are key determinants of cell fate specification. Although in the last decades we have learnt a lot of the specific actions of individual TFs, much less is known about their coordinated function as TF combinations. Importantly, considering TF pleiotropy, it is the combinatorial action the one responsible for the cell type specific actions of TFs.

At the beginning of this Thesis we aimed to increase our global understanding of TF combinatorial action in neural fate specification. To this purpose we focused on the clinically relevant population of monoaminergic neurons and decided to use the simple model organism *C. elegans* to perform an RNAi screen against all TFs in the worm genome.

This project, although is still unfinished has already provided new insights to complete the regulatory map of this fundamental neuronal populations. Future work will be focused on the in-depth characterization of the function of the TFs identified in this screen and the phylogenetic conservation of their actions.

1. RNAi is a powerful technique to identify new regulators of neural specification in *C. elegans*

Since not all tissues are affected in the same manner for the RNAi mechanism (Joyce, Gallagher, and Kuwabara 2006) and the selection a proper RNAi enhanced background depends on the tissue and the expected phenotype (Zhuang and Hunter 2011) our first aim was to establish a proper strain to obtain the best possible results.

We compared *nre-1 (hd20), lin-15b (hd126)* strain*, eri-1(mg366); lin-15b(n744)* strain*, rrf-3(pk1426)* strain and *rrf-3 (pk1426), unc-119::SID-1*. These mutations had previously been reported to increase the RNAi effects in neurons (Schmitz, Kinge, and Hutter 2007; Poole et al. 2011; Simmer et al. 2003). Although *eri-1(mg366); lin-15b(n744)* background is the most effective for the dopaminergic population for serotonergic neurons the highest efficiency was reached with *rrf-3(pk1426)*. *rrf-3*

(pk1426) was also the best background in other MA populations. These results reveal that not only different tissues respond differently to RNAi but even different subtypes of neurons respond differently. With these data and considering that the *rrf-3* mutant background also produced phenotypes in DA cells we decided to use *rrf-3 (pk1426)* for our screen.

We tried to improve efficiency by adding the neuronal expression of the *sid-1* transporter. However, to our surprise, we did not observe any significant improvement, even more in some cases *sid-1* expression had detrimental effects. Thus, it seems that the bottleneck of RNAi efficiency is to avoid the competition between RdRPs from endogenous and exogenous pathways rather than increase the availability of the dsRNA molecules in the cells.

Another important point to consider before starting the screen was the reporter strain to use. We decided to combine three fluorescent reporters in the same strain to extract more information about the role of each TF. In most cases, the scoring results were similar for the reporters in the same cell, suggesting either lineage defects, cell fate conversion or co-regulation of both genes by the TFs.

To validate our screen, we compared the number of observed visible phenotypes with previous reports and also if we retrieved the TFs previously known to be required in MA specification. The comparison of visual results with the data from Kamath and Simmer whole genome RNAi screens (Fraser et al. 2000; Kamath and Ahringer 2003; Simmer et al. 2003) showed that the 52.6% of our results overlap with what they reported. Moreover, only Simmer and colleges described characteristics for 17 TFs more than us. Considering that our main goal was not to detect visible phenotypes, it is possible that we did not report subtle defects; although this observation does not explain the variability in the results between both data sets. Perhaps the RNAi library had something to do with this variation, because in our case it was fully validated by sequencing before performing the experiments, whereas in their case the library had not been fully curated and it is described that in Arhinger library 17.5% genes need to be reannotated even they are reliable (Qu et al. 2011).

Nevertheless, the variability of RNAi technique has been a common issue in the past. It has been described that the comparison of the results obtained from different research groups can oscilate between 10% to 30% difference. And not only between laboratries, but also between different replicates in the same laboratory (Simmer et al. 2003). This is in agrement with our own observations: 127 clones out of 876 produced a phenotype in one out of the two replicates, this clones were assessed for a third time. This variability is related with the technical conditions of the experiment: the culture conditions of the RNAi clones, the concentration of IPTG levels for the induction of dsRNA production, the

time the IPTG is in the culture before seeding, the drying of the plates, the microscope used, the observer that carry out the scorings, etc. We were extremely cautios to reduce the variability, preserving products and protocols for every step of the experiments and trying to proceed always the same manner.

Additionally, when we compare our results with publised data, we also detected false negatives in our data. The number of false negative results reported in previous RNAi screen is high and vary between 25% to 55% (Rual et al. 2004). In our case, we estimate that the number of false negatives if around 22%, that is not very high but still concerning.

Finally, another caveat of the technique is the number of RNAi possitive that are not confirmed by mutant analysis. From a total of 10 evaluated mutants, 3 of them showed no phenotype in monoaminergic neurons. As RNAi is a downregulation of gene expression, we would have expected weaker phenotypes than in null mutants but, this turned out to be the opposite. However, RNAi phenotypes observed in the screen are not highly penetrant in general; therefore it is conceibable that weaker phentoypes turned to be false positives. This paradox appears to be common in other RNAi screenings (Poole et al. 2011). One possible explanation for the false positives are the unknown off target effects of some RNAi clones. Additionally, it could be that compensatory effects in the mutants mask the previously RNAi reported phenotypes. Finally, it has been described that redundancy is rather frecuent among *C. elegans* genes (Molin et al. 2000; Maduro et al. 2001; Pocock et al. 2004). This means that, as happens for example with *tbx-8/tbx-9*, the removal of both genes is essential to detect a phenotype, this downregulation of both paralogs can happen in RNAi but not in single mutant analysis.

In conclusion, our RNAi screen produced both false positive and negative results at ranges similar to previous reports (Kamath and Ahringer 2003; Simmer et al. 2003; Rual et al. 2004). Nonetheless, we described a phenotype, either visible or reporter specific, for 19,5% of all the TFs in *C. elegans*, which is the expected efficiency of RNAi screens (Cipriani and Piano 2011). There is still much work to do validating the list of candidates and dissecting their specific roles in each MA subpopulation.

2. A fully verified TF RNAi library of 876 clones available for the community.

Whole genome RNAi libraries are known to contain an stimated 10% of wrong clones, additionaly, there are also genes for which RNAi clones are not available. For example, the whole genome RNAi library from the Ahringer group, built in 2003, was the

first whole genome library generated and covers the 86% of the around 19000 predicted coding genes at that time (Qu et al. 2011).

We decided to perform a fully covered/fully verified TF RNAi screen . To this purpose we had generate 165 new RNAi clones. As we did not find any difference between the effectiveness of the clones of Ahringer and Vidal, this is between genomic or cDNA, we decided to use genomic DNA for our clonning. Furthermore, we targeted preferentially the 3' region of each gene to achieve the amplification of secondary siRNA by means of RdRPs. Another detail to keep in mind is that long transcripts are more successfully transfer though SID-1 channel (Joyce, Gallagher, and Kuwabara 2006). For this reason the average length of our targeted sequence is around a thousand base pairs.

The selection of the final list of TFs is not a trivial matter. The number of estimated TFs has been changing over time depending on the predictive method used. For our screen we contrasted the data base Cis-BP and the transcription factor compendium wTF2.0 (Narasimhan et al. 2015). The original number of stimated TFs was 934 genes (wTF2.0) and recently this number increased to 941 (wTF3.0) (Fuxman Bass et al. 2016). Howerver, we found some changes in *C. elegans* gene and protein catalog over time (dead genes, ncRNA, etc.), differences in domain clases, differences in domain score threshold and ambiguity in clasifiying some TF families such as C2H2 or NHR that made us reduce our list. It was important for us to compare different data bases, not only Cis-BP but also SMART or PFAM, because for many TFs their motif had only been predicted though bioinformatical tools with no experimental evidence. In those cases the domain score threshold brings us the only criteria to select the members of our bona fide TF list. Furthermore, in wTF3.0 we found several examples of proteins that are involved in other functions such us ZF – CCCH family, whose members are mainly RNA-binding proteins, or ZF – DHHC group, whose domain has palmitoyl transferase activity (Tavella et al. 2016; Kim et al. 2018). Consequently, those findings reduced the number of our list to number of 876 reliable transcription factor genes (Table A.4 in the annex).

We plan to make available our fully covered/fully verified TF RNAi library to other *C. elegans* labs as it can be very useful to perform additional screens to study many other biological processes.

3. bHLH, bZip, HD, ZF-C2H2 and ZF-NHR are the main TFs families involved in monoaminergic development and specification

We found a MA phenotype associated to 11% of all TF RNAi clones. From the candidates retrieved in our screen, the most represented TF families include bHLH, bZip,

Homeodomain, ZF-C2H2 and ZF-NHR members. Moreover, if we look the candidates for each monoaminergic subpopulation, we found TFs corresponding to each of these four families in all the three subtypes (Tables R.5, R.10, R.11). Importantly, normalizing to the size of each TF family, some families seem to be over-represented while from others we retrieved fewer candidates than would be expected. For example, 24% of HD RNAi clones produce a MA phenotype (compared to the 11% of global TFs) while only 3% of ZF-NHR RNAi clones have an effect on MA specification.

HDs have been extensively reported to be required for neuron subtype specification in *C. elegans* and mammals (Hobert 2016b), and MA specification seem to be no exception. In addition to HD role in terminal differentiation, in our RNAi screen we also found abundant examples of homeodomain TFs acting upon the lineage of the different monoaminergic subpopulations, such as *egl-5* in HSN, *lin-39* in VC4/5, *vab-15* in PDE. Interestingly, this effect was mainly observed in the cells generated in the posterior part of the body (HSN, VC4/5 and PDE). HD roles in neuronal specification seem to be evolutionary conserved, as they are essential in the first steps of nervous system generation in species like *Drosophila* and mouse (Holland 2012).

The reason for the under-representation of NHR family is less clear. We only find seven candidate genes from this family that is composed by 272 TFs. One possible explanation is that the elevated number of genes of this family could have redundant functions. Notwithstanding, it has been determined that very distinct NHRs can bind to very similar sets of sequences (Narasimhan et al. 2015). In this scenario, as previously explained, if all the genes implicated in one process are not removed, the phenotype can be mask and thus it will not be possible to detect it. On the other hand, NHR family is much larger in *C. elegans* than in other animals, 272 members compared to 48 in mouse and humans. Indeed, most NHR members do not have a mammalian ortholog. Nematode specific NHRs have been related to the robustness in adaptative changes to environmental cues, what suggests that these factors could act as environmental sensors in *C. elegans*, but not in neuronal specification processes (Arda et al. 2010), this could explain the lack of MA phenotypes associated to NHR RNAi.

Other TF family significantly present in the candidates of the screen is the bZIP family. It is especially interesting in the case of *C32E8.1*, *zip-10* and *zip-5* because they seem to have a role in specification of dopamingeric, ADF and RIC/RIM neurons respectively. This family, although is involved in the regulation of a plethora of processes from immunity to metabolism, had never been described before in *C. elegans* to participate in neuronal terminal fate although it has been described in mouse (Kautzmann et al. 2011). However the worm orthologue of CREB (the cAMP response element binding) is *crh-1*, a bZIP TF that is essential in some neurons to develop functions such as thermotaxis in AFD neuron (Nishida et al. 2011). In the case of RIC and

RIM we also noticed that not only *zip-5* but also *zip-6* could be performing a role in these neurons. As bZIP TFs display their activity forming dimers, it could be interesting to address if this may be the case of *zip-5* and *zip-6*.

The bHLH family is also highly represented and it has been studied in depth for its role in cell lineage (Lanjuin et al. 2006; Zhang et al. 2013) and also some of them, like Achaete Scute subfamily (*lin-32, hlh-2, hlh-3, hlh-4* and *hlh-14*), more specifically for its pro-neural action instructing blast cells to commit to a neuronal fate (Frank, Baum, and Garriga 2003). In some cases, when these TFs are not properly express, neurons differentiate into other cell lineages, such as hypodermal cells (Poole et al. 2011). Regarding neuronal differentiation, depending on when and where they are expressed, they can promote progenitor commitment towards neuronal lineages or they can tune the terminal fate of a neuron, as is the case of *hlh-4* in ADL neuron (Masoudi et al. 2018). Moreover, these TFs can function both as activators or repressors, what could explain the high number of ectopic phenotypes we observed from this family in the results from the screen. The presence of extra neurons in those cases could be motivated to the abolished function of a TF that is preventing that cell to express the monoaminergic reporters. Alternatively, ectopic cells can be generated by reiteration of lineages giving rise to MA neurons or by conversion of non-MA lineages, as it is the case of *lin-22*.

Regarding the role of bHLH TFs in neuronal lineage, we found different examples in our screen, where *lin-32* RNAi reported a drastically reduction in PDE neurons. We know through literature that this fact is due to the role of this TF in the lineage of PDE (Portman and Emmons 2000). In contrast, *hlh-3* is apparently only involved in the terminal fate of HSN (Lloret-Fernández et al. 2018). And finally, we noticed that *hlh-14* is involved not only in the lineage of some sensory neurons, but also in the maturation of ADF, as we will discuss later. While *hlh-14* in ADF exhibits loss of expression phenotype, in HSN this TF is involved in the migration of the neuron, showing a phenotype 50% penetrant, this is a nice example of the pleiotropic actions of TFs. As the null mutant of *hlh-3* also presented some missing phenotype in ADF (observation in the lab) we hypothesize that maybe both TF could interact in these neurons, given that both have been described to form heterodimers with other bHLH TFs (Grove et al. 2009). Interestingly, *hlh-3* and *hlh-14* are paralogs and also the closest in sequence to *Ascl1* mouse TF know to be involved in serotonergic specification (Pattyn et al. 2004) (Reece-Hoyes et al. 2005).

Together with homeodomain family, the Zn-C2H2 TFs are highly represented in the results of our screen. This is one of the largest families of TFs in *C. elegans* with 192 members and regarding probability, it does not surprise that we obtained several candidates from them. This family has important functions in development and cell identity maintenance, where they can act as activators of transcription even though most of them seem to function as repressors such us *sup-35*, *ref-2*, *tra-1*, *spr-3* or *hbl-1* (Razin

et al. 2012). Moreover, this group required most of P0 secondary scorings we performed due to the embryonic or larval lethality of some of its members (Table R.1). From our screen we reported two terminal selectors of the HSN neuron, *egl-46* and *sem-4* (Lloret-Fernández et al. 2018) and we also observed that *egl-43,* the worm ortholog of the protooncogene EVI1, could be involved in RIC or RIM specification, as is the case of UV neurons (Hwang, Meruelo, and Sternberg 2007).

In summary this screen has lead us with a compendium of TF candidates from a wide range of TF families. A deeper analysis of the role of this TFs could depict the regulatory landscape of the different monoaminergic neurons.

4. New members of *C. elegans* dopaminergic regulatory code have conserved roles in mammals.

The terminal regulatory logic of dopaminergic neurons in *C. elegans* has been studied prior to our RNAi screening (Doitsidou et al. 2013; Flames and Hobert 2009). A combination of three transcription factors *ast-1*, *ceh-43* and *ceh-20* are necessary and, in some contexts sufficient, to dictate gene expression in all dopaminergic neurons subtypes of the worm (CEPs, ADE and PDE). Interestingly, the role of these three TFs seems to be conserved in mouse OB where *Er81* (ortholog of *ast-1*), *Dlx2* (ortholog of *ceh-43*) and *Pbx1* (ortholog of *ceh-20*) are required for DA specification ((Doitsidou et al. 2013; Flames and Hobert 2009) and Remesal unpublished).

Our TF RNAi screen provided a list of candidates that could be involved in dopaminergic specification. Luckily for us the list included the already known terminal selectors, reinforcing the confidence in our method, as we have previously discussed. Moreover, the list also contains a new group of genes that we have validated (see Results section 3).

Our TF RNAi screen provided a list of additional candidates that could be involved in dopaminergic specification. From the evaluated candidates, *unc-62*, *vab-3* and *unc-55*, show the strongest evidences to be considered new members of the TF collective that selects the dopaminergic transcriptome in *C. elegans* DA neurons. We find loss off expression of DA pathway genes in mutants for these three TFs and evidence of functional binding sites in DA pathway CRMs.

It is not the first time these TFs are involved in neuronal specification. For example, *vab-3* is involved in the terminal fate of IL2, OLL and URY neurons (Hobert 2016b). Furthermore, there was previous evidences that this TF could be involved in dopaminergic specification (Doitsidou et al. 2008). Regarding *unc-55*, this TF is essential

for proper VD motorneurons specification (Walthall and Plunkett 1995). The role of *unc-55* in this neuronal type is required to create a synaptic pattern that distinguishes two classes of motorneurons. Interestingly, *unc-55* expression in motorneurons is dependent of *unc-62*, relating this gene to neuronal specification programs (Campbell and Walthall 2016). Finally, *unc-62* is a classical Hox co-factor from the Meis family (Rezsohazy et al. 2015). Meis often work together with PBX both as Hox co-factors. Interestingly, both *unc-62* (Meis) and *ceh-20* (Pbx) are required for neurogenesis of VNC motorneurons (Kalis et al. 2013) and other non-neuronal functions. On the other hand, *ceh-20* is a known member of the DA TF collective, therefore, it is not surprising that both factors could be acting together.

In contrast to the originally identified members of the DA TF collective, *vab-3*, *unc-55* and *unc-62* seem to have milder phenotypes or be expressed in only subtypes of DA cells. Nevertheless, as explained in the results, some of our reporters might not be good enough to reflect the endogenous expression of the gene. Additionally, the lack of phenotype in some DA neuron subtypes might be due to redundancy. A clear example of this is shown in *unc-55* mutant analysis. Whereas *unc-55 (e1170)* single mutant only affects the expression of *cat-2* in ADE, in combination with *ast-1 (hd1)* reveals it is necessary for *bas-1* in CEPD and *dat-1* in PDE. Thus, it is likely that these factors play a role in all DA subtypes that can be masked by redundancy with other factors.

Another example of pleiotropic actions of TFs is the requirement of *vab-3* and *unc-62* in DA lineage, revealed by ectopic neurons expressing the reporters in the corresponding mutants or RNAi screen (Table R.2). However, we could determine with the P0 RNAi experiments that *unc-62*, *unc-55* and *vab-3* perform a fundamental role in maintenance the phenotype apart from their earlier roles in lineage. (Figure R.12).

Of note, mouse othrologs for all DA TF collective members have been reported to have a role in OB DA specification: *Er81/ast-1, Dlx2/ceh-43, Pbx1/ceh-20, Pax6/vab-3, Meis2/unc-62* and *Couptf1/unc-55*. However, little is known about the specific actions of this TFs in DA OB specification and if they work as a TF collective directly orchestrating DA differentiation. Our results suggest this might be the case. It would be interesting to analyze if, as what we saw for the HSN TF collective, the presence of TFBS clusters for the DA TF collective can be used to *de novo* identify DA active enhancers.

Finally, we also revealed the possible role for *dro-1* in DA specification, *dro-1* is ortholog of *Dr1* (downregulation of transcription) in mammals. Interestingly, neither *dro-1* nor *Dr1* have been described to have roles in neuronal specification before. We find *Dr1* is expressed in adult mouse OB (Allen Brain Atlas), suggesting it could be a new member of the DA TF collective.

5. *lag-1* and *hlh-14* govern terminal fate of ADF serotonergic neuron and are essential for its functionality

From the results of our RNAi screen we observe that, unlike the dopaminergic population, different serotonergic neuron subtypes are regulated by distinct TF candidates. This is in agreement to what was described in previous work from our lab (Lloret-Fernández et al. 2018) and it is likely a reflection of the molecular diversity of 5-HT neuron classes. As the regulatory logic of ADF is the less characterized we focused our candidate validation in this neuron class.

RNAi against *lag-1*, the only *C. elegans* member of CSL TF family and transcriptional effector of Notch, gave the strongest phenotype. We confirmed *lag-1* role in ADF terminal differentiation with two different mutant alleles and reported, for the first time, *lag-1* expression in ADF. Moreover, we found *lag-1* action is direct upon the 5-HT pathway genes.

Interestingly, although *lag-1* is the main mediator of the Notch pathway, we found that *lag-1* action on ADF is Notch independent. Furthermore, although *lag-1* has been reported to act as a repressor, both in *Drosophila* and mammals, our results show that *lag-1* works mainly as an activator in ADF specification. CSL-Notch-independent activator activities have been reported in mouse, were *Rbpj* interacts with the bHLH TF *Ptf1* to induce gene expression (Johnson and MacDonald 2011). RBPJ/PTF1 complex acts in different cellular context such as pancreatic specification, GABA neuronal induction in cerebellum and spinal cord and amacrine neuron differentiation in the retina (Hori et al. 2008).

We find some evidences that *lag-1* could also interact with a bHLH TF (*hlh-14*) to induce ADF fate. We find that both *hlh-14* RNAi and mutant alleles show defects in ADF gene expression and, despite known roles of *hlh-14* in lineage specification, we find that in some contexts ADF is present and shows gene expression defects (such as both F1 and P0 RNAi). Moreover, we find evidence for functional bHLH binding sites at least in the *cat-1* promoter. Other proneuronal factors, such as ASC family members (in C. elegans *lin-32, hlh-2, hlh-3, hlh-4* and *hlh-14*) are known to have a dual role: first on progenitors, to commit them to neurons, and then in postmitotic neurons, to fine tune their cell fate. With available fosmid reporters, *hlh-14* expression is detected up to the moment when ADF is generated and then expression is quickly downregulated. Similar tight regulation of expression has been reported for other ASC factors in mouse and flies (Urbán et al. 2016; Guillemot and Hassan 2017).

We hypothesized that *hlh-14* early expression in ADF lineage could be necessary to induce neural fate while late *hlh-14* expression in the last division that generates ADF could be required to induce ADF identity together with *lag-1*.

Lack of detectable *hlh-14* expression in ADF at postembryonic stages contrasts with P0 RNAi phenotypes, both of gene expression and ADF mediated responses. Thus, either *hlh-14* is expressed at low levels or our RNAi are targeting other bHLH. One candidate for the off-target effects could be *hlh-3*, as we have observed *hlh-3* mutants show small but significant phenotype in ADF.

Finally, we have determined that *lag-1* and *hlh-14* loss of function leads to important perturbations of ADF function and ADF regulated behaviors. *lag-1* and *hlh-14* RNAi impedes ADF activation upon chemical stimuli, this experiment reveals that ADF might have other gene expression defects apart from those related to 5-HT biosynthesis. We are currently setting up the experiments that will allow us to sort ADF neurons from wildtype and *lag-1* mutant animals to perform RNAseq experiments. This data will unravel additional targets of *lag-1*.

6. *zip-5* is a novel TF candidate to select the identity of RIC and RIM neurons

The interneurons RIC and RIM are the less explored among the monoaminergic neurons. They synthesize tyramine and octopamine as neurotransmitters, which are restricted to invertebrates. However, these neurotransmitters are considered the counterparts of adrenaline and noradrenaline in vertebrates, because of their similarities ruling behavior (Flames and Hobert 2011; Roeder 2005). Today, very little is known about the specification of these two neurons and here, through the RNAi screen we have obtained a list of 22 transcription factors that could be involved in the development of tyramine and octopaminergic neurons.

These genes belong to different families but the most representatives are the HD and ZF-C2H2. Regarding homeodomain family, we detected that *ceh-12* and *ceh-13*, that are paralogue genes, presented missing phenotype in RIC and RIM. As paralogues, they share some similarities in sequence and thus, it could be that the RNAi clones used in the screen targeted both genes and only the validation through single mutant analysis will determine which of them originates the phenotype in RIC and RIM. Both TFs exert a role in neuron specification, such as *ceh-12* in VB motorneurons and *ceh-13* in touch receptor neurons (Von Stetina et al. 2007; Zheng, Jin, and Chalfie 2015).

Interestingly, we observed that a group of the candidates, *ceh-13*, *ceh-36*, *ceh-27* or *vab-7*, are under Wnt signaling regulation (Zacharias et al. 2015), suggesting that the generation of this neurons is influenced by this pathway. On the other hand, we also notice among the candidates for these neurons a TF involved sex dosage compensation, *sdc-1*, (Portman 2007). Although RIC and RIM neurons have not been described to be

sexually dimorphic, it would not be surprising that some of their features were different in hermaphrodites compare to males, as octopamine regulates egg laying behavior, a task exclusively performed by hermaphrodites (Horvitz et al. 1982).

The candidates producing a strongest phenotype for tyramine and octopaminergic neurons belong to the bZIP TF family, where we found *zip-5* and *zip-6*. bZIP members can bind to DNA as homo or heterodimers, although these last ones are more scarce in less evolved organisms such as *C. elegans* (Rodríguez-Martínez et al. 2017). In contrast to *ceh-12* and *ceh-13* that are paralogues, *zip-5* and *zip-6* do not present sequence similarities, what makes it unlikely that an RNAi clone targets both of them. This would support the idea of the heterodimerization between them.

Prior studies had involved another bZIP TF in octopamine signaling, *C. elegans* CREB orthologue, *crh-1*. It is postulated that AMPK can promote CREB (crh-1) and its coactivator, CRTC-1, to bind to the DNA and induce octopamine signaling to mediate mitochondrial metabolism and lifespan (Burkewitz et al. 2015). Trough RNAi we did not detect any phenotype attributed to *crh-1*, but this could be that the RNAi clone against this gene did not work efficiently. These effects of CREB/CRTC-1 are related to lifespan; however, we wonder whether CREB could bind to another coactivator to regulate distinct functions, such as octopamine synthesis. *zip-5* could be such a partner of CREB to drive *tdc-1* expression in other contexts. Another possible scenario is that *zip-5* forms a complex with CREB/CRTC-1. In both cases the interaction between CREB and *zip-5* could be through the formation of an heterodimer, as described for bZIP TFs (Xu et al. 2007).

On the other hand, *zip-5* mutant showed low tap habituation defects (Swierczek et al. 2011). In this behavior, the worms respond with a reversal turn of their foraging way after a sudden hit. This response is organized by RIM neurons, which integrates sensory information and coordinates motorneurons and muscles to execute a close turn to change direction. As more taps occur, worms finally habituate and do not perform any movement response (Lau et al. 2012). Curiously, the integration of the stimuli from RIM neurons requires *crh*-1/CREB mediation (Timbers and Rankin 2011). As stated above, the transcriptional activity of CREB requires a coactivator to bind to DNA that, in this context, could be *zip-5*. Finally, as we detected reduced expression of *tdc*-1 in RIM neuron, this defect in tap habituation of *zip-5* mutants could be related to deficits in tyramine.

Coming back to the AMPK signanling in RIC neuron, it has also been described that the TF *pqm-1* is also regulated by CREB/CTCR-1 to induce lifespan (Burkewitz et al. 2015). We reported a phenotype for this TF with our RNAi screen, *tdc-1* and *tbh-1*

expression is normal in *pqm-1* mutants. Furthermore, we did not detect *pqm-1* fosmid neither in RIC nor in RIM.

It seems clear that both tyramine and octopamine have important roles in development and metabolism in *C. elegans* and also in other invertebrates as *Drosophila*. However, these functions become restricted to this phylum, in vertebrates they are relieved for adrenaline and noradrenaline. However, as model organism, increase our knowledge in *C. elegans* about the genetic programs that select the fate of these neurons is essential to achieve further insights related to these catecholamines in more evolved organisms.

CONCLUSIONS

CONCLUSIONS

In this Thesis we have carried out an exhaustive screen on *C. elegans* transcription factors as a first step to complete the regulatory network involved in the specification of monoaminergic neurons. Our results have led us to the following conclusions:

1. The use of *rrf-3(pk1426)* mutant background for our RNAi screen has allowed us to identify TF candidates to be involved in the specification of the different neuron MA subtypes. We retrieved the maximum number of candidates for RIC/RIM neurons and the least for the NSM neuron.
2. We constructed a complete and fully verified RNAi library for all *C. elegans* TFs is composed by 876 clones: 548 are from the Ahringer's library, 163 from Vidal's library and 165 cloned in our laboratory.
3. The RNAi screen against the TFs of *C. elegans* revealed, 95 TF with a visible phenotype of which 84% had been previously described and 91 TF with phenotype in MA neurons. 76% of the factors that had previously been implicated in the differentiation of MA neurons were retrieved in our screen.
4. The TF families with more TF candidates are homeodomain, ZF-C2H2, bHLH, bZIP and ZF-NHR. However, considering the size of each *C. elegans* TF family, homeodomain candidates are over-represented (26% of total HD members retrieved as candidates) and nuclear hormone receptors are down-represented (2.57% of total members).
5. The most prominent phenotype was loss of expression of the reporters. Many of the candidates presented phenotype in more than one MA anatomical class and some candidates have reported defined functions, such as lineage specification, regulation of sexual dimorphism and heterochrony.
6. We identified three new factors for DA specification: *unc-62, vab-3* and *unc-55*. In addition, functional binding sites for the three factors are present in the *cis*-regulatory modules of *cat-2* and *dat-1* genes suggesting a terminal role.
7. We identified *lag-1* TF as a potential terminal selector for ADF serotonergic neuron. *lag-1* function is independent of Notch pathway and seems to cooperate with bHLH TF, *hlh-14*.
8. Finally, *zip-5* TF regulates specification of both tyraminergic (RIM) and octopaminergic (RIC) neurons.

BIBLIOGRAPHY

BIBLIOGRAPHY

Addis, Russell C., Fu-Chun Hsu, Rebecca L. Wright, Marc A. Dichter, Douglas A. Coulter, and John D. Gearhart. 2011. 'Efficient Conversion of Astrocytes to Functional Midbrain Dopaminergic Neurons Using a Single Polycistronic Vector', *PLOS ONE*, 6: e28719.

Agoston, Zsuzsa, Peer Heine, Monika S. Brill, Britta Moyo Grebbin, Ann-Christin Hau, Wiebke Kallenborn-Gerhardt, Jasmine Schramm, Magdalena Götz, and Dorothea Schulte. 2014. 'Meis2 is a Pax6 co-factor in neurogenesis and dopaminergic periglomerular fate specification in the adult olfactory bulb', *Development*, 141: 28.

Alkema, Mark J., Melissa Hunter-Ensor, Niels Ringstad, and H. Robert Horvitz. 2005. 'Tyramine Functions Independently of Octopamine in the *Caenorhabditis elegans* Nervous System', *Neuron*, 46: 247-60.

Alper, Scott, and Cynthia Kenyon. 2002. 'The zinc finger protein REF-2 functions with the Hox genes to inhibit cell fusion in the ventral epidermis of *C. elegans*', *Development*, 129: 3335.

Anderson, Alexandra, Henry Laurenson-Schafer, Frederick A. Partridge, Jonathan Hodgkin, and Rachel McMullan. 2013. 'Serotonergic Chemosensory Neurons Modify the *C. elegans* Immune Response by Regulating G-Protein Signaling in Epithelial Cells', *PLoS Pathogens*, 9: e1003787.

Andreeva, Liudmila, Björn Hiller, Dirk Kostrewa, Charlotte Lässig, Carina C. de Oliveira Mann, David Jan Drexler, Andreas Maiser, Moritz Gaidt, Heinrich Leonhardt, Veit Hornung, and Karl-Peter Hopfner. 2017. 'cGAS senses long and HMGB/TFAM-bound U-turn DNA by forming protein–DNA ladders', *Nature*, 549: 394.

Arda, H. Efsun, Stefan Taubert, Lesley T. MacNeil, Colin C. Conine, Ben Tsuda, Marc Van Gilst, Reynaldo Sequerra, Lynn Doucette-Stamm, Keith R. Yamamoto, and Albertha J. M. Walhout. 2010. 'Functional modularity of nuclear hormone receptors in a *Caenorhabditis elegans* metabolic gene regulatory network', *Molecular Systems Biology*, 6.

Arenas, Ernest, Mark Denham, and J. Carlos Villaescusa. 2015. 'How to make a midbrain dopaminergic neuron', *Development*, 142: 1918.

Badis, Gwenael, Michael F. Berger, Anthony A. Philippakis, Shaheynoor Talukder, Andrew R. Gehrke, Savina A. Jaeger, Esther T. Chan, Genita Metzler, Anastasia Vedenko, Xiaoyu Chen, Hanna Kuznetsov, Chi-Fong Wang, David Coburn, Daniel E. Newburger, Quaid Morris, Timothy R. Hughes, and Martha L. Bulyk. 2009. 'Diversity and complexity in DNA recognition by transcription factors', *Science (New York, N.Y.)*, 324: 1720-23.

Bargmann, C. I., and H. R. Horvitz. 1991. 'Control of larval development by chemosensory neurons in *Caenorhabditis elegans*', *Science (New York, N.Y.)*, 251: 1243.

Bauknecht, Philipp, and Gáspár Jékely. 2017. 'Ancient coexistence of norepinephrine, tyramine, and octopamine signaling in bilaterians', *BMC Biology*, 15: 6.

Baumeister, R., Y. Liu, and G. Ruvkun. 1996. 'Lineage-specific regulators couple cell lineage asymmetry to the transcription of the *Caenorhabditis elegans* POU gene *unc-86* during neurogenesis', *Genes & Development*, 10: 1395-410.

Bell, Adam C., Adam G. West, and Gary Felsenfeld. 1999. 'The Protein CTCF Is Required for the Enhancer Blocking Activity of Vertebrate Insulators', *Cell*, 98: 387-96.

Belton, Jon-Matthew, Rachel Patton McCord, Johan Harmen Gibcus, Natalia Naumova, Ye Zhan, and Job Dekker. 2012. 'Hi–C: A comprehensive technique to capture the conformation of genomes', *Methods*, 58: 268-76.

Beres, Thomas M., Toshihiko Masui, Galvin H. Swift, Ling Shi, R. Michael Henke, and Raymond J. MacDonald. 2006. 'PTF1 Is an Organ-Specific and Notch-Independent Basic Helix-Loop-Helix Complex Containing the Mammalian Suppressor of Hairless (RBP-J) or Its Paralogue, RBP-L', *Molecular and Cellular Biology*, 26: 117-30.

Berger, Michael F., Gwenael Badis, Andrew R. Gehrke, Shaheynoor Talukder, Anthony A. Philippakis, Lourdes Peña-Castillo, Trevis M. Alleyne, Sanie Mnaimneh, Olga B. Botvinnik, Esther T. Chan, Faiqua Khalid, Wen Zhang, Daniel Newburger, Savina A. Jaeger, Quaid D. Morris, Martha L. Bulyk, and Timothy R. Hughes. 2008. 'Variation in Homeodomain DNA Binding Revealed by High-Resolution Analysis of Sequence Preferences', *Cell*, 133: 1266-76.

Bertrand, Vincent, Paul Bisso, Richard J. Poole, and Oliver Hobert. 2011. 'Notch-dependent induction of left/right asymmetry in *C. elegans* interneurons and motoneurons', *Current biology : CB*, 21: 1225-31.

Blaiseau, Pierre-Louis, and Dominique Thomas. 1998. 'Multiple transcriptional activation complexes tether the yeast activator Met4 to DNA', *The EMBO Journal*, 17: 6327.

Blaugrund, E., T. D. Pham, V. M. Tennyson, L. Lo, L. Sommer, D. J. Anderson, and M. D. Gershon. 1996. 'Distinct subpopulations of enteric neuronal progenitors defined by time of development, sympathoadrenal lineage markers and Mash-1-dependence', *Development*, 122: 309.

Boutros, Michael , and Julie Ahringer. 2008. 'The art and design of generic screens: RNA interference', *Nature Reviews Genetics*, 9: 554-66.

Bovetti, Serena, Sara Bonzano, Donatella Garzotto, Serena Gea Giannelli, Angelo Iannielli, Maria Armentano, Michèle Studer, and Silvia De Marchis. 2013. 'COUP-TFI controls activity-dependent tyrosine hydroxylase expression in adult dopaminergic olfactory bulb interneurons', *Development*, 140: 4850.

Bozorgmehr, Tahereh, Evan L. Ardiel, Andrea H. McEwan, and Catharine H. Rankin. 2013. 'Mechanisms of plasticity in a Caenorhabditis elegans mechanosensory circuit', *Frontiers in Physiology*, 4: 88.

Brenner, S. 1974. 'The Genetics of CAENORHABDITIS ELEGANS', *Genetics*, 77: 71-94.

Brill, Monika S., Marina Snapyan, Hilde Wohlfrom, Jovica Ninkovic, Melanie Jawerka, Grant S. Mastick, Ruth Ashery-Padan, Armen Saghatelyan, Benedikt Berninger, and Magdalena Götz. 2008. 'A Dlx2- and Pax6-Dependent Transcriptional Code for Periglomerular Neuron Specification in the Adult Olfactory Bulb', *The Journal of Neuroscience*, 28: 6439.

Burkewitz, Kristopher, Ianessa Morantte, Heather J M. Weir, Robin Yeo, Yue Zhang, Frank K Huynh, Olga R Ilkayeva, Matthew D Hirschey, Ana R Grant, and William B

Mair. 2015. 'Neuronal CRTC-1 Governs Systemic Mitochondrial Metabolism and Lifespan via a Catecholamine Signal', *Cell*, 160: 842-55.
Caiazzo, Massimiliano, Maria Teresa Dell'Anno, Elena Dvoretskova, Dejan Lazarevic, Stefano Taverna, Damiana Leo, Tatyana D. Sotnikova, Andrea Menegon, Paola Roncaglia, Giorgia Colciago, Giovanni Russo, Piero Carninci, Gianni Pezzoli, Raul R. Gainetdinov, Stefano Gustincich, Alexander Dityatev, and Vania Broccoli. 2011. 'Direct generation of functional dopaminergic neurons from mouse and human fibroblasts', *Nature*, 476: 224.
Calixto, Andrea, Dattananda Chelur, Irini Topalidou, Xiaoyin Chen, and Martin Chalfie. 2010. 'Enhanced neuronal RNAi in C. elegans using SID-1', *Nature Methods*, 7: 554.
Campbell, Richard F., and Walter W. Walthall. 2016. 'Meis/UNC-62 isoform dependent regulation of CoupTF-II/UNC-55 and GABAergic motor neuron subtype differentiation', *Developmental Biology*, 419: 250-61.
Carey, Michael. 1998. 'The Enhanceosome and Transcriptional Synergy', *Cell*, 92: 5-8.
Carlsson, Arvid, Nicholas Waters, Susanna Holm-Waters, Joakim Tedroff, Marie Nilsson, and Maria L. Carlsson. 2001. 'Interactions Between Monoamines, Glutamate, and GABA in Schizophrenia: New Evidence', *Annual Review of Pharmacology and Toxicology*, 41: 237-60.
Cave, John W., Yosuke Akiba, Kasturi Banerjee, Shivraj Bhosle, RoseAnn Berlin, and Harriet Baker. 2010. 'Differential regulation of dopaminergic gene expression by *Er81*', *The Journal of neuroscience : the official journal of the Society for Neuroscience*, 30: 4717-24.
Caveney, Stanley, Wendy Cladman, LouAnn Verellen, and Cam Donly. 2006. 'Ancestry of neuronal monoamine transporters in the Metazoa', *Journal of Experimental Biology*, 209: 4858.
Chalfie, Martin, and John Sulston. 1981. 'Developmental genetics of the mechanosensory neurons of *Caenorhabditis elegans*', *Developmental Biology*, 82: 358-70.
Chamberlin, Helen M., Keith B. Brown, Paul W. Sternberg, and James H. Thomas. 1999. 'Characterization of Seven Genes Affecting *Caenorhabditis elegans* Hindgut Development', *Genetics*, 153: 731.
Chamberlin, Helen M., and Paul W. Sternberg. 1995. 'Mutations in the *Caenorhabditis elegans* Gene *vab-3* Reveal Distinct Roles in Fate Specification and Unequal Cytokinesis in an Asymmetric Cell Division', *Developmental Biology*, 170: 679-89.
Chang, Sarah, Robert J. Johnston, and Oliver Hobert. 2003. 'A transcriptional regulatory cascade that controls left/right asymmetry in chemosensory neurons of *C. elegans*', *Genes & Development*, 17: 2123-37.
Chen, Beth L., David H. Hall, and Dmitri B. Chklovskii. 2006. 'Wiring optimization can relate neuronal structure and function', *Proceedings of the National Academy of Sciences of the United States of America*, 103: 4723.
Chen, Zhe, and Min Han. 2001. 'Role of *C. elegans lin-40* MTA in vulval fate specification and morphogenesis', *Development*, 128: 4911.
Cheng Chi, Wa, Mei Yan Carol Hiu, Wah Choy Siu, Yu Hui Michelle Nga, Chi-Chung Hui, and Han Cheng Shuk. 2007. 'Zebrafish homologue *irx1a* is required for the differentiation of serotonergic neurons', *Developmental Dynamics*, 236: 2661-67.

Cheng, Leping, Chih-Li Chen, Ping Luo, Min Tan, Mengsheng Qiu, Randy Johnson, and Qiufu Ma. 2003. '*Lmx1b*, *Pet-1* and *Nkx2.2* Coordinately Specify Serotonergic Neurotransmitter Phenotype', *The Journal of Neuroscience*, 23: 9961.

Chisholm, A. 1991. 'Control of cell fate in the tail region of *C. elegans* by the gene *egl-5*', *Development*, 111: 921.

Christensen, S., V. Kodoyianni, M. Bosenberg, L. Friedman, and J. Kimble. 1996. '*lag-1*, a gene required for *lin-12* and *glp-1* signaling in *Caenorhabditis elegans*, is homologous to human CBF1 and *Drosophila* Su(H)', *Development*, 122: 1373.

Churgin, Matthew A., Richard J. McCloskey, Emily Peters, and Christopher Fang-Yen. 2017. 'Antagonistic Serotonergic and Octopaminergic Neural Circuits Mediate Food-Dependent Locomotory Behavior in *Caenorhabditis elegans*', *The Journal of Neuroscience*, 37: 7811.

Cipriani, Patricia G., and Fabio Piano. 2011. 'RNAi Methods and Screening: RNAi Based High-Throughput Genetic Interaction Screening.' in Joel H. Rothman and Andrew Singson (eds.), *Methods in cell biology* (Academic Press).

Clark, Scott G., Andrew D. Chisholm, and H. Robert Horvitz. 1993. 'Control of cell fates in the central body region of *C. elegans* by the homeobox gene *lin-39*', *Cell*, 74: 43-55.

Clark, Scott G., and Catherine Chiu. 2003. '*C. elegans* ZAG-1, a Zn-finger-homeodomain protein, regulates axonal development and neuronal differentiation', *Development*, 130: 3781.

Coppola, Eva, Fabien Autréaux, Filippo M. Rijli, and Jean-François Brunet. 2010. 'Ongoing roles of *Phox2* homeodomain transcription factors during neuronal differentiation', *Development*, 137: 4211.

D'Ausilio, Alessandro. 2012. 'Arduino: A low-cost multipurpose lab equipment', *Behavior Research Methods*, 44: 305-13.

Dalzell, Johnathan J., Paul McVeigh, Neil D. Warnock, Makedonka Mitreva, David McK Bird, Pierre Abad, Colin C. Fleming, Tim A. Day, Angela Mousley, Nikki J. Marks, and Aaron G. Maule. 2011. 'RNAi Effector Diversity in Nematodes', *PLoS Neglected Tropical Diseases*, 5: e1176.

de Melo, Jimmy, Xiangguo Qiu, Guoyan Du, Leah Cristante, and D. Eisenstat David. 2003. '*Dlx1*, *Dlx2*, *Pax6*, *Brn3b*, and *Chx10* homeobox gene expression defines the retinal ganglion and inner nuclear layers of the developing and adult mouse retina', *Journal of Comparative Neurology*, 461: 187-204.

Deneris, Evan S., and Oliver Hobert. 2014. 'Maintenance of postmitotic neuronal cell identity', *Nature neuroscience*, 17: 899-907.

Desai, Chand, Gian Garriga, Steven L. McLntire, and H. Robert Horvitz. 1988. 'A genetic pathway for the development of the *Caenorhabditis elegans* HSN motor neurons', *Nature*, 336: 638.

Dichoso, Daryl, Thomas Brodigan, Kyu Yeong Chwoe, Jin Sook Lee, Reymond Llacer, Morgan Park, Ann K. Corsi, Stephen A. Kostas, Andrew Fire, Joohong Ahnn, and Michael Krause. 2000. 'The MADS-Box Factor CeMEF2 Is Not Essential for *Caenorhabditis elegans* Myogenesis and Development', *Developmental Biology*, 223: 431-40.

Dittrich, R., T. Bossing, A. P. Gould, G. M. Technau, and J. Urban. 1997. 'The differentiation of the serotonergic neurons in the *Drosophila* ventral nerve cord depends on the

combined function of the zinc finger proteins Eagle and Huckebein', *Development*, 124: 2515.

Doitsidou, Maria, Nuria Flames, Albert C. Lee, Alexander Boyanov, and Oliver Hobert. 2008. 'Automated screening for mutants affecting dopaminergic-neuron specification in *C. elegans*', *Nature Methods*, 5: 869.

Doitsidou, Maria, Nuria Flames, Irini Topalidou, Namiko Abe, Terry Felton, Laura Remesal, Tatiana Popovitchenko, Richard Mann, Martin Chalfie, and Oliver Hobert. 2013. 'A combinatorial regulatory signature controls terminal differentiation of the dopaminergic nervous system in *C. elegans*', *Genes & Development*, 27: 1391-405.

Doitsidou, Maria, Gregory Minevich, Jason R. Kroll, Gwen Soete, Sriharsh Gowtham, Hendrik C. Korswagen, Jeroen Sebastiaan van Zon, and Oliver Hobert. 2018. 'A *Caenorhabditis elegans* Zinc Finger Transcription Factor, *ztf-6*, Required for the Specification of a Dopamine Neuron-Producing Lineage', *G3: Genes|Genomes|Genetics*, 8: 17.

Donnelly, Jamie L., Christopher M. Clark, Andrew M. Leifer, Jennifer K. Pirri, Marian Haburcak, Michael M. Francis, Aravinthan D. T. Samuel, and Mark J. Alkema. 2013. 'Monoaminergic Orchestration of Motor Programs in a Complex *C. elegans* Behavior', *PLOS Biology*, 11: e1001529.

Doonan, Ryan, Julia Hatzold, Saleel Raut, Barbara Conradt, and Aixa Alfonso. 2008. 'HLH-3 is a *C. elegans* Achaete/Scute protein required for differentiation of the hermaphrodite-specific motor neurons', *Mechanisms of Development*, 125: 883-93.

Dozier, Christine, Hiroshi Kagoshima, Gisela Niklaus, Giuseppe Cassata, and Thomas R. Bürglin. 2001. 'The *Caenorhabditis elegans* Six/sine oculis Class Homeobox Gene *ceh-32* Is Required for Head Morphogenesis', *Developmental Biology*, 236: 289-303.

Du, Hongping, and Martin Chalfie. 2001. 'Genes Regulating Touch Cell Development in *Caenorhabditis elegans*', *Genetics*, 158: 197.

Duchaine, Thomas F., James A. Wohlschlegel, Scott Kennedy, Yanxia Bei, Darryl Conte, Jr., KaMing Pang, Daniel R. Brownell, Sandra Harding, Shohei Mitani, Gary Ruvkun, John R. Yates, III, and Craig C. Mello. 2006. 'Functional Proteomics Reveals the Biochemical Niche of *C. elegans* DCR-1 in Multiple Small-RNA-Mediated Pathways', *Cell*, 124: 343-54.

Duerr, Janet S., Dennis L. Frisby, Jennifer Gaskin, Angie Duke, Karen Asermely, David Huddleston, Lee E. Eiden, and James B. Rand. 1999. 'The *cat-1* Gene of *Caenorhabditis elegans* Encodes a Vesicular Monoamine Transporter Required for Specific Monoamine-Dependent Behaviors', *The Journal of Neuroscience*, 19: 72.

Dupont, Cathérine, D. Randall Armant, and Carol A. Brenner. 2009. 'Epigenetics: Definition, Mechanisms and Clinical Perspective', *Seminars in reproductive medicine*, 27: 351-57.

Edelstein, Arthur, Nenad Amodaj, Karl Hoover, Ron Vale, and Nico Stuurman. 2010. 'Computer Control of Microscopes Using μManager', *Current Protocols in Molecular Biology*, 92: 14.20.1-14.20.17.

Ernsberger, Uwe, Eva Reissmann, Ivor Mason, and Hermann Rohrer. 2000. 'The expression of dopamine β-hydroxylase, tyrosine hydroxylase, and *Phox2* transcription factors in sympathetic neurons: evidence for common regulation during noradrenergic induction and diverging regulation later in development', *Mechanisms of Development*, 92: 169-77.

Evans, Nicole C., Christina I. Swanson, and Scott Barolo. 2012. 'Chapter four - Sparkling Insights into Enhancer Structure, Function, and Evolution.' in Serge Plaza and François Payre (eds.), *Current Topics in Developmental Biology* (Academic Press).

Fagan, Kelli A., Jintao Luo, Ross C. Lagoy, Frank C. Schroeder, Dirk R. Albrecht, and Douglas S. Portman. 2018. 'A Single-Neuron Chemosensory Switch Determines the Valence of a Sexually Dimorphic Sensory Behavior', *Current Biology*, 28: 902-14.e5.

Fang-Yen, Christopher, Mark J. Alkema, and Aravinthan D. T. Samuel. 2015. 'Illuminating neural circuits and behaviour in *Caenorhabditis elegans* with optogenetics', *Philosophical Transactions of the Royal Society B: Biological Sciences*, 370: 20140212.

Fire, Andrew, SiQun Xu, Mary K. Montgomery, Steven A. Kostas, Samuel E. Driver, and Craig C. Mello. 1998. 'Potent and specific genetic interference by double-stranded RNA in *Caenorhabditis elegans*', *Nature*, 391: 806.

Fischer, Sylvia E. J., Maurice D. Butler, Qi Pan, and Gary Ruvkun. 2008. 'Trans-splicing in *C. elegans* generates the negative RNAi regulator ERI-6/7', *Nature*, 455: 491.

Flames, Nuria, and Oliver Hobert. 2009. 'Gene regulatory logic of dopamine neuron differentiation', *Nature*, 458: 885.

———. 2011. 'Transcriptional Control of the Terminal Fate of Monoaminergic Neurons', *Annual Review of Neuroscience*, 34: 153-84.

Fontaine, Romain, Pierre Affaticati, Charlotte Bureau, Ingrid Colin, Michaël Demarque, Sylvie Dufour, Philippe Vernier, Kei Yamamoto, and Catherine Pasqualini. 2015. 'Dopaminergic Neurons Controlling Anterior Pituitary Functions: Anatomy and Ontogenesis in Zebrafish', *Endocrinology*, 156: 2934-48.

Frank, C. Andrew, Paul D. Baum, and Gian Garriga. 2003. 'HLH-14 is a *C. elegans* Achaete-Scute protein that promotes neurogenesis through asymmetric cell division', *Development*, 130: 6507.

Fraser, Andrew G., Ravi S. Kamath, Peder Zipperlen, Maruxa Martinez-Campos, Marc Sohrmann, and Julie Ahringer. 2000. 'Functional genomic analysis of *C. elegans* chromosome I by systematic RNA interference', *Nature*, 408: 325.

Fu, Jiajun, Haining Zhang, Wenming Huang, Xinyu Zhu, Yi Sheng, Eli Song, and Tao Xu. 2018. 'AIM interneurons mediate feeding suppression through the TYRA-2 receptor in *C. elegans*', *Biophysics Reports*, 4: 17-24.

Fuxman Bass, Juan I., Carles Pons, Lucie Koxlowski, John S. Reece-Hoyes, Shaleen Shrestha, Amy D. Holdorf, Akihiro Mori, Chad L. Myers, and Albertha J. M. Walhout. 2016. 'A gene-centered *C. elegans* protein–DNA interaction network provides a framework for functional predictions', *Molecular Systems Biology*, 12.

Gao, Zhen, Lu Liu, and Jianhua Ruan. 2017. 'Logo2PWM: a tool to convert sequence logo to position weight matrix', *BMC Genomics*, 18: 709.

García-Bellido, A. 1975. 'Genetic control of wing disc development in *Drosophila* ', *Ciba Found Symp.*, 29: 161-82.

Garvie, Colin W., James Hagman, and Cynthia Wolberger. 2001. 'Structural Studies of Ets-1/Pax5 Complex Formation on DNA', *Molecular Cell*, 8: 1267-76.
Gendrel, Marie, Emily G. Atlas, and Oliver Hobert. 2016. 'A cellular and regulatory map of the GABAergic nervous system of *C. elegans*', *eLIFE*, 5: e17686.
Gibcus, Johan H, and Job Dekker. 2013. 'The Hierarchy of the 3D Genome', *Molecular Cell*, 49: 773-82.
Gordân, Raluca, Ning Shen, Iris Dror, Tianyin Zhou, John Horton, Remo Rohs, and Martha L Bulyk. 2013. 'Genomic Regions Flanking E-Box Binding Sites Influence DNA Binding Specificity of bHLH Transcription Factors through DNA Shape', *Cell Reports*, 3: 1093-104.
Grishok, Alla. 2005. 'RNAi mechanisms in *Caenorhabditis elegans*', *FEBS Letters*, 579: 5932-39.
Grove, Christian A., Federico de Masi, M. Inmaculada Barrasa, Daniel E. Newburger, Mark J. Alkema, Martha L. Bulyk, and Albertha J. M. Walhout. 2009. 'A Multi-Parameter Network Reveals Extensive Divergence Between *C. elegans* bHLH Transcription Factors', *Cell*, 138: 314-27.
Guillemot, François, and Bassem A. Hassan. 2017. 'Beyond proneural: emerging functions and regulations of proneural proteins', *Current Opinion in Neurobiology*, 42: 93-101.
Guo, Min, Tai-Hong Wu, Yan-Xue Song, Ming-Hai Ge, Chun-Ming Su, Wei-Pin Niu, Lan-Lan Li, Zi-Jing Xu, Chang-Li Ge, Maha T. H. Al-Mhanawi, Shi-Ping Wu, and Zheng-Xing Wu. 2015. 'Reciprocal inhibition between sensory ASH and ASI neurons modulates nociception and avoidance in *Caenorhabditis elegans*', *Nature Communications*, 6: 5655.
Guo, Su, Jennifer Brush, Hiroki Teraoka, Audrey Goddard, Stephen W. Wilson, Mary C. Mullins, and Arnon Rosenthal. 1999. 'Development of Noradrenergic Neurons in the Zebrafish Hindbrain Requires BMP, FGF8, and the Homeodomain Protein *Soulless/Phox2a*', *Neuron*, 24: 555-66.
Gürel, Güliz, Megan A. Gustafson, Judy S. Pepper, H. Robert Horvitz, and Michael R. Koelle. 2012. 'Receptors and Other Signaling Proteins Required for Serotonin Control of Locomotion in *Caenorhabditis elegans*', *Genetics*, 192: 1359-71.
Hall, D. H., and R. L. Russell. 1991. 'The posterior nervous system of the nematode *Caenorhabditis elegans*: serial reconstruction of identified neurons and complete pattern of synaptic interactions', *The Journal of Neuroscience*, 11: 1.
Hall, David H., Robyn Lints, and Zeynep Altun. 2005. 'Nematode Neurons: Anatomy and Anatomical Methods in *Caenorhabditis elegans*.' in, *International Review of Neurobiology* (Academic Press).
Hansen, Anders S., Claudia Cattoglio, Xavier Darzacq, and Robert Tjian. 2018. 'Recent evidence that TADs and chromatin loops are dynamic structures', *Nucleus*, 9: 20-32.
Hartenstein, Volker, Shigeo Takashima, Parvana Hartenstein, Samuel Asanad, and Kian Asanad. 2017. 'bHLH proneural genes as cell fate determinants of entero-endocrine cells, an evolutionarily conserved lineage sharing a common root with sensory neurons', *Developmental Biology*, 431: 36-47.
Haspel, Gal, and Michael J. O'Donovan. 2012. 'A connectivity model for the locomotor network of *Caenorhabditis elegans*', *Worm*, 1: 125-28.

Haugas, Maarja, Laura Tikker, Kaia Achim, Marjo Salminen, and Juha Partanen. 2016. '*Gata2* and *Gata3* regulate the differentiation of serotonergic and glutamatergic neuron subtypes of the dorsal raphe', *Development*, 143: 4495.

Hills, Thomas, Penelope J. Brockie, and Andres V. Maricq. 2004. 'Dopamine and Glutamate Control Area-Restricted Search Behavior in *Caenorhabditis elegans*', *The Journal of Neuroscience*, 24: 1217.

Hobert, Oliver. 2008. 'Regulatory logic of neuronal diversity: Terminal selector genes and selector motifs', *Proceedings of the National Academy of Sciences*, 105: 20067.

———. 2011. 'Regulation of terminal differentiation programs in the nervous system', *Annu. Rev. Cell Dev. Biol.*, 27: 681–96.

———. 2016a. 'Chapter Twenty-Five - Terminal Selectors of Neuronal Identity.' in Paul M. Wassarman (ed.), *Current Topics in Developmental Biology* (Academic Press).

———. 2016b. 'A map of terminal regulators of neuronal identity in *Caenorhabditis elegans*', *Wiley Interdisciplinary Reviews: Developmental Biology*, 5: 474-98.

Hoekstra, Elisa J., Simone Mesman, Willem A. de Munnik, and Marten P. Smidt. 2013. 'LMX1B Is Part of a Transcriptional Complex with PSPC1 and PSF', *PLOS ONE*, 8: e53122.

Hoffman, Sandy, Daniel Martin, Alicia Meléndez, and Jill Bargonetti. 2014. '*C. elegans* CEP-1/p53 and BEC-1 Are Involved in DNA Repair', *PLOS ONE*, 9: e88828.

Hofmann, E. Randal, Stuart Milstein, Simon J. Boulton, Mianjia Ye, Jen J. Hofmann, Lilli Stergiou, Anton Gartner, Marc Vidal, and Michael O. Hengartner. 2002. '*Caenorhabditis elegans* HUS-1 Is a DNA Damage Checkpoint Protein Required for Genome Stability and EGL-1-Mediated Apoptosis', *Current Biology*, 12: 1908-18.

Holland, Peter W. H. 2012. 'Evolution of homeobox genes', *Wiley Interdisciplinary Reviews: Developmental Biology*, 2: 31-45.

Hong, Seok Jong, Thomas Lardaro, Myung Sook Oh, Youngbuhm Huh, Yunmin Ding, Un Jung Kang, Jutta Kirfel, Reinhard Buettner, and Kwang-Soo Kim. 2008. 'Regulation of the Noradrenaline Neurotransmitter Phenotype by the Transcription Factor AP-2β', *The Journal of Biological Chemistry*, 283: 16860-67.

Hori, Kei, Justyna Cholewa-Waclaw, Yuji Nakada, Stacey M. Glasgow, Toshihiko Masui, R. Michael Henke, Hendrik Wildner, Benedetta Martarelli, Thomas M. Beres, Jonathan A. Epstein, Mark A. Magnuson, Raymond J. MacDonald, Carmen Birchmeier, and Jane E. Johnson. 2008. 'A nonclassical bHLH–Rbpj transcription factor complex is required for specification of GABAergic neurons independent of Notch signaling', *Genes & Development*, 22: 166-78.

Horner, Michael A., Sophie Quintin, Mary Ellen Domeier, Judith Kimble, Michel Labouesse, and Susan E. Mango. 1998. '*pha-4*, anHNF-3 homolog, specifies pharyngeal organ identity in *Caenorhabditis elegans*', *Genes & Development*, 12: 1947-52.

Horvitz, H. R., M. Chalfie, C. Trent, J. E. Sulston, and P. D. Evans. 1982. 'Serotonin and octopamine in the nematode *Caenorhabditis elegans*', *Science (New York, N.Y.)*, 216: 1012.

Huang, Xinxin, E. Tian, Yanhua Xu, and Hong Zhang. 2009. 'The *C. elegans* engrailed homolog *ceh-16* regulates the self-renewal expansion division of stem cell-like seam cells', *Developmental Biology*, 333: 337-47.

Hwang, Byung Joon, Alejandro D. Meruelo, and Paul W. Sternberg. 2007. '*C. elegans* EVI1 proto-oncogene, EGL-43, is necessary for Notch-mediated cell fate specification and regulates cell invasion', *Development*, 134: 669.

Inoue, Takao, and Paul W. Sternberg. 2010. '*C. elegans* BED domain transcription factor BED-3 controls lineage-specific cell proliferation during organogenesis', *Developmental Biology*, 338: 226-36.

Inukai, Sachi, Kian Hong Kock, and Martha L. Bulyk. 2017. 'Transcription factor–DNA binding: beyond binding site motifs', *Current Opinion in Genetics & Development*, 43: 110-19.

Iwanir, Shachar, Adam S. Brown, Stanislav Nagy, Dana Najjar, Alexander Kazakov, Kyung Suk Lee, Alon Zaslaver, Erel Levine, and David Biron. 2016. 'Serotonin promotes exploitation in complex environments by accelerating decision-making', *BMC Biology*, 14: 9.

Jacobs, Frank M. J., Susan van Erp, Annemarie J. A. van der Linden, Lars von Oerthel, J. Peter H. Burbach, and Marten P. Smidt. 2009. '*Pitx3* potentiates *Nurr1* in dopamine neuron terminal differentiation through release of SMRT-mediated repression', *Development*, 136: 531.

Jannot, Guillaume, Marie-Eve L. Boisvert, Isabelle H. Banville, and Martin J. Simard. 2008. 'Two molecular features contribute to the Argonaute specificity for the microRNA and RNAi pathways in *C. elegans*', *RNA*, 14: 829-35.

Jarrell, Travis A., Yi Wang, Adam E. Bloniarz, Christopher A. Brittin, Meng Xu, J. Nichol Thomson, Donna G. Albertson, David H. Hall, and Scott W. Emmons. 2012. 'The Connectome of a Decision-Making Neural Network', *Science (New York, N.Y.)*, 337: 437.

Jiang, Yuan, Vanessa Horner, and Jun Liu. 2005. 'The HMX homeodomain protein MLS-2 regulates cleavage orientation, cell proliferation and cell fate specification in the *C. elegans* postembryonic mesoderm', *Development*, 132: 4119.

Johnson, Jane E., and Raymond J. MacDonald. 2011. 'Chapter three - Notch-Independent Functions of CSL.' in Carmen Birchmeier (ed.), *Current Topics in Developmental Biology* (Academic Press).

Johnson, W. A., and J. Hirsh. 1990. 'Binding of a Drosophila POU-domain protein to a sequence element regulating gene expression in specific dopaminergic neurons', *Nature*, 343: 467.

Jolma, Arttu, Yimeng Yin, Kazuhiro R. Nitta, Kashyap Dave, Alexander Popov, Minna Taipale, Martin Enge, Teemu Kivioja, Ekaterina Morgunova, and Jussi Taipale. 2015. 'DNA-dependent formation of transcription factor pairs alters their binding specificity', *Nature*, 527: 384.

Jorgensen, Erik M., and Susan E. Mango. 2002. 'The art and design of genetic screens: *Caenorhabditis elegans*', *Nature Reviews Genetics*, 3: 356-69.

Joshi, Rohit, Jonathan M. Passner, Remo Rohs, Rinku Jain, Alona Sosinsky, Michael A. Crickmore, Vinitha Jacob, Aneel K. Aggarwal, Barry Honig, and Richard S. Mann. 2007. 'Functional Specificity of a Hox Protein Mediated by the Recognition of Minor Groove Structure', *Cell*, 131: 530-43.

Joyce, Peter I., Joseph M. Gallagher, and Patricia E. Kuwabara. 2006. 'Manipulating and enhancing the RNAi response', *Journal of RNAi and Gene Silencing : An International Journal of RNA and Gene Targeting Research*, 2: 118-25.

Junion, Guillaume, Mikhail Spivakov, Charles Girardot, Martina Braun, E. Hilary Gustafson, Ewan Birney, and Eileen E M. Furlong. 2012. 'A Transcription Factor Collective Defines Cardiac Cell Fate and Reflects Lineage History', *Cell*, 148: 473-86.

Kalis, Andrea K., Djem U. Kissiov, Emily S. Kolenbrander, Zachary Palchick, Shraddha Raghavan, J. Tetreault Breanna, Erin Williams, M. Loer Curtis, and Ross Wolff Jennifer. 2013. 'Patterning of sexually dimorphic neurogenesis in the *Caenorhabditis elegans* ventral cord by Hox and TALE homeodomain transcription factors', *Developmental Dynamics*, 243: 159-71.

Kamath, Ravi S., and Julie Ahringer. 2003. 'Genome-wide RNAi screening in *Caenorhabditis elegans*', *Methods*, 30: 313-21.

Kamath, Ravi S., Maruxa Martinez-Campos, Peder Zipperlen, Andrew G. Fraser, and Julie Ahringer. 2000. 'Effectiveness of specific RNA-mediated interference through ingested double-stranded RNA in *Caenorhabditis elegans*', *Genome Biology*, 2: research0002.1.

Kamhi, J. Frances, Sara Arganda, Corrie S. Moreau, and James F. A. Traniello. 2017. 'Origins of Aminergic Regulation of Behavior in Complex Insect Social Systems', *Frontiers in Systems Neuroscience*, 11.

Kandel, E. R. , J. H. Schwartz, and T. M. Jessell. 1991. 'Principles of neural science', *Appleton & Lange*: pp. 1135.

Kantidakis, Theodoros, and Robert J. White. 2010. 'Dr1 (NC2) is present at tRNA genes and represses their transcription in human cells', *Nucleic Acids Research*, 38: 1228-39.

Kaslin, Jan, and Pertti Panula. 2001. 'Comparative anatomy of the histaminergic and other aminergic systems in zebrafish (*Danio rerio*)', *Journal of Comparative Neurology*, 440: 342-77.

Kautzmann, Marie-Audrey I., Douglas S. Kim, Marie-Paule Felder-Schmittbuhl, and Anand Swaroop. 2011. 'Combinatorial Regulation of Photoreceptor Differentiation Factor, Neural Retina Leucine Zipper Gene Nrl, Revealed by *in Vivo* Promoter Analysis', *Journal of Biological Chemistry*, 286: 28247-55.

Kennedy, Scott, Duo Wang, and Gary Ruvkun. 2004. 'A conserved siRNA-degrading RNase negatively regulates RNA interference in *C. elegans*', *Nature*, 427: 645.

Khan, Aziz, Oriol Fornes, Arnaud Stigliani, Marius Gheorghe, Jaime A. Castro-Mondragon, Robin van der Lee, Adrien Bessy, Jeanne Chèneby, Shubhada R. Kulkarni, Ge Tan, Damir Baranasic, David J. Arenillas, Albin Sandelin, Klaas Vandepoele, Boris Lenhard, Benoît Ballester, Wyeth W. Wasserman, François Parcy, and Anthony Mathelier. 2018. 'JASPAR 2018: update of the open-access database of transcription factor binding profiles and its web framework', *Nucleic Acids Research*, 46: D1284-D84.

Khoueiry, Pierre, Charles Girardot, Lucia Ciglar, Pei-Chen Peng, E. Hilary Gustafson, Saurabh Sinha, and Eileen E. M. Furlong. 2017. 'Uncoupling evolutionary changes in DNA sequence, transcription factor occupancy and enhancer activity', *eLIFE*, 6: e28440.

Kim, J., and K. Struhl. 1995. 'Determinants of half-site spacing preferences that distinguish AP-1 and ATF/CREB bZIP domains', *Nucleic Acids Research*, 23: 2531-37.

Kim, Jongpil, Susan C Su, Haoyi Wang, Albert W Cheng, John P Cassady, Michael A Lodato, Christopher J Lengner, Chee-Yeun Chung, Meelad M Dawlaty, Li-Huei Tsai, and Rudolf Jaenisch. 2011. 'Functional Integration of Dopaminergic Neurons Directly Converted from Mouse Fibroblasts', *Cell Stem Cell*, 9: 413-19.

Kim, Kyuhyung, Rinho Kim, and Piali Sengupta. 2010. 'The HMX/NKX homeodomain protein MLS-2 specifies the identity of the AWC sensory neuron type via regulation of the *ceh-36* Otx gene in *C. elegans*', *Development (Cambridge, England)*, 137: 963-74.

Kim, Tae Kook, and Tom Maniatis. 1997. 'The Mechanism of Transcriptional Synergy of an In Vitro Assembled Interferon-b Enhanceosome', *Molecular Cell*, 1: 119-29.

Kim, Yujin, Hayoung Yang, Jeong-Ki Min, Young-Jun Park, Seung Hun Jeong, Sung-Wuk Jang, and Sungbo Shim. 2018. 'CCN3 secretion is regulated by palmitoylation via ZDHHC22', *Biochemical and Biophysical Research Communications*, 495: 2573-78.

Klemm, Juli D., Mark A. Rould, Rajeev Aurora, Winship Herr, and Carl O. Pabo. 1994. 'Crystal structure of the Oct-1 POU domain bound to an octamer site: DNA recognition with tethered DNA-binding modules', *Cell*, 77: 21-32.

Kramer, J. M., R. P. French, E. C. Park, and J. J. Johnson. 1990. 'The *Caenorhabditis elegans rol-6* gene, which interacts with the *sqt-1* collagen gene to determine organismal morphology, encodes a collagen', *Molecular and Cellular Biology*, 10: 2081-89.

Kulkarni, Meghana M., and David N. Arnosti. 2003. 'Information display by transcriptional enhancers', *Development*, 130: 6569.

Kuroyanagi, Hidehito, Tomomi Kimura, Kazuhiro Wada, Naoki Hisamoto, Kunihiro Matsumoto, and Masatoshi Hagiwara. 2000. 'SPK-1, a *C. elegans* SR protein kinase homologue, is essential for embryogenesis and required for germline development', *Mechanisms of Development*, 99: 51-64.

Lackner, Mark R., Rachel M. Kindt, Pamela M. Carroll, Katherine Brown, Michael R. Cancilla, Changyou Chen, Heshani de Silva, Yvonne Franke, Bo Guan, Tim Heuer, Tak Hung, Kevin Keegan, Jae Moon Lee, Veeraswamy Manne, Carol O'Brien, Dianne Parry, Juan J. Perez-Villar, Rajashekar K. Reddy, Hong Xiao, Hangjun Zhan, Mark Cockett, Greg Plowman, Kevin Fitzgerald, Michael Costa, and Petra Ross-Macdonald. 2005. 'Chemical genetics identifies Rab geranylgeranyl transferase as an apoptotic target of farnesyl transferase inhibitors', *Cancer Cell*, 7: 325-36.

Lai, Chun-Hung, Chang-Yuan Chou, Lan-Yang Ch'ang, Chung-Shyan Liu, and Wen-chang Lin. 2000. 'Identification of Novel Human Genes Evolutionarily Conserved in *Caenorhabditis elegans* by Comparative Proteomics', *Genome research*, 10: 703-13.

Lambie, E. J., and J. Kimble. 1991. 'Two homologous regulatory genes, *lin-12* and *glp-1*, have overlapping functions', *Development*, 112: 231.

Lanjuin, Anne, Julia Claggett, Mayumi Shibuya, Craig P. Hunter, and Piali Sengupta. 2006. 'Regulation of neuronal lineage decisions by the HES-related bHLH protein REF-1', *Developmental Biology*, 290: 139-51.

Lau, H. L., T. A. Timbers, R. Mahmoud, and C. H. Rankin. 2012. 'Genetic dissection of memory for associative and non-associative learning in *Caenorhabditis elegans*', *Genes, Brain and Behavior*, 12: 210-23.

LeBoeuf, Brigitte, Paola Correa, Changhoon Jee, and L. René García. 2014. 'Caenorhabditis elegans male sensory-motor neurons and dopaminergic support cells couple ejaculation and post-ejaculatory behaviors', *eLIFE*, 3: e02938.

Lee, Hyung-Kook, and Martha J. Lundell. 2007. 'Differentiation of the *Drosophila* serotonergic lineage depends on the regulation of *Zfh-1* by Notch and Eagle', *Molecular and cellular neurosciences*, 36: 47-58.

Lehner, Ben, Andrea Calixto, Catriona Crombie, Julia Tischler, Angelo Fortunato, Martin Chalfie, and Andrew G. Fraser. 2006. 'Loss of LIN-35, the *Caenorhabditis elegans* ortholog of the tumor suppressor p105Rb, results in enhanced RNA interference', *Genome Biology*, 7: R4.

Lelli, Katherine M., Matthew Slattery, and Richard S. Mann. 2012. 'Disentangling the Many Layers of Eukaryotic Transcriptional Regulation', *Annual Review of Genetics*, 46: 43-68.

Lenhard, Boris, Albin Sandelin, and Piero Carninci. 2012. 'Metazoan promoters: emerging characteristics and insights into transcriptional regulation', *Nature Reviews Genetics*, 13: 233.

Leung, Thomas H., Alexander Hoffmann, and David Baltimore. 2004. 'One Nucleotide in a kB Site Can Determine Cofactor Specificity for NF-kB Dimers', *Cell*, 118: 453-64.

Levine, Michael, and Robert Tjian. 2003. 'Transcription regulation and animal diversity', *Nature*, 424: 147.

Levine, Mike. 2010. 'Transcriptional Enhancers in Animal Development and Evolution', *Current Biology*, 20: R754-R63.

Levo, Michal, and Eran Segal. 2014. 'In pursuit of design principles of regulatory sequences', *Nature Reviews Genetics*, 15: 453.

Liberman, Louisa M., and Angelike Stathopoulos. 2009. 'Design flexibility in cis-regulatory control of gene expression: Synthetic and comparative evidence', *Developmental Biology*, 327: 578-89.

Lillesaar, Christina, Birgit Tannhäuser, Christian Stigloher, Elisabeth Kremmer, and Laure Bally-Cuif. 2007. 'The serotonergic phenotype is acquired by converging genetic mechanisms within the zebrafish central nervous system', *Developmental Dynamics*, 236: 1072-84.

Lints, Robyn, and D. H. Hall. 2009. 'Male introduction', *WormAtlas*.

Lloret-Fernández, Carla, Miren Maicas, Carlos Mora-Martínez, Alejandro Artacho, Angela Jimeno-Martín, Laura Chirivella, Peter Weinberg, and Nuria Flames. 2018. 'A combinatorial transcription factor signature defines the HSN serotonergic neuron regulatory landscape', *eLIFE*, 7: e32785.

Loer, C. M., and C. J. Kenyon. 1993. 'Serotonin-deficient mutants and male mating behavior in the nematode *Caenorhabditis elegans*', *The Journal of Neuroscience*, 13: 5407.

Löhr, Heiko, Soojin Ryu, and Wolfgang Driever. 2009. 'Zebrafish diencephalic A11-related dopaminergic neurons share a conserved transcriptional network with neuroendocrine cell lineages', *Development*, 136: 1007.

Long, Hannah K., Sara L. Prescott, and Joanna Wysocka. 2016. 'Ever-changing landscapes: transcriptional enhancers in development and evolution', *Cell*, 167: 1170-87.

Lundell, Martha J., Quynh Chu-LaGraff, Chris Q. Doe, and Jay Hirsh. 1996. 'The *engrailed* and *huckebein* Genes Are Essential for Development of Serotonin Neurons in the *Drosophila* CNS', *Molecular and Cellular Neuroscience*, 7: 46-61.

Luo, Guang Rui, Yi Chen, Xu Ping Li, Ting Xi Liu, and Wei Dong Le. 2008. '*Nr4a2* is essential for the differentiation of dopaminergic neurons during zebrafish embryogenesis', *Molecular and Cellular Neuroscience*, 39: 202-10.

Maduro, Morris F., Russell J. Hill, Paul J. Heid, Erin D. Newman-Smith, Jiangwen Zhu, James R. Priess, and Joel H. Rothman. 2005. 'Genetic redundancy in endoderm specification within the genus *Caenorhabditis*', *Developmental Biology*, 284: 509-22.

Maduro, Morris F., Marc D. Meneghini, Bruce Bowerman, Gina Broitman-Maduro, and Joel H. Rothman. 2001. 'Restriction of Mesendoderm to a Single Blastomere by the Combined Action of SKN-1 and a GSK-3b; Homolog Is Mediated by MED-1 and -2 in *C. elegans*', *Molecular Cell*, 7: 475-85.

Malin, Jennifer A., Maxime J. Kinet, Mary C. Abraham, Elyse S. Blum, and Shai Shaham. 2016. 'Transcriptional control of non-apoptotic developmental cell death in *C. elegans*', *Cell Death and Differentiation*, 23: 1985-94.

Masel, Joanna, and Mark L. Siegal. 2009. 'Robustness: mechanisms and consequences', *Trends in genetics : TIG*, 25: 395-403.

Masoudi, Neda, Saeed Tavazoie, Lori Glenwinkel, Leesun Ryu, Kyuhyung Kim, and Oliver Hobert. 2018. 'Unconventional function of an Achaete-Scute homolog as a terminal selector of nociceptive neuron identity', *PLOS Biology*, 16: e2004979.

Massari, Mark Eben, and Cornelis Murre. 2000. 'Helix-Loop-Helix Proteins: Regulators of Transcription in Eucaryotic Organisms', *Molecular and Cellular Biology*, 20: 429-40.

Matsui, Hideaki, and Atsushi Sugie. 2017. 'An optimized method for counting dopaminergic neurons in zebrafish', *PLOS ONE*, 12: e0184363.

Meijsing, Sebastiaan H., Miles A. Pufall, Alex Y. So, Darren L. Bates, Lin Chen, and Keith R. Yamamoto. 2009. 'DNA Binding Site Sequence Directs Glucocorticoid Receptor Structure and Activity', *Science (New York, N.Y.)*, 324: 407-10.

Mello, C. C., J. M. Kramer, D. Stinchcomb, and V. Ambros. 1991. 'Efficient gene transfer in *C. elegans*: extrachromosomal maintenance and integration of transforming sequences', *The EMBO Journal*, 10: 3959-70.

Mercer, Elinore M, Yin C Lin, Christopher Benner, Suchit Jhunjhunwala, Janusz Dutkowski, Martha Flores, Mikael Sigvardsson, Trey Ideker, Christopher K Glass, and Cornelis Murre. 2011. 'Multilineage Priming of Enhancer Repertoires Precedes Commitment to the B and Myeloid Cell Lineages in Hematopoietic Progenitors', *Immunity*, 35: 413-25.

Merika, Menie, Amy J. Williams, Guoying Chen, Tucker Collins, and Dimitris Thanos. 1998. 'Recruitment of CBP/p300 by the IFNb Enhanceosome Is Required for Synergistic Activation of Transcription', *Molecular Cell*, 1: 277-87.

Molin, L., A. Mounsey, S. Aslam, P. Bauer, J. Young, M. James, A. Sharma-Oates, and I. A. Hope. 2000. 'Evolutionary conservation of redundancy between a diverged pair of forkhead transcription factor homologues', *Development*, 127: 4825.

Mong, Jamie, Lia Panman, Zhanna Alekseenko, Nigel Kee, W. Stanton Lawrence, Johan Ericson, and Thomas Perlmann. 2013. 'Transcription Factor-Induced Lineage

Programming of Noradrenaline and Motor Neurons from Embryonic Stem Cells', *STEM CELLS*, 32: 609-22.

Montgomery, Mary K., SiQun Xu, and Andrew Fire. 1998. 'RNA as a target of double-stranded RNA-mediated genetic interference in *Caenorhabditis elegans*', *Proceedings of the National Academy of Sciences*, 95: 15502.

Moss, Eric G. 2007. 'Heterochronic Genes and the Nature of Developmental Time', *Current Biology*, 17: R425-R34.

Narasimhan, Kamesh, Samuel A. Lambert, Ally W. H. Yang, Jeremy Riddell, Sanie Mnaimneh, Hong Zheng, Mihai Albu, Hamed S. Najafabadi, John S. Reece-Hoyes, Juan I. Fuxman Bass, Albertha J. M. Walhout, Matthew T. Weirauch, and Timothy R. Hughes. 2015. "Mapping and analysis of *Caenorhabditis elegans* transcription factor sequence specificities." In *eLIFE*.

Neckameyer, W. S., C. M. Coleman, S. Eadie, and S. F. Goodwin. 2007. 'Compartmentalization of neuronal and peripheral serotonin synthesis in *Drosophila melanogaster*', *Genes, Brain and Behavior*, 6: 756-69.

Nefzger, Christian M., John M. Haynes, and Colin W. Pouton. 2011. 'Directed Expression of *Gata2*, *Mash1*, and *Foxa2* Synergize to Induce the Serotonergic Neuron Phenotype During In Vitro Differentiation of Embryonic Stem Cells', *STEM CELLS*, 29: 928-39.

Nishida, Yukuo, Takuma Sugi, Mayu Nonomura, and Ikue Mori. 2011. 'Identification of the AFD neuron as the site of action of the CREB protein in *Caenorhabditis elegans* thermotaxis', *EMBO reports*, 12: 855.

Niu, Wei, Zhi John Lu, Mei Zhong, Mihail Sarov, John I. Murray, Cathleen M. Brdlik, Judith Janette, Chao Chen, Pedro Alves, Elicia Preston, Cindie Slightham, Lixia Jiang, Anthony A. Hyman, Stuart K. Kim, Robert H. Waterston, Mark Gerstein, Michael Snyder, and Valerie Reinke. 2011. 'Diverse transcription factor binding features revealed by genome-wide ChIP-seq in *C. elegans*', *Genome research*, 21: 245-54.

Noble, Tallie, Jonathan Stieglitz, and Supriya Srinivasan. 2013. 'An Integrated Serotonin and Octopamine Neuronal Circuit Directs The Release of An Endocrine Signal to Control *C. elegans* Body Fat', *Cell metabolism*, 18: 10.1016/j.cmet.2013.09.007.

Otte, Christian, Stefan M. Gold, Brenda W. Penninx, Carmine M. Pariante, Amit Etkin, Maurizio Fava, David C. Mohr, and Alan F. Schatzberg. 2016. 'Major depressive disorder', *Nature Reviews Disease Primers*, 2: 16065.

Page, B. D., W. Zhang, K. Steward, T. Blumenthal, and J. R. Priess. 1997. 'ELT-1, a GATA-like transcription factor, is required for epidermal cell fates in *Caenorhabditis elegans* embryos', *Genes & Development*, 11: 1651-61.

Pak, Julia, Jay Mahesh Maniar, Cecilia Cabral Mello, and Andrew Fire. 2012. 'Protection from feed-forward amplification in an amplified RNAi mechanism', *Cell*, 151: 885-99.

Papantonis, Argyris, and Peter R. Cook. 2010. 'Genome architecture and the role of transcription', *Current Opinion in Cell Biology*, 22: 271-76.

Park, Seong Kyun, Vit Na Choi, and Byung Joon Hwang. 2013. 'LIN-12/Notch Regulates *lag-1* and *lin-12* Expression during Anchor Cell/Ventral Uterine Precursor Cell Fate Specification', *Molecules and Cells*, 35: 249-54.

Parraga, A., L. Bellsolell, A. R. Ferré-D'Amaré, and Stephen K. Burley. 1998. 'Co-crystal structure of sterol regulatory element binding protein 1a at 2.3 resolution', *Structure*, 6: 661-72.

Pattyn, A., X. Morin, H. Cremer, C. Goridis, and J. F. Brunet. 1997. 'Expression and interactions of the two closely related homeobox genes *Phox2a* and *Phox2b* during neurogenesis', *Development*, 124: 4065.

Pattyn, Alexandre, Nicolas Simplicio, J. Hikke van Doorninck, Christo Goridis, François Guillemot, and Jean-François Brunet. 2004. '*Ascl1/Mash1* is required for the development of central serotonergic neurons', *Nature neuroscience*, 7: 589.

Pavelec, Derek M., Jennifer Lachowiec, Thomas F. Duchaine, Harold E. Smith, and Scott Kennedy. 2009. 'Requirement for the ERI/DICER Complex in Endogenous RNA Interference and Sperm Development in *Caenorhabditis elegans*', *Genetics*, 183: 1283.

Pereira, Laura, Paschalis Kratsios, Esther Serrano-Saiz, Hila Sheftel, Avi E. Mayo, David H. Hall, John G. White, Brigitte LeBoeuf, L. Rene Garcia, Uri Alon, and Oliver Hobert. 2015. 'A cellular and regulatory map of the cholinergic nervous system of *C. elegans*', *eLIFE*, 4: e12432.

Pirri, Jennifer K., Adam D. McPherson, Jamie L. Donnelly, Michael M. Francis, and Mark J. Alkema. 2009. 'A Tyramine-Gated Chloride Channel Coordinates Distinct Motor Programs of a *Caenorhabditis elegans* Escape Response', *Neuron*, 62: 526-38.

Pocock, Roger, Julie Ahringer, Michael Mitsch, Sara Maxwell, and Alison Woollard. 2004. 'A regulatory network of T-box genes and the *even-skipped* homologue *vab-7* controls patterning and morphogenesis in *C. elegans*', *Development*, 131: 2373.

Poole, Richard J., Enkelejda Bashllari, Luisa Cochella, Eileen B. Flowers, and Oliver Hobert. 2011. 'A Genome-Wide RNAi Screen for Factors Involved in Neuronal Specification in *Caenorhabditis elegans*', *PLOS Genetics*, 7: e1002109.

Portman, D. S., and S. W. Emmons. 2000. 'The basic helix-loop-helix transcription factors LIN-32 and HLH-2 function together in multiple steps of a *C. elegans* neuronal sublineage', *Development*, 127: 5415.

Portman, Douglas S. 2007. 'Genetic Control of Sex Differences in *C. elegans* Neurobiology and Behavior.' in, *Advances in Genetics* (Academic Press).

———. 2017. 'Sexual modulation of sex-shared neurons and circuits in *C. elegans*', *Journal of neuroscience research*, 95: 527-38.

Potts, Malia B., David P. Wang, and Scott Cameron. 2009. 'Trithorax, Hox, and TALE-class homeodomain proteins ensure cell survival through repression of the BH3-only gene *egl-1*', *Developmental Biology*, 329: 374-85.

Qiao, L., J. L. Lissemore, P. Shu, A. Smardon, M. B. Gelber, and E. M. Maine. 1995. 'Enhancers of *glp-1,* a gene required for cell-signaling in *Caenorhabditis elegans*, define a set of genes required for germline development', *Genetics*, 141: 551.

Qu, Qiuhao, Guoqiang Sun, Wenwu Li, Su Yang, Peng Ye, Chunnian Zhao, Ruth T. Yu, Fred H. Gage, Ronald M. Evans, and Yanhong Shi. 2010. 'Orphan nuclear receptor TLX activates Wnt/β-catenin signalling to stimulate neural stem cell proliferation and self-renewal', *Nature cell biology*, 12: 31-9.

Qu, Wubin, Changhong Ren, Yuan Li, Jinping Shi, Jiye Zhang, Xiaolei Wang, Xingyi Hang, Yiming Lu, Dongsheng Zhao, and Chenggang Zhang. 2011. 'Reliability analysis of

the Ahringer *Caenorhabditis elegans* RNAi feeding library: a guide for genome-wide screens', *BMC Genomics*, 12: 170-70.

Quintin, Sophie, Grégoire Michaux, Laura McMahon, Anne Gansmuller, and Michel Labouesse. 2001. 'The *Caenorhabditis elegans* Gene *lin-26* Can Trigger Epithelial Differentiation without Conferring Tissue Specificity', *Developmental Biology*, 235: 410-21.

Razin, S. V., V. V. Borunova, O. G. Maksimenko, and O. L. Kantidze. 2012. 'Cys2His2 zinc finger protein family: Classification, functions, and major members', *Biochemistry (Moscow)*, 77: 217-26.

Razin, S. V., A. A. Gavrilov, A. Pichugin, M. Lipinski, O. V. Iarovaia, and Yegor S. Vassetzky. 2011. 'Transcription factories in the context of the nuclear and genome organization', *Nucleic Acids Research*, 39: 9085-92.

Reece-Hoyes, John S., Bart Deplancke, Jane Shingles, Christian A. Grove, Ian A. Hope, and Albertha J. M. Walhout. 2005. 'A compendium of *Caenhorabditis elegans* regulatory transcription factors: a resource for mapping transcription regulatory networks', *Genome Biology*, 6: R110-R10.

Rezával, Carolina, Tetsuya Nojima, Megan C Neville, Andrew C Lin, and Stephen F Goodwin. 2014. 'Sexually Dimorphic Octopaminergic Neurons Modulate Female Postmating Behaviors in *Drosophila*', *Current Biology*, 24: 725-30.

Rezsohazy, René, Andrew J. Saurin, Corinne Maurel-Zaffran, and Yacine Graba. 2015. 'Cellular and molecular insights into Hox protein action', *Development*, 142: 1212.

Richmond, Janet E., Warren S. Davis, and Erik M. Jorgensen. 1999. 'UNC-13 is required for synaptic vesicle fusion in *C. elegans*', *Nature neuroscience*, 2: 959-64.

Rieder, Dietmar, Zlatko Trajanoski, and James G. McNally. 2012. 'Transcription factories', *Frontiers in Genetics*, 3: 221.

Rodríguez-Martínez, José A., Aaron W. Reinke, Devesh Bhimsaria, Amy E. Keating, and Aseem Z. Ansari. 2017. 'Combinatorial bZIP dimers display complex DNA-binding specificity landscapes', *eLIFE*, 6: e19272.

Roeder, Thomas. 2003. 'Metabotropic histamine receptors—nothing for invertebrates?', *European Journal of Pharmacology*, 466: 85-90.

———. 2005. 'Tyramine and Octopamine: Ruling Behavior and Metabolism', *Annual Review of Entomology*, 50: 447-77.

Rual, Jean-François, Julian Ceron, John Koreth, Tong Hao, Anne-Sophie Nicot, Tomoko Hirozane-Kishikawa, Jean Vandenhaute, Stuart H. Orkin, David E. Hill, Sander van den Heuvel, and Marc Vidal. 2004. 'Toward Improving *Caenorhabditis elegans* Phenome Mapping With an ORFeome-Based RNAi Library', *Genome research*, 14: 2162-68.

Ryu, Soojin, Julia Mahler, Dario Acampora, Jochen Holzschuh, Simone Erhardt, Daniela Omodei, Antonio Simeone, and Wolfgang Driever. 2007. 'Orthopedia Homeodomain Protein Is Essential for Diencephalic Dopaminergic Neuron Development', *Current Biology*, 17: 873-80.

Sarin, Sumeet, Celia Antonio, Baris Tursun, and Oliver Hobert. 2009. 'The *C. elegans* Tailless/TLX transcription factor *nhr-67* controls neuronal identity and left/right asymmetric fate diversification', *Development*, 136: 2933.

Sarov, Mihail, Susan Schneider, Andrei Pozniakovski, Assen Roguev, Susanne Ernst, Youming Zhang, A. Anthony Hyman, and A. Francis Stewart. 2006. 'A recombineering pipeline for functional genomics applied to *Caenorhabditis elegans*', *Nature Methods*, 3: 839.

Sarthy, P. Vijay. 1991. 'Histamine: A Neurotransmitter Candidate for *Drosophila* Photoreceptors', *Journal of Neurochemistry*, 57: 1757-68.

Sawin, Elizabeth R., Rajesh Ranganathan, and H. Robert Horvitz. 2000. '*C. elegans* Locomotory Rate Is Modulated by the Environment through a Dopaminergic Pathway and by Experience through a Serotonergic Pathway', *Neuron*, 26: 619-31.

Schindelman, Gary, Jolene S. Fernandes, Carol A. Bastiani, Karen Yook, and Paul W. Sternberg. 2011. 'Worm Phenotype Ontology: Integrating phenotype data within and beyond the *C. elegans* community', *BMC Bioinformatics*, 12: 32.

Schmidt, Mirko, Shengyin Lin, Manuela Pape, Uwe Ernsberger, Matthias Stanke, Kazuto Kobayashi, Marthe J. Howard, and Hermann Rohrer. 2009. 'The bHLH transcription factor *Hand2* is essential for the maintenance of noradrenergic properties in differentiated sympathetic neurons', *Developmental Biology*, 329: 191-200.

Schmitz, Caroline, Parag Kinge, and Harald Hutter. 2007. 'Axon guidance genes identified in a large-scale RNAi screen using the RNAi-hypersensitive *Caenorhabditis elegans* strain *nre-1(hd20) lin-15b(hd126)*', *Proceedings of the National Academy of Sciences of the United States of America*, 104: 834-39.

Sengupta, Piali, and I. Bargmann Cornelia. 1998. 'Cell fate specification and differentiation in the nervous system of *Caenorhabditis elegans*', *Developmental Genetics*, 18: 73-80.

Serrano-Saiz, Esther, Richard J Poole, Terry Felton, Feifan Zhang, Estanisla Daniel De La Cruz, and Oliver Hobert. 2013. 'Modular Control of Glutamatergic Neuronal Identity in *C. elegans* by Distinct Homeodomain Proteins', *Cell*, 155: 659-73.

Shan, Ge, Kyuhyung Kim, Chris Li, and W. W. Walthall. 2005. 'Convergent genetic programs regulate similarities and differences between related motor neuron classes in *Caenorhabditis elegans*', *Developmental Biology*, 280: 494-503.

Shlyueva, Daria, Gerald Stampfel, and Alexander Stark. 2014. 'Transcriptional enhancers: from properties to genome-wide predictions', *Nature Reviews Genetics*, 15: 272.

Siggers, Trevor, and Raluca Gordân. 2014. 'Protein–DNA binding: complexities and multi-protein codes', *Nucleic Acids Research*, 42: 2099-111.

Sijen, Titia, Jamie Fleenor, Femke Simmer, Karen L. Thijssen, Susan Parrish, Lisa Timmons, Ronald H. A. Plasterk, and Andrew Fire. 2001. 'On the Role of RNA Amplification in dsRNA-Triggered Gene Silencing', *Cell*, 107: 465-76.

Simmer, Femke, Celine Moorman, Alexander M. van der Linden, Ewart Kuijk, Peter V. E. van den Berghe, Ravi S. Kamath, Andrew G. Fraser, Julie Ahringer, and Ronald H. A. Plasterk. 2003. 'Genome-Wide RNAi of *C. elegans* Using the Hypersensitive *rrf-3* Strain Reveals Novel Gene Functions', *PLOS Biology*, 1: e12.

Simmer, Femke, Marcel Tijsterman, Susan Parrish, Sandhya P. Koushika, Michael L. Nonet, Andrew Fire, Julie Ahringer, and Ronald H. A. Plasterk. 2002. 'Loss of the Putative RNA-Directed RNA Polymerase RRF-3 Makes *C.elegans* Hypersensitive to RNAi', *Current Biology*, 12: 1317-19.

Simon Horst, H., Lavinia Bhatt, Daniel Gherbassi, Paola SgadÓ, and Lavinia AlberÍ. 2006. 'Midbrain Dopaminergic Neurons', *Annals of the New York Academy of Sciences*, 991: 36-47.

Singhvi, Aakanksha, C. Andrew Frank, and Gian Garriga. 2008. 'The T-Box Gene *tbx-2*, the Homeobox Gene *egl-5* and the Asymmetric Cell Division Gene *ham-1* Specify Neural Fate in the HSN/PHB Lineage', *Genetics*, 179: 887-98.

Sinha, Amit, and Robbie Rae. 2016. 'Genome-Wide RNAi Screens in *C. elegans* to Identify Genes Influencing Lifespan and Innate Immunity.' in David O. Azorsa and Shilpi Arora (eds.), *High-Throughput RNAi Screening: Methods and Protocols* (Springer New York: New York, NY).

Smidt, Marten P., Simone M. Smits, and J. Peter H. Burbach. 2003. 'Molecular mechanisms underlying midbrain dopamine neuron development and function', *European Journal of Pharmacology*, 480: 75-88.

Song, Bo-mi, and Leon Avery. 2012. 'Serotonin Activates Overall Feeding by Activating Two Separate Neural Pathways in *Caenorhabditis elegans*', *The Journal of Neuroscience*, 32: 1920.

Spitz, Francois, and Denis Duboule. 2008. 'Chapter 6 Global Control Regions and Regulatory Landscapes in Vertebrate Development and Evolution.' in, *Advances in Genetics* (Academic Press).

Spitz, François, and Eileen E. M. Furlong. 2012. 'Transcription factors: from enhancer binding to developmental control', *Nature Reviews Genetics*, 13: 613.

Spitz, François, Federico Gonzalez, and Denis Duboule. 2003. 'A Global Control Region Defines a Chromosomal Regulatory Landscape Containing the *HoxD* Cluster', *Cell*, 113: 405-17.

Stefanakis, Nikolaos, Ines Carrera, and Oliver Hobert. 2015. 'Regulatory logic of pan-neuronal gene expression in *C. elegans*', *Neuron*, 87: 733-50.

Sugimoto, Asako. 2004. 'High-throughput RNAi in *Caenorhabditis elegans*: genome-wide screens and functional genomics', *Differentiation*, 72: 81-91.

Sulston, J., M. Dew, and S. Brenner. 1975. 'Dopaminergic neurons in the nematode *Caenorhabditis elegans*', *Journal of Comparative Neurology*, 163: 215-26.

Sulston, J. E., and H. R. Horvitz. 1977. 'Post-embryonic cell lineages of the nematode *Caenorhabditis elegans*', *Developmental Biology*, 56: 110-56.

Sulston, J. E., E. Schierenberg, J. G. White, and J. N. Thomson. 1983. 'The embryonic cell lineage of the nematode *Caenorhabditis elegans*', *Developmental Biology*, 100: 64-119.

Sulston, John E., and H. Robert Horvitz. 1981. 'Abnormal cell lineages in mutants of the nematode *Caenorhabditis elegans*', *Developmental Biology*, 82: 41-55.

Suo, Satoshi, Joseph G. Culotti, and Hubert H. M. Van Tol. 2009. 'Dopamine counteracts octopamine signalling in a neural circuit mediating food response in *C. elegans*', *The EMBO Journal*, 28: 2437-48.

Suo, Satoshi, and Shoichi Ishiura. 2013. 'Dopamine Modulates Acetylcholine Release via Octopamine and CREB Signaling in *Caenorhabditis elegans*', *PLOS ONE*, 8: e72578.

Swierczek, Nicholas A., Andrew C. Giles, Catharine H. Rankin, and Rex A. Kerr. 2011. 'High-throughput behavioral analysis in *C. elegans*', *Nature Methods*, 8: 592.

Swoboda, Peter, Haskell T. Adler, and James H. Thomas. 2000. 'The RFX-Type Transcription Factor DAF-19 Regulates Sensory Neuron Cilium Formation in *C. elegans*', *Molecular Cell*, 5: 411-21.

Sze, Ji Ying, Martin Victor, Curtis Loer, Yang Shi, and Gary Ruvkun. 2000. 'Food and metabolic signalling defects in a *Caenorhabditis elegans* serotonin-synthesis mutant', *Nature*, 403: 560.

Sze, Ji Ying, Shenyuan Zhang, Jie Li, and Gary Ruvkun. 2002. 'The *C. elegans* POU-domain transcription factor UNC-86 regulates the *tph-1* tryptophan hydroxylase gene and neurite outgrowth in specific serotonergic neurons', *Development*, 129: 3901.

Tabara, Hiroaki, Alla Grishok, and Craig C. Mello. 1998. 'RNAi in *C. elegans* Soaking in the Genome Sequence', *Science (New York, N.Y.)*, 282: 430.

Tavella, Davide, Laura M. Deveau, Troy W. Whitfield, and Francesca Massi. 2016. 'Structural basis of the disorder in the tandem zinc finger domain of the RNA-binding protein Tristetraprolin', *Journal of chemical theory and computation*, 12: 4717-25.

Tavernarakis, Nektarios, Shi L. Wang, Maxim Dorovkov, Alexey Ryazanov, and Monica Driscoll. 2000. 'Heritable and inducible genetic interference by double-stranded RNA encoded by transgenes', *Nature genetics*, 24: 180.

Taylor, W. Robert, Yi-Wen Hsieh, T. Joshua Gamse, and Chiou-Fen Chuang. 2010. 'Making a difference together: reciprocal interactions in

C. elegans and zebrafish asymmetric neural development', *Development*, 137: 681-91.

Tepper, Ronald G, Jasmine Ashraf, Rachel Kaletsky, Gunnar Kleemann, Coleen T Murphy, and Harmen J Bussemaker. 2013. 'PQM-1 Complements DAF-16 as a Key Transcriptional Regulator of DAF-2-Mediated Development and Longevity', *Cell*, 154: 676-90.

Thivierge, Caroline, Neetha Makil, Mathieu Flamand, Jessica J. Vasale, Craig C. Mello, James Wohlschlegel, Darryl Conte Jr, and Thomas F. Duchaine. 2012. 'Tudor domain ERI-5 tethers an RNA-dependent RNA polymerase to DCR-1 to potentiate endo-RNAi', *Nature Structural &Amp; Molecular Biology*, 19: 90.

Thompson, Kenneth W., Pradeep Joshi, Jessica S. Dymond, Lakshmi Gorrepati, Harold Smith, Michael Krause, and David M. Eisenmann. 2016. 'The Paired-box protein PAX-3 regulates the choice between lateral and ventral epidermal cell fates in *C. elegans*', *Developmental Biology*, 412: 191-207.

Thor, Stefan, and John B. Thomas. 1997. 'The *Drosophila Islet* Gene Governs Axon Pathfinding and Neurotransmitter Identity', *Neuron*, 18: 397-409.

Tian, Chenxi, Herong Shi, Clark Colledge, Michael Stern, Robert Waterston, and Jun Liu. 2011. 'The *C. elegans* SoxC protein SEM-2 opposes differentiation factors to promote a proliferative blast cell fate in the postembryonic mesoderm', *Development*, 138: 1033.

Tian, Lin, S. Andrew Hires, Tianyi Mao, Daniel Huber, M. Eugenia Chiappe, Sreekanth H. Chalasani, Leopoldo Petreanu, Jasper Akerboom, Sean A. McKinney, Eric R. Schreiter, Cornelia I. Bargmann, Vivek Jayaraman, Karel Svoboda, and Loren L. Looger. 2009. 'Imaging neural activity in worms, flies and mice with improved GCaMP calcium indicators', *Nature Methods*, 6: 875.

Timbers, Tiffany A., and Catharine H. Rankin. 2011. 'Tap withdrawal circuit interneurons require CREB for long-term habituation in *Caenorhabditis elegans*', *Behavioral Neuroscience*, 125: 560-66.

Timmons, Lisa, Donald L. Court, and Andrew Fire. 2001. 'Ingestion of bacterially expressed dsRNAs can produce specific and potent genetic interference in *Caenorhabditis elegans*', *Gene*, 263: 103-12.

Topalidou, Irini, and Martin Chalfie. 2011. 'Shared gene expression in distinct neurons expressing common selector genes', *Proceedings of the National Academy of Sciences*, 108: 19258.

Tsialikas, Jennifer, Mitchell A. Romens, Allison Abbott, and Eric G. Moss. 2017. 'Stage-Specific Timing of the microRNA Regulation of *lin-28* by the Heterochronic Gene l*in-14* in *Caenorhabditis elegans*', *Genetics*, 205: 251.

Turlejski, Krzysztof 1996. 'Evolutionary ancient roles of serotonin: long-lasting regulation of activity and development', *Acta Neurobiol. Exp.*, 56: 619-36.

Ueno, Shunsuke, Kiichi Yasutake, Daisuke Tohyama, Tsutomu Fujimori, Dai Ayusawa, and Michihiko Fujii. 2012. 'Systematic screen for genes involved in the regulation of oxidative stress in the nematode *Caenorhabditis elegans*', *Biochemical and Biophysical Research Communications*, 420: 552-57.

Urbán, Noelia, Debbie L. C. van den Berg, Antoine Forget, Jimena Andersen, Jeroen A. A. Demmers, Charles Hunt, Olivier Ayrault, and François Guillemot. 2016. 'Return to quiescence of mouse neural stem cells by degradation of a proactivation protein', *Science (New York, N.Y.)*, 353: 292.

Van Auken, Kimberly, Daniel Weaver, Barbara Robertson, Meera Sundaram, Tassa Saldi, Lois Edgar, Ulrich Elling, Monica Lee, Queta Boese, and William B. Wood. 2002. 'Roles of the Homothorax/Meis/Prep homolog UNC-62 and the Exd/Pbx homologs CEH-20 and CEH-40 in *C. elegans* embryogenesis', *Development*, 129: 5255.

van der Linden, Alexander M., Katherine M. Nolan, and Piali Sengupta. 2007. 'KIN-29 SIK regulates chemoreceptor gene expression via an MEF2 transcription factor and a class II HDAC', *The EMBO Journal*, 26: 358-70.

Vierbuchen, Thomas, Austin Ostermeier, Zhiping P. Pang, Yuko Kokubu, Thomas C. Südhof, and Marius Wernig. 2010. 'Direct conversion of fibroblasts to functional neurons by defined factors', *Nature*, 463: 1035.

Vincentz, Joshua W., Nathan J. VanDusen, Andrew B. Fleming, Michael Rubart, Beth A. Firulli, Marthe J. Howard, and Anthony B. Firulli. 2012. 'A *Phox2*- and *Hand2*-dependent *Hand1 cis*-regulatory element reveals a unique gene dosage requirement for *Hand2* during sympathetic neurogenesis', *The Journal of Neuroscience*, 32: 2110-20.

Voglis, Giannis, and Nektarios Tavernarakis. 2008. 'A synaptic DEG/ENaC ion channel mediates learning in *C. elegans* by facilitating dopamine signalling', *The EMBO Journal*, 27: 3288-99.

Vömel, Matthias, and Christian Wegener. 2008. 'Neuroarchitecture of Aminergic Systems in the Larval Ventral Ganglion of *Drosophila melanogaster*', *PLOS ONE*, 3: e1848.

Von Stetina, Stephen E., Rebecca M. Fox, Kathie L. Watkins, Todd A. Starich, Jocelyn E. Shaw, and David M. Miller. 2007. 'UNC-4 represses CEH-12/HB9 to specify

synaptic inputs to VA motor neurons in *C. elegans*', *Genes & Development*, 21: 332-46.
Walthall, W. W., and J. A. Plunkett. 1995. 'Genetic transformation of the synaptic pattern of a motoneuron class in *Caenorhabditis elegans*', *The Journal of Neuroscience*, 15: 1035.
Wang, Duo, Scott Kennedy, Darryl Conte Jr, John K. Kim, Harrison W. Gabel, Ravi S. Kamath, Craig C. Mello, and Gary Ruvkun. 2005. 'Somatic misexpression of germline P granules and enhanced RNA interference in retinoblastoma pathway mutants', *Nature*, 436: 593.
Wang, Fushun, and Alfredo Pereira. 2016. 'Neuromodulation, Emotional Feelings and Affective Disorders', *Mens Sana Monographs*, 14: 5-29.
Watanabe, Kiichi, Hui Chiu, Barret D. Pfeiffer, Allan M. Wong, Eric D. Hoopfer, Gerald M. Rubin, and David J. Anderson. 2017. 'A Circuit Node that Integrates Convergent Input from Neuromodulatory and Social Behavior-Promoting Neurons to Control Aggression in *Drosophila*', *Neuron*, 95: 1112-28.e7.
Webster, Christopher M., Elizabeth C. Pino, Christopher E. Carr, Lianfeng Wu, Ben Zhou, Lucydalila Cedillo, Michael C. Kacergis, Sean P. Curran, and Alexander A. Soukas. 2017. 'Genome-wide RNAi Screen for Fat Regulatory Genes in *C. elegans* Identifies a Proteostasis-AMPK Axis Critical for Starvation Survival', *Cell Reports*, 20: 627-40.
Weirauch, Matthew T, Ally Yang, Mihai Albu, Atina G. Cote, Alejandro Montenegro-Montero, Philipp Drewe, Hamed S Najafabadi, Samuel A Lambert, Ishminder Mann, Kate Cook, Hong Zheng, Alejandra Goity, Harm van Bakel, Jean-Claude Lozano, Mary Galli, Mathew G. Lewsey, Eryong Huang, Tuhin Mukherjee, Xiaoting Chen, John S Reece-Hoyes, Sridhar Govindarajan, Gad Shaulsky, Albertha J M. Walhout, François-Yves Bouget, Gunnar Ratsch, Luis F Larrondo, Joseph R Ecker, and Timothy R Hughes. 2014. 'Determination and Inference of Eukaryotic Transcription Factor Sequence Specificity', *Cell*, 158: 1431-43.
Wenzel, Dirk, Francesca Palladino, and Monika Jedrusik-Bode. 2011. 'Epigenetics in *C. elegans*: Facts and challenges', *genesis*, 49: 647-61.
White, J. G., Eileen Southgate, J. N. Thomson, and Sydney Brenner. 1986. 'The structure of the nervous system of the nematode *Caenorhabditis elegans*', *Philosophical Transactions of the Royal Society of London. B, Biological Sciences*, 314: 1.
Wilczyński, Bartek, and Eileen E. M. Furlong. 2010. 'Dynamic CRM occupancy reflects a temporal map of developmental progression', *Molecular Systems Biology*, 6.
Willis, Gregory L. 1987. 'Amine accumulation in Parkinson's disease and other disorders', *Neuroscience & Biobehavioral Reviews*, 11: 97-105.
Wingender, Edgar, Torsten Schoeps, and Jürgen Dönitz. 2013. 'TFClass: an expandable hierarchical classification of human transcription factors', *Nucleic Acids Research*, 41: D165-D70.
Winston, William M., Christina Molodowitch, and Craig P. Hunter. 2002. 'Systemic RNAi in *C. elegans* Requires the Putative Transmembrane Protein SID-1', *Science (New York, N.Y.)*, 295: 2456.
Wolberger, Cynthia. 1999. 'Multiprotein-DNA complexes in transcriptional regulation', *Annual Review of Biophysics and Biomolecular Structure*, 28: 29-56.

Wragg, Rachel T., Vera Hapiak, Sarah B. Miller, Gareth P. Harris, John Gray, Patricia R. Komuniecki, and Richard W. Komuniecki. 2007. 'Tyramine and Octopamine Independently Inhibit Serotonin-Stimulated Aversive Behaviors in *Caenorhabditis elegans* through Two Novel Amine Receptors', *The Journal of Neuroscience*, 27: 13402.

Wrischnik, L. A., and C. J. Kenyon. 1997. 'The role of *lin-22*, a *hairy/enhancer of split* homolog, in patterning the peripheral nervous system of *C. elegans*', *Development*, 124: 2875.

Wullimann, Mario F., and Elke Rink. 2002. 'The teleostean forebrain: a comparative and developmental view based on early proliferation, *Pax6* activity and catecholaminergic organization', *Brain Research Bulletin*, 57: 363-70.

Xie, Yusu, Mustapha Moussaif, Sunju Choi, Lu Xu, and Ji Ying Sze. 2013. 'RFX Transcription Factor DAF-19 Regulates 5-HT and Innate Immune Responses to Pathogenic Bacteria in *Caenorhabditis elegans*', *PLOS Genetics*, 9: e1003324.

Xu, Wu, Lawryn H Kasper, Stephanie Lerach, Trushar Jeevan, and Paul K Brindle. 2007. 'Individual CREB-target genes dictate usage of distinct cAMP-responsive coactivation mechanisms', *The EMBO Journal*, 26: 2890-903.

Yanase, Sumino, Hitoshi Suda, Kayo Yasuda, and Naoaki Ishii. 2017. 'Impaired p53/CEP-1 is associated with lifespan extension through an age-related imbalance in the energy metabolism of *C. elegans*', *Genes to Cells*, 22: 1004-10.

Yang, Jichen, and Stephen A. Ramsey. 2015. 'A DNA shape-based regulatory score improves position-weight matrix-based recognition of transcription factor binding sites', *Bioinformatics*, 31: 3445-50.

Yáñez-Cuna, J. Omar, Evgeny Z. Kvon, and Alexander Stark. 2013. 'Deciphering the transcriptional *cis*-regulatory code', *Trends in Genetics*, 29: 11-22.

Zacharias, Amanda L., Travis Walton, Elicia Preston, and John Isaac Murray. 2015. 'Quantitative Differences in Nuclear β-catenin and TCF Pattern Embryonic Cells in *C. elegans*', *PLOS Genetics*, 11: e1005585.

Zaret, Kenneth S., and Jason S. Carroll. 2011. 'Pioneer transcription factors: establishing competence for gene expression', *Genes & Development*, 25: 2227-41.

Zhang, Feifan, Abhishek Bhattacharya, Jessica C. Nelson, Namiko Abe, Patricia Gordon, Carla Lloret-Fernandez, Miren Maicas, Nuria Flames, Richard S. Mann, Daniel A. Colón-Ramos, and Oliver Hobert. 2014. 'The LIM and POU homeobox genes *ttx-3* and *unc-86* act as terminal selectors in distinct cholinergic and serotonergic neuron types', *Development*, 141: 422.

Zhang, Jingyan, Xia Li, Angela R. Jevince, Liying Guan, Jiaming Wang, David H. Hall, Xun Huang, and Mei Ding. 2013. 'Neuronal Target Identification Requires AHA-1-Mediated Fine-Tuning of Wnt Signaling in *C. elegans*', *PLOS Genetics*, 9: e1003618.

Zheng, Chaogu, Felix Qiaochu Jin, and Martin Chalfie. 2015. 'Hox Proteins Act as Transcriptional Guarantors to Ensure Terminal Differentiation', *Cell Reports*, 13: 1343-52.

Zheng, Chaogu, Siavash Karimzadegan, Victor Chiang, and Martin Chalfie. 2013. 'Histone Methylation Restrains the Expression of Subtype-Specific Genes during Terminal Neuronal Differentiation in *Caenorhabditis elegans*', *PLOS Genetics*, 9: e1004017.

Zheng, Xianwu, Shinjae Chung, Takahiro Tanabe, and Ji Ying Sze. 2005. 'Cell-type specific regulation of serotonergic identity by the *C.elegans* LIM-homeodomain factor LIM-4', *Developmental Biology*, 286: 618-28.

Zhou, Xing, Fang Liu, Miao Tian, Zhejun Xu, Qifei Liang, Chunyang Wang, Jiwen Li, Zhidong Liu, Ke Tang, Miao He, and Zhengang Yang. 2015. 'Transcription factors COUP-TFI and COUP-TFII are required for the production of granule cells in the mouse olfactory bulb', *Development*, 142: 1593.

Zhuang, Jimmy J., and Craig P. Hunter. 2011. 'Tissue Specificity of *Caenorhabditis elegans* Enhanced RNA Interference Mutants', *Genetics*, 188: 235-37.

RESUMEN

(CASTELLANO)

RESUMEN

Introducción

La adquisición de la identidad celular a lo largo del desarrollo embrionario ha sido uno de los temas de interés para los científicos en las últimas décadas. Durante el proceso de diferenciación, las células comienzan a expresar marcadores específicos de su identidad final. Para conseguir tal objetivo, se selecciona un perfil transcripcional que dota a la célula de sus características diferenciadoras.

La expresión de dichos genes característicos de la identidad celular, denominados genes efectores (Hobert 2016a) es controlada por factores de transcripción (FT) que se unen a las secuencias reguladoras del ADN, promotores y potenciadores (*enhancers*). Ahora bien, los factores de transcripción son pleiotrópicos, es decir, se expresan en múltiples tipos celulares, de modo que es la combinación de distintos FT lo que otorga la especificidad a la regulación transcripcional en cada tipo celular.

Los FT presentan una región, en la conformación estructural de la proteína, con la que se unen al ADN para ejercer su función reguladora, denominada dominio de unión al ADN. En función de estos dominios, se unen a unos motivos, o secuencias del ADN, con mayor probabilidad. Esta característica conduce a agrupar los FT en familias en función de sus dominios de unión. En humanos se han descrito 111 familias de FT, mientras que en *C. elegans* hay 48 (Narasimhan et al. 2015).

Como se ha mencionado, la combinación de FT es necesaria para conseguir la especificidad de cada programa transcripcional, por lo que los FT habitualmente interaccionan de cara a su unión a las secuencias reguladoras. Esto da lugar a fenómenos de cooperación entre dos factores para promover la unión de ambos; o bien, puede ser la unión de dos factores lo que promueva el reclutamiento de un tercero o cofactor, que se una a ellos formando un complejo más estable, de modo que finalmente den lugar a una sinergia en la expresión del gen. Por otra parte, la unión entre factores puede provocar cambios conformacionales en alguna de las proteínas y, así, que se altere la especificidad de unión del factor al ADN, en un fenómeno de alosterismo.

Teniendo en cuenta todos estos mecanismos, se han propuesto distintos modelos para explicar la ocupación de las secuencias reguladoras por parte de los FT. Dichos modelos se basan en la presencia, constante o cambiante, de motivos de unión para el grupo de FT; además tienen en cuenta si los factores se unen exclusivamente al ADN o si alguno de los miembros del grupo puede interaccionar también con el resto de FT. Uno de los modelos del que se encuentran varios ejemplos en la naturaleza consiste en que un mismo grupo de FT forma un colectivo encargado de regular los genes efectores pero

cuya unión para promover la expresión de cada gen es variable, dependiendo de los motivos presentes y de cómo interaccionen entre sí los FT (Doitsidou et al. 2013; Lloret-Fernández et al. 2018).

Aunque los FT son esenciales en la regulación transcripcional, hay otros elementos que contribuyen a la expresión génica, como el estado de la cromatina, las marcas epigenéticas, así como la organización tridimensional del genoma. Todo ello aporta capas de complejidad en la regulación que, al mismo tiempo, también intervienen y afinan la ejecución de los programas reguladores.

Uno de los tejidos donde la identidad celular es especialmente variada es en el sistema nervioso. En este tejido se encuentra una gran variedad tanto estructural como funcional de tipos neuronales, además de células de soporte. Por ejemplo, en el nematodo *C. elegans*, hay 302 neuronas en su forma hermafrodita, las cuales se pueden agrupar en 118 categorías diferentes. En este tejido se ha llevado a cabo una amplia labor para estudiar los FT que dirigen los programas de determinación de la identidad neuronal. Más concretamente, ha dado lugar a acuñar el término de selectores terminales (Hobert 2011, 2008) para aquellos FT cuya combinación regula la expresión de los genes efectores que caracterizan la madurez de la célula.

En el caso de las neuronas, de entre los genes efectores podemos encontrar aquellos encargados en la síntesis, empaquetamiento, liberación y recaptación del neurotransmisor, además de canales iónicos, receptores y transportadores cuya correcta expresión es uno de los rasgos de la madurez funcional de las neuronas.

El estudio de los programas reguladores tradicionalmente ha seguido una perspectiva en la que se estudiaba el papel de un elemento concreto de la red de regulación y todos aquellos procesos en los que participaba. Sin embargo, el uso de otros modelos animales como el nematodo *Caenorhabditis elegans* permite una perspectiva diferente mediante la que abordar el estudio directamente sobre un elevado número de genes.

Los estudios con este modelo comenzaron en los años sesenta por Sydney Brenner, que, junto con Jonh Sulston, realizaron un análisis exhaustivo de mutantes para cientos de genes y describieron el linaje completo de todas las células de *C. elegans*. El fácil mantenimiento en el laboratorio y el corto ciclo de vida de este nematodo, que alcanza la madurez en tres días, afianzaron su uso como modelo experimental. *C. elegans* se reproduce mediante la puesta de huevos que, una vez eclosionan, se desarrollan a través de cuatro estadios larvarios hasta alcanzar la madurez. En esta especie nos encontramos con dos formas, hermafroditas en su mayoría y un pequeño porcentaje de machos que facilitan el intercambio genético (Brenner 1974).

Debido a estas características, *C. elegans* permite llevar a cabo protocolos de cribado masivo de genes mediante los que abordar el estudio de cientos de secuencias para identificar las que intervienen en un proceso de interés. Tradicionalmente estos procesos de cribado se basaban en el uso de un agente mutágeno, como el EMS (etilmetanosulfonato) para posteriormente aislar aquellos genes donde la mutación había producido un fenotipo de interés. Sin embargo, en este tipo de cribado, la mutación de los genes no era dirigida, lo que suponía posteriormente un largo período de aislamiento e identificación. No obstante, con la aplicación de la técnica de ARN de interferencia (ARNi), los procesos de cribado adquirieron un matiz direccional.

El fundamento del ARN de interferencia se basa la respuesta de la célula cuando detecta la presencia de moléculas de ARN doble cadena (ARNdc), ya que pone en marcha la maquinaria para degradarlas. La técnica aprovecha esta característica para provocar esta respuesta mediante la introducción en el animal de moléculas de ARN de doble cadena. Además, si la secuencia de dichas moléculas introducidas es complementaria a la del mensajero de un gen concreto, la maquinaria celular acaba degradando su propio mensajero, con lo que se consigue disminuir la expresión del gen diana.

Una característica que ha afianzado el uso del ARNi en *C. elegans* es que sus células presentan transportadores de ácidos nucleicos de doble cadena, de tal modo que es posible alimentar al nematodo con bacterias que produzcan moléculas de ARNdc que, al ser ingeridas por el animal liberarán el material genético que será transportado a lo largo del cuerpo de *C. elegans* y, por consiguiente, la degradación del mensajero endógeno se dará en todas sus células. Esto ha llevado a la construcción de genotecas de ARN de interferencia en las que cada clon bacteriano contiene un plásmido con un fragmento de un gen de *C. elegans.* Estas genotecas cubren el genoma completo del animal y han facilitado su uso para procesos de cribado masivo (Boutros and Ahringer 2008).

Ahora bien, esta técnica varía su eficiencia dependiendo del tejido estudiado. En el caso del sistema nervioso, por ejemplo, las células son refractarias al ARN de interferencia. Sin embargo, se han descrito mutaciones en ciertos genes que incrementan la eficacia de la interferencia, lo que ha llevado a la aplicación exitosa de esta técnica en neuronas, sobre todo con el objetivo de descubrir aquellos factores de transcripción que participan en su regulación terminal. Una de las poblaciones particularmente interesantes por su relevancia clínica, son las neuronas monoaminérgicas (MA).

Esta población neuronal se caracteriza por sintetizar sus neurotransmisores a partir de aminoácidos aromáticos y, en función del tipo de neurotransmisor que produzcan, se clasifican en seis tipos diferentes: dopaminérgicas (DA), serotonérgicas (5-HT), noradrenérgicas (NA), adrenérgicas (A), tiraminérgicas (TA) y octopaminérgicas (OA).

Las neuronas NA y A se encuentran exclusivamente en vertebrados, siendo las TA y OA sus homólogas en invertebrados (Roeder 2005).

Como se ha mencionado anteriormente, una de las características que definen la madurez funcional de las neuronas es la expresión de aquellos genes que intervienen en la síntesis, empaquetamiento y liberación de los neurotransmisores. Dichos genes efectores, en esta población neuronal, se denominan de modo general *genes de la vía de las monoaminas*. Defectos en la expresión de estos genes conducen a enfermedades como el Parkinson o la esquizofrenia, además de trastornos como el bipolar o depresión. El estudio de la regulación de estos genes ha servido para comprender el componente genético de estas patologías, así como punto de partida para determinar qué FT intervienen en la regulación terminal de estas neuronas.

Las neuronas MA están ampliamente conservadas en la evolución. En los sistemas nerviosos de vertebrados, como el pez cebra o el ratón, y en los de invertebrados, como *Drosophila melanogaster* o *C. elegans*, encontramos núcleos neuronales que emplean estos neurotransmisores. En el caso de *C. elegans*, en su forma hermafrodita se han descrito cuatro pares de neuronas DA (CEPV/D, ADE y PDE), cuatro pares (NSM, ADF, HSN y AIM) y una neurona unilateral (RIH) que emplean serotonina; una pareja de neuronas TA (RIM) y otra pareja OA (RIC) (Flames and Hobert 2011).

Además de la presencia de estas neuronas, se han descrito numerosos casos en los que un FT intervenía en la diferenciación de un subtipo MA en un organismo, y su ortólogo funcional en otro organismo también jugaba un papel en la diferenciación del mismo tipo de neurona MA. Por ejemplo, en *C. elegans* se ha descrito que tres FT, *ast-1*, un factor de la familia ETS; *ceh-43*, de la familia de los homeodominio (HD); y *ceh-20*, de la familia PBX, dirigen la diferenciación terminal de las neuronas dopaminérgicas y en ratón, la diferenciación de las neuronas DA del bulbo olfatorio está controlada por los ortólogos de dichos factores, a saber, *Er81* (ETS), *Dlx2* (HD) y *Pbx1* (PBX) (Doitsidou et al. 2013). Por otra parte, un fenómeno similar se ha descrito entre la diferenciación terminal de la neurona HSN de *C. elegans* y las neuronas serotonérgicas de los núcleos del raphe del ratón, en este caso es una combinación de seis FT la que está conservada: *ast-1/Pet1*, *unc-86/Brn2*, *sem-4/Sall2*, *egl-46/Insm1*, *egl-18/Gata2/3* and *hlh-3/Ascl1* (Lloret-Fernández et al. 2018).

Objetivos

En definitiva, la relevancia de las neuronas monoaminérgicas, debido a la gran cantidad de funciones que controlan, desde las emociones al aprendizaje y la coordinación del movimiento, unido a su conservación a lo largo de la escala evolutiva,

nos ha llevado establecer como finalidad de esta Tesis desvelar aquellos factores de transcripción que intervienen en el programa regulador de la identidad celular de las neuronas monoaminérgicas, empleando para ello el modelo animal de *C. elegans*. Para abordar este trabajo, nos hemos propuesto los siguientes objetivos:

1. Optimizar la estrategia de ARN de interferencia para llevar a cabo un cribado mediante la esta técnica, altamente eficiente y contra todos los FT de *C. elegans.*
2. Construir una genoteca de ARN de interferencia para todos los FT de *C. elegans* con la que disminuir la expresión de dichos genes y así detectar cuáles de ellos participan en la especificación de las neuronas monoaminérgicas.
3. Validar y determinar con precisión la función de los candidatos obtenidos mediante el proceso de cribado que presenten los fenotipos más penetrantes para cada una de las neuronas monoaminérgicas.

Resultados y Metodología

2.1. Optimización de la estrategia de ARNi para identificar los FT de *C. elegans* que participan en la especificación de neuronas MA.

En la sección anterior se mencionaba cómo la eficiencia del ARNi variaba en función del tejido estudiado y que, sin embargo, se han descrito diversas mutaciones que aumentan la efectividad de este método. Por tanto, dado que en el tejido nervioso la eficiencia es baja, hicimos un ensayo piloto para comprobar cuál de las mutaciones descritas nos permitía ver el mayor fenotipo posible.

Probamos la eficiencia de los fondos genéticos mutantes: *nre-1 (hd20), lin-15b (hd126); eri-1 (mg366), lin-15b (n744);* and *rrf-3 (pk1426).* Para ello evaluamos la pérdida de expresión de reporteros fluorescentes que marcasen, las distintas neuronas monoaminérgicas, con el reportero *cat-1::gfp*; las neuronas dopaminérgicas, con *cat-2::gfp*; y las neuronas serotonérgicas, con *tph-1::gfp*. Los resultados demostraron que, para las neuronas dopaminérgicas, el fondo genético con el que se conseguía mayor eficiencia era *eri-1 (mg366), lin-15b (n744)*. No obstante, teniendo en cuenta todas las neuronas MA, la mutación que mostró fenotipo en todas ellas fue *rrf-3 (pk1426)*, por lo que optamos por ella para incorporarla a la cepa final con la que se llevaría a cabo el proceso de cribado. Además, probamos la combinación de dicha mutación con la expresión del transportador de ácidos nucleicos, *sid-1*, específicamente en el tejido nervioso. Sin embargo, no conseguimos mejorar el fenotipo ya obtenido con el mutante *rrf-3 (pk1426)*.

Finalmente decidimos emplear el fondo genético *rrf-3 (pk14266)* para nuestro cribado de ARNi. Pero además incorporamos tres reporteros para visualizar las neuronas MA y determinar el papel de cada factor de trascripción en las mismas. Dichos reporteros fueron: *cat-1::gfp*, para todas las neuronas MA; para las neuronas DA, *dat-1::mCherry*; y para las neuronas 5-HT con *tph-1::dsRed*. Con este sistema evaluamos la regulación de cada FT sobre estos tres genes.

1.2. Construcción de una genoteca de ARNi para los FT de *C. elegans*

Para llevar a cabo el proceso de cribado, se alimentó a los animales con bacterias con la capacidad de producir ARN de doble cadena. Dichas bacterias, *E. coli* HT1115 (DE3), son deficientes en la expresión de la ARN exonucleasa, lo que aumenta la vida media del ARN de doble cadena. Además, se les ha insertado una copia de la polimerasa del fago T7, mediante la cual son capaces de unirse a un promotor del fago T7 y producir ARN de doble cadena a partir del ADN. Esta característica se ha aprovechado para subclonar un fragmento de cada FT de *C. elegans* en un plásmido cuyo sitio de clonación está flanqueado por dos promotores T7, de tal modo que cuando se expresa la polimerasa de T7, se comienza a producir el ARNdc. Para controlar la expresión de la polimerasa, dicho gen se encuentra bajo control de un promotor inducible por IPTG, un compuesto químico que se añade al caldo de cultivo de las bacterias tres horas antes de sembrarlas en las placas donde se depositará a los gusanos para que se alimenten de las mismas e ingieran el ARNi. Los experimentos duran una semana, desde que se siembran las placas y trasladan los gusanos, hasta que la progenie de la generación inicialmente depositada en la placa alcanzaba el estadio de adulto joven. En ese momento se analizaban las neuronas MA de los animales a través del microscopio de fluorescencia.

Ya hay genotecas de ARNi contra todos los genes de *C. elegans*, entre las que destacan las de los laboratorios de Julie Ahringer y Marc Vidal (Rual et al. 2004; Kamath and Ahringer 2003). Sin embargo, estas genotecas, generadas por un proceso de clonación masiva, suelen tener un porcentaje de genes sin recoger. Por tanto, nos propusimos extraer, en primer lugar, los clones contra los FT de la genoteca de Ahringer. Comprobamos por secuenciación si su anotación era correcta y los que no encontramos o eran erróneos los buscamos en la genoteca de Vidal. Repetimos el proceso de comprobar la anotación mediante la secuenciación de los clones y, para completar nuestra genoteca de ARNi para FT, llevamos a cabo nuestro propio proceso de clonación. Finalmente, la composición de la librería de 876 clones es la siguiente: 548 clones de Ahringer, 163 clones de Vidal y 165 clones generados en nuestro laboratorio.

2.1. Valoración de la eficacia del cribado de ARNi mediante fenotipos visibles y aquellos fenotipos previamente descritos

Cuando llevamos a cabo los experimentos de ARNi, analizábamos la población de neuronas MA de al menos 30 gusanos alimentados con ARNi, donde observamos

distintos fenotipos. En primer lugar, en caso de que el FT evaluado controlase la expresión de los reporteros de nuestra cepa o interviniese en el linaje de alguna de las neuronas MA, nos encontramos con una pérdida de fluorescencia, bien por la nula expresión del reportero o porque la neurona no se hubiera generado. Por otra parte, también detectamos alteraciones en la morfología del axón en distintas neuronas MA, así como defectos de migración en algunas de ellas. Finalmente, también describimos casos en los que la aplicación de un ARNi daba lugar a la aparición de neuronas ectópicas. Los recuentos bajo el microscopio dieron lugar a la detección de 91 FT con fenotipo significativo (en >10% de la población) en las neuronas MA.

Además de los resultados detectados bajo el microscopio, algunos fenotipos también fueron visibles bajo la lupa de disección convencional, como defectos en el patrón de movimiento que daban lugar al fenotipo conocido como *unc* (del inglés, descoordinado o *uncoordinated*) o rol, en el que los animales giraban sobre sí mismos. Pero sin duda el más claro de todos se producía cuando el ARNi administrado provocaba letalidad embrionaria, dado que el número de animales de la placa se veía reducido drásticamente. Este tipo de características fueron detectadas en 95 FT.

La detección de dichos fenotipos nos sirvió para comparar la efectividad de nuestro método de cribado con otros cribados similares realizados previamente por Simmer y colaboradores y por Kamath y colaboradores. Estos grupos habían buscado fenotipos visuales, como los que acabamos de describir, en sus cribados. Así pudimos comprobar que el 51% de nuestros fenotipos también habían sido descritos por los otros dos grupos. Además, buscamos si el resto de genes que no solapaban con los de Simmer y Kamath habían presentado fenotipo y habían sido descritos en otros cribados. Para ello buscamos la información en WormBase (W257) sobre dichos genes y nos encontramos con que solo de 16 de ellos no se había descrito previamente ningún fenotipo.

Los fenotipos visibles no son los únicos que nos han servido para determinar la eficacia del cribado de ARNi para los FT, sino que algunos de ellos ya se ha visto que desempeñan un papel en las neuronas MA. De entre los candidatos ya conocidos unos 17 aproximadamente, nuestro cribado había servido para reproducir el resultado de 14 de ellos. Este resultado, junto al de fenotipos visibles, refuerza la confianza en nuestro protocolo de cribado.

2.2. Análisis global de los resultados obtenidos en el cribado de ARN de interferencia

Como ya se ha mencionado, el cribado proporcionó 91 FT involucrados en el desarrollo de las neuronas MA. De entre las familias con más candidatos entre los resultados destacan: Homeodominio (24), ZF-C2H2 (21), bHLH (7), bZIP (6) y ZF-NHR (7). Además, el fenotipo mayoritario observado es la pérdida de fluorescencia por parte

de los reporteros. Si atendemos a este fenotipo, vemos que los candidatos se reparten entre todas las neuronas MA, siendo RIC/RIM los que más candidatos tienen (22) y NSM la que menos (2). Además, entre los candidatos con este fenotipo observamos que algunos de ellos presentan pérdida de expresión en varios subtipos de neuronas MA, como es el caso de *ceh-27* en las neuronas ADF y RIC/RIM.

Otra rasgo que llama la atención de nuestros resultados es la presencia de genes que intervienen en la regulación de características de dimorfismo sexual, como *sex-1* que presenta fenotipo de pérdida de expresión en ADF; *tra-1*, en el caso de VC4/5 o *sdc-1*, en RIC/RIM. En esta últimas, no se había descrito hasta el momento ningún tipo de dimorfismo entre machos y hermafroditas en *C. elegans* (Portman 2007).

Por otra parte, también obtuvimos como candidatos genes heterocrónicos, que intervienen en la expresión de ciertos genes a partir de momentos concretos del desarrollo. Un ejemplo de esto es la maduración funcional de la neurona HSN que interviene en la puesta de huevos y que, aunque nace en el estadio larvario L1, no es funcional hasta el estadio de adulto joven, proceso en el que interviene el gen *hbl-1*. Lo que destaca es el gen heterocrónico *lin-14* como candidato de la neurona NSM, donde no se había descrito previamente la acción de ningún gen de heterocronía (Tsialikas et al. 2017).

Una vez acabado el cribado, procedimos a validar aquellos candidatos que presentaron el fenotipo más penetrante para cada subpoblación monoaminérgica.

3. Validación de los candidatos requeridos para la especificación de neuronas dopaminérgicas

La población de neuronas DA en *C. elegans* había sido estudiada con anterioridad y se había descrito el papel de tres factores de transcripción implicados en su diferenciación terminal, *ceh-20, ceh-43* y *ast-1*. Estos tres candidatos estaban presentes entre los resultados obtenidos para esta población, pero además observamos la presencia de otros FT cuyo fenotipo abarcaba varias neuronas DA, entre los que destacaban por la penetrancia de su fenotipo: *unc-62, vab-3, unc-55, dro-1, mef-2* y *cep-1*.

Los seis candidatos tenían un fenotipo significativo mediante ARNi, por lo que comenzamos la validación analizando la expresión del reportero *cat-2::gfp* (específico de DA) en el mutante nulo de cada uno de los candidatos para comprobar que también presentaran fenotipo en las neuronas DA. Además, estudiamos el patrón de expresión de cada candidato con el fin de determinar si se expresaban en dichas neuronas.

En primer lugar, *cep-1* y *mef-2* no mostraron fenotipo al analizar sus mutantes, es más, *cep-1* no se expresaba tampoco en esta población. Esto nos llevó a descartar ambos candidatos. Al evaluar el mutante de *dro-1*, observamos defectos de expresión en la

neurona ADE, sin embargo, el reportero no mostró expresión del gen en ninguna de las neuronas. Aunque es posible que un reportero más fiable o CRISPR nos llevase a resultados diferentes, por limitaciones de tiempo, no continuamos validando este gen. Posteriormente, la evaluación de los mutantes de *unc-62, vab-3, unc-55* demostró que los tres presentaban fenotipo de pérdida de expresión en las neuronas DA, no solo con el reportero *cat-2* sino con otros reporteros de genes efectores, además de expresión en las mismas, por lo que continuamos validando el papel de los tres candidatos.

El factor *unc-55* fue el que menos fenotipo mostró, afectando solamente a la neurona ADE, por lo que nos planteamos que quizá este factor podría estar interaccionando con otros factores para dirigir la expresión de los reporteros. Decidimos cruzar el mutante de este gen con el mutante hipomorfo para el candidato *ast-1*. El análisis mostró que ambos FT interaccionan para controlar la expresión de los genes *bas-1* y *dat-1*, característicos de la producción y recaptación de DA.

Finalmente, quisimos responder a la pregunta de si *unc-62, vab-3* y *unc-55*, se unen directamente a las secuencias reguladoras de los genes efectores dopaminérgicos. Para ello llevamos a cabo experimentos de mutagénesis dirigida contra posibles motivos de unión para nuestros candidatos en las secuencias reguladoras mínimas de los genes *cat-2* y *dat-1*. En todos ellos la mutación de los motivos para los tres candidatos reveló un fenotipo de pérdida de expresión, lo que indica que *unc-62, vab-3* y *unc-55* controlan la expresión de los genes efectores mediante su unión directa al ADN.

Todos estos datos nos llevan a concluir que el colectivo de FT que regulan la especificación de las neuronas dopaminérgicas podría ser más amplio que el inicialmente descrito y que podría incluir a los tres nuevos candidatos *unc-62, vab-3* y *unc-55.*

4. Validación de los candidatos requeridos para la especificación de neuronas serotonérgicas

Las neuronas serotonérgicas de *C. elegans* pueden separarse en dos categorías, aquellas que son capaces de fabricar serotonina, NSM, ADF y HSN; y aquellas que solo son capaces de emplear la serotonina que liberan al medio las primeras, y que son AIM, RIH y VC4/5. Con la excepción de AIM y RIH, no visibles en nuestro proceso de cribado, obtuvimos candidatos para las demás. En el caso de NSM y HSN, que habían sido previamente estudiadas, los FT involucrados en la especificación de dichas neuronas también estaban entre los resultados del cribado de ARNi Sin embargo, elegimos centrar el proceso de validación en los candidatos obtenidos para la neurona ADF, de la que no se conocían hasta el momento posibles FT que controlasen su diferenciación.

El candidato con un fenotipo de pérdida de expresión más penetrante era *lag-1*, el efector transcripcional de la ruta Notch de señalización. Decidimos analizar la expresión de los genes de la vía serotonérgica, encargados de la síntesis y liberación de 5-HT, en el fondo genético mutante para dicho gen. Así pudimos comprobar que, en ausencia de la expresión de este factor, había una pérdida significativa de expresión de los reporteros evaluados.

En vista de estos resultados, quisimos comprobar si la señalización mediante la vía Notch estaba también implicada en la diferenciación de ADF. Sin embargo, al evaluar la expresión del gen *tph-1*, enzima limitante en la síntesis de 5-HT, en el fondo genético mutante para Notch, no observamos ningún fenotipo similar al observado en el mutante de *lag-1*, por lo que concluimos que *lag-1* estaría actuando mediante una vía independiente de Notch para dirigir la especificación de ADF.

Se ha descrito que el ortólogo de *lag-1* en mamíferos, *Rbpj*, puede actuar en una vía de acción independiente de Notch mediante su unión a un factor de la familia bHLH. Dado que otro de los candidatos obtenidos para ADF era de esta familia, *hlh-14*, decidimos estudiar este factor (Johnson and MacDonald 2011). Los mutantes para este factor son letales, además de que se ha visto que la ausencia de este gen afecta la generación de las neuronas del linaje de ADF. Por lo que evaluamos mediante ARNi, que produce un fenotipo menos penetrante que el mutante nulo, el papel de este factor en los genes *tph-1* y *cat-1*, donde la pérdida de expresión era similar a la que experimentaban en el mutante de *lag-1.* Por tanto, *hlh-14* podría ser el compañero de *lag-1* para dirigir la diferenciación de ADF.

El siguiente paso que llevamos a cabo fue la identificación de sitios funcionales de unión de ambos candidatos a las secuencias reguladoras de los genes de la síntesis de 5-HT, mediante mutagénesis dirigida. Los resultados obtenidos mostraron que ambos factores tenían sitios de unión funcionales, por lo que su modo de regulación sugiere su unión directa al ADN.

Finalmente, quisimos comprobar la relevancia de estos dos factores en la respuesta funcional de ADF mediante el estudio de dos comportamientos en los que participa activamente la neurona. El primero de ellos fue la respuesta de deceleración aumentada que exhiben los animales al acercarse a la comida después de haber pasado por un período de ayuno. En este comportamiento, la neurona ADF detecta las moléculas liberadas por las bacterias de las que se alimentan y, por tanto, comienza a liberar serotonina para hacer que el animal se detenga, lo que se consigue con la liberación de serotonina también por parte de la neurona NSM en la fase final de la respuesta. En los grupos de animales tratados con ARNi contra *lag-1* y *hlh-14*, la deceleración inicial debida a la actividad de ADF, no tuvo lugar (Iwanir et al. 2016).

La segunda característica funcional de esta neurona consiste en su capacidad para detectar compuestos químicos disueltos en el ambiente. Para ello llevamos a cabo experimentos de imagen de calcio para ver y cuantificar la activación de la neurona cuando se la exponía a un medio con 10 mM de cobre y pH4. Estos experimentos revelaron que la neurona no es capaz de responder cuando se trata a los animales con ARNi contra *lag-1* y *hlh-14*.

Con estos dos tipos de experimentos pudimos comprobar que tanto *lag-1* como *hlh-14* son esenciales para la diferenciación terminal de la neurona ADF y para que pueda llevar a cabo la señalización y respuesta a cambios en el medio que rodea al animal.

5. Validación de los candidatos requeridos para la especificación de neuronas tiraminérgicas y octopaminérgicas

Estos dos tipos de neuronas, como ya hemos mencionado, están presentes en invertebrados en lugar de las adrenérgicas y noradrenérgicas. Hasta el momento no se conocía posibles FT implicados en su diferenciación, pero nuestro cribado de ARNi puso de manifiesto 22 candidatos con fenotipo de pérdida de expresión del reportero *cat-1*. En general, observamos que entre dichos candidatos muchos de ellos participaban en la vía de señalización por Wnt (*ceh-13*, *ceh-36*, *ceh-27* o *vab-7*), por lo que esta podría estar implicada en la especificación de RIC y RIM (Zacharias et al. 2015).

Para comenzar la validación, escogimos el FT con mayor fenotipo, *zip-5*, y otro gen cuyas funciones en el metabolismo del animal están relacionadas con la liberación de octopamina, el gen *pqm-1*.

En primer lugar, llevamos a cabo el análisis de los mutantes para ambos genes, evaluando la expresión de los reporteros *tdc-1* y *tbh-1*, enzimas necesarias para la producción de TA y OA en el primer caso, y de OA en el segundo. Los resultados mostraron que *pqm-1* no afectaba a la expresión de ninguno de los dos reporteros; sin embargo, la expresión de *tdc-1* en el mutante de *zip-5* presentó una reducción significativa de la expresión tanto en RIC como en RIM. Por otra parte, al analizar el patrón de expresión de ambos factores, encontramos que solo *zip-5* se encontraba expresado en las dos neuronas, por lo que finalmente concluimos que este FT podría ser un sólido candidato a dirigir la diferenciación terminal de RIC y RIM.

Conclusiones

En esta Tesis hemos llevado a cabo un estudio exhaustivo de los factores de transcripción de *C. elegans* y hemos dado un primer paso para completar el mapa de

factores reguladores que intervienen en la especificación de las neuronas monoaminérgicas. Dichos resultados nos han llevado a las siguientes conclusiones:

1. El fondo genético mutante *rrf-3 (pk1426)* ha sido eficaz para llevar a cabo un cribado de ARNi en *C. elegans* y ha permitido obtener diversos fenotipos en la población de neuronas monoaminérgicas observados mediante los reporteros fluorescentes *cat-1, dat-1* y *tph-1*.
2. La construcción de una genoteca de ARNi, completa y verificada, para todos los FT de *C. elegans* cuenta con 876 clones de los cuales 548 proceden de la genoteca de Ahringer, 163 de Vidal y 165 generados en nuestro laboratorio.
3. El proceso de cribado de ARNi contra los FT de *C. elegans* reveló, 95 FT con un fenotipo visible de los que el 84% ya había sido previamente descrito y 91 FT con fenotipo en las neuronas MA, de entre los cuales se reprodujo el resultado del 76% de los factores que habían sido previamente implicados en la diferenciación de neuronas MA.
4. Las familias de factores de transcripción más representadas entre los resultados fueron homeodominios, ZF-C2H2, bHLH, bZIP y ZF-NHR. El fenotipo más destacado fue el de pérdida de expresión de los reporteros. Muchos de los candidatos presentaron fenotipo en más de una neurona y se obtuvieron candidatos con funciones definidas en linaje, regulación del dimorfismo sexual y heterocronía.
5. En la población de neuronas dopaminérgicas se describió el papel de tres factores, *unc-62, vab-3* y *unc-55* en la regulación de genes característicos de esta población; además se descubrieron sitios de unión funcionales de los tres factores en las regiones reguladoras mínimas de los genes *cat-2* y *dat-1.*
6. Para la neurona serotonérgica ADF, se descubrió que el gen *lag-1* está implicado en la regulación de la batería de genes efectores a cargo de la síntesis y liberación de 5-HT, la cual lleva a cabo mediante una vía independiente de Notch, gracias a su cooperación con el factor *hlh-14*. Ambos, presentan sitios de unión funcionales en los genes efectores para la producción y liberación de 5-HT.
7. En la neurona TA, RIM, y en la neurona OA, RIC, el factor de transcripción *zip-5* regula la expresión del gen efector *tdc-1*, esencial para la síntesis de sus respectivos neurotransmisores, lo que lo convierte en el primer FT descrito para la especificación de estas dos neuronas en *C. elegans*.

RESUM
(VALENCIÀ)

RESUM

Introducció

L'adquisició de la identitat cel·lular al llarg del desenvolupament embrionari ha sigut un dels temes d'interès per als científics en les últimes dècades. Durant el procés de diferenciació, les cèl·lules comencen a expressar marcadors específics de la seua identitat final. Per a aconseguir tal objectiu, es selecciona un perfil transcripcional que dota a la cèl·lula de les seues característiques diferenciadores.

L'expressió d'aquests gens característics de la identitat cel·lular, denominats gens efectors (Hobert 2016a) és controlada per factors de transcripció (FT) que s'uneixen a les seqüències reguladores de l'ADN, promotors i potenciadors (del anglés *enhancers*). Ara bé, els factors de transcripció són pleiotròpics, és a dir, s'expressen en múltiples tipus cel·lulars, de manera que és la combinació de diferents FT el que atorga l'especificitat a la regulació transcripcional en cada tipus cel·lular.

Els FT presenten una regió, en la conformació estructural de la proteïna, amb la qual s'uneixen a l'ADN per a exercir la seua funció reguladora, denominada domini d'unió a l'ADN. En funció d'aquests dominis, s'uneixen a uns motius, o seqüències de l'ADN, amb major probabilitat. Aquesta característica condueix a agrupar els FT en famílies en funció dels seus dominis d'unió. En humans s'han descrit 111 famílies de FT, mentre que en *Caenorhabditis elegans* es coneixen 48 (Narasimhan et al. 2015).

Com s'ha esmentat, la combinació de FT és necessària per a aconseguir l'especificitat de cada programa transcripcional, pel que els FT habitualment interaccionen de cara a la seua unió a les seqüències reguladores. Açò dóna lloc a fenòmens de cooperació entre dos factors per a promoure la unió de tots dos; o bé, pot ser la unió de dos factors el que promoga el reclutament d'un tercer factor o cofactor, que s'unisca a ells formant un complex més estable, de manera que finalment donen lloc a una sinergia en l'expressió del gen. D'altra banda, la unió entre factors pot provocar canvis conformacionals en alguna de les proteïnes i, així, que s'altere l'especificitat d'unió del factor a l'ADN, en un fenomen de alosterisme (Siggers and Gordân 2014).

Tenint en compte tots aquests mecanismes, s'han proposat diferents models per a explicar l'ocupació de les seqüències reguladores per part dels FT. Aquests models es basen en la presència, constant o canviant, de motius d'unió per al grup de FT; i a més tenen en compte si els factors s'uneixen exclusivament a l'ADN o si algun dels membres del grup pot interaccionar també amb la resta de FT. Un dels models del que es troben diversos exemples en la naturalesa consisteix en que un mateix grup de FT forma un col·lectiu encarregat de regular els gens efectors, però la seua unió per a promoure

l'expressió de cada gen és variable i depén dels motius presents i de com interaccionen entre si els FT (Doitsidou et al. 2013; Lloret-Fernández et al. 2018).

Encara que els FT són essencials en la regulació transcripcional, hi ha altres elements que contribueixen a l'expressió gènica, com l'estat de la cromatina, les marques epigenètiques, així com l'organització tridimensional del genoma. Tot açò aporta capes de complexitat en la regulació que, al mateix temps, també intervenen i afinen l'execució dels programes reguladors.

Un dels teixits on la identitat cel·lular és especialment variada és el sistema nerviós. En aquest teixit es troba una gran varietat tant estructural com a funcional de tipus neuronals, a més de cèl·lules de suport. Per exemple, en el nematode *C. elegans* hi ha 302 neurones en la seua forma hermafrodita, les quals es poden agrupar en 118 categories diferents. En aquest teixit s'ha dut a terme una àmplia labor per a estudiar els FT que dirigeixen els programes de determinació de la identitat neuronal. Més concretament, ha donat lloc a encunyar el terme de selectors terminals (Hobert 2011, 2008) per a aquells FT la combinació dels quals regula l'expressió dels gens efectors que caracteritzen la maduresa de la cèl·lula.

En el cas de les neurones, d'entre els gens efectors podem trobar aquells encarregats de la síntesi, empaquetament, alliberament i recaptació del neurotransmissor, a més de canals iònics, receptors i transportadors, la correcta expressió dels quals és un dels trets de la maduresa funcional de les neurones.

L'estudi dels programes reguladors tradicionalment ha seguit la perspectiva d'estudiar el paper d'un element concret de la xarxa de regulació. No obstant açò, l'ús d'altres models animals com el nematode *C. elegans* permet una perspectiva diferent mitjançant la qual abordar l'estudi directament sobre un elevat nombre de gens.

Els estudis amb aquest model van començar en els anys seixanta per Sydney Brenner i, junt amb Jonh Sulston, van realitzar una anàlisi exhaustiva de mutants per a centenars de gens i van descriure el llinatge complet de totes les cèl·lules de *C. elegans*. El fàcil manteniment en el laboratori i el curt cicle de vida d'aquest nematode, que aconsegueix la maduresa sexual en tres dies, van afermar el seu ús com a model experimental. *C. elegans* es reprodueix mitjançant la posada d'ous que, una vegada eclosionen, es desenvolupen a través de quatre estadis larvaris fins a aconseguir la maduresa. En aquesta espècie ens trobem amb dues formes, hermafrodites en la seua majoria i un xicotet percentatge de mascles que faciliten l'intercanvi genètic (Brenner 1974).

A causa d'aquestes característiques, *C. elegans* permet dur a terme protocols de garbellat massiu de gens mitjançant els quals abordar l'estudi de centenars de seqüències per a identificar les que intervenen en un procés d'interès. Tradicionalment

aquests processos de garbellat es basaven en l'ús d'un agent mutagen, com l'EMS (etilmetanosulfonat) per a posteriorment aïllar aquells gens on la mutació havia produït un fenotip d'interès. En aquest tipus de garbellat la mutació dels gens no era dirigida, la qual cosa suposava posteriorment un llarg període d'aïllament i identificació. No obstant açò, amb l'aplicació de la tècnica d'ARN d'interferència (ARNi), els processos de garbellat van adquirir un matís direccional.

El fonament de l'ARN d'interferència es basa la resposta de la cèl·lula quan detecta la presència de molècules d'ARN doble cadena (ARNdc), ja que engega la maquinària per degradar-les. La tècnica aprofita aquesta característica per provocar aquesta resposta mitjançant la introducció en l'animal de molècules d'ARNdc. A més, si la seqüència d'aquestes molècules introduïdes és complementària a la del missatger d'un gen concret, la maquinària cel·lular acaba degradant el seu propi missatger, amb el que s'aconsegueix disminuir l'expressió del gen diana.

Una característica que ha afermat l'ús de l'ARNi en *C. elegans* és que les seves cèl·lules presenten transportadors d'àcids nucleics de doble cadena, de tal manera que és possible alimentar al nematode amb bacteris que produeixin molècules d'ARNdc que, en ser ingerides per l'animal, alliberaran el material genètic que serà transportat al llarg del cos del nematode i, per tant, la degradació del missatger endogen es donarà en totes les seves cèl·lules. Això ha portat a la construcció de genoteques d'ARNi en les quals cada clon bacterià conté un plasmidi amb un fragment d'un gen de *C. elegans*. Aquestes genoteques cobreixen el genoma complet de l'animal i han facilitat el seu ús per a processos de garbellat massiu (Boutros and Ahringer 2008).

Ara bé, aquesta tècnica varia la seva eficiència depenent del teixit estudiat. En el cas del sistema nerviós, per exemple, les cèl·lules són refractàries a l'ARNi. No obstant això, s'han descrit mutacions en certs gens que incrementen l'eficàcia de la interferència, la qual cosa ha portat a l'aplicació exitosa d'aquesta tècnica en neurones, sobretot amb l'objectiu de descobrir aquells FT que participen en la seva regulació terminal. Una de les poblacions particularment interessants per la seva rellevància clínica, són les neurones monoaminérgiques (MA).

Aquesta població neuronal es caracteritza per sintetitzar els seus neurotransmisors a partir d'aminoàcids aromàtics i, en funció del tipus de neurotransmissor que produeixin, es classifiquen en sis tipus diferents: dopaminèrgiques (DA), serotonèrgiques (5-HT), noradrenèrgiques (NA), adrenèrgiques (A), tiraminèrgiques (TA) i octopaminèrgiques (OA). Les neurones NA i A es troben exclusivament en vertebrats, sent les TA i OA les seues homòlogues en invertebrats (Roeder 2005).

Com s'ha esmentat anteriorment, una de les característiques que defineixen la maduresa funcional de les neurones és l'expressió d'aquells gens que intervenen en la síntesi, empaquetament i alliberament dels neurotransmisors. Aquests gens efectors, en aquesta població neuronal, es denominen de manera general *gens de la via de les monoamines*. Defectes en l'expressió d'aquests gens condueixen a malalties com el Parkinson o l'esquizofrènia, a més de trastorns com el bipolar o depressió. L'estudi de la regulació d'aquests gens ha servit per comprendre el component genètic d'aquestes patologies, així com punt de partida per determinar què FT intervenen en la regulació terminal d'aquestes neurones.

Les neurones MA estan àmpliament conservades en l'evolució. En els sistemes nerviosos de vertebrats, com el peix zebra o el ratolí, i en els de invertebrats, com *Drosophila melanogaster* o *C. elegans*, trobem nuclis neuronals que empren aquests neurotransmisors. En el cas de *C. elegans,* en la seua forma hermafrodita s'han descrit quatre parells de neurones DA (CEPV/D, ADE i PDE), quatre parells (NSM, ADF, HSN i AIM) i una neurona unilateral (RIH) que emprenen serotonina; una parella de neurones TA (RIM) i una altra parella OA (RIC) (Flames and Hobert 2011).

A més de la presència d'aquestes neurones, s'han descrit nombrosos casos en els quals un FT intervenia en la diferenciació d'un subtipus MA en un organisme, i el seu ortòleg funcional en un altre organisme també jugava un paper en la diferenciació del mateix tipus de neurona MA. Per exemple, en *C. elegans* s'ha descrit que tres FT, *ast-1*, un factor de la família ETS; *ceh-43*, de la família dels homeodominis (HD); i *ceh-20*, de la família PBX, dirigeixen la diferenciació terminal de les neurones DA. En ratolí, la diferenciació de les neurones DA del bulb olfactori està controlada pels ortòlegs d'aquests factors, a saber, Er81 (ETS), Dlx2 (HD) i Pbx1 (PBX) (Doitsidou et al. 2013). D'altra banda, un fenomen similar s'ha descrit entre la diferenciació terminal de la neurona HSN de *C. elegans* i les neurones serotonèrgiques dels nuclis del raphe del ratolí. En aquest cas es tracta de una combinació de sis FT la que està conservada: *ast-1*/Pet1, *unc-86*/Brn2, *sem-4*/Sall2, *egl-46*/Insm1*, egl-18*/Gata2/3 i *hlh-3*/Ascl1 (Lloret-Fernández et al. 2018).

Objectius

En definitiva, la rellevància de les neurones MA, degut a la gran quantitat de funcions que controlen, des de les emocions a l'aprenentatge i la coordinació del moviment, unit a la seua conservació al llarg de l'escala evolutiva, ens ha portat a establir com a finalitat d'aquesta Tesi desvetlar aquells factors de transcripció que intervenen en el programa regulador de la identitat cel·lular de les neurones MA, emprant el model animal de *C. elegans*. Per a abordar aquest treball, ens hem proposat els següents objectius:

1. Optimitzar l'estratègia d'ARN d'interferència per a dur a terme un garbellat mitjançant aquesta tècnica altament eficient i contra tots els FT de *C. elegans*.
2. Construir una genoteca d'ARN d'interferència per a tots els FT de *C. elegans* amb la qual disminuir l'expressió d'aquests gens i així detectar quins d'ells participen en l'especificació de les neurones monoaminèrgiques.
3. Validar i determinar amb precisió la funció dels candidats obtinguts mitjançant el procés de garbellat que presenten els fenotips més penetrants per a cadascuna de les neurones monoaminérgicas.

Resultats i Metodologia

1.1. Optimització de l'estratègia d'ARNi per a identificar els FT de *C. elegans* que participen en l'especificació de neurones MA.

En la secció anterior s'esmentava com l'eficiència de l'ARNi varia en funció del teixit estudiat i que, no obstant açò, s'han descrit diverses mutacions que augmenten l'efectivitat d'aquest mètode. Per tant, atès que en el teixit nerviós l'eficiència és baixa, vam fer un assaig pilot per a comprovar quina de les mutacions descrites ens permetia veure el major fenotip possible.

Provàrem l'eficiència dels fons genètics mutants: *nre-1 (hd20), lin-15b (hd126); eri-1 (mg366), lin-15b (n744)* i *rrf-3 (pk1426)*. Per a açò avaluem la pèrdua d'expressió de reporters fluorescents que marcaren les diferents neurones MA, amb el reporter *cat-1::gfp*; les neurones dopaminérgicas, amb *cat-2::gfp*; i les neurones serotonèrgiques, amb *tph-1::gfp.* Els resultats van demostrar que, per a les neurones DA, el fons genètic amb el qual s'aconseguia major eficiència era *eri-1 (mg366), lin-15b (n744).* No obstant açò, tenint en compte totes les neurones MA, la mutació que va mostrar fenotip en totes elles va ser *rrf-3 (pk1426).* A més, provárem la combinació d'aquesta mutació amb l'expressió del transportador d'àcids nucleics, *sid-1*, específicament en el teixit nerviós. No obstant açò, no aconseguim millorar el fenotip ja obtingut amb el mutant *rrf-3 (pk1426),* que va ser el triat per a dur a terme el procés de garbellat.

A més de emprar el fons genètic *rrf-3 (pk14266),* incorporàrem tres reporters per a visualitzar les neurones MA i determinar el paper de cada factor de trasncripció en les mateixes. Aquests reporters van ser: *cat-1::gfp*, per a totes les neurones MA; *dat-1::mCherry,* per a les neurones DA; i *tph-1::dsRed* per a les neurones 5-HT. Amb aquest sistema avaluem la regulació de cada FT sobre aquests tres gens.

1.2. Construcció d'una genoteca d'ARNi per als FT de *C. elegans*

Per a dur a terme el procés de garbellat, es va alimentar als animals amb bacteris amb la capacitat de produir ARNdc. Aquests bacteris, *E. coli* HT1115 (DE3), són deficients en l'expressió de l'ARN exonucleasa, la qual cosa augmenta la vida mitjana de l'ARNdc. A més, se'ls ha inserit una còpia de la polimerasa del fago T7, mitjançant la qual són capaços d'unir-se a un promotor del fago T7 i produir ARNdc a partir de l'ADN. Aquesta característica s'ha aprofitat per a subclonar un fragment de cada FT de C*. elegans* en un plasmidi, flanquejat per dues promotors T7, de tal manera que, quan s'expressa la polimerasa de T7, es comença a produir l'ARNdc. Per a controlar l'expressió de la polimerasa, aquest gen es troba baix control d'un promotor inducible per IPTG, un compost químic que s'afig al brou de cultiu dels bacteris tres hores abans de sembrar-les en les plaques on es dipositarà als cucs perquè s'alimenten de les mateixes i ingerisquen l'ARNi. Els experiments duren una setmana, des que se sembren les plaques i traslladen els cucs, fins que la progenie de la generació inicialment dipositada en la placa aconsegueix l'estadi d'adult jove. En aqueix moment s'analitzen les neurones MA dels animals mitjançant el microscopi de fluorescència.

Ja hi ha genoteques d'ARNi contra tots els gens de *C. elegans*, entre les quals destaquen les dels laboratoris de Julie Ahringer i Marc Vidal (Rual et al. 2004; Kamath and Ahringer 2003). No obstant açò, en aquestes genoteques generades per un procés de clonació massiva sol faltar un percentatge de gens. Per tant, ens vam proposar extraure, en primer lloc, els clons contra els FT de la genoteca d'Ahringer. Comprovàrem per seqüenciació si la seua anotació era correcta i, els que no trovárem o eren erronis, els cercàrem en la genoteca de Vidal. Repetírem el procés de comprovar l'anotació mitjançant la seqüenciació dels clons i, per a completar la nostra genoteca d'ARNi per a FT, vam dur a terme el nostre propi procés de clonació. Finalment, la composició de la llibreria de 876 clons és la següent: 548 clons d'Ahringer, 163 clons de Vidal i 165 clons generats en el nostre laboratori.

2.1. Valoració de l'eficàcia del garbellat d'ARNi mitjançant fenotips visibles i aquells fenotips prèviament descrits

Després dels experiments d'ARNi, analitzàvem la població de neurones MA d'almenys 30 cucs alimentats amb ARNi, on observem diferents fenotips. En primer lloc, en els casos en que el FT avaluat controla l'expressió dels reporters del nostre cep o interve en el llinatge d'alguna de les neurones MA, ens trobem amb una pèrdua de fluorescència, bé per la nul·la expressió del reporter o perquè la neurona no s'ha generat. D'altra banda, també detectem alteracions en la morfologia de l'axó en diferents neurones MA, així com defectes de migració en algunes d'elles. Finalment, també descrivim casos en els quals l'aplicació d'un ARNi dona lloc a l'aparició de neurones

ectòpiques. Els recomptes sota el microscopi van donar lloc a la detecció de 91 FT amb fenotip significatiu (en >10% de la població) en les neurones MA.

A més dels resultats detectats sota el microscopi, alguns fenotips també van ser visibles sota la lupa de dissecció convencional, com a defectes en el patró de moviment que donaven lloc al fenotip conegut com *unc* (de l'anglès, *uncoordinated* o descoordinat) o *rol*, en el qual els animals giren sobre si mateixos. Però sens dubte el més clar de tots es produïa quan l'ARNi administrat provocava letalitat embrionària, atès que el nombre d'animals de la placa es veia reduït dràsticament. Aquest tipus de característiques van ser detectades en 95 FT.

La detecció d'aquests fenotips ens va servir per a comparar l'efectivitat del nostre mètode de garbellat amb altres garbellats similars realitzats prèviament per Simmer i col·laboradors i per Kamath i col·laboradors. Aquests grups havien cercat fenotips visuals, com els que acabem de descriure, en els seus garbellats. Així vam poder comprovar que el 51% dels nostres fenotips també havien sigut descrits pels altres dos grups. A més, cercàrem si la resta de gens que no solapaven amb els de Simmer i Kamath havien presentat fenotip i havien sigut descrits en altres garbellats. Per a açò cercàrem la informació en WormBase (W257) sobre aquests gens i ens trobàrem amb que tan sols de 16 d'ells no s'havia descrit prèviament cap fenotip.

Els fenotips visibles no són els únics que ens han servit per a determinar l'eficàcia del garbellat d'ARNi per als FT, sinó que alguns d'ells ja s'havia vist que exerceixen un paper en les neurones MA. D'entre els candidats ja coneguts, uns 17 aproximadament, el nostre garbellat ha reproduït el resultat de 14 d'ells. Aquest resultat, al costat del de fenotips visibles, reforça la confiança en el nostre protocol de garbellat.

2.2. Anàlisi global dels resultats obtinguts en el garbellat d'ARN d'interferència

Com ja s'ha esmentat, el garbellat va proporcionar 91 FT involucrats en el desenvolupament de les neurones MA. D'entre les famílies amb més candidats entre els resultats destaquen: Homeodomini (24), ZF-C2H2 (21), bHLH (7), bZIP (6) i ZF-NHR (7). A més, el fenotip majoritari observat és la pèrdua de fluorescència per part dels reporters. Si atenem a aquest fenotip, veiem que els candidats es reparteixen entre totes les neurones MA, sent RIC/RIM els que més candidats tenen (22) i NSM la que menys (2). A més, entre els candidats amb aquest fenotip observem que alguns d'ells presenten pèrdua d'expressió en diversos subtipus de neurones MA, com és el cas de *ceh-27* en les neurones ADF i RIC/RIM.

Un altre tret que crida l'atenció dels nostres resultats és la presència de gens que intervenen en la regulació de característiques de dimorfisme sexual com *sex-1,* que

presenta fenotip de pèrdua d'expressió en ADF; *tra-1*, en el cas de VC4/5; o *sdc-1*, en RIC/RIM. En estes últimes neurones no s'havia descrit cap tipus de dimorfisme entre mascles i hermafrodites en *C. elegants* (Portman 2007).

D'altra banda, també vam obtenir com a candidats gens heterocrònics, que intervenen en l'expressió de certs gens a partir de moments concrets del desenvolupament. Un exemple d'açò és la maduració funcional de la neurona HSN que intervé en la posada d'ous i que, encara que naix en l'estadi larvari L1, no és funcional fins a l'estadi d'adult jove, procés en el qual intervé el gen *hbl-1*. Curiosament, el gen heterocrònic *lin-14* apareix com a candidat de la neurona NSM, on no s'havia descrit prèviament l'acció de cap gen d'heterocronia (Tsialikas et al. 2017).

Una vegada acabat el garbellat, vam procedir a validar aquells candidats que van presentar el fenotip més penetrant per a cada subpoblació MA.

3. Validació dels candidats requerits per a l'especificació de neurones dopaminèrgiques

La població de neurones DA en *C. elegans* havia sigut estudiada amb anterioritat i s'havia descrit el paper de tres factors de transcripció implicats en la seua diferenciació terminal, *ceh-20, ceh-43* i *ast-1*. Aquests tres candidats estaven presents entre els resultats obtinguts per a aquesta població, però a més observem la presència de FT addicionals amb fenotips que afectaven a diverses neurones DA. Per la penetrància del seu fenotip destaquen: *unc-62, vab-3, unc-55, dro-1, mef-2* i *cep-1.*

Els sis candidats tenien un fenotip significatiu mitjançant ARNi, per tant, començàrem la validació analitzant l'expressió del reporter *cat-2::gfp* (específic de DA) en el mutant nul de cadascun dels candidats per a comprovar que també presentaren fenotip en les neurones DA. A més, estudiàrem el patró d'expressió de cada candidat amb la finalitat de determinar si s'expressaven en aquestes neurones.

En primer lloc, ni *cep-1* ni *mef-2* mostraren fenotip en analitzar els seus mutants; és més, *cep-1* tampoc s'expressava en aquesta població. Açò ens va portar a descartar tots dos candidats. En avaluar el mutant de *dro-1*, observárem defectes d'expressió en la neurona ADE, però, desafortunadament, el reporter no va mostrar expressió del gen en cap de les neurones. Encara que és possible que un reporter més fiable (fòsmid) o endogen (CRISPR) ens portara a resultats diferents, degut a limitacions de temps, no continuáreem validant aquest gen. Posteriorment, l'avaluació dels mutants de *unc-62, vab-3* i *unc-55* va revelar un fenotip de pèrdua d'expressió en les neurones DA, no només amb el reporter *cat-2* sinó amb altres reporters de gens efectors, a més d'expressió en les mateixes neurones afectades en els mutants. Per tant, continuàrem validant el paper dels tres candidats.

El factor *unc-55* va ser el que menys fenotip va mostrar, afectant únicament a la neurona ADE, pel que ens vam plantejar que potser aquest factor podria estar interaccionant amb altres factors per a dirigir l'expressió dels reporters. Decidim creuar el mutant d'aquest gen amb el mutant hipomorf per al candidat *ast-1*. L'anàlisi va mostrar que tots dos FT interaccionen per a controlar l'expressió dels gens *bas-1* i *dat-1*, característics de la producció i recaptació de DA.

Finalment, vam voler respondre a la pregunta de si *unc-62*, *vab-3* i *unc-55*, s'uneixen directament a les seqüències reguladores dels gens efectors dopaminèrgics. Amb aquest fi vam dur a terme experiments de mutagènesi dirigida contra possibles motius d'unió per als nostres candidats en les seqüències reguladores mínimes dels gens *cat-2* i *dat-1*. En tots ells la mutació dels motius per als tres candidats va revelar un fenotip de pèrdua d'expressió, el que indica que *unc-62, vab-3* i *unc-55* controlen l'expressió dels gens efectors mitjançant la seua unió directa a l'ADN.

Totes aquestes dades ens porten a concloure que el col·lectiu de FT que regulen l'especificació de les neurones DA podria ser més ampli que l'inicialment descrit i que podria incloure als tres nous candidats *unc-62, vab-3* i *unc-55*.

4. Validació dels candidats requerits per a l'especificació de neurones serotonèrgiques

Les neurones 5-HT de *C. elegans* poden classificar-se en dues categories, aquelles que són capaços de fabricar serotonina (NSM, ADF i HSN) i aquelles que només són capaços d'emprar la serotonina que alliberen al mitjà les primeres (AIM, RIH i VC4/5). Amb l'excepció de AIM i RIH, no detectables en el nostre mètode de garbellat, vam obtindre candidats per a les altres quatre parelles. En el cas de NSM i HSN, que ja havien sigut prèviament estudiades, els FT involucrats en l'especificació d'aquestes neurones també apareixien entre els resultats del nostre garbellat de ARNi. No obstant açò, decidirem centrar el procés de validació en els candidats obtinguts per a la neurona ADF, de la qual no es coneixien fins al moment possibles FT que controlen la seua diferenciació.

El candidat amb un fenotip de pèrdua d'expressió més penetrant era *lag-1*, l'efector transcripcional de la ruta Notch de senyalització en *C. elegans*. Decidim analitzar l'expressió dels gens de la via serotonèrgica, encarregats de la síntesi i alliberament de serotonina, en el fons genètic mutant para aquest gen. Així vam poder comprovar que, en absència de l'expressió d'aquest factor, hi havia una pèrdua significativa d'expressió dels reporters avaluats.

En vista d'aquests resultats, vam voler comprovar si la senyalització mitjançant la via Notch estava també implicada en la diferenciació de la neurona ADF. No obstant açò, en avaluar l'expressió del gen *tph-1*, enzim limitant en la síntesi de serotonina, en el fons

genètic mutant per a Notch, no observàrem cap fenotip similar a l'observat en el mutant de *lag-1*, concloent que *lag-1* estaria actuant mitjançant una via independent de Notch per a dirigir l'especificació d'ADF.

S'ha descrit que l'ortòleg de *lag-1* en mamífers, Rbpj, pot actuar en una via d'acció independent de Notch mitjançant la seua unió a un factor de la família bHLH. Atès que un altre dels candidats obtinguts per a ADF era d'aquesta família, *hlh-14*, decidírem estudiar aquest factor (Johnson and MacDonald 2011). Els mutants per a aquest factor són letals i, a més, s'ha vist que l'absència d'aquest gen afecta a la generació de les neurones del llinatge de la neurona ADF. Per tant, decidírem avaluar mitjançant ARNi, que produeix un fenotip menys penetrant que el mutant nul, el paper d'aquest factor sobre els gens *tph-1* i *cat-1*. La pèrdua d'expressió observada era similar a la experimentada en el mutant de *lag-1*, pel que *hlh-14* podria ser efectivament el company de *lag-1* a l'hora de dirigir la diferenciació de'ADF.

El següent pas que duem a terme va ser la identificació de llocs funcionals d'unió de tots dos candidats a les seqüències reguladores dels gens de la síntesi de serotonina, mitjançant mutagènesi dirigida. Els resultats obtinguts van mostrar que tots dos factors tenien llocs d'unió funcionals, per la qual cosa la seua manera de regulació suggereix la seua unió directa a l'ADN.

Finalment, vam voler comprovar la rellevància d'aquests dos factors en la resposta funcional d'ADF mitjançant l'estudi de dos comportaments en els quals participa activament la neurona. El primer d'ells va ser la resposta de deceleració augmentada que exhibeixen els animals en acostar-se al menjar després d'haver passat per un període de dejuni. En aquest comportament, la neurona ADF detecta les molècules alliberades pels bacteris de les quals s'alimenten i, per tant, comença a alliberar serotonina per a fer que l'animal es detinga, la qual cosa s'aconsegueix amb l'alliberament de serotonina també per part de la neurona NSM en la fase final de la resposta. En els grups d'animals tractats amb ARNi contra *lag-1* i *hlh-14*, la deceleració inicial deguda a l'activitat d'ADF, no va tindre lloc.

La segona característica funcional d'aquesta neurona consisteix en la seua capacitat per a detectar compostos químics dissolts en l'ambient. Per a açò duem a terme experiments d'imatge de calci per a veure i quantificar l'activació de la neurona quan li l'exposava a un mitjà amb 10 mm de coure i pH4. Aquests experiments van revelar que la neurona no és capaç de respondre quan es tracta als animals amb ARNi contra *lag-1* i *hlh-14*.

Amb aquests dos tipus d'experiments vam poder comprovar que tant *lag-1* com *hlh-14* són essencials per a la diferenciació terminal de la neurona ADF i perquè puga dur a terme la senyalització i resposta a canvis en el mitjà que envolta a l'animal.

5. Validació dels candidats requerits per a l'especificació de neurones tiraminèrgiques i octopaminèrgiques

Aquests dos tipus de neurones, com ja hem esmentat, estan presents en invertebrats en lloc de les A i NA. Fins al moment no es coneixia cap FT implicat en la seua diferenciació, però el nostre garbellat d'ARNi va posar de manifest 22 candidats amb fenotip de pèrdua d'expressió del reporter *cat-1*. En general, observem que entre aquests candidats molts d'ells participaven en la via de senyalització per Wnt (*ceh-13, ceh-36, ceh-27* o *vab-7*), i que aquesta podria estar implicada en l'especificació de RIC i RIM (Zacharias et al. 2015).

Per a començar la validació, vam escollir el FT amb major fenotip, *zip-5*, i un altre gen les funcions del qual estan relacionades amb l'alliberament de octopamina, en el metabolisme de l'animal, el gen *pqm-1*.

En primer lloc, duem a terme l'anàlisi dels mutants per a tots dos gens, avaluant l'expressió dels reporters *tdc-1* i *tbh-1*, enzims necessaris per a la producció de TA i OA en el primer cas, i de OA en el segon. Els resultats van mostrar que *pqm-1* no afecta a l'expressió de cap dels dos reporters; no obstant açò, l'expressió de *tdc-1* en el mutant de *zip-5* va presentar una reducció significativa de l'expressió tant en RIC com en RIM. D'altra banda, en analitzar el patró d'expressió de tots dos factors, trobem que només *zip-5* es trobava expressat en les dues neurones, per la qual cosa finalment concloem que aquest FT podria ser un sòlid candidat a dirigir la diferenciació terminal de RIC i RIM.

Conclusions

En aquesta Tesi hem dut a terme un estudi exhaustiu dels factors de transcripció de *C. elegans* i hem donat un primer pas per a completar el mapa de factors reguladors que intervenen en l'especificació de les neurones monoaminérgicas. Aquests resultats ens han portat a les següents conclusions:

1. El fons genètic mutant *rrf-3 (pk1426)* ha sigut eficaç per a dur a terme un garbellat d'ARNi en *C. elegans* i ha permès obtindre diversos fenotips en la població de neurones MA observats mitjançant els reporters fluorescents *cat-1, dat-1* i *tph-1.*

2. La construcció d'una genoteca d'ARNi, completa i verificada, per a tots els FT de *C. elegans compta* amb 876 clons dels quals 548 procedeixen de la genoteca de Ahringer, 163 de Vidal i 165 generats en el nostre laboratori.
3. El procés de garbellat d'ARNi contra els FT de *C. elegans* revela 95 FT amb un fenotip visible dels quals el 84% ja haN sigut prèviament descrit i 91 FT amb fenotip en les neurones DA, d'entre els quals es va reproduir el resultat del 76% dels factors que havien sigut prèviament implicats en la diferenciació de neurones DT..
4. Les famílies de factors de transcripció més representades entre els resultats son homeodominis, ZF-C2H2, bHLH, bZIP i ZF-NHR. El fenotip més destacat es el de pèrdua d'expressió dels reporters. Molts dels candidats van presentar fenotip en més d'una neurona i es van obtenir candidats amb funcions definides en llinatge, regulació del dimorfisme sexual i heterocronia.
5. En la població de neurones DA s'ha descrit el paper de tres factors, *unc-62, vab-3* i *unc*-55 en la regulació de gens característics d'aquesta població; a més es van descobrir llocs d'unió funcionals dels tres factors en les regions reguladores mínimes dels gens *cat-2 i dat-1.*
6. Per a la neurona 5-HT ADF, s'ha descobert que el gen l*ag-1* està implicat en la regulació de la bateria de gens efectors a càrrec de la síntesi i alliberament de 5-HT, la qual du a terme mitjançant una via independent de Notch, gràcies a la seua cooperació amb el factor *hlh-14*. Tots dos, presenten llocs d'unió funcionals en els gens efectors per a la producció i alliberament de 5-HT.
7. En la neurona TA, RIM, i en la neurona OA, RIC, el factor de transcripció *zip-5* regula l'expressió del gen efector *tdc-1*, essencial per a la síntesi dels seus respectius neurotransmisors, convertint-lo en el primer FT descrit per a l'especificació d'aquestes dues neurones en C*. elegans*.

ANNEX

ANNEX

Table A.1. Terminal selectors in *C. elegans*

NEURONAL TERMINAL SELECTORS IN *C. elegans*

Neuron	NT	Type	Terminal Selectors	Neuron	NT	Type	Terminal Selectors
ADE	DA	sensory	*ast-1, ceh-43, ceh-20/ceh-40*	IL2	Ach	sensory	*unc-86, cfi-1*
ADL	Glu	sensory	*lin-11*	OLL	Glu	sensory	*sox-2, vab-3*
AFD	Glu	sensory	*ttx-1, ceh-14*	PDA	Ach	motor	*unc-3*
AIA	Ach	inter	*ttx-3*	PDB	Ach	motor	*unc-3*
AIB	Glu	inter	*unc-42*	PDE	DA	sensory	*ceh-43, ceh-20/ceh-40*
AIM	Glu, 5-HT	inter	*unc-86, ceh-14*	PHA	Glu	sensory	*ceh-14*
AIY	Ach	inter	*ttx-3, ceh-10*	PHB	Glu	sensory	*ceh-14*
AIZ	Glu	inter	*unc-86, ceh-14*	PHC	Glu	sensory	*ceh-14*
ALA	GABA	sensory	*ceh-14, ceh-17*	PLM	Glu	sensory	*unc-86, mec-3*
ALM	Glu	sensory	*unc-86, mec-3*	PQR	Glu	sensory	*unc-86, egl-13, ahr-1*
AQR	Glu	sensory	*unc-86, egl-13, ahr-1*	PVC	Ach	inter	*ceh-14, cfi-1*
AS	Ach	motor	*unc-3*	PVD	Glu	sensory	*unc-86, mec-3*
ASE	Glu	sensory	*che-1*	PVM	(-)	sensory	*unc-86, mec-3*
ASG	Glu	sensory	*lin-11, ceh-37*	PVN	Ach	inter	*unc-3, ceh-14*
ASH	Glu	sensory	*unc-42*	PVP	Ach	inter	*lin-11, unc-30*
ASJ	Ach	sensory	*sptf-1*	PVQ	Glu	inter	*pag-3, zag-1*
ASK	Glu	sensory	*ttx-3*	PVR	Glu	inter	*unc-86, ceh-14*
AUA	Glu	inter	*ceh-6*	RID	(-)	inter	*lim-4*
AVG	Ach	inter	*lin-11, ast-1*	RIH	Ach, 5-HT	inter	*unc-86*
AVK	(-)	inter	*unc-42, fax-1*	RIS	GABA	inter	*nhr-67, lim-6*
AVL	GABA	motor	*nhr-67, lim-6*	RIV	Ach	inter	*unc-42*
AVM	Glu	sensory	*unc-86, mec-3*	RMD	Ach	motor	*unc-42*
AWA	(-)	sensory	*odr-7*	RME	GABA	motor	*nhr-67, ceh-10, tab-1*
AWB	Ach	sensory	*lim-4, sox-2*	SAA	Ach	inter	*sox-3*
AWC	Glu	sensory	*ceh-36, sox-2*	SAB	Ach	motor	*unc-3*
BAG	Glu	sensory	*ets-5, ceh-37, egl-13, egl-46*	SMB	Ach	motor	*lim-4*
BDU	(-)	inter	*pag-3, zag-1*	SMD	Ach	motor	*unc-42*
CEP	DA	sensory	*ast-1, ceh-43, ceh-20/ceh-40*	URA	Ach	sensory	*unc-86, cfi-1*
DA	Ach	motor	*unc-3*	URB	Ach	sensory	*unc-86*
DB	Ach	motor	*unc-3*	URX	Ach	sensory	*unc-86, ahr-1, egl-13*
DD	GABA	motor	*unc-30*	URY	Glu	sensory	*vab-3*
DVC	Glu	inter	*ceh-14*	VA	Ach	motor	*unc-3*
FLP	Glu	sensory	*unc-86, mec-3*	VB	Ach	motor	*unc-3*
HSN	Ach, 5-HT	motor	*unc-86, sem-4*	VD	GABA	motor	*unc-30*
IL1	Glu	sensory	*sox-2, vab-3*				

Tabla A.1. Main TFs described as terminal selectors in *C. elegans* in neurons. Adapted from *Hobert 2016* and *Carla Lloret PhD manuscript*.

Table A.2. *C. elegans* strains used in this Thesis

Table A.2. *C. elegans* strains used in this Thesis

Strain Name	Genotype	Source
OH7196	*ast-1(hd1)rol-6(e187)II; vtIs1 (dat-1::gfp)V*	Harald Hutter
NFB772	*cat-1::mCherry I; nIs60[vab-3::GFP + lin-15(+)]*	This work
CE1255	*cep-1(ep347) I*	CGC
NFB1774	*cep-1(ep347) I; nIs118 (cat-2::gfp)*	This work
TG12	*cep-1(lg12501) I; unc-119(ed4) III; gtIs1[CEP-1::GFP + unc-119(+)]*	CGC
BC1282	*dpy-18(e364)/eT1 III; unc-62(s472) unc-46(e177)/eT1 V*	CGC
FX14560	*dro-1 (tm4702) II; eTv1 (III/V)*	Mitani (Japan)
NFB50	*eri-1(mg366) (IV);lin-15b (n744) (X); otIs199 (I) (cat-2::gfp,rgfef-1::red)*	This work
NFB1788	*gtIs1[CEP-1::GFP + unc-119(+)] III; otIs181*	This work
EM66	*him-5(e1490) V; vab-3(bx23) X.*	CGC
EL301	*lag-1(om13) IV.*	CGC
NFB1332	*lag-1(om13)IV; otex2435 [bas-1prom1::gfp (50ng/ul), rol6]*	Dr. Maicas
NFB1770	*lag-1(q385)/dpy-13(e184) unc-24(e138) IV; otex2433 [bas1prom1 gfp (50ng/ul), rol6]*	Dr. Maicas
JK1313	*lin-12(n941) glp-1(q46)/dpy-19(e1259) unc-69(e587) III.*	CGC
MT8457	*lin-15B&lin-15A(n765) X; nIs60[vab-3::GFP + lin-15(+)].*	CGC
NFB1785	*mef-2 (gv1) I; nIs118 (cat-2::gfp)*	This work
KM134	*mef-2(gv1) I; ayIs.*	CGC
VC1402	*mef-2(gk633) I*	CGC
NFB1775	*mef-2(gk633) I; nIs118 (cat-2::gfp)*	This work
VC1172	*nhr-129&nhr-168(gk538) V.*	CGC
MT9971	*nIs107 [tbh-1::GFP + lin-15(+)] III.*	CGC
unknown	*nIs118 (cat-2::gfp)*	This work
NFB25	*nre-1(hd20), lin15b(hd126) X; otIs199 (I) (cat-2::gfp,rgfef-1::red)*	This work
NFB1838	*otIs181 III; vlcEx1074 [dro-1p::gfp, rol-6]*	This work
NFB1022	*otIs181 III; vlcEx498 (prom-unc-55::gpf; rol-6)*	This work
NFB1016	*otIs181 III; vlcEx545(vab-3fosmid::gfp + ttx-3::mCherry + rol-6)*	This work
NFB1813	*otIs181 III; wgIs301 [mef-2::TY1::EGFP::3xFLAG + unc-119(+)]*	This work
NFB897	*otIs181 III; wgIs600*	This work
OH7193	*otIs181[dat-1::mCherry + ttx-3::mCherry]III; him-8(e1489) IV*	This work
NFB771	*otIs181[dat-1::mCherry + ttx-3::mCherry]III; nIs60[vab-3::GFP + lin-15(+)]*	This work
NFB752	*otIs181[dat-1::mCherry + ttx-3::mCherry]III; otIs224[cat-1::gfp] V; lin-15B(n765) X; vsIs97[tph-1p::DsRed2 + lin-15(+)]X*	This work
NFB876	*otIs181[dat-1::mCherry + ttx-3::mCherry]III; vab-3(ot346)X*	This work
OH7547	*otIs199 [cat-2::GFP + rgef-1(F25B3.3)::dsRed + rol-6(su1006)] I*	This work
NFB885	*otIs199 [cat-2::GFP + rgef-1(F25B3.3)::dsRed + rol-6(su1006)] I; unc-62(e644) dpy-11(e224) V*	This work

NFB883	*otIs199 [cat-2::GFP + rgef-1(F25B3.3)::dsRed + rol-6(su1006)] I; unc-62(e917) V*	This work
NFB881	*otIs199 [cat-2::GFP + rgef-1(F25B3.3)::dsRed + rol-6(su1006)] I; unc-62(mu232) muIs35 V*	This work
NFB826	*otIs199 [cat-2::GFP + rgef-1(F25B3.3)::dsRed + rol-6(su1006)]; vab-3 (ot346) X.*	This work
NFB826	*otIs199 [cat-2::GFP + rgef-1(F25B3.3)::dsRed + rol-6(su1006)]; vab-3 (ot346) X.*	This work
NFB1835	*otIs199 I; dro-1 (tm4702) II; eTv1 (III/V)*	This work
NFB1001	*otIs199; wpSi6 II; eri-1(mg366) IV; rde-1(ne219) V; lin-15B(n744) X*	This work
OH8480	*otIs221 (cat-1::gfp) III; him-8 (e1489) IV*	CGC
NFB1772	*otIs221(cat-1::gfp) III; nhr-129&nhr-168(gk538) V*	This work
NFB1330	*otIs221[cat-1::gfp]III; lag-1(om13)IV*	Dr. Maicas
NFB1759	*otIs221[cat-1::gfp]III; lag-1(q385)/dpy-13(e184) unc-24(e138) IV*	Dr. Maicas
NFB643	*otIs221[cat-1::gfp]III; rrf-3 (pk1426)II*	This work
OH8249	*otIs224 [cat-1(2493bp)::GFP] V*	CGC
NFB884	*otIs224[cat-1::gfp] III; unc-62(e644) dpy-11(e224) V*	This work
NFB874	*otIs224[cat-1::gfp]III; vab-3(ot346)X*	This work
OH8250	*otIs225 [cat-4::GFP] II*	CGC
NFB1725	*otIs225(cat-4::gfp) II; zdIs10(tdc-1::mCherry)IV; otIs199(cat-2::gfp + rol-6) I*	This work
NFB1760	*otIs225[cat-4::gfp]II; lag-1(q385)/dpy-13(e184) unc-24(e138) IV.*	Dr. Maicas
NFB1200	*otIs225[cat-4::gfp]II; unc-62 (e917) V*	This work
NFB1344	*otIs225[cat-4::gfp]II; vab-3(bx23) X.*	This work
NFB872	*otIs225[cat-4::gfp]II; vab-3(ot346)X*	This work
OH8251	*otIs226(bas-1::gfp)IV*	CGC
NFB1199	*otIs226[bas-1::gfp]IV; unc-62 (e917) V*	This work
NFB873	*otIs226[bas-1::gfp]IV; vab-3(ot346)X*	This work
NFB1210	*otIs236 (asic-1prom::gfp); unc-62 (e917) V*	This work
OH8510	*otIs236(asic-1prom1::gfp)*	This work
NFB1201	*otIs259 [dat-1p::gfp + rol-6 (su1006)]; unc-62 (e917) V*	This work
NFB177	*otIs259(dat-1::gfp)*	This work
NFB1812	*otIs266 (cat-1prom1::mcherry); Ex (zip-5::gfp)*	This work
NFB1736	*otIs266 [cat-1p::mCherry] I; rrf-3 (pk1246) II; nIs107 [tbh-1::GFP + lin-15(+)] III;*	This work
NFB1614	*otIs517[(tph-1::SL2::YFP::H2B),ttx-3::mCherry, rol-6] III; lin-12(n941) glp-1(q46)/dpy-19(e1259) unc-69(e587) III*	Dr. Maicas
NFB1340	*otIs517[(tph-1::SL2::YFP::H2B),ttx-3::mCherry, rol-6]; lag-1(om13)IV*	Dr. Maicas
NFB689	*otIs517[(tph-1::SL2::YFP::H2B),ttx-3::mCherry, rol-6]; rrf3 (pk1426) II*	This work
NFB911	*oxIs364 [unc-17p::channelrhodopsin::mCherry + lin-15(+) + Litmus] X; sEx10929 [rCes C27H5.3::GFP + pCeh361]*	This work
NFB1786	*pqm-1 (ok485) II; nIs107 (tbh-1::gfp) III*	This work
RB711	*pqm-1(ok485) II*	CGC
NFB1773	*pqm-1(ok485) II; zfIs10(tdc-1::m-cherry)IV*	This work
WM27	*rde-1(ne219) V*	CGC

NFB1366	*rrf-3 (1426) II; vlcEx119(cat-1prom37::gfp (50ng/ul),rol-6)*	This work
NFB1367	*rrf-3 (1426) II; vlcEx149(cat-1prom14::gfp (50ng/ul),rol-6)*	This work
NFB1364	*rrf-3 (1426) II; vlcEx15(bas-1prom7::gfp (50ng/ul, rol-6))*	This work
NFB1365	*rrf-3 (1426) II; vlcEx159(cat-4prom6::gfp (50ng/ul),rol-6)*	This work
NFB1443	*rrf-3 (pk1426) II; Ex[psrh-142::TeTx-mCherry punc122::GFP]*	This work
NFB1444	*rrf-3 (pk1426) II; Ex[psrh-142::TeTx-mCherry punc122::GFP]*	This work
NFB1731	*rrf-3 (pk1426) II; nIs107 [tbh-1::GFP + lin-15(+)] III.*	This work
NFB676	*rrf3 (pk1426) II; vlcEx365(tph-1 prom17::GFP)*	This work
NFB745	*rrf-3 (pk1426) II; vlcEx400 [cat-1p3::iGFP (100 ng/uL); txt-3::mCherry (30 ng/uL)]*	This work
NFB1363	*rrf-3 (pk1426) II; vlcEx809(srh-142prom::gpf, rol-6 (50 ng/microL)*	This work
NFB1445	*rrf-3 (pk1426); lite-1(ce314); Ex[Psrh-142::mcherry::SL2::GCaMP3 punc122::RFP]*	This work
NFB1447	*rrf-3 (pk1426); lite-1(ce314); Ex[ptph-1:::Chr2-mCherry punc-122::GFP]*	This work
NFB1448	*rrf-3 (pk1426); lite-1(ce314); Ex[ptph-1:::Chr2-mCherry punc-122::GFP]*	This work
NFB1449	*rrf-3 (pk1426); unc-13 (e51); lite-1(ce314); Ex[Psrh-142::mcherry::SL2::GCaMP3 punc122::RFP]*	This work
NFB51	*rrf-3(pk1426) (II); vtIs1 (V); otIs199 (I) (cat-2::gfp,rgfef-1::red)*	This work
NFB49	*rrf-3(pk1426) (II); zdIs13(IV) (tph-1::gfp)*	This work
NL2099	*rrf-3(pk1426) II*	CGC
NFB48	*rrf-3(pk1426)(II); otIs199 (I) (cat-2::gfp,rgfef-1::red)*	This work
NFB753	*rrf-3(pk1426)II; otIs181[dat-1::mCherry + ttx-3::mCherry]III; otIs224[cat-1::gfp] ¿V?; lin-15B(n765) X; vsIs97[tph-1p::DsRed2 + lin-15(+)]X*	This work
LC108	*uIs69 [pCFJ90(myo-2p::mCherry) + unc-119p::sid-1]*	CGG
NFB600	*uIs69 [pCFJ90(myo-2p::mCherry) + unc-119p::sid-1] (V); rrf-3(pk1426) (II); zdIs13(tph-1::gfp)(IV)*	This work
UL2177	*unc-119 (ed3); Ex [zip-5:gfp; unc-119 +]*	Ian A. Hope
OP340	*unc-119(ed3) III; wgIs340 [nhr-129::TY1::EGFP::3xFLAG + unc-119(+)].*	CGC
OP201	*unc-119(tm4063) III; wgIs201 [pqm-1::TY1::EGFP::3xFLAG(92C12) + unc-119(+)]*	CGC
OP301	*unc-119(tm4063) III; wgIs301 [mef-2::TY1::EGFP::3xFLAG + unc-119(+)]*	CGC
OP634	*unc-119(tm4063) III; wgIs634 [zip-10::TY1::EGFP::3xFLAG + unc-119(+)]*	CGC
MT7929	*unc-13(e51) I*	CGC
NFB1023	*unc-55 (e1170) I; ast-1 (hd1); otIs226 (bast-1::gfp) IV*	This work
NFB1002	*unc-55 (e1170) I; ast-1(ot417)II; vtIs1*	This work
CB1170	*unc-55(e1170) I*	CGC
NFB998	*unc-55(e1170) I; ast-1(hd1)rol-6(e187)II; vtIs1 [dat-1p::GFP + rol-6(su1006)] V*	This work
NFB863	*unc-55(e1170) I; nIs118 (cat-2p::gfp)*	This work
NFB769	*unc-55(e1170) I; otIs1(dat-1::gfp) V.*	This work

NFB770	*unc-55(e1170) I; otIs224 (cat-1::gfp) III.*	This work
NFB864	*unc-55(e1170) I; otIs225[cat-4::gfp]II*	This work
NFB865	*unc-55(e1170) I; otIs226[bas-1::gfp]IV*	This work
CB2030	*unc-62(e644) dpy-11(e224) V*	CGC
CZ1072	*unc-62(e917) V*	CGC
NFB838	*vab-3 (ot346) X*	This work
NFB1729	*vlcEx1046(vab-3fosmid::gfp + ttx-3::mCherry + rol-6)*	This work
NFB1730	*vlcEx1047(vab-3fosmid::gfp + ttx-3::mCherry + rol-6)*	This work
NFB1798	*vlcEx1061(bas-1prom91::gfp (50ng/ul, rol-6))*	Dr. Maicas
NFB1836	*vlcEx1074 [dro-1p::gfp, rol-6]*	This work
NFB1837	*vlcEx1075 [dro-1p::gfp, rol-6]*	This work
NFB396	*vlcEx224(tph-1prom42::gfp (50ng/ul),rol-6)*	Dr. Maicas
NFB397	*vlcEx225(tph-1prom42::gfp (50ng/ul),rol-6)*	Dr. Maicas
NFB420	*vlcEx239(cat-1prom72::gfp (50ng/ul),rol-6)*	Dr. Maicas
NFB421	*vlcEx240(cat-1prom72::gfp (50ng/ul),rol-6)*	Dr. Maicas
NFB610	*vlcEx325(bas-1prom74::gfp (50ng/ul),rol-6)*	Dr. Maicas
NFB611	*vlcEx326(bas-1prom74::gfp (50ng/ul),rol-6)*	Dr. Maicas
NFB620	*vlcEx331(cat-1prom77::gfp (50ng/ul),rol-6)*	Dr. Maicas
NFB621	*vlcEx332(cat-4prom69::gfp (50ng/ul),rol-6)*	Dr. Maicas
NFB622	*vlcEx333(cat-4prom69::gfp (50ng/ul),rol-6)*	Dr. Maicas
NFB631	*vlcEx341(cat-1prom77::gfp (50ng/ul),rol-6)*	Dr. Maicas
NFB737	*vlcEx395(cat-1prom81::gfp (50ng/ul),rol-6)*	Dr. Maicas
NFB739	*vlcEx397(cat-1prom81::gfp (50ng/ul),rol-6)*	Dr. Maicas
NFB740	*vlcEx398(cat-1prom80::gfp (50ng/ul),rol-6)*	Dr. Maicas
NFB741	*vlcEx399(cat-1prom80::gfp (50ng/ul),rol-6)*	Dr. Maicas
NFB777	*vlcEx414(Mdat-1prom1::gfp (50ng/ul),rol-6)*	This work
NFB778	*vlcEx415(Mdat-1prom1::gfp (50ng/ul),rol-6)*	This work
NFB820	*vlcEx454(Mdat-1prom2::gfp (50ng/ul),rol-6)*	This work
NFB821	*vlcEx455(Mdat-1prom2::gfp (50ng/ul),rol-6)*	This work
NFB822	*vlcEx456(Mdat-1prom3::gfp (50ng/ul),rol-6)*	This work
NFB823	*vlcEx457(Mdat-1prom3::gfp (50ng/ul),rol-6)*	This work
NFB833	*vlcEx461(Mcat-2prom2::gfp (50ng/ul),rol-6)*	This work
NFB904	*vlcEx49[Mcat-2prom-1::gfp, rol-6 (50 ng/microL)]*	This work
NFB903	*vlcEx490[Mcat-2prom-1::gfp, rol-6 (50ng/microL)]*	This work
NFB905	*vlcEx492[Mcat-2prom-3::gfp, rol-6 (50 ng/microL)]*	This work
NFB906	*vlcEx493[Mcat-2prom-3::gfp, rol-6 (50 ng/microL)]*	This work
NFB933	*vlcEx498 (prom-unc-55::gfp; rol-6)*	This work
NFB932	*vlcEx498 (prom-unc-55::gpf; rol-6)*	This work
NFB1007	*vlcEx539(Mdat-1prom4::gfp (50ng/ul),rol-6)*	This work
NFB1008	*vlcEx540(Mdat-1prom4::gfp (50ng/ul),rol-6)*	This work
NFB1009	*vlcEx541 (Mdat-1prom5::gfp (50ng/ul),rol-6)*	This work
NFB1010	*vlcEx542(Mdat-1prom5::gfp (50ng/ul),rol-6)*	This work
NFB1011	*vlcEx543(Mdat-1prom6::gfp (50ng/ul),rol-6)*	This work
NFB1012	*vlcEx544(Mdat-1prom6::gfp (50ng/ul),rol-6)*	This work
NFB1013	*vlcEx545(vab-3fosmid::gfp + ttx-3::mCherry + rol-6)*	This work
NFB1019	*vlcEx549(Mdat-1prom7::gfp (50ng/ul),rol-6)*	This work

NFB1019	*vlcEx549(Mdat-1prom7::gfp (50ng/ul),rol-6)*	This work
NFB1021	*vlcEx551 (Mdat-1prom8::gfp (50ng/ul),rol-6)*	This work
NFB1022	*vlcEx552 (Mdat-1prom8::gfp (50ng/ul),rol-6)*	This work
NFB1023	*vlcEx553 (Mdat-1prom9::gfp (50ng/ul),rol-6)*	This work
NFB1024	*vlcEx554 (Mdat-1prom9::gfp (50ng/ul),rol-6)*	This work
NFB1093	*vlcEx602 (Mcat-2prom-2::gfp, rol-6)*	This work
NFB1101	*vlcEx607(cat-4prom71::gfp (50ng/ul),rol-6)*	Dr. Maicas
NFB1102	*vlcEx608(cat-4prom71::gfp (50ng/ul),rol-6)*	Dr. Maicas
NFB1320	*vlcEx782(cat-4prom73::gfp (50ng/ul),rol-6)*	Dr. Maicas
NFB1321	*vlcEx783(cat-4prom73::gfp (50ng/ul),rol-6)*	Dr. Maicas
NFB1322	*vlcEx784(cat-1prom90::gfp (50ng/ul),rol-6)*	Dr. Maicas
NFB1323	*vlcEx785(cat-1prom90::gfp (50ng/ul),rol-6)*	Dr. Maicas
NFB1360	*vlcEx807(bas-1prom90::gfp (50ng/ul, rol-6))*	Dr. Maicas
NFB1361	*vlcEx808(bas-1prom90::gfp (50ng/ul, rol-6))*	Dr. Maicas
NFB1783	*vlcIs8[tph-1::T2A::mNeonGreen]II; lag-1(om13) IV*	Dr. Maicas
NFB1841	*vsIs97 [tph-1p::DsRed2 + lin-15(+)] X; vlcEx1076 [zip-10p::gpf, rol-6]*	This work
BY200	*vtIs1 [dat-1p::GFP + rol-6(su1006)] V*	This work
OH4254	*vtIs1 V; vab-3(ot266) X.*	CGC
NFB875	*vtIs1(dat-1::gfp, rol-6)V; vab-3(ot346)X*	This work
OH7058	*vtIs1(dat-1p::GFP + rol-6); vsIs33 (dop-3::RFP); vab-3(ot346)X*	CGG
NFB1831	*wgIs339 [nhr-129::TY1::EGFP::3xFLAG + unc-119(+)]wgIs339 [nhr-129::TY1::EGFP::3xFLAG + unc-119(+)]; otIs266 (cat-1p::mCherry)II*	This work
NFB1832	*wgIs340 [nhr-129::TY1::EGFP::3xFLAG + unc-119(+)]wgIs339 [nhr-129::TY1::EGFP::3xFLAG + unc-119(+)]; otIs266 (cat-1p::mCherry)II*	This work
SD1871	*wgIs600 [unc-62::TY1::EGFP::3xFLAG(92C12) + unc-119(+)]*	CGC
NFB1833	*wgIs634 [zip-10::TY1::EGFP::3xFLAG + unc-119(+)]; vsIs97 [tph-1p::DsRed2 + lin-15(+)] X*	This work
XE1474	*wpSi6 II; eri-1(mg366) IV; rde-1(ne219) V; lin-15B(n744) X.*	CGC
NFB14	*zfIs10(tdc-1::mCherry)IV*	This work
NFB1811	*zfIs10(tdc-1::mCherry)IV; Ex (zip-5::gfp)*	This work
NFB1787	*zfIs10(tdc-1::mCherry)IV; wgIs201 [pqm-1::TY1::EGFP::3xFLAG(92C12) + unc-119(+)]*	This work
VC1392	*zip-5 (gk646)V*	CGC
NFB1783	*zip-5 (gk646); nIs107 [tbh-1::GFP + lin-15(+)] III*	This work
NFB1784	*zip-5 (gk646); zfIs10 (tdc-1::mCherry) IV*	This work

Table A.3. RNAi clones *de novo* generated for the TF RNAi screen

Table A.3. RNAi clones *de novo* generated for TF RNAi screen

Gene name	DBD	Length	Forward primer	Reverse primer
C46C2.7	AP-2	948	ttgtcttgatgccagctttcg	tccaattatcttcggttgacg

arid-1	ARID - RBP	1460	accactaaccttgtcatcgtc	tgagcaagtcgatgaagaag
swsn-7	ARID - RFX	1575	aatggaaccgtggaagtgtgc	tcgactctttcatcggagctg
wrm-1	Beta-catenin/ Armadillo	1051	attgtgacggtagaagtgctg	tgtacccgcacaaagattcattc
bar-1	Beta-catenin/ Armadillo	1300	tcaccctgaattaggtaacg	gtgcaacaaatatccgactg
hmp-2	Beta-catenin/ Armadillo	950	tgctgtagatggagttccaatg	attgtgattagggcgcatttg
hlh-17	bHLH	1200	gtactgtaactttggaggcggag	aactgggagaccaatatactcagc
lin-22	bHLH	650	ttccgtaggcaggtttgaatgag	aaactaggccgaaaccctgc
hlh-4	bHLH	953	aaatggcaagatgtgcttcc	tctgaacagccactgcacat
hlh-14	bHLH	1000	tgccagaaatgagagagaacg	agtatggagacccgtaaatgc
hlh-16	bHLH	938	gattatgtcttcggaatcac	catgttgatgtgatgcagtc
ZK177.11	bHLH	262	ttctccagagtggaacgtcag	tcaagtatcatgtgttcagtccatc
Y44A6D.3	Brinker	1302	atccaggcactccgtatagtc	ggattgtttgattcggcaacg
cebp-2	bZIP	416	tgcaatttcaagcgatgagtgg	ttgttatctacacggcggaagaag
atf-8	bZIP	1615	agcctatgtgctcatccttcaac	gttgctgactagcactgtactcc
C32E8.1	bZIP	400	gaagcaagaggattgcagaagc	gcattcggtgcaaattgtgtg
C32E8.1	bZIP	400	gaagcaagaggattgcagaagc	gcattcggtgcaaattgtgtg
zip-9	bZIP	785	ttgatcttcttcccaagggtg	taacaagagtttgtccgggag
F41H10.4	bZIP	814	atgaagctgcaaagaaccacg	ttcacggacatctgaatctcg
maf-1	bZIP	1039	agaaacgtggtgatgcaatgg	gtattgttgttggcgcaatcg
Y60A3A.25	bZIP	892	tggctactcgtgtatgttctcg	acaaccgcttgctaaagtacc
hpo-39	bZIP	716	agacggatttcttcgctttctc	atcgttggtcatatcgcgtc
egrh-3	C2H2 ZF	1111	tttccaacgacgtttagccag	atttggctgctgtgagcttc
bnc-1	C2H2 ZF	854	tacatacgtggtgtcaggatgc	taaggttagtgactcgggcatg
ztf-9	C2H2 ZF	696	aattcgcccttgtcagtcac	gtcaataaccatgtcgcagtcg
Y75B8A.6	CxxC	1068	cctcgtaatggagtttcacagc	cttgtcccttcatatcctgtgc
ets-4	ETS	1180	ttcagccgcctagaaactgt	acaccaaacgctgcttcttt
ets-10	ETS	300	tagtttacgcaatgcccagc	tgaatccagaggcatgttca
ceh-87	HD	1023	ttctggagtcttcgcaggttgag	gcgccggtgtttgttattgc
ceh-90	HD	1778	aaatagccgagttagggcttc	tttgcgtccgatactctgattg
ceh-99	HD	1261	ttcagattcgcagatggttc	acatttctaaagttcggctccag
ceh-63	HD	1014	taagaacatcaaaccgccacc	tcgtcagacttcttcatcatgc
ceh-92	HD	435	aagcaagataaatggccgctg	aaacgaacccgttgagaaacc
nsy-7	HD	930	acagacgaaatctaccgaacc	tagttgtgtcaagccgtcgtc
ceh-93	HD - 2domains	1308	gaaggcaacaacactcacaag	ggtgatgtgggaaactccaag
ceh-44	HD - CUT	381	tcgcgtagaaaactgtgacg	tgtttctagatccccgaacg

ceh-16	HD - HOX	1159	agaagatatgcgccgagaaagg	gcctaccgtaaccgcctaac
ceh-62	HD - HOX	1178	taatgtcagtagtcggcagc	ttgggtcgaataatggaggag
ceh-75	HD - NK	684	attgtgttgactgccattggtg	tgctgctcatcttcattgagtc
ceh-1	HD - NK	786	ggctttcgtgtcgaagatttgc	gccaagtttcaagctcatgtg
ceh-30	HD - NK	1474	agttctcttccggggtcaat	tcatcatccacgaacagcat
ceh-9	HD - NK	933	ctgacttgctcttccaactacttcaaccc	cacaatctgatcatccggtatttctcc
pha-2	HD - NK	526	gcagcggatcactaatcataacg	accgtactcttattgacccattcc
ceh-31	HD - NK	960	tagatccatctcctacctcc	caggagatactgatggtgattc
ceh-5	HD - NK	662	cttgattcaactatgccttctgc	tgatagaaatgcagcggctgtc
ceh-83	HD - POU - 2 domains	1161	tgagctgagctattccttgg	cacattcagcctacttcatc
ceh-84	HD - PRD	1142	cttccagaagtaaagcgcgactc	gatttcttagtccgggtaacgctc
ttx-1	HD - PRD	1186	aaacctagtcaatatgggtgtc	aaaccggagagatttgtgtg
pax-2	HD - PRD	1182	tttgtagcagggctgtttgg	cattggagttctcattgcccag
sem-2	HMG box	1950	aaaccgcccaacttcatgctg	ctacatcctaccgtactcccaaac
ZC247.1	HTH-Pipsqueak	1124	tgtttcaatcagcgcgagaag	ttgtcttgctcggcgaattg
madf-11	MADF	1310	ttggacgacaaggtgtattggtgg	acgtgtgactctacctccagcatc
madf-5	MADF	1130	agaccgactacttgcacaaac	ttgagccattcaagagcaacc
madf-3	MADF - 2 domains	695	tctcgatgtgctcgaagtctg	aattaggagcaggtgtagacggag
flt-1/baz-2	MBD	943	tctggaagaccaatgtgcatg	aaactgattccagcacgtcc
sma-4	MH1/SMAD	952	gaaggaaggttatgtcttggagc	ccagtatttgtagaggacggtg
K11D2.5	mTERF	966	tcgttgatcgccacaaattcc	aaccgggtgctaatttccatg
chd-7	MYB	2000	cactatgctcattgccggtgc	tgacggctgctgttgttgttg
R151.8	MYB	1224	aaagagacaaaccaacggcag	tttcttcttgggcgtggtcttc
nhr-61	NHR	1194	tgcaaagccaaccgacgaacg	atcggtgatcccgaagctcttg
nhr-146	NHR	873	gaagctgtgacgtaagcagtg	ttgaaatcaagttgcccagtcg
nhr-286	NHR	1032	gtgaacgtgaagtaaggcagtg	gttcacggaagagttcttgtcg
ZK1037.13	NHR	1112	ggttgaggaaacgtaagggaag	tcggctatgttcggcatttg
myrf-1	p53	922	ttacagggcctcgacaatgg	tgttggttggacacaagtgg
F19F10.9	SART-1	1034	agagatcaaggaggatggttgg	atcaagagttcccagtggagtg
Y73E7A.1	Sox	709	gtgcctcatttcggcttgatc	tgacgagaaaccgaaaccgag
chpf-2	STAT	697	tctttaacggcgcacacatg	tcctcgcgtgtgatgtagttg
tbx-37	T-box	2160	tgcacctctccttctggaattg	ctgctgccagtaccattgtctc
tbx-7	T-box	899	tcttttcttttccagcgtcc	gaactatgtgaaaccgggga
tbx-43	T-box	800	aacttaggccaccattcttgtc	agtctggtgatgaattggacg
tbx-7	T-box	899	tcttttcttttccagcgtcc	gaactatgtgaaaccgggga

tbx-2	T-box	954	tcatcgctgttacggcttatc	atcgtaacggatgatgagctg
tlf-1	TBP	742	agtgaggcggattgtaaacgag	ttcttcagatgggtctcgacg
egl-44	TEA/ATTS	1057	actcgttctactcaagtcgtg	ctggttgcacatgatgagac
C30G4.4	TSC-22/dip/bun	1500	ccctcctatatcgtgtgtctgtttg	aatcaggaatcaatcgagggacg
nhr-273	Unknown	746	agatattcgatgtatgtgccgtgc	tcataggatggcttgaagagtc
dpy-27	Unknown	1157	ggtgttcgggattatgcgatg	attggtggtggagatggagttg
ets-8	WH - ETS	1993	tctcacctatcttatccgtccagc	aaattggagcaaagtaggtcgtgg
fkh-9	WH - Fork Head	1935	agttcagagttcagcaacctcc	gtgcaaactaggagcacaacc
efl-1	WH-TDP	1500	tcgtttccaaccatgagctac	tatgaattgtgtgggcactgtgg
grl-25	WT1 - 2 domains	1400	gcgcccatttcacaacactataac	acagtgctcacgattctctcc
bed-1	ZF - BED	1380	cacctcttccatcgagcactg	ttggttattcttcgtgctcttgg
C27A2.7	ZF - C2H2	836	ttcctgaacaccatcagttcc	aatgactggagtagcttgatgag
D2092.10	ZF - C2H2	754	gaatgttcatggtgagtcagg	gcattagctttcaccaactcag
egrh-2	ZF - C2H2	1071	atttgcgcgatgtgatgaacg	tgtctatcggttcgcaaatgtc
C02F5.12	ZF - C2H2 - 1 finger	1692	agaaaacgattggttgtccg	tggagaaccacacattccaa
C52E12.1	ZF - C2H2 - 1 finger	614	cagtaacaaaatcgctggca	cgtgctcatttgctctgtgt
F52B5.7	ZF - C2H2 - 1 finger	1866	cctatcaccgcttcttcgcac	tcatcactttcaacaccggcatc
K11D12.12	ZF - C2H2 - 1 finger	1200	cgtaacaacgaagcatctggaac	atccgctggtttctaagcgac
Y37F4.6	ZF - C2H2 - 1 finger	1400	tttccagactcacagaggtcttc	ctgacacagattgagcgggac
T06G6.5	ZF - C2H2 - 1 finger	780	aaatctctcgatatgccagcag	gtgtttacatggtaagtggcgag
W04D2.4	ZF - C2H2 - 1 finger	1240	aagttgtcgaaacgcagacg	cgctaagttcgtcttcgattgg
saeg-1	ZF - C2H2 - 1 finger, MYB	2078	acgtgggacaccactcaatatc	ttgttgttgtggagtgagtggag
K04C1.3	ZF - C2H2 - 1 finger, WH - Fork Head	947	acggattcgatgtgctagtg	gagatgacgaaagtatggcag
Y48G8AL.10	ZF - C2H2 - 12 fingers	1400	aatgatatgcgcctcaacctg	gttgggcattccgagattac
lin-13	ZF - C2H2 - 15 fingers	1730	atcgtgtaagacttgccactgc	tttctggttctccaatggctgc
nhr-202	ZF - C2H2 - 2 fingers	438	ccaatttcactctacaactcacc	tggtcttggtagatgaattgctgg
Y17G7B.22	ZF - C2H2 - 2 fingers	2150	cccggtgcaagaaacacttaac	agccaaatgctgctccaacac
Y71A12B.8	ZF - C2H2 - 2 fingers	721	acattgccgagcacatcttcc	acaagatgttggagtttggctgg

ztf-29	ZF - C2H2 - 2 fingers	1300	aatgccttaccgtccagaagc	aagccgacgacgagaaattgg
R144.3	ZF - C2H2 - 2 fingers	950	ggccatcctcgtcttcttatag	ccatcatatttagggtcaccag
ztf-17	ZF - C2H2 - 2 fingers	963	aggtgtgcgcctttaagatg	atatgacaaagtgcagagaggtg
slr-2	ZF - C2H2 - 3 fingers	417	tccagtgtcaattcctccacaac	acctcatcttcactccattgctc
Y67H2A.10	ZF - C2H2 - 3 fingers	1600	gcagtttccgatgttcaagacg	ggaggtggcatttgttgcattg
ZK686.5	ZF - C2H2 - 3 fingers	770	tgagccatgaatctgtaggatgc	tgggttctcaacgattgcttgtc
ztf-26	ZF - C2H2 - 3 fingers	940	aactgcaaatgcgaacacatcc	ccagtagatgttcccgcatgag
F47E1.3	ZF - C2H2 - 3 fingers	1012	acagtgtggcgtcattaacag	tcgtggacgtgaagaatgtg
ztf-20	ZF - C2H2 - 3 fingers	720	cacctagagcaactcaaacacg	ccgaacattccgcacaaatc
lst-5	ZF - C2H2 - 4 fingers	947	tcaggtttgatccgagtagg	tctgccttggttaatcgtttcg
Y111B2A.10	ZF - C2H2 - 6 fingers	1155	aactcacgaatggtactgcaag	tgtgcttcctcaattctgatgg
M03D4.4	ZF - C2H2 - 6 fingers	1066	ttgatgattcattccggtggac	acgttgaagattccgaagcag
sma-9	ZF - C2H2 - 7 fingers	1270	tcgataccacggattgtgagaag	ggtcgcttgttgtgtagacg
ztf-16	ZF - C2H2 - 8 fingers	870	actgttcactcggacttggagc	cagcacaatgcactccgagc
mex-6	ZF - CCCH - 2 domains	1289	tcaacaagctgctccaatgtac	acgagtgagcaatctggagtg
dmd-7	ZF - DM	1529	tttctgccgcaaatgcgaag	tgtgtgagtgcttgtgtgtagac
mab-23	ZF - DM	1700	tccagtcctatttgagcctcttc	tcaatgacgtggcagattctcc
dmd-8	ZF - DM - 2 domains	1700	gcatcccttatcttgtagccctc	aatcaatcggtttcagcgcagc
flh-2	ZF - FLYWCH	1145	ctcaatcaatgcagcagcaac	aaatgtagcgtgcagcgaaac
elt-4	ZF - GATA	214	acagtttcgaaatgccagga	tccaattgcaatggtacgaa
nhr-101	ZF - NHR	1400	ggtcttgtgctttcaaactctgc	gccaactttgcttggagagaaac
nhr-107	ZF - NHR	2200	ttcctctgtctctacctctcacac	tttgggctaacttctgcgacg
nhr-109	ZF - NHR	938	atacgctgatgcctgaatgg	agtcatctccatgtcatcctg
nhr-114	ZF - NHR	902	aattacagcctccaccaatctcg	caacctttcgattgccgtgtc
nhr-118	ZF - NHR	1335	tttccagccgttgcgacattg	gactccactcacatcaagttcc
nhr-122	ZF - NHR	778	attggacttgccgaagttgc	tcaacgctgatagtgccaag
nhr-129	ZF - NHR	1372	agttgctttccagatcattccac	tttgcattctttgctgtcgttcc
nhr-131	ZF - NHR	744	ttcggtcagtttgccaccatag	aacgcaactcactatctcaactg
nhr-138	ZF - NHR	1505	aattggcaaacgctatacacg	agggagatagttacagaggtagg

nhr-145	ZF - NHR	1484	gcgagttatccggctccttg	acgatttcttcggttgtcaggtc
nhr-156	ZF - NHR	739	tctcgttctgcaaagtttgtg	ccaacctgtaattcgtgtgac
nhr-161	ZF - NHR	1439	atgctgtgcaagatttgtgacg	tgtggacctcctcttgaaacc
nhr-189	ZF - NHR	1753	aagagaccgaggaagtcaaagc	actgttagcgtcttccgatgtc
nhr-203	ZF - NHR	1585	ttccatttgtaagttggccgtc	gatcttccgcacttccattgac
nhr-238	ZF - NHR	1179	tttgtggtgtttgtgagcattcc	gtattagaataaggtctccggtcc
nhr-239	ZF - NHR	1288	ttgagactcttcgcaccaac	aataagactgctcatggagcttc
nhr-241	ZF - NHR	1500	gatcttccctccacatcatcc	gtgcctggcaacatgactttattc
nhr-255	ZF - NHR	874	gccaaggtgagcaagacagaaatc	tgatagcaaatcaccaaagcgac
nhr-274	ZF - NHR	576	caggacctcccaaacacaaac	tcggtaattgttgggcttgttgg
nhr-275	ZF - NHR	1000	gatttccaatacaaccgtgacc	tttcagcttctccctccgttc
nhr-283	ZF - NHR	1242	aactttcaggtgttgtgttgc	ggcccacggattgagttaagaatg
nhr-285	ZF - NHR	1350	gctccaacgtgctctatttgc	gcttcttcttcgtaaccgcaaatc
nhr-36	ZF - NHR	887	tcaggttagccgtcagtttcaag	cgaccagaaatctaggacaccag
nhr-48	ZF - NHR	760	tgcgaatgtttaggagccac	gcgctactccacctttaagttc
nhr-5	ZF - NHR	1389	aatttcagtcacctcggcaacg	agctcaccctcaaatcatccaac
nhr-52	ZF - NHR	1100	aacgaaatctcacgagtggac	tgcacaaagcagtaatcttccac
nhr-86	ZF - NHR	1340	agcacagtcctgctatttaccaac	cctgaagcgcaggtaacaatg
nhr-261	ZF - NHR	522	atcacaccggctcagcaatg	cgatttccatgtcgctcagtttc
nhr-264	ZF - NHR	1023	tgccgagcctgtaggtataac	aatttctgagtgcagcggtaac
nhr-78	ZF - NHR	1343	cattcgacttccgctcgtac	aagttccattacttcggcctg
nhr-210	ZF - NHR	1074	ttcattgatgtcagctacctgc	ccaactcaattcgtggtctctg
nhr-112	ZF - NHR	1002	gaggacagggatagagtaggtttg	atgattcatctcgcacaccaac
nhr-248	ZF - NHR	956	gacgatttggagcacttgcatg	ttcaccgaatctttccactccac
nhr-252	ZF - NHR	1117	aggattactgtgtgccgagtc	tcgattccgtccttgaccag
nhr-136	ZF - NHR	873	acttgtctaggcgcatgtgtc	cgattaagttcatgtcggagcac
nhr-209	ZF - NHR	1119	agtcaacgactgtgcaaagg	cggatgtgagcattctcgttg
nhr-242	ZF - NHR	1002	ttgccgagatggtcgagtag	gagtttagttgcacttcgccag
srt-58	ZF - NHR	688	atcagctacctgtgcaaacg	tgattgtgttgggagttgtgg
nhr-201	ZF - NHR	1023	agagggacccgtataagcag	ttccacattgtgcttcggac
nhr-41	ZF - NHR	1020	gtagcgtgaatcaaatggcgtc	agcgaagatgttgagagagtatcc
nhr-167	ZF - NHR	1130	agccctggacagacttacaac	tatgctgcttcaatgccatcc
nhr-171	ZF - NHR	1288	attcaggcagtctcctgtgaag	aggtaggagagcttgagtcatg
nhr-177	ZF - NHR	985	aatgagcaacttggagcaactg	gggtttgaaattcgtgggttg
nhr-42	ZF - NHR	535	acacacgtctcccaatgttgc	tgggtcttgagcgtttgcttg
nhr-245	ZF - NHR	1023	agtagacgggttcagcaagatc	gatgatacatccgagccatgtc

nhr-31	ZF - NHR	1107	gccgatttggaaacttgttgc	gtcattctggaaggcactgtc
nhr-32	ZF - NHR	997	ggaatcctggaaacgtacagc	cagactccgctgagaacatcg
nhr-135	ZF - NHR	1747	cgcatagtttgtagttgatcggtg	ttatgagacacgcttctgggtcc

Table A.4. Complete and verified TF RNAi library

Table A.4 TF RNAi library

Gene Name	Sequence Name	Domain	Library	Source	Comments
aptf-1	K06A1.1	AP-2	JA	wTF2.0	
aptf-4	F28C6.1	AP-2	MV	wTF2.0	
aptf-3	F28C6.2	AP-2	JA	wTF2.0	
aptf-2	Y62E10A.17	AP-2	JA	wTF2.0	
C46C2.7	C46C2.7	AP-2	AJM	Cis-BP	
arid-1	Y108G3AL.7	ARID - RBP	AJM	Cis-BP	
swsn-7	C08B11.3	ARID - RFX	AJM	Cis-BP, wTF2.0	P0 scoring
let-526	C01G8.9	ARID/BRIGHT	JA	Cis-BP, wTF2.0	P0 scoring
rbr-2	ZK593.4	ARID/BRIGHT	JA	Cis-BP, wTF2.0	
cfi-1	T23D8.8	ARID/BRIGHT	JA	Cis-BP, wTF2.0	
athp-2	H20J04.2	AT Hook	JA	wTF2.0	
saeg-2	T23G5.6	AT Hook	JA	wTF2.0	
attf-5	T04G9.1	AT Hook	JA	wTF2.0	
attf-4	C05D10.1	AT Hook	JA	wTF2.0	
attf-6	Y18D10A.1	AT Hook x2	JA	wTF2.0	P0 scoring
mel-28	C38D4.3	AT Hook x2	JA	wTF2.0	
xnd-1/gak-1	C05D2.5	AT Hook x2	JA	wTF2.0	
athp-1	C44B9.4	AT Hook x2	JA	wTF2.0	
lin-15B	ZK662.4	AT Hook x2, ZF - THAP	JA	Cis-BP, wTF2.0	
hmg-11	T05A7.4	AT Hook x3	JA	wTF2.0	
attf-2	F09G2.9	AT Hook x3	JA	wTF2.0	
athp-3	Y116A8C.22	AT Hook x5/PHD	MV	Cis-BP, wTF2.0	
hmg-12	Y17G7A.1	AT Hook x7	JA	Cis-BP, wTF2.0	
isw-1	F37A4.8	AT Hook, MYB x2	MV	wTF2.0	
attf-1	C44F1.2	AT Hook, SAND	JA	wTF2.0	
spe-44	C25G4.4	AT Hook, SAND	JA	wTF2.0	
aha-1	C25A1.11	bHLH	JA	Cis-BP, wTF2.0	
ahr-1	C41G7.5	bHLH	JA	Cis-BP, wTF2.0	
cnd-1	C34E10.7	bHLH	MV	Cis-BP, wTF2.0	
cky-1	C15C8.2	bHLH	MV	Cis-BP, wTF2.0	

hif-1	F38A6.3	bHLH	JA	Cis-BP, wTF2.0	
hlh-1	B0304.1	bHLH	JA	Cis-BP, wTF2.0	
hlh-10	ZK682.4	bHLH	JA	Cis-BP, wTF2.0	
hlh-11	F58A4.7	bHLH	JA	Cis-BP, wTF2.0	
hlh-12	C28C12.8	bHLH	JA	Cis-BP, wTF2.0	
hlh-13	F48D6.3	bHLH	JA	Cis-BP, wTF2.0	
hlh-14	C18A3.8	bHLH	AJM	Cis-BP, wTF2.0	
hlh-15	C43H6.8	bHLH	JA	Cis-BP, wTF2.0	
hlh-16	DY3.3	bHLH	AJM	Cis-BP, wTF2.0	
hlh-17	F38C2.2	bHLH	AJM	Cis-BP, wTF2.0	
hlh-19	F57C12.3	bHLH	JA	Cis-BP, wTF2.0	
hlh-2	M05B5.5	bHLH	MV	Cis-BP, wTF2.0	
hlh-25	C17C3.7	bHLH	JA	Cis-BP, wTF2.0	
hlh-26	C17C3.8	bHLH - 2 domains	JA	Cis-BP, wTF2.0	
hlh-27	C17C3.10	bHLH	JA	Cis-BP, wTF2.0	
hlh-28	F31A3.2	bHLH - 2 domains	JA	Cis-BP, wTF2.0	
hlh-29	F31A3.4	bHLH - 2 domains	MV	Cis-BP, wTF2.0	
hlh-3	T24B8.6	bHLH	JA	Cis-BP, wTF2.0	
hlh-30	W02C12.3	bHLH	JA	Cis-BP, wTF2.0	
hlh-31	F38C2.8	bHLH	JA	Cis-BP, wTF2.0	Overlapping clones
hlh-32	Y105C5B.29	bHLH	JA	Cis-BP, wTF2.0	
hlh-33	Y39A3CR.6	bHLH	JA	Cis-BP, wTF2.0	
hlh-34	T01D3.2	bHLH	MV	Cis-BP, wTF2.0	
hlh-4	T05G5.2	bHLH	MV	Cis-BP, wTF2.0	
hlh-6	T15H9.3	bHLH	JA	Cis-BP, wTF2.0	
hlh-8	C02B8.4	bHLH	JA	Cis-BP, wTF2.0	
hnd-1	C44C10.8	bHLH	MV	Cis-BP, wTF2.0	
lin-22	Y54G2A.1	bHLH	AJM	Cis-BP, wTF2.0	
lin-32	T14F9.5	bHLH	JA	Cis-BP, wTF2.0	
mdl-1	R03E9.1	bHLH	MV	Cis-BP, wTF2.0	
mml-1	T20B12.6	bHLH	MV	Cis-BP, wTF2.0	
mxl-1	T19B10.11	bHLH	JA	Cis-BP, wTF2.0	
mxl-2	F40G9.11	bHLH	JA	Cis-BP, wTF2.0	
mxl-3	F46G10.6	bHLH	MV	Cis-BP, wTF2.0	
ngn-1	Y69A2AR.29	bHLH	JA	Cis-BP, wTF2.0	
ref-1	T01E8.2	bHLH - 2 domains	JA	Cis-BP, wTF2.0	
sbp-1	Y47D3B.7	bHLH	JA	Cis-BP, wTF2.0	
ZK177.11	ZK177.11	bHLH	AJM	CisBP	
Y44A6D.3	Y44A6D.3	Brinker	AJM	CisBP	

F21D5.4	F21D5.4	Brinker	MV	CisBP	
C18C4.5	C18C4.5	bZIP	MV	CisBP	
C32E8.1	C32E8.1	bZIP	AJM	CisBP	
F15A4.10	F15A4.10	bZIP	MV	CisBP	
zip-9	F17C11.17	bZIP	AJM	CisBP	
F41H10.4	F41H10.4	bZIP	AJM	CisBP	
maf-1	F45H11.6	bZIP	AJM	CisBP	
lmn-1	DY3.2	bZIP	MV	CisBP	
Y60A3A.25	Y60A3A.25	bZIP	AJM	CisBP	
atf-2	K08F8.2	bZIP - 2 domains	JA	Cis-BP, wTF2.0	
atf-5	T04C10.4	bZIP	JA	Cis-BP, wTF2.0	
atf-6	F45E6.2	bZIP	JA	Cis-BP, wTF2.0	
atf-7	C07G2.2	bZIP	MV	Cis-BP, wTF2.0	
atf-8	F17A9.3	bZIP	AJM	Cis-BP, wTF2.0	
atfs-1	ZC376.7	bZIP	MV	Cis-BP, wTF2.0	
cebp-1	D1005.3	bZIP	JA	Cis-BP, wTF2.0	
cebp-2	C48E7.11	bZIP	AJM	Cis-BP, wTF2.0	
ces-2	ZK909.4	bZIP	JA	Cis-BP, wTF2.0	
crh-1	Y41C4A.4	bZIP	MV	Cis-BP, wTF2.0	
crh-2	C27D6.4	bZIP	JA	Cis-BP, wTF2.0	
jun-1	T24H10.7	bZIP	JA	Cis-BP, wTF2.0	
hpo-39	Y61A9LA.9	bZIP	AJM	CisBP	
let-607	F57B10.1	bZIP (CREB)	JA	Cis-BP, wTF2.0	P0 scoring
lfi-1	ZC8.4	bZIP	JA	Cis-BP, wTF2.0	
sknr-1	W02H5.7	bZIP	JA	Poole et al 2011	
xbp-1	R74.3	bZIP	JA	Cis-BP, wTF2.0	
zip-1	Y75B8A.35	bZIP	MV	Cis-BP, wTF2.0	
zip-10	T27F2.4	bZIP	JA	Cis-BP, wTF2.0	P0 scoring
zip-11	W08E12.1	bZIP	JA	Cis-BP, wTF2.0	
zip-2	K02F3.4	bZIP	JA	Cis-BP, wTF2.0	
zip-3	W07G1.3	bZIP		Cis-BP, wTF2.0	
zip-4	Y44E3B.1	bZIP	JA	Cis-BP, wTF2.0	
zip-5	C34D1.5	bZIP	JA	Cis-BP, wTF2.0	
zip-6	R07H5.10	bZIP	JA	Cis-BP, wTF2.0	
zip-7	Y51H4A.4	bZIP	JA	Cis-BP, wTF2.0	
zip-8	F23F12.9	bZIP	JA	Cis-BP, wTF2.0	
fos-1	F29G9.4	bZIP	JA	Cis-BP, wTF2.0	P0 scoring
nfya-1	T08D10.1	CBF	JA	Cis-BP, wTF2.0	
nfya-2	Y53H1A.5	CBF	JA	Cis-BP, wTF2.0	

nfyc-1	F23F1.1	CBF	JA	Cis-BP, wTF2.0	
drap-1	F40F9.7	CBF	AJM	Cis-BP, wTF2.0	
dro-1	F53A2.5	CBF	JA	Cis-BP, wTF2.0	
T26A5.8	T26A5.8	CBF	JA	Cis-BP, wTF2.0	
nfyb-1	W10D9.4	CBF	MV	Cis-BP, wTF2.0	
Y53F4B.3	Y53F4B.3	CBF	JA	Cis-BP, wTF2.0	
F23B12.7	F23B12.7	CBF	JA	Cis-BP, wTF2.0	
Y48G1C.6	Y48G1C.6	CENPB	MV	CisBP	
cey-1	F33A8.3	COLD BOX	JA	Cis-BP, wTF2.0	
cey-2	F46F11.2	COLD BOX	JA	Cis-BP, wTF2.0	
cey-3	M01E11.5	COLD BOX	JA	Cis-BP, wTF2.0	
cey-4	Y39A1C.3	COLD BOX	JA	Cis-BP, wTF2.0	
lin-28	F02E9.2	COLD BOX	MV	Cis-BP, wTF2.0	
grh-1	Y48G8AR.1	CP2	JA	Cis-BP, wTF2.0	
lag-1	K08B4.1	CSL	MV	Cis-BP, wTF2.0	P0 scoring
lin-54	JC8.6	CxC	MV	CisBP	P0 scoring
Y75B8A.6	Y75B8A.6	CxxC	AJM	CisBP	
ceh-52	C07E3.5	HD	JA	Cis-BP, wTF2.0	
ceh-54	T13C5.4	HD	MV	Cis-BP, wTF2.0	
ceh-7	C34C6.8	HD	JA	Cis-BP, wTF2.0	
ceh-74	ZC376.4	HD	JA	Cis-BP, wTF2.0	
ceh-79	C26E1.3	HD	JA	Cis-BP, wTF2.0	
ceh-81	F45C12.3	HD	JA	Cis-BP, wTF2.0	
ceh-82	F45C12.2	HD	JA	Cis-BP, wTF2.0	
ceh-85	F59H6.6	HD	JA	Cis-BP, wTF2.0	
ceh-86	F42G2.6	HD	JA	Cis-BP, wTF2.0	
ceh-87	F34D6.2	HD	AJM	Cis-BP, wTF2.0	
ceh-90	R03E1.4	HD	AJM	Cis-BP, wTF2.0	
ceh-91	Y66A7A.5	HD - 2 domains	JA	Cis-BP, wTF2.0	
ceh-93	R04A9.5	HD - 2 domains	AJM	Cis-BP, wTF2.0	
ceh-63	C02F12.10	HD	AJM	CisBP	
C50B6.1	C50B6.1	HD	MV	CisBP	
ceh-99	T21B4.17	HD	AJM	CisBP	
ceh-92	Y66D12A.5	HD	AJM	CisBP	
dve-1	ZK1193.5	HD - 2 domains	JA	Cis-BP, wTF2.0	
nsy-7	C18F3.4	HD	AJM	Cis-BP	
ceh-21	T26C11.6	HD - CUT	JA	Cis-BP, wTF2.0	
ceh-38	F22D3.1	HD - CUT	MV	Cis-BP, wTF2.0	
ceh-39	T26C11.7	HD - CUT	MV	Cis-BP, wTF2.0	

ceh-41	T26C11.5	HD - CUT	JA	Cis-BP, wTF2.0	
ceh-44	Y54F10AM.4	HD - CUT	AJM	Cis-BP, wTF2.0	
ceh-48	C17H12.9	HD - CUT	MV	Cis-BP, wTF2.0	
ceh-49	F17A9.6	HD - CUT	JA	Cis-BP, wTF2.0	
hmbx-1	F54A5.1	HD - HNF	JA	Cis-BP, wTF2.0	
ceh-12	F33D11.4	HD - HOX	MV	Cis-BP, wTF2.0	
ceh-13	R13A5.5	HD - HOX	JA	Cis-BP, wTF2.0	
ceh-16	C13G5.1	HD - HOX	AJM	Cis-BP, wTF2.0	
ceh-19	F20D12.6	HD - HOX	MV	Cis-BP, wTF2.0	
ceh-51	Y80D3A.3	HD - HOX	JA	Cis-BP, wTF2.0	
ceh-58	C07E3.6	HD - HOX	JA	Cis-BP, wTF2.0	
ceh-62	R06F6.6	HD - HOX	AJM	Cis-BP, wTF2.0	
ceh-83	F45C12.15	HD - HOX - 2 domains	AJM	Cis-BP, wTF2.0	
ceh-89	F28H6.2	HD - HOX	JA	Cis-BP, wTF2.0	
egl-5	C08C3.1	HD - HOX	JA	Cis-BP, wTF2.0	
lin-39	C07H6.7	HD - HOX	JA	Cis-BP, wTF2.0	
mab-5	C08C3.3	HD - HOX	JA	Cis-BP, wTF2.0	
nob-1	Y75B8A.2	HD - HOX	JA	Cis-BP, wTF2.0	
pal-1	C38D4.6	HD - HOX	JA	Cis-BP, wTF2.0	P0 scoring
php-3	Y75B8A.1	HD - HOX	JA	Cis-BP, wTF2.0	P0 scoring
vab-7	M142.4	HD - HOX	JA	Cis-BP, wTF2.0	
duxl-1	ZC204.2	HD - HOX - 2 domains	JA	Cis-BP, wTF2.0	
ceh-100	Y38E10A.6	HD - HOX	JA	Cis-BP, wTF2.0	
ceh-14	F46C8.5	HD - LIM	JA	Cis-BP, wTF2.0	
lim-4	ZC64.4	HD - LIM	JA	Cis-BP, wTF2.0	
lim-6	K03E6.1	HD - LIM	JA	Cis-BP, wTF2.0	
lim-7	C04F1.3	HD - LIM	MV	Cis-BP, wTF2.0	
lin-11	ZC247.3	HD - LIM	JA	Cis-BP, wTF2.0	
mec-3	F01D4.6	HD - LIM	JA	Cis-BP, wTF2.0	
ttx-3	C40H5.5	HD - LIM	JA	Cis-BP, wTF2.0	
ceh-1	F16H11.4	HD - NK	AJM	Cis-BP, wTF2.0	
ceh-2	C27A12.5	HD - NK	JA	Cis-BP, wTF2.0	
ceh-22	F29F11.5	HD - NK	JA	Cis-BP, wTF2.0	
ceh-23	ZK652.5	HD - NK	JA	Cis-BP, wTF2.0	
ceh-24	F55B12.1	HD - NK	JA	Cis-BP, wTF2.0	
ceh-27	F46F3.1	HD - NK	MV	Cis-BP, wTF2.0	
ceh-28	K03A11.3	HD - NK	JA	Cis-BP, wTF2.0	
ceh-30	C33D12.7	HD - NK	AJM	Cis-BP, wTF2.0	
ceh-31	C33D12.1	HD - NK	AJM	Cis-BP, wTF2.0	

ceh-43	C28A5.4	HD - NK	JA	Cis-BP, wTF2.0	
ceh-5	C16C2.1	HD - NK	AJM	Cis-BP, wTF2.0	
ceh-75	C50H2.6	HD - NK	AJM	Cis-BP, wTF2.0	
ceh-9	Y65B4BR.9	HD - NK	AJM	Cis-BP, wTF2.0	
cog-1	R03C1.3	HD - NK	MV	Cis-BP, wTF2.0	
mls-2	C39E6.4	HD - NK	JA	Cis-BP, wTF2.0	
pha-2	M6.3	HD - NK	AJM	Cis-BP, wTF2.0	
tab-1	F31E8.3	HD - NK	JA	Cis-BP, wTF2.0	
vab-15	R07B1.1	HD - NK	MV	Cis-BP, wTF2.0	
ceh-18	ZC64.3	HD - POU	JA	Cis-BP, wTF2.0	
ceh-6	K02B12.1	HD - POU	JA	Cis-BP, wTF2.0	
unc-86	C30A5.7	HD - POU	JA	Cis-BP, wTF2.0	
alr-1	R08B4.2	HD - PRD	MV	Cis-BP, wTF2.0	
ceh-10	W03A3.1	HD - PRD	JA	Cis-BP, wTF2.0	
ceh-17	D1007.1	HD - PRD	JA	Cis-BP, wTF2.0	
ceh-36	C37E2.4	HD - PRD	JA	Cis-BP, wTF2.0	
ceh-37	C37E2.5	HD - PRD	JA	Cis-BP, wTF2.0	
ceh-45	ZK993.1	HD - PRD	JA	Cis-BP, wTF2.0	
ceh-53	C09G12.1	HD - PRD	JA	Cis-BP, wTF2.0	
ceh-8	ZK265.4	HD - PRD - 2 domains	JA	Cis-BP, wTF2.0	
ceh-84	C40D2.4	HD - PRD	AJM	Cis-BP, wTF2.0	
dsc-1	C18B12.3	HD - PRD	JA	Cis-BP, wTF2.0	
ttx-1	Y113G7A.6	HD - PRD	AJM	Cis-BP, wTF2.0	
unc-4	F26C11.2	HD - PRD	JA	Cis-BP, wTF2.0	
unc-42	F58E6.10	HD - PRD	JA	Cis-BP, wTF2.0	
eyg-1	Y53C12C.1	HD - PRD,Paired Domian - CPAX	JA	Cis-BP, wTF2.0	
vab-3	F14F3.1	HD - PRD,Paired Domian - FULL	JA	Cis-BP, wTF2.0	
pax-3	F27E5.2	HD - PRD,Paired Domian - FULL	JA	Cis-BP, wTF2.0	
unc-30	B0564.10	HD - PRD, bHLH	MV	Cis-BP, wTF2.0	
ceh-26	K12H4.1	HD - PROX	JA	Cis-BP, wTF2.0	
ceh-32	W05E10.3	HD - SIX	JA	Cis-BP, wTF2.0	
ceh-33	C10G8.7	HD - SIX	JA	Cis-BP, wTF2.0	
ceh-34	C10G8.6	HD - SIX	MV	Cis-BP, wTF2.0	
unc-39	F56A12.1	HD - SIX	JA	Cis-BP, wTF2.0	
ceh-20	F31E3.1	HD - TALE	JA	Cis-BP, wTF2.0	P0 scoring
ceh-40	F17A2.5	HD - TALE	JA	Cis-BP, wTF2.0	
ceh-60	F22A3.5	HD -TALE	JA	Cis-BP, wTF2.0	
ceh-88	C49C3.5	HD - TALE	JA	Cis-BP, wTF2.0	

irx-1	C36F7.1	HD - TALE	JA	Cis-BP, wTF2.0	
unc-62	T28F12.2	HD - TALE	JA	Cis-BP, wTF2.0	P0 scoring
egl-13	T22B7.1	HMG box	JA	Cis-BP, wTF2.0	
gei-3	T22H6.6	HMG box	JA	Cis-BP, wTF2.0	
hmg-1.1	Y48B6A.14	HMG box	MV	Cis-BP, wTF2.0	
hmg-1.2	F47D12.4	HMG box - 2 domains	JA	Cis-BP, wTF2.0	P0 scoring
hmg-20	W02D9.3	HMG box	JA	Cis-BP, wTF2.0	
hmg-3	C32F10.5	HMG box	JA	Cis-BP, wTF2.0	
hmg-4	T20B12.8	HMG box	JA	Cis-BP, wTF2.0	P0 scoring
hmg-5	F45E4.9	HMG box - 2 domains	JA	Cis-BP, wTF2.0	
hmg-6	F47G4.6	HMG box	JA	Cis-BP, wTF2.0	
pop-1	W10C8.2	HMG box	JA	Cis-BP, wTF2.0	P0 scoring
sem-2	C32E12.5	HMG box	AJM	Cis-BP, wTF2.0	
sox-2	K08A8.2	HMG box	JA	Cis-BP, wTF2.0	P0 scoring
sox-3	F40E10.2	HMG box	JA	Cis-BP, wTF2.0	
sox-4	C12D12.5	HMG box	JA	Cis-BP, wTF2.0	
swsn-3	Y71H2AM.17	HMG box	JA	Cis-BP, wTF2.0	P0 scoring
Y73E7A.1	Y73E7A.1	HMG box	AJM	CisBP	Secondary targets
mbf-1	H21P03.1	HTH	JA	wTF2.0	
mbr-1	T01C1.2	HTH-Pipsqueak	JA	Cis-BP	
ZC247.1	ZC247.1	HTH-Pipsqueak	AJM	CisBP	
unc-3	Y16B4A.1	IPT/TIG	JA	wTF2.0	
camt-1	T05C1.4	IPT/CAMTA	JA	Cis-BP, wTF2.0	
madf-1	Y55F3BR.5	MADF	JA	Cis-BP	
madf-10	Y106G6H.4	MADF	JA	Cis-BP, wTF2.0	
madf-11	C05D2.6	MADF	AJM	Cis-BP, wTF2.0	
madf-2	F36D1.1	MADF	JA	Cis-BP, wTF2.0	
madf-3	H20J04.3	MADF - 2 domains	AJM	Cis-BP, wTF2.0	
madf-4	T07C12.11	MADF	JA	Cis-BP, wTF2.0	
madf-5	C01G12.1	MADF	AJM	Cis-BP, wTF2.0	
madf-6	C54G6.1	MADF	MV	Cis-BP	
madf-7	C06A5.4	MADF	JA	Cis-BP, wTF2.0	
madf-8	C46F11.3	MADF	JA	Cis-BP, wTF2.0	
madf-9	ZC416.1	MADF	JA	Cis-BP, wTF2.0	
C06A6.2	C06A6.2	MADF	MV	CisBP	
mef-2	W10D5.1	MADS box	JA	Cis-BP, wTF2.0	
unc-120	D1081.2	MADS box	MV	Cis-BP, wTF2.0	
flt-1/baz-2	ZK783.4	MBD	AJM	CisBP	
daf-3	F25E2.5	MH1	JA	Cis-BP, wTF2.0	

daf-8	R05D11.1	MH1/ZnF-GATA?	MV	wTF2.0	
nfi-1	ZK1290.4	MH1	JA	Cis-BP, wTF2.0	
sma-2	ZK370.2	MH1	MV	Cis-BP, wTF2.0	
sma-3	R13F6.9	MH1/SMAD	MV	Cis-BP, wTF2.0	
sma-4	R12B2.1	MH1/SMAD	AJM	wTF2.0	
tag-68	F37D6.6	MH1	JA	Cis-BP, wTF2.0	
C50F4.12	C50F4.12	mTERF	MV	CisBP	
K11D2.5	K11D2.5	mTERF	AJM	CisBP	
B0261.1	B0261.1	MYB	JA	Cis-BP, wTF2.0	
chd-7	T04D1.4	MYB	AJM	wTF2.0	
ekl-4	Y105E8A.17	MYB	MV	Cis-BP, wTF2.0	P0 scoring
F10E7.11	F10E7.11	MYB	JA	Cis-BP, wTF2.0	
R151.8	R151.8	MYB	AJM	wTF2.0	
swsn-1	Y113G7B.23	MYB	JA	wTF2.0	P0 scoring
T07F8.4	T07F8.4	MYB	MV	Cis-BP, wTF2.0	
cdc-5L	D1081.8	MYB - 2 domains	JA	Cis-BP, wTF2.0	P0 scoring
dnj-11	F38A5.13	MYB - 2 domains	JA	Cis-BP, wTF2.0	
F54F2.9	F54F2.9	MYB - 2 domains	JA	Cis-BP, wTF2.0	
gei-8	C14B9.6	MYB - 2 domains	JA	Cis-BP, wTF2.0	
spr-1	D1014.8	MYB - 2 domains	JA	Cis-BP, wTF2.0	
snpc-4	F32H2.1	MYB - 5 domains	JA	Cis-BP, wTF2.0	P0 scoring
cep-1	F52B5.5	p53	JA	wTF2.0	
myrf-1	F59B10.1	p53	AJM	Cis-BP, wTF2.0	
myrf-2	F21A10.2	p53	JA	Cis-BP, wTF2.0	
egl-38	C04G2.7	Paired Domain - FULL	MV	Cis-BP, wTF2.0	
npax-1	F21D12.5	Paired Domain - NPAX	JA	Cis-BP, wTF2.0	
npax-2	F48B9.5	Paired Domain - NPAX	MV	Cis-BP, wTF2.0	
npax-3	R13.2	Paired Domain - NPAX	JA	Cis-BP, wTF2.0	
npax-4	C09G9.7	Paired Domain - NPAX	MV	Cis-BP, wTF2.0	
pax-1	K07C11.1	Paired Domain - FULL	JA	Cis-BP, wTF2.0	
pax-2	K06B9.5	Paired Domain - FULL	AJM	Cis-BP, wTF2.0	
rnt-1	B0414.2	RNT	JA	Cis-BP, wTF2.0	
gmeb-1	C01B12.2	SAND	JA	Cis-BP, wTF2.0	
gmeb-2	F53H4.5	SAND	JA	Cis-BP, wTF2.0	
F19F10.9	F19F10.9	SART-1	AJM	CisBP	P0 scoring
chpf-2	F59D6.7	STAT	AJM	CisBP	
sta-1	Y51H4A.17	STAT	JA	Cis-BP, wTF2.0	
mab-9	T27A1.6	T-box	JA	Cis-BP, wTF2.0	
mls-1	H14A12.4	T-box	JA	Cis-BP, wTF2.0	

sea-1	F19B10.9	T-box	JA	Cis-BP, wTF2.0	
tbx-11	F40H6.4	T-box	JA	Cis-BP, wTF2.0	
tbx-2	F21H11.3	T-box	AJM	Cis-BP, wTF2.0	
tbx-30	Y59E9AR.3	T-box	JA	Cis-BP, wTF2.0	
tbx-31	C36C9.2	T-box	JA	Cis-BP, wTF2.0	
tbx-32	ZK380.1	T-box	JA	Cis-BP, wTF2.0	
tbx-33	Y66A7A.8	T-box	JA	Cis-BP, wTF2.0	
tbx-34	Y47D3A.10	T-box	MV	Cis-BP, wTF2.0	
tbx-35	ZK177.10	T-box	JA	Cis-BP, wTF2.0	
tbx-36	ZK829.5	T-box	JA	Cis-BP, wTF2.0	
tbx-37	Y47D3A.12	T-box	AJM	Cis-BP, wTF2.0	
tbx-38	C24H11.3	T-box	JA	Cis-BP, wTF2.0	
tbx-39	Y73F8A.16	T-box	MV	Cis-BP, wTF2.0	
tbx-40	Y73F8A.17	T-box	MV	Cis-BP, wTF2.0	
tbx-41	T26C11.1	T-box	JA	Cis-BP, wTF2.0	
tbx-42	Y59E9AR.5	T-box	JA	Cis-BP, wTF2.0	
tbx-43	Y46E12A.4	T-box	AJM	Cis-BP	
tbx-7	ZK328.8	T-box	AJM	Cis-BP, wTF2.0	
tbx-8	T07C4.2	T-box	JA	Cis-BP, wTF2.0	
tbx-9	T07C4.6	T-box	JA	Cis-BP, wTF2.0	
taf-11.3	F43D9.5	TBP	MV	Wormbook, Wormbase	
tbp-1	T20B12.2	TBP	MV	CisBP	P0 scoring
tlf-1	F39H11.2	TBP	AJM	CisBP	
egl-44	F28B12.2	TEA/ATTS	AJM	Cis-BP, wTF2.0	
C30G4.4	C30G4.4	TSC-22/dip/bun	AJM	SMART, PFAM	
T18D3.7	T18D3.7	TSC-22/dip/bun	JA	SMART, PFAM	
Y48C3A.12	Y48C3A.12	TSC-22/dip/bun	MV	SMART, PFAM	
wrm-1	B0336.1	Beta-catenin/ARmadillo	AJM	wTF2.0	P0 scoring
bar-1	C54D1.6	Beta-catenin/ARmadillo	AJM	wTF2.0	
hmp-2	K05C4.6	Beta-catenin/ARmadillo	AJM	wTF2.0	
ham-1	F53B2.6	WH	MV	wTF2.0	
dac-1	B0412.1	WH - DAC	JA	SMART, PFAM	
ast-1	T08H4.3	WH - ETS	MV	Cis-BP, wTF2.0	
elf-1	C24A1.2	WH - ETS	MV	Cis-BP, wTF2.0	
ets-4	F22A3.1	WH - ETS	AJM	Cis-BP, wTF2.0	
ets-5	C42D8.4	WH - ETS	JA	Cis-BP, wTF2.0	
ets-7	F19F10.5	WH - ETS	JA	Cis-BP, wTF2.0	
ets-8	C50A2.4	WH - ETS	AJM	Cis-BP, wTF2.0	
ets-9	C52B9.2	WH - ETS	JA	Cis-BP, wTF2.0	

ets-10	C52B9.11	WH - ETS	AJM	Wormbase	
F19F10.1	F19F10.1	WH - ETS	JA	Cis-BP, wTF2.0	
lin-1	C37F5.1	WH - ETS	JA	Cis-BP, wTF2.0	Secondary target: *elk-2*
tag-97	C33A11.4	WH - ETS	JA	Cis-BP, wTF2.0	
daf-16	R13H8.1	WH - Fork Head, AT Hook	JA	Cis-BP, wTF2.0	
fkh-10	C25A1.2	WH - Fork Head	JA	Cis-BP, wTF2.0	
fkh-2	T14G12.4	WH - Fork Head	MV	Cis-BP, wTF2.0	
fkh-3	C29F7.4	WH - Fork Head	JA	Cis-BP, wTF2.0	
fkh-4	C29F7.5	WH - Fork Head	MV	Cis-BP, wTF2.0	
fkh-5	F26A1.2	WH - Fork Head	MV	Cis-BP, wTF2.0	
fkh-6	B0286.5	WH - Fork Head	JA	Cis-BP, wTF2.0	
fkh-8	F40H3.4	WH - Fork Head	MV	Cis-BP, wTF2.0	
fkh-9	K03C7.2	WH - Fork Head	AJM	Cis-BP, wTF2.0	
let-381	F26B1.7	WH - Fork Head	JA	Cis-BP, wTF2.0	
lin-31	K10G6.1	WH - Fork Head	JA	Cis-BP, wTF2.0	
pes-1	T28H11.4	WH - Fork Head	JA	Cis-BP, wTF2.0	
pha-4	F38A6.1	WH - Fork Head	JA	Cis-BP, wTF2.0	
T27A8.2	T27A8.2	WH - Fork Head	JA	Cis-BP, wTF2.0	
unc-130	C47G2.2	WH - Fork Head	JA	Cis-BP, wTF2.0	
hsf-1	Y53C10A.12	WH - HSF	JA	Cis-BP, wTF2.0	
daf-19	F33H1.1	WH - RFX	JA	Cis-BP, wTF2.0	
dpl-1	T23G7.1	WH - TDP	MV	Cis-BP, wTF2.0	
efl-1	Y102A5C.18	WH - TDP	AJM	Cis-BP, wTF2.0	
efl-2	Y48C3A.17	WH - TDP	MV	Cis-BP, wTF2.0	
efl-3	F49E12.6	WH - TDP - 2 domains	MV	Cis-BP, wTF2.0	
grl-25	ZK643.8	WT1 - 2 domains	AJM	wTF2.0	
gfl-1	M04B2.3	YEATS	MV	SMART, PFAM	
bed-1	Y39B6A.12	ZF - BED	AJM	wTF2.0	
bed-2	Y47D3B.9	ZF - BED	JA	wTF2.0	
bed-3	F25H8.6	ZF - BED	MV	Cis-BP, PBM	P0 scoring
K09A11.1	K09A11.1	ZF - BED	JA	wTF2.0	
egl-46	K11G9.4	ZF - C2H2 - 1 finger	JA	Cis-BP, wTF2.0	
2L52.1	2L52.1	ZF - C2H2 - 1 finger	JA	wTF2.0	
C01F6.9	C01F6.9	ZF - C2H2 - 1 finger	JA	wTF2.0	
C02F5.12	C02F5.12	ZF - C2H2 - 1 finger	AJM	wTF2.0	
C06E2.1	C06E2.1	ZF - C2H2 - 1 finger	JA	Cis-BP, wTF2.0	
ztf-3	C53D5.4	ZF - C2H2 - 1 finger	JA	Cis-BP, wTF2.0	
pqn-21	C37A2.5	ZF - C2H2 - 1 finger	MV	wTF2.0	

C38D4.7	C38D4.7	ZF - C2H2 - 1 finger	JA	wTF2.0	
C46E10.8	C46E10.8	ZF - C2H2 - 1 finger	JA	Cis-BP, wTF2.0	
C52E12.1	C52E12.1	ZF - C2H2 - 1 finger	AJM	wTF2.0	
D1046.2	D1046.2	ZF - C2H2 - 1 finger	JA	wTF2.0	
D2030.7	D2030.7	ZF - C2H2 - 1 finger	JA	wTF2.0	
repo-1	F11A10.2	ZF - C2H2 - 1 finger	JA	wTF2.0	P0 scoring
lin-26	F18A1.2	ZF - C2H2 - 1 finger	JA	wTF2.0	
lir-1	F18A1.3	ZF - C2H2 - 1 finger	JA	wTF2.0	P0 scoring
lir-2	F18A1.4	ZF - C2H2 - 1 finger	JA	wTF2.0	
lir-3	F37H8.1	ZF - C2H2 - 1 finger	JA	wTF2.0 and CisBP	
F21D5.9	F21D5.9	ZF - C2H2 - 1 finger	JA	wTF2.0 and CisBP	
F21G4.5	F21G4.5	ZF - C2H2 - 1 finger	MV	wTF2.0	
ubxn-1	F23C8.4	ZF - C2H2 - 1 finger	JA	wTF2.0	
F27D4.6	F27D4.6	ZF - C2H2 - 1 finger	JA	wTF2.0	
F37B4.10	F37B4.10	ZF - C2H2 - 1 finger	JA	wTF2.0	
sptf-1	F45H11.1	ZF - C2H2 - 1 finger	JA	wTF2.0 and CisBP	
F52B5.7	F52B5.7	ZF - C2H2 - 1 finger	AJM	wTF2.0 and CisBP	
lect-2	K05F1.5	ZF - C2H2 - 1 finger	JA	wTF2.0	
cid-1	K10D2.3	ZF - C2H2 - 1 finger	MV	wTF2.0	
sea-2	K10G6.3	ZF - C2H2 - 1 finger	JA	wTF2.0	
K11D12.12	K11D12.12	ZF - C2H2 - 1 finger	AJM	wTF2.0 and CisBP	
K12H6.12	K12H6.12	ZF - C2H2 - 1 finger	JA	wTF2.0	
somi-1	M04G12.4	ZF - C2H2 - 1 finger	JA	wTF2.0	P0 scoring
R02D3.7	R02D3.7	ZF - C2H2 - 1 finger	JA	wTF2.0	
R05D3.3	R05D3.3	ZF - C2H2 - 1 finger	MV	wTF2.0	
R07E5.5	R07E5.5	ZF - C2H2 - 1 finger	JA	wTF2.0 and CisBP	
T06G6.5	T06G6.5	ZF - C2H2 - 1 finger	AJM	wTF2.0	
zim-1	T07G12.6	ZF - C2H2 - 1 finger	MV	WormBase	
zim-2	T07G12.10	ZF - C2H2 - 1 finger	JA	wTF2.0	
zim-3	T07G12.11	ZF - C2H2 - 1 finger	JA	wTF2.0	
him-8	T07G12.12	ZF - C2H2 - 1 finger	JA	wTF2.0	
T08G5.7	T08G5.7	ZF - C2H2 - 1 finger	JA	wTF2.0	Secondary targets
ztf-27	T09F3.1	ZF - C2H2 - 1 finger	JA	wTF2.0 and CisBP	
ztf-4	T10B11.3	ZF - C2H2 - 1 finger	JA	wTF2.0	
eea-1	T10G3.5	ZF - C2H2 - 1 finger	JA	wTF2.0	

T22C8.3	T22C8.3	ZF - C2H2 - 1 finger	JA	wTF2.0 and CisBP	
T22C8.4	T22C8.4	ZF - C2H2 - 1 finger	JA	wTF2.0 and CisBP	
T23F11.4	T23F11.4	ZF - C2H2 - 1 finger	JA	wTF2.0	
tlp-1	T23G4.1	ZF - C2H2 - 1 finger	JA	wTF2.0	
ztf-18	T24C4.7	ZF - C2H2 - 1 finger	JA	wTF2.0	
W04B5.2	W04B5.2	ZF - C2H2 - 1 finger	JA	wTF2.0	
W04D2.4	W04D2.4	ZF - C2H2 - 1 finger	AJM	wTF2.0	P0 scoring
Y37F4.6	Y37F4.6	ZF - C2H2 - 1 finger	AJM	wTF2.0	
rabs-5	Y42H9AR.3	ZF - C2H2 - 1 finger	MV	wTF2.0	
sup-35	Y48A6C.3	ZF - C2H2 - 1 finger	JA	wTF2.0	
ztf-22	Y48C3A.4	ZF - C2H2 - 1 finger	MV	wTF2.0	
lin-38	Y48E1B.7	ZF - C2H2 - 1 finger	JA	wTF2.0	
mcd-1	Y51H1A.6	ZF - C2H2 - 1 finger	JA	wTF2.0	
dxbp-1	Y52B11A.9	ZF - C2H2 - 1 finger	JA	wTF2.0	
Y53F4B.5	Y53F4B.5	ZF - C2H2 - 1 finger	JA	wTF2.0	
Y53H1A.2	Y53H1A.2	ZF - C2H2 - 1 finger	JA	wTF2.0 and CisBP	
Y56A3A.18	Y56A3A.18	ZF - C2H2 - 1 finger	JA	wTF2.0	P0 scoring
Y57A10A.31	Y57A10A.31	ZF - C2H2 - 1 finger	JA	wTF2.0	
Y82E9BR.17	Y82E9BR.17	ZF - C2H2 - 1 finger	JA	wTF2.0	
ZK177.3	ZK177.3	ZF - C2H2 - 1 finger	JA	wTF2.0	
ZK185.1	ZK185.1	ZF - C2H2 - 1 finger	JA	wTF2.0	
snu-23	ZK686.4	ZF - C2H2 - 1 finger	JA	wTF2.0	
F33H1.4	F33H1.4	ZF - C2H2 - 1 finger, AT Hook x3	JA	wTF2.0	
lin-36	F44B9.6	ZF - C2H2 - 1 finger, ZF - THAP	JA	wTF2.0 and CisBP	
K04C1.3	K04C1.3	ZF - C2H2 - 1 finger, WH - Fork Head	AJM	wTF2.0	
pbrm-1	C26C6.1	ZF - C2H2 - 1 finger, HMG box	JA	wTF2.0 and CisBP	
ada-2	F32A5.1	ZF - C2H2 - 1 finger, MYB	JA	wTF2.0 and CisBP	
saeg-1	F53H10.2	ZF - C2H2 - 1 finger, MYB	AJM	wTF2.0 and CisBP	
Y48G8AL.10	Y48G8AL.10	ZF - C2H2 - 12 fingers	AJM	wTF2.0	
spr-4	C09H6.1	ZF - C2H2 - 14 fingers	MV	wTF2.0	
lin-13	C03B8.4	ZF - C2H2 - 15 fingers	AJM	wTF2.0	P0 scoring
ham-2	C07A12.1	ZF - C2H2 - 2 fingers	JA	wTF2.0 and CisBP	
B0035.1	B0035.1	ZF - C2H2 - 2 fingers	JA	wTF2.0	
B0310.2	B0310.2	ZF - C2H2 - 2 fingers	JA	wTF2.0 and CisBP	

ztf-30	C06E1.8	ZF - C2H2 - 2 fingers	JA	wTF2.0 and CisBP	
scrt-1	C55C2.1	ZF - C2H2 - 2 fingers	AJM	wTF2.0 and CisBP	
F21A9.2	F21A9.2	ZF - C2H2 - 2 fingers	MV	wTF2.0	
ztf-28	F36F12.8	ZF - C2H2 - 2 fingers	JA	wTF2.0 and CisBP	
F44E2.7	F44E2.7	ZF - C2H2 - 2 fingers	JA	wTF2.0	
lsy-1	F47H4.1	ZF - C2H2 - 2 fingers	JA	wTF2.0 and CisBP	
sdc-1	F52E10.1	ZF - C2H2 - 2 fingers	JA	wTF2.0 and CisBP	
ztf-13	F52E4.8	ZF - C2H2 - 2 fingers	JA	wTF2.0	
K09H9.7	K09H9.7	ZF - C2H2 - 2 fingers	JA	wTF2.0	
K10B3.5	K10B3.5	ZF - C2H2 - 2 fingers	JA	wTF2.0	
R10E4.11	R10E4.11	ZF - C2H2 - 2 fingers	JA	wTF2.0	
R144.3	R144.3	ZF - C2H2 - 2 fingers	AJM	wTF2.0	
dnj-17	T03F6.2	ZF - C2H2 - 2 fingers	JA	wTF2.0	
ztf-17	T09A5.12	ZF - C2H2 - 2 fingers	MV	wTF2.0	
T20F7.1	T20F7.1	ZF - C2H2 - 2 fingers	JA	wTF2.0 and CisBP	
T20H4.2	T20H4.2	ZF - C2H2 - 2 fingers	JA	wTF2.0	
ztf-6	W06H12.1	ZF - C2H2 - 2 fingers	JA	wTF2.0 and CisBP	
Y17G7B.22	Y17G7B.22	ZF - C2H2 - 2 fingers	AJM	wTF2.0	
Y22D7AL.16	Y22D7AL.16	ZF - C2H2 - 2 fingers	JA	wTF2.0	
Y56A3A.28	Y56A3A.28	ZF - C2H2 - 2 fingers	JA	wTF2.0 and CisBP	
ztf-29	Y66D12A.12	ZF - C2H2 - 2 fingers	AJM	wTF2.0 and CisBP	
ztf-25	Y6G8.3	ZF - C2H2 - 2 fingers	JA	wTF2.0 and CisBP	
Y71A12B.8	Y71A12B.8	ZF - C2H2 - 2 fingers	AJM	wTF2.0	
Y82E9BR.1	Y82E9BR.1	ZF - C2H2 - 2 fingers	JA	wTF2.0 and CisBP	
sdz-38	ZK892.7	ZF - C2H2 - 2 fingers	JA	wTF2.0 and CisBP	
die-1	C18D1.1	ZF - C2H2 - 3 fingers	JA	wTF2.0 and CisBP	P0 scoring
ztf-26	F55H12.6	ZF - C2H2 - 3 fingers	AJM	wTF2.0 and CisBP	
odd-1	B0280.4	ZF - C2H2 - 3 fingers	JA	wTF2.0 and CisBP	
C04F5.9	C04F5.9	ZF - C2H2 - 3 fingers	JA	wTF2.0 and CisBP	
mnm-2	C10A4.8	ZF - C2H2 - 3 fingers	MV	wTF2.0 and CisBP	
C16A3.4	C16A3.4	ZF - C2H2 - 3 fingers	JA	wTF2.0	P0 scoring
egrh-1	C27C12.2	ZF - C2H2 - 3 fingers	JA	wTF2.0 and CisBP	

odd-2	C34H3.2	ZF - C2H2 - 3 fingers	JA	wTF2.0 and CisBP	
ref-2	C47C12.3	ZF - C2H2 - 3 fingers	MV	wTF2.0 and CisBP	
unc-98	F08C6.7	ZF - C2H2 - 3 fingers	MV	wTF2.0 and CisBP	
ztf-2	F13G3.1	ZF - C2H2 - 3 fingers	JA	wTF2.0 and CisBP	
bcl-11	F13H6.1	ZF - C2H2 - 3 fingers	JA	wTF2.0 and CisBP	
F26A10.2	F26A10.2	ZF - C2H2 - 3 fingers	JA	wTF2.0	
pqm-1	F40F8.7	ZF - C2H2 - 3 fingers	JA	wTF2.0	
F47E1.3	F47E1.3	ZF - C2H2 - 3 fingers	AJM	wTF2.0 and CisBP	
klf-2	F53F8.1	ZF - C2H2 - 3 fingers	JA	wTF2.0 and CisBP	
klf-3	F54H5.4	ZF - C2H2 - 3 fingers	MV	wTF2.0 and CisBP	
klf-1	F56F11.3	ZF - C2H2 - 3 fingers	JA	wTF2.0 and CisBP	
F57C9.4	F57C9.4	ZF - C2H2 - 3 fingers	JA	wTF2.0 and CisBP	
K11D2.4	K11D2.4	ZF - C2H2 - 3 fingers	JA	wTF2.0 and CisBP	
sptf-2	T22C8.5	ZF - C2H2 - 3 fingers	JA	wTF2.0 and CisBP	
pat-9	T27B1.2	ZF - C2H2 - 3 fingers	JA	wTF2.0 and CisBP	P0 scoring
W02D7.6	W02D7.6	ZF - C2H2 - 3 fingers	JA	wTF2.0 and CisBP	
Y37E11B.1	Y37E11B.1	ZF - C2H2 - 3 fingers	JA	wTF2.0 and CisBP	
ztf-20	Y39B6A.46	ZF - C2H2 - 3 fingers	AJM	wTF2.0 and CisBP	
sptf-3	Y40B1A.4	ZF - C2H2 - 3 fingers	JA	wTF2.0 and CisBP	P0 scoring
slr-2	Y59A8B.13	ZF - C2H2 - 3 fingers	AJM	wTF2.0 and CisBP	
Y67H2A.10	Y67H2A.10	ZF - C2H2 - 3 fingers	AJM	wTF2.0	
Y79H2A.3	Y79H2A.3	ZF - C2H2 - 3 fingers	JA	wTF2.0	
klu-2	ZC328.2	ZF - C2H2 - 3 fingers	JA	wTF2.0 and CisBP	
ztf-8	ZC395.8	ZF - C2H2 - 3 fingers	MV	wTF2.0	
ZK546.5	ZK546.5	ZF - C2H2 - 3 fingers	JA	wTF2.0	
ZK686.5	ZK686.5	ZF - C2H2 - 3 fingers	AJM	wTF2.0 and CisBP	
C46E10.9	C46E10.9	ZF - C2H2 - 4 fingers	JA	wTF2.0	
lst-5	C52E12.6	ZF - C2H2 - 4 fingers	AJM	wTF2.0 and CisBP	
che-1	C55B7.12	ZF - C2H2 - 4 fingers	JA	wTF2.0 and CisBP	
F10B5.3	F10B5.3	ZF - C2H2 - 4 fingers	JA	wTF2.0 and CisBP	

blmp-1	F25D7.3	ZF - C2H2 - 4 fingers	JA	wTF2.0 and CisBP
ces-1	F43G9.11	ZF - C2H2 - 4 fingers	JA	wTF2.0 and CisBP
ztf-7	F46B6.7	ZF - C2H2 - 4 fingers	MV	wTF2.0 and CisBP
ztf-1	F54F2.5	ZF - C2H2 - 4 fingers	JA	wTF2.0
F56D1.1	F56D1.1	ZF - C2H2 - 4 fingers	MV	wTF2.0 and CisBP
H16D19.3	H16D19.3	ZF - C2H2 - 4 fingers	MV	wTF2.0
snai-1	K02D7.2	ZF - C2H2 - 4 fingers	AJM	wTF2.0
egl-43	R53.3	ZF - C2H2 - 4 fingers	JA	wTF2.0 and CisBP
T07D10.3	T07D10.3	ZF - C2H2 - 4 fingers	JA	wTF2.0
klu-1	ZK337.2	ZF - C2H2 - 4 fingers	MV	wTF2.0 and CisBP
syd-9	ZK867.1	ZF - C2H2 - 4 fingers	MV	wTF2.0 and CisBP
lin-48	F34D10.5	ZF - C2H2 - 4 fingers	MV	wTF2.0 and CisBP
zag-1	F28F9.1	ZF - C2H2 - 4 fingers, HD - ZFHD	JA	wTF2.0 and CisBP
C28G1.4	C28G1.4	ZF - C2H2 - 5 fingers	JA	wTF2.0
row-1	F37D6.2	ZF - C2H2 - 5 fingers	MV	wTF2.0
pag-3	F45B8.4	ZF - C2H2 - 5 fingers	MV	wTF2.0 and CisBP
lsy-2	F49H12.1	ZF - C2H2 - 5 fingers	MV	wTF2.0 and CisBP
lsl-1	F52F12.4	ZF - C2H2 - 5 fingers	JA	wTF2.0 and CisBP
mep-1	M04B2.1	ZF - C2H2 - 5 fingers	JA	wTF2.0
ztf-15	R06C7.9	ZF - C2H2 - 5 fingers	JA	wTF2.0 and CisBP
lin-29	W03C9.4	ZF - C2H2 - 5 fingers	JA	wTF2.0 and CisBP
fezf-1	Y38H8A.5	ZF - C2H2 - 5 fingers	JA	wTF2.0 and CisBP
tra-1	Y47D3A.6	ZF - C2H2 - 5 fingers	JA	wTF2.0 and CisBP
Y5F2A.4	Y5F2A.4	ZF - C2H2 - 5 fingers	JA	wTF2.0 and CisBP
sup-37	C01B7.1	ZF - C2H2 - 6 fingers	JA	wTF2.0
C09F5.3	C09F5.3	ZF - C2H2 - 6 fingers	JA	wTF2.0 and CisBP
C27A12.2	C27A12.2	ZF - C2H2 - 6 fingers	JA	wTF2.0 and CisBP
let-391	C27A12.3	ZF - C2H2 - 6 fingers	JA	wTF2.0 and CisBP
F26F4.8	F26F4.8	ZF - C2H2 - 6 fingers	JA	wTF2.0 and CisBP
tra-4	F53B3.1	ZF - C2H2 - 6 fingers	JA	wTF2.0

F58G1.2	F58G1.2	ZF - C2H2 - 6 fingers	MV	wTF2.0 and CisBP	
M03D4.4	M03D4.4	ZF - C2H2 - 6 fingers	AJM	wTF2.0 and CisBP	
pzf-1	T05G11.1	ZF - C2H2 - 6 fingers	JA	wTF2.0 and CisBP	
Y111B2A.10	Y111B2A.10	ZF - C2H2 - 6 fingers	AJM	wTF2.0 and CisBP	
ztf-23	Y54E10BR.8	ZF - C2H2 - 6 fingers	JA	wTF2.0 and CisBP	
ehn-3	ZK616.10	ZF - C2H2 - 6 fingers	MV	wTF2.0 and CisBP	
spr-3	C07A12.5	ZF - C2H2 - 7 fingers	JA	wTF2.0	
sdz-12	F12E12.5	ZF - C2H2 - 7 fingers	MV	wTF2.0 and CisBP	
sem-4	F15C11.1	ZF - C2H2 - 7 fingers	AJ	wTF2.0 and CisBP	
zpf-2	F35H8.3	ZF - C2H2 - 7 fingers	JA	wTF2.0 and CisBP	
sma-9	T05A10.1	ZF - C2H2 - 7 fingers	AJM	wTF2.0 and CisBP	
ztf-16	R08E3.4	ZF - C2H2 - 8 fingers	AJM	wTF2.0 and CisBP	
eor-1	R11E3.6	ZF - C2H2 - 9 fingers	MV	wTF2.0 and CisBP	
hbl-1	F13D11.2	ZF - C2H2 - 9 fingers	JA	wTF2.0 and CisBP	
hinf-1	F39B2.1	ZF - C2H2 - 9 fingers	JA	wTF2.0 and CisBP	
Y55F3AM.14	Y55F3AM.14	ZF - C2H2 - 9 fingers	MV	wTF2.0 and CisBP	
zfh-2	ZC123.3	ZF - C2H2 - 9 fingers, HD - 3 domains	JA	wTF2.0 and CisBP	
ztf-11	F52F12.6	ZF - C2HC 2 fingers	JA	wTF2.0 and CisBP	
C27A2.7	C27A2.7	ZF - C2H2	AJM	CisBP	
D2092.10	D2092.10	ZF - C2H2	AJM	CisBP	
egrh-2	Y55F3AM.7	ZF - C2H2	AJM	CisBP	Secondary target: *egrh-1*
egrh-3	Y94H6A.11	ZF - C2H2	AJM	CisBP	
bnc-1	F55C5.11	ZF - C2H2	AJM	CisBP	
ztf-9	ZK287.6	ZF - C2H2	AJM	CisBP	
mex-6	AH6.5	ZF - CCCH - 2 domains	AJM	wTF2.0 and CisBP	
dmd-10	C34D1.1	ZF - DM	JA	wTF2.0 and CisBP	
dmd-11	C34D1.2	ZF - DM	JA	wTF2.0 and CisBP	
dmd-3	Y43F8C.10	ZF - DM	JA	wTF2.0 and CisBP	
dmd-4	C27C12.6	ZF - DM	JA	wTF2.0 and CisBP	

dmd-5	F10C1.5	ZF - DM	JA	wTF2.0 and CisBP
dmd-6	F13G11.1	ZF - DM	JA	wTF2.0 and CisBP
dmd-7	K08B12.2	ZF - DM	AJM	wTF2.0 and CisBP
dmd-9	Y67D8A.3	ZF - DM	JA	wTF2.0 and CisBP
mab-23	C32C4.5	ZF - DM	AJM	wTF2.0 and CisBP
dmd-8	T22H9.4	ZF - DM - 2 domains	AJM	wTF2.0 and CisBP
mab-3	Y53C12B.5	ZF - DM - 2 domains	MV	wTF2.0 and CisBP
flh-1	Y11D7A.12	ZF - FLYWCH	JA	wTF2.0 and CisBP
flh-2	C26E6.2	ZF - FLYWCH	AJM	wTF2.0 and CisBP
flh-3	Y11D7A.13	ZF - FLYWCH	JA	wTF2.0 and CisBP
peb-1	T14F9.4	ZF - FLYWCH	JA	wTF2.0 and CisBP
egl-18	F55A8.1	ZF - GATA	JA	wTF2.0 and CisBP
elt-1	W09C2.1	ZF - GATA - 2 domains	JA	wTF2.0 and CisBP
elt-2	C33D3.1	ZF - GATA	JA	wTF2.0 and CisBP
elt-3	K02B9.4	ZF - GATA	JA	wTF2.0 and CisBP
elt-4	C39B10.6	ZF - GATA	AJM	wTF2.0 and CisBP
elt-6	F52C12.5	ZF - GATA	JA	wTF2.0 and CisBP
elt-7	C18G1.2	ZF - GATA	MV	wTF2.0 and CisBP
end-1	F58E10.2	ZF - GATA	JA	wTF2.0 and CisBP
end-3	F58E10.5	ZF - GATA	JA	wTF2.0 and CisBP
med-1	T24D3.1	ZF - GATA	JA	wTF2.0 and CisBP
med-2	K04C2.6	ZF - GATA	JA	wTF2.0 and CisBP
egl-27	C04A2.3	ZF - GATA, MYB	JA	wTF2.0 and CisBP
lin-40	T27C4.4	ZF - GATA, MYB	JA	wTF2.0 and CisBP
rcor-1	Y74C9A.4	ZF - GATA, MYB (2x)	MV	wTF2.0 and CisBP
miz-1	R13.1	ZF - MIZ	JA	WormBase
nfx-1	C16A3.7	ZF - NF-X1 - 10 domains	JA	wTF2.0 and CisBP
nhr-150	C06B8.1	ZF - NHR	MV	wTF2.0 and CisBP

nhr-63	C06C6.4	ZF - NHR	MV	wTF2.0 and CisBP	
nhr-50	C06C6.5	ZF - NHR	JA	wTF2.0 and CisBP	
nhr-152	C12D5.2	ZF - NHR	MV	wTF2.0 and CisBP	
nhr-94	C12D5.8	ZF - NHR	JA	wTF2.0 and CisBP	
nhr-155	C14C6.4	ZF - NHR	JA	wTF2.0 and CisBP	
nhr-257	C17A2.1	ZF - NHR	JA	wTF2.0 and CisBP	
nhr-72	C17A2.8	ZF - NHR	JA	wTF2.0 and CisBP	
nhr-30	C25E10.1	ZF - NHR	JA	wTF2.0 and CisBP	
nhr-258	C26B2.4	ZF - NHR	MV	wTF2.0 and CisBP	
nhr-74	C27C7.3	ZF - NHR	JA	wTF2.0 and CisBP	
nhr-73	C27C7.4	ZF - NHR	MV	wTF2.0 and CisBP	
nhr-43	C29E6.5	ZF - NHR	MV	wTF2.0 and CisBP	
nhr-162	C33G8.10	ZF - NHR	MV	wTF2.0 and CisBP	
nhr-107	C33G8.11	ZF - NHR	AJM	wTF2.0 and CisBP	
nhr-163	C33G8.12	ZF - NHR	JA	wTF2.0 and CisBP	
nhr-42	C33G8.6	ZF - NHR	AJM	wTF2.0 and CisBP	
nhr-161	C33G8.7	ZF - NHR	AJM	wTF2.0 and CisBP	
nhr-139	C33G8.8	ZF - NHR	JA	wTF2.0 and CisBP	
nhr-140	C33G8.9	ZF - NHR	JA	wTF2.0 and CisBP	
nhr-164	C41G6.5	ZF - NHR	MV	wTF2.0 and CisBP	
nhr-165	C47F8.2	ZF - NHR	JA	wTF2.0 and CisBP	
nhr-81	C47F8.8	ZF - NHR	JA	wTF2.0 and CisBP	
nhr-75	C49D10.6	ZF - NHR	JA	wTF2.0 and CisBP	
nhr-261	C49D10.9	ZF - NHR	AJM	wTF2.0 and CisBP	Secondatry target *nhr-257*
nhr-167	C49F5.4	ZF - NHR	AJM	wTF2.0 and CisBP	
nhr-169	C54C8.1	ZF - NHR	JA	wTF2.0 and CisBP	
nhr-170	C54E10.5	ZF - NHR	JA	wTF2.0 and CisBP	
nhr-171	C54F6.8	ZF - NHR	AJM	wTF2.0 and CisBP	

nhr-172	C54F6.9	ZF - NHR	JA	wTF2.0 and CisBP	
nhr-137	C56E10.4	ZF - NHR	JA	wTF2.0 and CisBP	
nhr-89	E03H4.13	ZF - NHR	JA	wTF2.0 and CisBP	
nhr-174	E03H4.6	ZF - NHR	JA	wTF2.0 and CisBP	
nhr-264	F14A5.1	ZF - NHR	AJM	wTF2.0 and CisBP	Secondaty target *nhr-267*
nhr-176	F14H3.11	ZF - NHR	MV	wTF2.0 and CisBP	
nhr-281	F16B12.8	ZF - NHR	JA	wTF2.0 and CisBP	
nhr-177	F16B4.1	ZF - NHR	AJM	wTF2.0 and CisBP	
nhr-179	F16B4.11	ZF - NHR	MV	wTF2.0 and CisBP	
nhr-117	F16B4.12	ZF - NHR	MV	wTF2.0 and CisBP	
nhr-178	F16B4.9	ZF - NHR	JA	wTF2.0 and CisBP	
nhr-45	F16H11.5	ZF - NHR	JA	wTF2.0 and CisBP	
nhr-27	F16H9.2	ZF - NHR	JA	wTF2.0 and CisBP	
nhr-180	F31F4.12	ZF - NHR	JA	wTF2.0 and CisBP	
nhr-15	F33E11.1	ZF - NHR	MV	wTF2.0 and CisBP	
nhr-108	F35E8.12	ZF - NHR	JA	wTF2.0 and CisBP	
nhr-78	F36A4.14	ZF - NHR	AJM	wTF2.0 and CisBP	
nhr-54	F36D3.2	ZF - NHR	JA	wTF2.0 and CisBP	
nhr-183	F41B5.10	ZF - NHR	MV	wTF2.0 and CisBP	
nhr-182	F41B5.9	ZF - NHR	JA	wTF2.0 and CisBP	
nhr-82	F41D3.1	ZF - NHR	JA	wTF2.0 and CisBP	
nhr-265	F41D3.3	ZF - NHR	JA	wTF2.0 and CisBP	
nhr-20	F43C1.4	ZF - NHR	MV	wTF2.0 and CisBP	
nhr-39	F44A2.4	ZF - NHR	JA	wTF2.0 and CisBP	
nhr-126	F44C8.10	ZF - NHR	JA	wTF2.0 and CisBP	
nhr-96	F44C8.11	ZF - NHR	JA	wTF2.0 and CisBP	
nhr-134	F44C8.2	ZF - NHR	JA	wTF2.0 and CisBP	
nhr-18	F44C8.3	ZF - NHR	JA	wTF2.0 and CisBP	

nhr-103	F44C8.4	ZF - NHR	JA	wTF2.0 and CisBP	
nhr-128	F44C8.5	ZF - NHR	JA	wTF2.0 and CisBP	
nhr-56	F44C8.6	ZF - NHR	JA	wTF2.0 and CisBP	
nhr-133	F44C8.8	ZF - NHR	MV	wTF2.0 and CisBP	
nhr-184	F44C8.9	ZF - NHR	JA	wTF2.0 and CisBP	
nhr-185	F47C10.1	ZF - NHR	JA	wTF2.0 and CisBP	
nhr-186	F47C10.3	ZF - NHR	JA	wTF2.0 and CisBP	
nhr-187	F47C10.4	ZF - NHR	JA	wTF2.0 and CisBP	
nhr-188	F47C10.7	ZF - NHR	JA	wTF2.0 and CisBP	
nhr-189	F47C10.8	ZF - NHR	AJM	wTF2.0 and CisBP	
nhr-83	F48G7.3	ZF - NHR	JA	wTF2.0 and CisBP	
nhr-7	F54D1.4	ZF - NHR	JA	wTF2.0 and CisBP	
nhr-266	F56H1.2	ZF - NHR	JA	wTF2.0 and CisBP	
nhr-283	F57A10.6	ZF - NHR	AJM	wTF2.0 and CisBP	
nhr-193	F57G8.6	ZF - NHR	JA	wTF2.0 and CisBP	
nhr-195	F59E11.10	ZF - NHR	JA	wTF2.0 and CisBP	
nhr-143	F59E11.11	ZF - NHR	JA	wTF2.0 and CisBP	
nhr-267	H22D14.1	ZF - NHR	JA	wTF2.0 and CisBP	
nhr-51	K06B4.1	ZF - NHR	JA	wTF2.0 and CisBP	
nhr-199	K06B4.10	ZF - NHR	JA	wTF2.0 and CisBP	
nhr-53	K06B4.11	ZF - NHR	MV	wTF2.0 and CisBP	Secondary target *nhr-199*
nhr-196	K06B4.5	ZF - NHR	MV	wTF2.0 and CisBP	
nhr-268	K06B4.6	ZF - NHR	JA	wTF2.0 and CisBP	
nhr-71	K11E4.5	ZF - NHR	JA	wTF2.0 and CisBP	
nhr-99	M02H5.1	ZF - NHR	MV	wTF2.0 and CisBP	
nhr-98	M02H5.6	ZF - NHR	MV	wTF2.0 and CisBP	
nhr-123	M02H5.7	ZF - NHR	JA	wTF2.0 and CisBP	
nhr-125	R02D1.1	ZF - NHR	JA	wTF2.0 and CisBP	

nhr-12	R04B5.4	ZF - NHR	MV	wTF2.0 and CisBP
nhr-269	R08H2.9	ZF - NHR	JA	wTF2.0 and CisBP
dpr-1	R10D12.2	ZF - NHR	JA	wTF2.0 and CisBP
nhr-132	R11G11.1	ZF - NHR	MV	wTF2.0 and CisBP
nhr-210	R11G11.12	ZF - NHR	AJM	wTF2.0 and CisBP
nhr-58	R11G11.2	ZF - NHR	JA	wTF2.0 and CisBP
nhr-131	T01G6.2	ZF - NHR	AJM	wTF2.0 and CisBP
nhr-106	T01G6.4	ZF - NHR	JA	wTF2.0 and CisBP
nhr-211	T01G6.5	ZF - NHR	MV	wTF2.0 and CisBP
nhr-212	T01G6.6	ZF - NHR	JA	wTF2.0 and CisBP
nhr-55	T01G6.7	ZF - NHR	JA	wTF2.0 and CisBP
nhr-130	T01G6.8	ZF - NHR	JA	wTF2.0 and CisBP
nhr-271	T03E6.3	ZF - NHR	JA	wTF2.0 and CisBP
nhr-57	T05B4.2	ZF - NHR	JA	wTF2.0 and CisBP
nhr-213	T06C12.13	ZF - NHR	MV	wTF2.0 and CisBP
nhr-102	T06C12.6	ZF - NHR	MV	wTF2.0 and CisBP
nhr-84	T06C12.7	ZF - NHR	MV	wTF2.0 and CisBP
nhr-272	T07C5.2	ZF - NHR	JA	wTF2.0 and CisBP
nhr-214	T07C5.3	ZF - NHR	JA	wTF2.0 and CisBP
nhr-215	T07C5.4	ZF - NHR	JA	wTF2.0 and CisBP
nhr-216	T09D3.4	ZF - NHR	JA	wTF2.0 and CisBP
nhr-217	T09E11.2	ZF - NHR	JA	wTF2.0 and CisBP
nhr-109	T12C9.5	ZF - NHR	AJM	wTF2.0 and CisBP
nhr-218	T13F3.2	ZF - NHR	JA	wTF2.0 and CisBP
nhr-77	T15D6.6	ZF - NHR	JA	wTF2.0 and CisBP
odr-7	T18D3.2	ZF - NHR	JA	wTF2.0 and CisBP
nhr-44	T19A5.4	ZF - NHR	JA	wTF2.0 and CisBP
nhr-220	T19H12.8	ZF - NHR	JA	wTF2.0 and CisBP

nhr-285	T26E4.16	ZF - NHR	AJM	wTF2.0 and CisBP	
nhr-223	T26E4.8	ZF - NHR	JA	wTF2.0 and CisBP	
nhr-79	T26H2.9	ZF - NHR	MV	wTF2.0 and CisBP	
nhr-59	T27B7.1	ZF - NHR	JA	wTF2.0 and CisBP	
nhr-115	T27B7.4	ZF - NHR	JA	wTF2.0 and CisBP	
nhr-227	T27B7.5	ZF - NHR	JA	wTF2.0 and CisBP	
nhr-228	T27B7.6	ZF - NHR	MV	wTF2.0 and CisBP	
nhr-229	Y116A8C.18	ZF - NHR	JA	wTF2.0 and CisBP	
nhr-230	Y17D7A.1	ZF - NHR	JA	wTF2.0 and CisBP	
nhr-231	Y17D7B.1	ZF - NHR	JA	wTF2.0 and CisBP	
nhr-232	Y22F5A.1	ZF - NHR	JA	wTF2.0 and CisBP	
tag-122	Y32B12B.6	ZF - NHR	JA	wTF2.0 and CisBP	
nhr-234	Y38E10A.18	ZF - NHR	MV	wTF2.0 and CisBP	
nhr-95	Y39B6A.17	ZF - NHR	JA	wTF2.0 and CisBP	
nhr-92	Y41D4B.8	ZF - NHR	JA	wTF2.0 and CisBP	
nhr-122	Y41D4B.9	ZF - NHR	AJM	wTF2.0 and CisBP	
nhr-110	Y46H3D.5	ZF - NHR	MV	wTF2.0 and CisBP	
nhr-275	Y5H2A.2	ZF - NHR	AJM	wTF2.0 and CisBP	
nhr-13	Y5H2B.2	ZF - NHR	JA	wTF2.0 and CisBP	
nhr-241	Y69H2.8	ZF - NHR	AJM	wTF2.0 and CisBP	
nhr-112	Y70C5C.6	ZF - NHR	AJM	wTF2.0 and CisBP	
nhr-276	Y71A12C.1	ZF - NHR	JA	wTF2.0 and CisBP	
nhr-243	Y80D3A.4	ZF - NHR	MV	wTF2.0 and CisBP	
nhr-277	Y94H6A.1	ZF - NHR	MV	wTF2.0 and CisBP	
nhr-245	ZK1025.10	ZF - NHR	AJM	wTF2.0 and CisBP	Secondary target *nhr-73* and *nhr-74*
nhr-113	ZK1025.9	ZF - NHR	JA	wTF2.0 and CisBP	
nhr-248	ZK218.6	ZF - NHR	AJM	wTF2.0 and CisBP	

nhr-9	ZK418.1	ZF - NHR	MV	wTF2.0 and CisBP
nhr-250	ZK488.1	ZF - NHR	JA	wTF2.0 and CisBP
nhr-90	ZK488.2	ZF - NHR	JA	wTF2.0 and CisBP
nhr-251	ZK488.4	ZF - NHR	JA	wTF2.0 and CisBP
nhr-252	ZK6.2	ZF - NHR	AJM	wTF2.0 and CisBP
nhr-253	ZK6.4	ZF - NHR	MV	wTF2.0 and CisBP
nhr-254	ZK6.5	ZF - NHR	JA	wTF2.0 and CisBP
nhr-255	ZK678.2	ZF - NHR	AJM	wTF2.0 and CisBP
nhr-256	ZK697.2	ZF - NHR	JA	wTF2.0 and CisBP
nhr-10	B0280.8	ZF - NHR	JA	wTF2.0 and CisBP
nhr-23	C01H6.5	ZF - NHR	JA	wTF2.0 and CisBP
nhr-17	C02B4.2	ZF - NHR	JA	wTF2.0 and CisBP
nhr-76	C05G6.1	ZF - NHR	JA	wTF2.0 and CisBP
nhr-35	C07A12.3	ZF - NHR	JA	wTF2.0 and CisBP
nhr-67	C08F8.8	ZF - NHR	JA	wTF2.0 and CisBP
nhr-28	C11G6.4	ZF - NHR	MV	wTF2.0 and CisBP
nhr-153	C13C4.1	ZF - NHR	JA	wTF2.0 and CisBP
nhr-154	C13C4.2	ZF - NHR	JA	wTF2.0 and CisBP
nhr-136	C13C4.3	ZF - NHR	AJM	wTF2.0 and CisBP
nhr-124	C17E7.8	ZF - NHR	MV	wTF2.0 and CisBP
nhr-47	C24G6.4	ZF - NHR	JA	wTF2.0 and CisBP
nhr-120	C25B8.6	ZF - NHR	JA	wTF2.0 and CisBP
nhr-31	C26B2.3	ZF - NHR	MV	wTF2.0 and CisBP
nhr-100	C28D4.1	ZF - NHR	JA	wTF2.0 and CisBP
nhr-138	C28D4.9	ZF - NHR	AJM	wTF2.0 and CisBP
nhr-2	C32F10.6	ZF - NHR	JA	wTF2.0 and CisBP
nhr-260	C38C3.9	ZF - NHR	JA	wTF2.0 and CisBP
nhr-64	C45E1.1	ZF - NHR	JA	wTF2.0 and CisBP

nhr-46	C45E5.6	ZF - NHR	MV	wTF2.0 and CisBP
nhr-6	C48D5.1	ZF - NHR	JA	wTF2.0 and CisBP
nhr-166	C49D10.2	ZF - NHR	JA	wTF2.0 and CisBP
nhr-129	C50B6.14	ZF - NHR	AJM	wTF2.0 and CisBP
nhr-168	C50B6.8	ZF - NHR	JA	wTF2.0 and CisBP
nhr-173	C56E10.1	ZF - NHR	JA	wTF2.0 and CisBP
nhr-19	E02H1.7	ZF - NHR	JA	wTF2.0 and CisBP
nhr-121	E02H9.8	ZF - NHR	JA	wTF2.0 and CisBP
nhr-262	F09C6.8	ZF - NHR	JA	wTF2.0 and CisBP
nhr-116	F09C6.9	ZF - NHR	JA	wTF2.0 and CisBP
nhr-175	F09F3.10	ZF - NHR	JA	wTF2.0 and CisBP
daf-12	F11A1.3	ZF - NHR	JA	wTF2.0 and CisBP
nhr-25	F11C1.6	ZF - NHR	JA	wTF2.0 and CisBP
nhr-118	F13A2.8	ZF - NHR	AJM	wTF2.0 and CisBP
nhr-21	F21D12.1	ZF - NHR	MV	wTF2.0 and CisBP
nhr-141	F25E5.6	ZF - NHR	MV	wTF2.0 and CisBP
nhr-4	F32B6.1	ZF - NHR	JA	wTF2.0 and CisBP
nhr-8	F33D4.1	ZF - NHR	JA	wTF2.0 and CisBP
nhr-181	F38H12.3	ZF - NHR	MV	wTF2.0 and CisBP
sex-1	F44A6.2	ZF - NHR	JA	wTF2.0 and CisBP
nhr-37	F44C4.2	ZF - NHR	JA	wTF2.0 and CisBP
nhr-142	F44E7.8	ZF - NHR	JA	wTF2.0 and CisBP
nhr-111	F44G3.9	ZF - NHR	MV	wTF2.0 and CisBP
unc-55	F55D12.4	ZF - NHR	JA	wTF2.0 and CisBP
fax-1	F56E3.4	ZF - NHR	JA	wTF2.0 and CisBP
nhr-60	F57A10.5	ZF - NHR	JA	wTF2.0 and CisBP
nhr-192	F57A8.5	ZF - NHR	JA	wTF2.0 and CisBP
nhr-34	F58G6.5	ZF - NHR	MV	wTF2.0 and CisBP

nhr-3	H01A20.1	ZF - NHR	MV	wTF2.0 and CisBP
nhr-80	H10E21.3	ZF - NHR	JA	wTF2.0 and CisBP
nhr-68	H12C20.3	ZF - NHR	JA	wTF2.0 and CisBP
nhr-101	H12C20.6	ZF - NHR	AJM	wTF2.0 and CisBP
nhr-97	H27C11.1	ZF - NHR	JA	wTF2.0 and CisBP
nhr-38	K01H12.3	ZF - NHR	JA	wTF2.0 and CisBP
nhr-22	K06A1.4	ZF - NHR	JA	wTF2.0 and CisBP
nhr-52	K06B4.2	ZF - NHR	AJM	wTF2.0 and CisBP
nhr-197	K06B4.7	ZF - NHR	JA	wTF2.0 and CisBP
nhr-198	K06B4.8	ZF - NHR	MV	wTF2.0 and CisBP
nhr-88	K08A2.5	ZF - NHR	JA	wTF2.0 and CisBP
nhr-32	K08H2.8	ZF - NHR	MV	wTF2.0 and CisBP
nhr-49	K10C3.6	ZF - NHR	JA	wTF2.0 and CisBP
nhr-119	K12H6.1	ZF - NHR	JA	wTF2.0 and CisBP
nhr-204	R02C2.4	ZF - NHR	JA	wTF2.0 and CisBP
nhr-205	R04B5.3	ZF - NHR	MV	wTF2.0 and CisBP
nhr-206	R07B7.13	ZF - NHR	JA	wTF2.0 and CisBP
nhr-207	R07B7.14	ZF - NHR	JA	wTF2.0 and CisBP
nhr-208	R07B7.15	ZF - NHR	JA	wTF2.0 and CisBP
nhr-209	R07B7.16	ZF - NHR	AJM	wTF2.0 and CisBP
nhr-1	R09G11.2	ZF - NHR	MV	wTF2.0 and CisBP
nhr-104	R11E3.5	ZF - NHR	JA	wTF2.0 and CisBP
nhr-270	R13D11.8	ZF - NHR	JA	wTF2.0 and CisBP
nhr-14	T01B10.4	ZF - NHR	JA	wTF2.0 and CisBP
nhr-40	T03G6.2	ZF - NHR	MV	wTF2.0 and CisBP
nhr-26	T07C5.5	ZF - NHR	JA	wTF2.0 and CisBP
nhr-66	T09A12.4	ZF - NHR	JA	wTF2.0 and CisBP
nhr-273	T12C9.1	ZF - NHR	AJM	wTF2.0 and CisBP

nhr-16	T12C9.6	ZF - NHR	MV	wTF2.0 and CisBP
nhr-127	T13F3.3	ZF - NHR	JA	wTF2.0 and CisBP
nhr-69	T23H4.2	ZF - NHR	MV	wTF2.0 and CisBP
nhr-225	T27B7.2	ZF - NHR	JA	wTF2.0 and CisBP
nhr-226	T27B7.3	ZF - NHR	JA	wTF2.0 and CisBP
nhr-61	W01D2.2	ZF - NHR	AJM	wTF2.0 and CisBP
nhr-85	W05B5.3	ZF - NHR	JA	wTF2.0 and CisBP
nhr-91	Y15E3A.1	ZF - NHR	MV	wTF2.0 and CisBP
nhr-65	Y17D7A.3	ZF - NHR	MV	wTF2.0 and CisBP
nhr-145	Y39B6A.47	ZF - NHR	AJM	wTF2.0 and CisBP
nhr-86	Y40B10A.8	ZF - NHR	AJM	wTF2.0 and CisBP
nhr-274	Y41D4B.21	ZF - NHR	AJM	wTF2.0 and CisBP
nhr-87	Y41D4B.7	ZF - NHR	JA	wTF2.0 and CisBP
nhr-114	Y45G5AM.1	ZF - NHR	AJM	wTF2.0 and CisBP
nhr-70	Y51A2D.17	ZF - NHR	MV	wTF2.0 and CisBP
nhr-239	Y54F10AM.1	ZF - NHR	AJM	wTF2.0 and CisBP
nhr-62	Y67A6A.2	ZF - NHR	JA	wTF2.0 and CisBP
nhr-242	Y69A2AR.26	ZF - NHR	AJM	wTF2.0 and CisBP
nhr-5	Y73F8A.21	ZF - NHR	AJM	wTF2.0 and CisBP
nhr-11	ZC410.1	ZF - NHR	JA	wTF2.0 and CisBP
nhr-247	ZK1037.5	ZF - NHR	JA	wTF2.0 and CisBP
nhr-33	ZK455.6	ZF - NHR	JA	wTF2.0 and CisBP
nhr-48	ZK662.3	ZF - NHR	AJM	wTF2.0 and CisBP
nhr-148	C03G6.10	ZF - NHR	JA	wTF2.0 and CisBP
nhr-149	C03G6.12	ZF - NHR	JA	wTF2.0 and CisBP
nhr-147	C03G6.8	ZF - NHR	JA	wTF2.0 and CisBP
nhr-105	C06G3.1	ZF - NHR	JA	wTF2.0 and CisBP
nhr-156	C17E7.1	ZF - NHR	MV	wTF2.0 and CisBP

nhr-157	C17E7.5	ZF - NHR	JA	wTF2.0 and CisBP
nhr-158	C17E7.6	ZF - NHR	JA	wTF2.0 and CisBP
nhr-159	C17E7.7	ZF - NHR	JA	wTF2.0 and CisBP
srt-58	C29G2.5	ZF - NHR	AJM	wTF2.0 and CisBP
nhr-36	F07C3.10	ZF - NHR	AJM	wTF2.0 and CisBP
nhr-190	F48G7.11	ZF - NHR	JA	wTF2.0 and CisBP
nhr-201	M02H5.3	ZF - NHR	AJM	wTF2.0 and CisBP
nhr-202	M02H5.4	ZF - NHR	AJM	wTF2.0 and CisBP
nhr-203	M02H5.5	ZF - NHR	AJM	wTF2.0 and CisBP
nhr-222	T24A6.11	ZF - NHR	JA	wTF2.0 and CisBP
nhr-221	T24A6.8	ZF - NHR	JA	wTF2.0 and CisBP
nhr-41	Y104H12A.1	ZF - NHR	AJM	wTF2.0 and CisBP
nhr-237	Y46H3D.6	ZF - NHR	MV	wTF2.0 and CisBP
nhr-238	Y46H3D.7	ZF - NHR	AJM	wTF2.0 and CisBP
nhr-146	Y41D4B.27	ZF - NHR	AJM	CisBP
nhr-236	Y38F2AL.5	ZF - NHR	MV	CisBP
nhr-286	VC5.6	ZF - NHR	AJM	CisBP
ZK1037.13	ZK1037.13	ZF - NHR	AJM	CisBP
nhr-219	T19A5.5	ZF - NHR - 2 domains	JA	wTF2.0 and CisBP
nhr-135	VC5.5	ZF - NHR - 2 domains	AJM	wTF2.0 and CisBP
B0336.7	B0336.7	ZF - THAP	JA	wTF2.0 and CisBP
cdc-14	C17G10.4	ZF - THAP	MV	wTF2.0 and CisBP
ctbp-1	F49E10.5	ZF - THAP	JA	wTF2.0 and CisBP
him-17	T09E8.2	THAP finger	MV	CisBP
Y50E8A.12	Y50E8A.12	THAP finger	MV	CisBP
dpy-27	R13G10.1	Unknown	AJM	CisBP
lin-14	T25C12.1	Unknown	MV	CisBP

Table A.4. Composition of TF RNAi library. The libraries used to build this TF RNAi library were Julie Ahringer's libraty (JA), Marc Vidal's library (MV) and generated clones in our lab (AJM).

Table A.5. RNAi and mutant scores of dopaminergic candidates

Table A.5. RNAi and mutant scores of DA candidates								
TF	**Neuron**	**Reporter**	**RNAi**			**Mutant**		
			Stage	%	SEP	Allele	%	SEP
cep-1	CEPV	*cat-2*	P0	86	4,48	*ep347*	96	1,96
	CEPD			88	4,20	*ep347*	92	2,71
	ADE			86	4,48	*ep347*	97	1,71
	PDE			80	5,16	*ep347*	100	0,00
	CEPV	*cat-1*	F1	86	4,48			
	CEPD			86	4,48			
	ADE			87	4,34			
	PDE			97	2,20			
mef-2	CEPV	*cat-2*	P0	88	4,20	*gk633*	96	1,96
						gv1	98	1,40
	CEPD			87	4,34	*gk633*	94	2,37
						gv1	100	0,00
	ADE			92	3,50	*gk633*	100	0,00
						gv1	97	1,71
	PDE			85	4,61	*gk633*	100	0,00
						gv1	100	0,00
	CEPV	*cat-1*	F1	88	4,20			
	CEPD			86	4,48			
	ADE			89	4,04			
	PDE			95	2,81			
dro-1	CEPV	*cat-2*	P0	86	4,48	*tm4702*	95	2,18
	CEPD			86	4,48			
	ADE			82	4,96	*tm4702*	95	2,18
	PDE			71	5,86	*tm4702*	86	3,47
	CEPV	*cat-1*	F1	81	5,06			
	CEPD			81	5,06			
	ADE			78	5,35			
	PDE			72	5,80			
unc-55	CEPV	*cat-2*	P0	98	1,81	*e1170*	98	1,40
	CEPD			90	3,87	*e1170*	98	1,40
	ADE			51	6,45	*e1170*	85	3,57
	PDE			34	6,12	*e1170*	100	0,00
	CEPV	*cat-1*	F1	88	4,20	*e1170*	94	2,37
	CEPD			89	4,04	*e1170*	96	1,96

	ADE			97	2,20	*e1170*	94	2,37
	PDE			95	2,81	*e1170*	100	0,00
	CEPV	*cat-4*				*e1170*	100	0,00
	CEPD					*e1170*	100	0,00
	ADE					*e1170*	94	2,37
	PDE					*e1170*	100	0,00
	CEPV	*bas-1*				*e1170*	95	2,18
	CEPD					*e1170*	100	0,00
	ADE					*e1170*	93	2,55
	PDE					*e1170*	96	1,96
	CEPV	*dat-1*				*e1170*	94	2,37
	CEPD					*e1170*	100	0,00
	ADE					*e1170*	100	0,00
	PDE					*e1170*	95	2,18
vab-3	CEPV	*cat-2*	P0	86	4,48	*ot346*	20	4,00
	CEPD			95	2,81			
	ADE			61	6,30	*ot346*	85	3,57
	PDE			30	5,92	*ot346*	85	3,57
	CEPV	*cat-1*	F1	78	5,35			
	CEPD			94	3,07			
	ADE			77	5,43			
	PDE			79	5,26			
	CEPV	*dat-1*				*ot346*	30	4,58
	CEPD							
	ADE					*ot346*	100	0,00
	PDE					*ot346*	100	0,00
unc-62	CEPV	*cat-2*	P0	90	3,87	*e644*	89	3,13
						mu232	92	2,71
						e917	88	3,25
	CEPD			99	1,28	*e644*	89	3,13
						mu232	90	3,00
						e917	90	3,00
	ADE			78	5,35	*e644*	86	3,47
						mu232	83	3,76
						e917	70	4,58
	PDE			58	6,37	*e644*	93	2,55
						mu232	97	1,71
						e917	70	4,58
	CEPV	*cat-1*	F1	83	4,85	*e917*	87	3,36

	CEPD			82	4,96	*e917*	90	3,00
	ADE			66	6,12	*e917*	88	3,25
	PDE			65	6,16	*e917*	66	4,74
	CEPV	*cat-4*				*e917*	94	2,37
	CEPD					*e917*	98	1,40
	ADE					*e917*	83	3,76
	PDE					*e917*	64	4,80
	CEPV	*bas-1*				*e917*	100	0,00
	CEPD					*e917*	100	0,00
	ADE					*e917*	85	3,57
	PDE					*e917*	72	4,49
	CEPV	*dat-1*				*e917*	94	2,37
	CEPD					*e917*	94	2,37
	ADE					*e917*	75	4,33
	PDE					*e917*	81	3,92

Table A.5. RNAi and mutant scores of dopaminergic candidates. Grey boxes indicate results that we did not achieve. For each score is included its standar error of the proportion (SEP).

Table A.6. RNAi and mutant scores of serotonergic, tyraminergic and octopaminergic candidates

TF	Neuron	Reporter	RNAi			Mutant		
			Stage	%	SEP	Allele	%	SEP
lag-1	ADF	*tph-1*	P0	32	6,02	*om13*	41	4,92
						q385	0	0,00
		cat-4				*om13*	73	4,44
						q385	40	4,90
		bas-1				*om13*	66	4,74
						q385	31	4,62
		cat-1	P0	45	6,42	*om13*	88	3,25
						q385	24	4,27
		srh-142	P0	100	0,00			
hlh-14	ADF	*tph-1*	P0	72	5,80			
			F1	49	6,45			
		cat-1	P0	97	2,20			

			F1	56	6,41			
		srh-142	P0	98	1,81			
			F1	65	6,16			
zip-5	RIM	*cat-1*	F1	65	6,16			
		tdc-1				*gk646*	79	4,07
	RIC	*cat-1*	F1	65	6,16			
		tdc-1				*gk646*	58	4,94
		tbh-1				*gk646*	98	1,40
pqm-1	RIM	*cat-1*	F1	76	5,51			
		tdc-1				*ok485*	98	1,40
	RIC	*cat-1*	F1	76	5,51			
		tdc-1				*ok485*	97	1,71
		tbh-1				*ok485*	100	0,00

Table A.6. RNAi and mutant scores of serotonergic, tyraminergic and octopmainergic candidates. Grey boxes indicate results that we did not achieve. For each score is included its standar error of the proportion (SEP).